Identification of Novel Therapeutic Vulnerabilities in Multiple Myeloma

Steven Findlay

Division of Experimental Medicine
Department of Medicine
McGill University
Montréal, Québec, Canada

2022

A thesis submitted to McGill University in partial fulfillment of the requirement of the degree of Doctor of Philosophy

Table of Contents

Abstract vi

Résumé viii

Contents of Manuscript x

Contributions of authors xii

Chapter 1: Introduction ..... ***xii***

Chapter 2: The mitochondrial pyruvate carrier complex modulates the response to proteasome inhibitors in multiple myeloma ..... ***xii***

Chapter 3: SHLD2/FAM35A co-operates with REV7 to coordinate DNA double-strand break repair pathway choice. ..... ***xii***

Chapter 4: Discussion ..... ***xiii***

Original contributions to knowledge xiv

Acknowledgements xv

List of Abbreviations xvi

Chapter 1: General Introduction 1

1.1 Multiple myeloma epidemiology ***2***

1.2 Pathophysiology and MM development ***3***

1.2.1 Plasma cell development 3

1.2.2 Cytogenetics of multiple myeloma 4

1.2.2.1 Primary oncogenic events *4*

1.2.2.2 Secondary oncogenic events *5*

1.2.3 Monoclonal gammopathy of undetermined significance (MGUS) 6

1.2.4 Smoldering multiple myeloma (SMM) 7

1.2.5 Symptomatic multiple myeloma (MM) 7

1.2.5.1 International staging system (ISS) *9*

1.3 Multiple myeloma bone marrow microenvironment ***10***

1.3.1 Osteoblasts/osteoclasts 11

1.3.2 Hypoxic bone marrow 12

1.4 MM therapeutic options: ***13***

1.4.1 Chemotherapy and DNA damage 14
1.4.2 DNA damage and genomic instability 15
1.4.2.1 DNA damage response 16
1.4.2.2 DSB recognition 16
1.4.2.3 Homologous recombination 17
1.4.2.3.1 RAD51 recombinase nucleofilaments, homology search and invasion 18
1.4.2.4 Non-homologous end-joining 18
1.4.2.4.1 Blunt end ligation 19
1.4.2.4.2 Polymerase-dependent pathway and alternative end joining 19
1.4.3 Genomic instability and multiple myeloma 20
1.4.4 Proteasome Inhibitors (PIs) 22
1.4.5 Immunomodulatory drugs and monoclonal antibodies 24
1.5 CRISPR Technology and Screening Strategies 25
1.6 Cellular Metabolism and Energetics 26
1.6.1 Mitochondria Pyruvate Carrier: 27
1.6.2 Cancer Metabolism: 28
1.6.3 Glutamine Metabolism: 29
1.6.4 Reactive Oxygen Species: 31
1.6.5 Energetic Stress: 32
1.6.6 Mitochondria and Multiple Myeloma 33

Chapter 2: The mitochondrial pyruvate carrier complex potentiates the efficacy of proteasome inhibitors in multiple myeloma 35

2.1 Abstract 36

2.2 Introduction 37

2.3 Materials and Methods 39

2.4 Results 45

2.5 Discussion 51

2.6 References 69

Chapter 3: SHLD2/FAM35A co-operates with REV7 to coordinate DNA double-strand break repair pathway choice 73

3.1 Preface to the manuscript 74

3.2 Abstract 78

3.3 Introduction ... *79*

3.4 Results ... *81*

3.4.1 Mapping of REV7 proximal/interacting partners relevant for DNA repair pathway choice ... 81

3.4.2 SHLD2 promotes DSB repair in human cells ... 82

3.4.3 SHLD2 is recruited to DSBs through its N-terminal domain ... 83

3.4.4 SHLD2 associates with REV7 to promote NHEJ and limit HR ... 85

3.4.5 SHLD2 associates with SHLD1 to promote NHEJ ... 86

3.4.6 SHLD2 levels correlate with a poorer prognosis in a subset of breast cancer patients ... 88

3.5 Discussion ... *89*

3.6 Materials and Methods ... *91*

3.7 References ... *127*

Chapter 4: Discussion and Future Directions ... **133**

4.1 The MPC in MM biology and BTZ treatment ... *133*

4.2 The role of DNA repair and the Shieldin complex in MM biology. ... *140*

References ... **146**

List of Figures

Figure 1.1 Multiple Myeloma Development 8
Figure 1.2 Revised international staging system (R-ISS) for multiple myeloma 10
Figure 1.3 Multiple Myeloma Treatment Options 14
Figure 1.4 Genomic instability and DNA repair in MM 22
Figure 1.5 Biological consequences of BTZ treatment in MM 24
Figure 1.6 Mitochondrial Metabolism Overview 29

Figure 2.1 CRISPR screening identifies MPC1 as a modulator of BTZ response in MM cells. 54
Figure 2.2 Targeting the MPC complex exacerbates BTZ-induced apoptosis of MM cells. 56
Figure 2.3 The MPC complex is required for bioenergetic capacity of MM cells. 58
Figure 2.4 Lack of mitochondrial pyruvate import alters glutamine metabolism and BTZ-driven proteasomal inhibition in MM cells. 60
Figure 2.5 Pyruvate metabolism has prognostic potential for MM patients. 62

Supplemental Figure 2.1 CRISPR-based genome-wide screen analysis of BTZ-treated MM cells. 63
Supplemental Figure 2.2 Characterization of MPC1-deficient MM cells. 64
Supplemental Figure 2.3 Impact of MPC1 depletion on ECAR and OCR. 66
Supplemental Figure 2.4 Loss of MPC1 alters glutaminolysis. 67
Supplemental Figure 2.5 Pyruvate metabolism expression in MM development 68

Figure 3.1 The Shieldin complex is a prognostic mark of bortezomib treatment efficacy in MM patients. 76
Figure 3.2 Identification of novel REV7 interactors relevant for the NHEJ pathway. 104
Figure 3.3 SHLD2 plays a critical in DNA repair. 106
Figure 3.4 SHLD2 is recruited and accumulates at DNA damage sites. 108
Figure 3.5 SHLD2 is an effector of REV7 in promoting NHEJ and antagonizing HR. 110
Figure 3.6 SHLD1 cooperates with SHLD2 and REV7 to promote NHEJ and restrict HR. 112
Figure 3.7 SHLD2 levels are candidate marker for the prognosis of subset of breast cancer. 114

Supplemental Figure 3.1 Analysis of REV7 interactome. 115
Supplemental Figure 3.2 Evaluation of the impact of SHLD2 on DNA repair. 117
Supplemental Figure 3.3 Structure-Function analysis of SHLD2. 119
Supplemental Figure 3.4 Characterization of the role of SHLD2 in the NHEJ pathway. 121
Supplemental Figure 3.5 Characterization of the role of SHLD2 in the HR pathway. 123
Supplemental Figure 3.6 Identification of SHLD2 interactome. 125

Abstract

Multiple myeloma (MM) is one of the most common hematological malignancies in the western world, with an incidence rate that has increased over the last 20 years by 126%. Despite significant advancements in therapeutic options, MM remains an incurable disease with the vast majority of patients relapsing due to genetic alterations and clonal evolution. CRISPR functional genomics is a powerful tool that allows for the identification of novel genetic vulnerabilities in different disease models including hematological malignancies. Using this technology, the goal my doctoral studies was to gain a better understanding of MM pathobiology by identifying both essential and synthetic lethality genes influencing proteasome inhibitor toxicity (e.g. Bortezomib; BTZ) in MM cell lines. Using CRISPR-Cas9 genome-wide screening, I identified several novel genetic targets that when disrupted, sensitize cells to BTZ treatment. These include MPC1, a subunit of the mitochondrial pyruvate carrier (MPC), and SHLD1, a component of the Shieldin complex. Both complexes had unknown roles in MM biology and warranted further investigation. First, I focused my attention on characterizing the role of the role of the MPC in MM cell lines through genetic manipulation and pharmacological inhibition (UK5099). Interestingly, I showed that both UK5099 treatment and CRISPR-mediated knockout of MPC1 in MM cells enhances the toxicity of proteasome inhibitors *in vitro*. Bioenergetic profiling of MM cells indicated that disruption of the MPC leads to limited bioenergetic capacity driven by a reduced maximal respiration capacity in the electron transport chain. In-depth metabolomics analysis identified imbalances in key sources of energy upon inhibition of the MPC in MM cells, including reduced citric acid cycle intermediates and intracellular glutamine and glutathione concentrations along with increased concentrations of pyruvate and lactate, and glucose consumption, suggesting a metabolic rewiring towards a glycolytic state. Importantly, RNA expression analysis identified MPC2 alongside other metabolic-related genes (e.g. LDHA, LDHB, CS, ACO2) as a strong predictors of MM patient overall survival. Subsequently, I investigated the relevance of the previously unknown factor SHLD1, previously annotated as C20orf196 and RINN1, in MM cells. My CRISPR-based functional genomics approach identified SHLD1 as one of the top sensitizers to BTZ *in vitro*. Interestingly, SHLD1 expression strongly predicts the overall survival of MM patients, suggesting a key role in the pathobiology of MM. Both mass spectrometry and a CRISPR-based approaches showed that SHLD1 is part of a multi-protein complex including SHLD2 and the adaptor protein REV7 that play a critical role

in the repair of DNA double-strand breaks by the non-homologous end-joining (NHEJ) pathway. SHLD1 and SHLD2 depletion impairs NHEJ-mediated DNA repair and compromises antibody diversification by class switch recombination in B cells. In fact, SHLD1 and SHLD2 accumulate at DSBs in a 53BP1, RIF1, and REV7-dependent manner and antagonizes homologous recombination by limiting DNA end resection. CRISPR-based functional genomics allowed me to identify two new complexes that influence MM cell response to BTZ *in vitro*: the mitochondrial pyruvate carrier and the Shieldin complex. These are two novel complexes that are part of the metabolic and DNA repair biological pathways that have been previously shown to influence MM therapy. My data indicates that disruption of the MPC leads to mitochondrial dysfunction and reduced bioenergetic capacity, thereby increasing proteasome inhibitor toxicity in MM cells. Additionally, my systematic screening suggests a key role of the Shieldin complex in the response to BTZ treated MM cells, by controlling the decision-making process during DSB repair. Altogether, my thesis positions the MPC and the Shieldin complex as novel biomarkers and potential therapeutic targets for the treatment of MM patients.

Résumé

Le myélome multiple (MM) est l'une des hémopathies malignes les plus courantes dans le monde, avec un taux d'incidence qui a augmenté 126 % au cours des 20 dernières années. Malgré des avancées dans les options thérapeutiques, la grande majorité des patients rechutant en raison d'altérations génétiques et d'une évolution clonale. La technologie CRISPR est un outil puissant qui permet l'identification de nouvelles vulnérabilités génétiques dans les hémopathies malignes. En utilisant cette technologie, l'objectif de mes études doctorales était de mieux comprendre la pathobiologie du MM en identifiant les gènes de létalité essentiels et synthétiques associés aux inhibiteurs du protéasome (par exemple, Bortezomib ; BTZ) dans les lignées cellulaires de MM. À l'aide du dépistage pangénomique CRISPR-Cas9, j'ai identifié plusieurs nouvelles cibles génétiques qui, sensibilisent les cellules au traitement BTZ. Ceux-ci incluent MPC1, une sous-unité du transporteur de pyruvate mitochondrial (MPC), et SHLD1, un composant du complexe Shieldin. Les deux complexes avaient des rôles inconnus dans la biologie du MM et justifiaient une enquête plus approfondie.

Tout d'abord, j'ai concentré sur la caractérisation du MPC dans les cellulaires MM par manipulation génétique et inhibition pharmacologique (UK5099). J'ai montré que le traitement par UK5099 ou l'inactivation médiée par CRISPR de MPC1 dans les cellules MM améliore la toxicité des inhibiteurs du protéasome *en vitro*. Le profilage bioénergétique des cellules MM a indiqué que la perturbation du MPC conduit à une flexibilité d'approvisionnement énergétique limitée en raison d'une capacité respiratoire maximale réduite dans la chaîne de transport d'électrons. Des analyses métabolomiques approfondies ont identifié des déséquilibres dans les principales sources d'énergie lors de l'inhibition du MPC dans les cellules MM. J’ai montré une réduction des intermédiaires du cycle de l'acide citrique, une réduction des concentrations intracellulaires de glutamine, et une augmentation des concentrations de pyruvate, lactate, et la consommation de glucose. Il est important de noter que l'analyse de l'expression de l'ARN a identifié MPC2 aux côtés d'autres gènes liés au métabolisme (par exemple, LDHA, LDHB, CS, ACO2) comme de puissants prédicteurs de la survie globale des patients atteints de MM.

Par la suite, j'ai étudié la pertinence du facteur auparavant inconnu SHLD1, précédemment annoté comme C20orf196 et RINN1, dans les cellules MM. Mon approche de génomique fonctionnelle basée sur CRISPR a identifié ce gène comme l'un des principaux sensibilisateurs au BTZ *en vitro*. Fait intéressant, l'expression de SHLD1 prédit fortement la survie globale des

patients atteints de MM, suggérant un rôle clé dans la pathobiologie du MM. La spectrométrie de masse a montré que SHLD1 fait partie d'un complexe multi-protéique comprenant SHLD2 et la protéine adaptatrice REV7 qui jouent un rôle essentiel dans la réparation des cassures double brin de l'ADN par le non-homologue de jonction terminale (NHEJ). En fait, SHLD1 et SHLD2 s'accumulent au niveau des DSB de manière dépendante de 53BP1, RIF1 et REV7, antagoniste de la recombinaison homologue en limitant la résection de l'extrémité de l'ADN.

La génomique fonctionnelle basée sur CRISPR m'a permis d'identifier le porteur mitochondrial du pyruvate et le complexe Shieldin comme complexes influencent la réponse des cellules MM au BTZ *en vitro*. Mes données indiquent que la perturbation du MPC entraîne un dysfonctionnement mitochondrial et une réduction de la flexibilité énergétique, augmentant ainsi la toxicité des inhibiteurs du protéasome dans les cellules MM. De plus, le complexe Shieldin contrôlant le processus de prise de décision lors de la réparation du DSB et augment la toxicité de BTZ. Ma thèse positionne le MPC et le complexe Shieldin comme de nouveaux biomarqueurs et des cibles thérapeutiques potentielles pour le traitement des patients atteints de MM.

Contents of Manuscript

This is a manuscript-based thesis consisting of one published research article and one research article under peer-review.

Chapter 2

Findlay, S., Cajelot, A., Kaiser, Z., Aryanpour, Z., Heath, J., St-Louis, C., Papadopoli, D., St-Pierre, J., Toposirovic, I., Sebag, M., Hulea, L,. Orthwein, A. (2022). The mitochondrial pyruvate carrier complex modulates the response to proteasome inhibitors in multiple myeloma (Under revision at Blood Advances November 2022).

Chapter 3

Findlay, S.*, Heath, J.*, Luo, V. M., Malina, A., Morin, T., Coulombe, Y., Djerir, B., Li, Z., Samiei, A., Simo-Cheyou, E., Karam, M., Bagci, H., Rahat, D., Grapton, D., Lavoie, E. G., Dove, C., Khaled, H., Kuasne, H., Mann, K. K., Klein, K. O., … Orthwein, A. (2018). SHLD2/FAM35A co-operates with REV7 to coordinate DNA double-strand break repair pathway choice. *The EMBO journal*, *37*(18), e100158. https://doi.org/10.15252/embj.2018100158

* Co-authorship

Publications that include work performed by Steven Findlay but not included in this dissertation:

Heath, J., Cheyou, E. S., Findlay, S., Luo, V. M., Carpio, E. P., Lee, J., Djerir, B., Chen, X., Morin, T., Lebeau, B., Karam, M., Bagci, H., Grapton, D., Ursini-Siegel, J., Côté, J. F., Witcher, M., Richard, S., Maréchal, A., & Orthwein, A. (2022). POGZ promotes homology-directed DNA repair in an HP1-dependent manner. *EMBO reports*, *23*(1), e51041. https://doi.org/10.15252/embr.202051041

Sherill-Rofe, D., Rahat, D., Findlay, S., Mellul, A., Guberman, I., Braun, M., Bloch, I., Lalezari, A., Samiei, A., Sadreyev, R., Goldberg, M., Orthwein, A., Zick, A., & Tabach, Y. (2019). Mapping global and local coevolution across 600 species to identify novel homologous

recombination repair genes. *Genome research*, *29*(3), 439–448. https://doi.org/10.1101/gr.241414.118

Sherill-Rofe, D.*, Raban, O.*, Findlay, S.*, Rahat, D., Unterman, I., Samiei, A., Yasmeen, A., Kaiser, Z., Kuasne, H., Park, M., Foulkes, W. D., Bloch, I., Zick, A., Gotlieb, W. H., Tabach, Y., & Orthwein, A. (2022). Multi-omics data integration analysis identifies the spliceosome as a key regulator of DNA double-strand break repair. *NAR cancer*, *4*(2), zcac013. https://doi.org/10.1093/narcan/zcac013

* Co-authorship

Contributions of authors

Chapter 1: Introduction

SF wrote the complete chapter under the guidance and editorial supervision of AO.

Chapter 2: The mitochondrial pyruvate carrier complex modulates the response to proteasome inhibitors in multiple myeloma

Chapter 2 contains scientific material that is included in a manuscript that is currently submitted to Blood Advances as an original research article. Conception and design of the work was done by SF and AO. Most of the experiments in this study were designed, executed and analyzed by SF under the supervision of AO. Liquid chromatography- mass spectrometry was performed and analyzed by the Metabolomics Innovation Resource (MIR) at McGill University. The composition of the manuscript and design of experimental figures were done under the supervision of AO.

Chapter 3: SHLD2/FAM35A co-operates with REV7 to coordinate DNA double-strand break repair pathway choice.

Chapter 3 was published as an original research article. SF and JH designed, performed and analyzed the data of most of the experiments presented in this manuscript. VML designed and performed the CSR experiments and analyzed the data. AMal designed, performed the CRISPR/Cas9-based genome-wide screen and the clonogenic experiments, and analyzed the data. TM and BD performed the laser stripe micro-irradiation, and AMar designed the experiments and analyzed the data. YC purified recombinant SHLD2 and performed the *in vitro* DNA-binding assays under the supervision of J-YM. ZL generated most of the constructs used in this manuscript, designed, and performed the ChIP experiments, and analyzed the data. AS designed and performed the comet assay experiments and analyzed the data. ES-C, HB, DG, CD and HKh, and EGL performed the MS experiments and analyzed the data under the supervision of J-FC. MK performed the initial characterization of SHDL2 in the FokI system. DR performed the phylogenetic analysis profiling under the supervision of YT. KKM performed

the pathway analysis of SHLD2. HKu and KOK performed the RNA-seq analysis and the patient cohort analysis under the supervision of CMG. MP provided the RNA-seq data and the related patient outcome of the TNBC cohort. AO conceived the study, designed the research, provided supervision, and wrote the manuscript with input from all the other authors.

Chapter 4: Discussion

SF wrote the complete chapter under the guidance and editorial supervision of AO.

Original contributions to knowledge

Chapter 2:

- Identified the Shieldin complex as an effector of the 53BP1-RIF1-REV7 axis in NHEJ mediated repair.
- Shieldin complex is composed of SHLD1 and SHLD2 and interacts with REV7 independent of DNA damage.
- Shieldin complex recruitment to sites of damage is dependent on 53BP1, RIF1 and REV7.
- Shieldin complex is critical for antibody diversification, NHEJ repair and limiting DNA end resection.
- Identified components of the Shieldin complex (SHLD1 and SHLD2) as prognostic factors in MM patient survival

Chapter 3:

- Successfully completed two complex genome-wide CRISPR Cas9 screens in multiple myeloma cell lines (U266 and JJN3) under bortezomib treatment.
- Identified MPC1 as a genetic vulnerability that increased sensitivity to bortezomib resulting in apoptosis.
- First to describe how disruption of the mitochondria pyruvate carrier in multiple myeloma cells leads to a reduced bioenergetic capacity and metabolic reprogramming favoring glycolysis and glutamine utilization in multiple myeloma cells.
- Identified pyruvate metabolism as a prognostic marker for MM patient outcome.

Acknowledgements

I would like to begin by thanking Dr. Alexandre Orthwein, who provided the resources, and supervision of each component of this thesis. When I began my graduate research at McGill, Alex was kind enough to provide me with the opportunity to learn and grow as a scientist and at the LDI. I would also like to thank the members of my thesis advisory committee, Dr. Sidong Huang, Dr. Josie Ursini-Siegel, Dr. François Mercier and Dr. Laura Hulea for their support, comments and invaluable expertise that they provided throughout my thesis.

To the members of my lab and colleagues of the LDI, without you this thesis would not be possible. In order to accomplish your goals and succeed in your PhD you require an incredible support system. Throughout all the adversity of my degree, my fellow lab members (Joey Heath, Vincent Luo, Edgar and others.) have supported me and made this experience all the more rewarding. Specifically, Joey who would spend hours with me bouncing scientific ideas and rationale back and forth.

Saving the best for last, I would like to thank my friends and family, Mom, Dad, Jackie and Marc for their unwavering support and love that they have provided through all these years. Never once did they question my graduate studies and consistently provided me with the will to push through some of the most difficult times of my degree. Jackie, you were there through the highs and lows of my PhD and always knew what to say to keep me pushing forward.

Onto the next challenge and pursuit!

List of Abbreviations

Abbreviation	Definition
53BP1	DNA damage response protein p53 binding protein
AID	Activation induced deaminase
AMPK	AMP activated protein kinase
ASCT	Autologous stem cell transplantation
ATM	Ataxia-telangiectasia-mutated
ATP	Adenosine triphosphate
ATR	Ataxia telangiectasia and rad3 related
BCMA	B-cell maturation antigen
BER	Base excision repair
BM	Bone marrow
BTZ	Bortezomib
CFZ	Carfilzomib
CNA	Copy number alterations
CRISPR	Clustered regularly interspaced short palindromic repeats
CSR	Class switch recombination
DDR	DNA damage response
DNA-PKcs	DNA-dependent protein kinase catalytic subunit
DSB	Double strand break
dsDNA	Double strand DNA
ECAR	Extracellular acidification rate
ECM	Extracellular matrix
ETC	Electron transport chain
FISH	Fluorescent in situ hybridization
GC	Germinal center
GSH	Glutathione
HD	Hyperdiploid disease
HIF	Hypoxia inducible factor
HR	Homologous recombination
ICL	Interstrand crosslink

IMiD	Immunomodulatory drugs
IMM	Inner mitochondrial membrane
IR	Ionizing radiation
ISS	International staging system
IWMG	International myeloma working group
LDHA	Lactate dehydrogenase A
LLPC	Long lived plasma cell
M-Protein	Monoclonal protein
MCT	Monocarboxylate transporters
MDC1	Mediator of DNA damage checkpoint 1
MDE	Myeloma defining events
MDSC	Myeloid derived suppressor cells
MGUS	Monoclonal gammopathy of undetermined significance
MM	Multiple myeloma
MMR	Mismatch repair
MMRF	Multiple myeloma research foundation
MP(T)	Melphalan-prednisone-(thalidomide)
MPC	Mitochondrial pyruvate carrier
MRI	Magnetic resonance imaging
MRN	MRE11/RAD50/NBS1
NCS	Neocarzinostatin
NER	Nucleotide excision repair
NGS	Next generation sequencing
NHD	Non-hyperdiploid disease
NHEJ	Non-homologous end joining
NMD	Nonsense mediated decay
NRF1	Nuclear respiratory factor 1
OCR	Oxygen consumption rate
OMM	Outer mitochondrial membrane
OXPHOS	Oxidative phosphorylation
PC	Plasma cell

PCL	Plasma cell leukemia
PDH	Pyruvate dehydrogenase
PGC1α	Peroxisome proliferator-activated receptor coactivator 1α
PI	Proteasome inhibitor
PIKK	Phosphatidylinositol-3 kinase-related kinases
PPP	Pentose phosphate pathway
RAP80	Receptor associated protein 80
RIF1	Replication timing regulatory factor
RNAi	RNA interference
ROS	Reactive oxygen species
RPA	Replication protein A
SHM	Somatic hypermutation
SLPC	Short lived plasma cell
SMM	Smoldering multiple myeloma
SNP	Single nucleotide polymorphisms
SPR	Spare respiratory capacity
SSA	Single strand annealing
SSB	Single strand break
ssDNA	Single strand DNA
TCA	Tricarboxylic acid cycle/ Citric acid cycle
TLS	Translesion synthesis
UPR	Unfolded protein response
VCd	Bortezomib, cyclophosphamide, dexamethasone
VDAC	Voltage dependent anion channels
VEGF	Vascular endothelial growth factor
VRd	Bortezomib, lenalidomide, dexamethasone
VTD	Bortezomib, thalidomide, dexamethasone
XRCC4	X-ray repair-cross complementing protein

Chapter 1: General Introduction

1.1 Multiple myeloma epidemiology

Multiple Myeloma (MM) is a fatal hematological malignancy characterized by the uncontrolled expansion of mutated plasma B-cells (PC) within the bone marrow (BM). MM is the second most common hematological malignancy behind Non-Hodgkin's lymphoma and accounts for 1% of all cancers[1, 2]. In 2019, MM had a global incidence of 155,688 cases per year and was responsible for 13,474 deaths annually[3]. Since 1990, MM incidence has increased by 126%, attributable to population growth (40.4%) and aging of the general population (52.9%)[4]. Geographically, North America, Australasian and western European populations present with the highest incidence and death rates. Meanwhile Asia, Oceania and Sub-Saharan Africa are some regions among the lowest MM incidences[4]. In Canada, there are a reported 3800 new cases and 1600 new deaths annually[5]. Paradoxically, the incidence of MM in the African American population is twice that of the European American population in the USA [3, 6]. Various explanations have been proposed to understand the variability in MM incidence including socioeconomic status[7], treatment availability, diagnosis technology and aging populations, age gender and body mass [3]. Genetically, t[11;14], t[14,16] and t[14,20] translocations occur more frequently in African American populations[8, 9]. Justifiably, recent emphasis has been placed on ensuring equal racial and ethnic representation in clinical trials. From 2006 to 2019, 19 global clinical trials comprising over 10,000 patients of which 84% were Caucasian [10]. One ongoing clinical trial or project that can begin to investigate racial and ethnic considerations in MM is the "Stand Up 2 Cancer Multiple Myeloma Dream Team". Investigating early detection of precursor myeloma conditions in high risk populations via blood samples collected from approximately 50,000 volunteers, this group hopes to identify molecular and immune factors that could lead to disease progression. Such a large cohort of participants ensures that targeted population analysis should have a large enough sample size to ensure robust statistical analysis to gain a clearer understanding of how ethnicity influences MM development.

The median age of diagnosis for MM patients 66-70 years old with only 37% of the patients being under the age of 65 years old and 93.1% of patients above the age of 50 years old at diagnosis[3, 11]. Based on the progressive increase in incidence, deaths and age of diagnosis, there is a necessity for increased research into MM biomarkers, risk factors and treatment options to help address the ever-growing burden on the healthcare system[12].

1.2 Pathophysiology and MM development

Throughout MM disease development and progression, the monoclonal disease acquires various chromosomal aberrations and mutations leading to disease heterogeneity and subclonal populations[13]. This heterogeneity is amplified as the disease progresses from monoclonal gammopathy of undetermined significance (MGUS) to smoldering multiple myeloma (SMM) to symptomatic myeloma (MM)[14] (Figure 1.1). Each stage of progression is associated with numerous physiological changes, including BM infiltration and osteolytic bone lesions.

1.2.1 Plasma cell development

Antibody producing PCs are the cell of origin that gives rise to MM, and play an important role in humoral immunity. PCs are a differentiated stage of B-cells that have gone through the germinal center (GC) reaction, a process that diversifies antibodies/immunoglobulins by class switch recombination and somatic hypermutation[15]. B-cells are then terminally differentiated into short lived plasmablasts, memory B-cells and long-lived PCs (LLPCs)[16]. Differentiation of B-cells into antibody producing PCs is associated with profound changes in morphology and cellular homeostasis to support high rates of antibody production[16]. IRF4, BLIMP1 and XBP1 are transcription factors that favor the differentiation to antibody secreting cells and have been shown to be involved in MM development. IRF4 represses BCL6 and activates BLIMP1, with BLIMP1 regulating components of the unfolded protein response (UPR) via XBP1 and ATF6. Control of the UPR allows cells to acquire the capacity to sustain high levels of antibody secretion[17-19]. LLPCs traffic and reside in the BM to provide sustained antibody production for decades. Their long-lived nature is dependent on their ability to access their protective niche in the BM, secondary lymphoid organs, and mucosa. Gut-associated lymphoid tissue PCs primarily produce IgA while BM PCs produce IgG, IgA and IgM, although IgG is the predominant isotype[20-22]. Upon activation, LLPCs rely on fatty acid utilization and mitochondrial oxidation to sustain metabolic requirements for proliferation and antibody production[23]. LLPCs have also upregulated the glucose transporter, GLUT1, to glycosylate antibodies[24]. The current model of MM initiation stipulates that the developing PCs must acquire multiple genetic alterations (hits) to transform from a normal functioning PC to a malignant MM cell. The dysregulation of regulatory survival

mechanisms and the favorable microenvironment in the BM allows MM, the long-lived PC neoplasm, to persist.

1.2.2 Cytogenetics of multiple myeloma

MM heterogeneity has been well documented both in a single patient throughout MM progression, and between different MM patients. Such variability between patients influences disease progression and treatment outcomes[25]. Historically, MM was thought to have randomly distributed driver mutations that lead to the development of the disease, however recent MM cytogenetics can temporally track clonal expansion and identify two sequential oncogenic events that accumulate to produce a heterogenous disease[26, 27]. By looking at common cytogenetic abnormalities shared amongst MGUS and MM patients, it is clear that there are primary oncogenic events that persist throughout disease progression and more numerous secondary oncogenic events that lead to clonal heterogeneity in later stages of MM[28] (Figure 1.1). To improve patient stratification and risk assessment, certain chromosomal abnormalities and single nucleotide polymorphisms (SNPs) were incorporated by the international myeloma working group (IMWG) into staging systems such as the international staging system (ISS) and the revised version (R-ISS) of MM[29].

1.2.2.1 Primary oncogenic events

Primary oncogenic events lead to the pathogenic development of MM from post-germinal center B-cells and they can be broadly divided into two groups: i) non-hyperdiploid disease (NHD); and ii) hyperdiploid disease (HD). NHD is characterized by chromosomal translocations at 14q32 including t(4;14), t(14;16), t(11;14) and t(14;20) which involve the immunoglobulin heavy chain (IgH) genes. Translocations involving the IgH locus (14q32) or one of the IgL loci are present in at least half of MM cases. These translocations usually result in the dysregulated expression of an oncogene that is juxtaposed to strong Ig enhancers, such as FGFR3 and MMSET[30, 31]. It has long been hypothesized that these translocations are the result from errors during the physiological process of CSR since the breakpoints are usually located near or within IgH switch regions. The most dysregulated oncogenes include CYCLIND (40%)[32], MAF (8%)[33] and MMSET/FGFR3 (15%)[30] with these translocation groups being mutually

exclusive. NHD is also associated with an increased likelihood of disease progression, aggressiveness, and a poorer overall prognosis. On the other hand, HD is characterized by trisomy of odd numbered chromosomes 3, 5, 7, 9, 11, 15, 19, 21[34-37]. The ploidy status is stable over time in MM patients and HD MM patients have a better prognosis, and account for 40-50% of all MM cases[28, 34, 38]. Only 15% of MM patients present with both trisomy and IgH translocations, with 85% of patients either diagnosed with HD or NHD MM exclusively[39]. Patients with the highest risk of progression have t(14;16), t(14;20) and del(17p) which affect MAF, MAFB and TP53 respectively[40]. Intermediate risk patients have t(4;14) and gain of chromosome 1q21 which impacts CCND3 and CSK1B which influence cell cycle functions[41, 42]. Despite the heterogeneity, the primary chromosome translocations and ploidy status continue to mark the tumor clone throughout disease progression.

1.2.2.2 Secondary oncogenic events

Throughout disease progression, secondary alterations increase the disease heterogeneity of the monoclonal PC population. The most frequent mutations in MM patients KRAS (23%), NRAS (20%), FAM46C (11%), TP53 (8%) and DIS3 (11%)[43] as well as other notable mutations including BRAF, XBP1, IRF4, PRDM1 and RB1 at lower frequencies. These mutations are hypothesized to occur via cytosine deamination (AID)[44], kataegis (localized hypermutation)[45] and APOBEC (somatic mutagenesis pathway)[46] (Figure 1.1). Interestingly, these mutations do not cluster with a particular biological pathway, rather they influence several cellular signaling pathways highlighting the extent of MM patient genetic diversity. To confound this complexity, different biopsy sites within the same patient revealed different genetic mutations[47]. These genetic mutations are associated with the longevity of MM cells as subclonal development of the disease increases the likelihood of cellular survival, persistence, and limit the efficacy of therapeutic drugs[26, 48]. Upon relapse, the frequency of subclonal populations will shift to favor the resistant clone to escape treatment related toxicity and therapeutic selection drives the clonal evolution of the disease[48]. Apart from mutational status, epigenetic modifications are also known to play a role in MM clonal heterogeneity. DNA methylation is known to play a critical role in controlling nuclear architecture and gene expression[49]. In MM patients, targeted loci including tumor suppressor genes are hypermethylated resulting in epigenetic inhibition[50]. Furthermore, expression of DNA

methyltransferase 1 (DNMT1)[51], enhancer of zeste homolog 2 (EZH2) [52], multiple myeloma SET domain (MMSET)[53] have all been reported to be highly expressed in MM patients compared to healthy controls and are associated with a worse overall prognosis. Due to this research DNA methyltransferase inhibitors (DNMTi) are being tested in clinical trials to ascertain it's therapeutic potential in MM[54].

1.2.3 Monoclonal gammopathy of undetermined significance (MGUS)

MGUS represents the earliest stage of MM development. Approximately 3% of the adult population over the age of 50 are expected to have MGUS, but diagnosis is quite complex due to the absence of symptoms and lack of standardized screening procedures[55]. Largely undiagnosed, MGUS is a condition characterized by abnormal changes of PCs in the BM, leading to the release of abnormal monoclonal protein (M-protein) into the blood[56]. One of the only ways to diagnose the asymptomatic disease is through blood tests resulting in abnormal concentrations of serum monoclonal proteins. Although considered to be a benign condition with no recognizable symptoms, it represents the first indication of abnormal PC biology that increases the susceptibility of a patient to develop various hematological malignancies, such as MM, light chain amyloidosis, waldenstrom macroglobulinemia, and lymphoma. Despite these challenges, the IMWG has outlined clinically relevant procedures and criteria to diagnose MGUS. Any patient with a serum monoclonal protein concentration of <30g/L, clonal bone marrow plasma cells <10%, and absence of any end organ damage is diagnosed with MGUS[57]. Despite the apparent asymptomatic nature of MGUS patients, recent evidence suggests that these patients have an increased risk of bone fractures, which could serve as a prognostic metric for the progression and development of symptomatic MM[58]. Additional progression risk factors include, increased serum M-protein, type of M protein (IgG, IgM, IgA)[59], percentage of clonal PCs in the bone marrow[60] and the presence of circulating PCs[61]. Each year, 1-2% of MGUS patients progress to SMM and symptomatic MM. Historically, 82% of MM patients have been previously diagnosed with MGUS within 8 years of developing symptomatic MM[62]. Since MGUS is currently labelled as an asymptomatic diagnosis, the treatment recommendation is increased monitoring for disease progression. That being said, there has been increased research focusing on early detection of clonal subpopulations that are associated with increased risk of progression which may require

earlier treatment intervention[63]. New research in the characterization of MGUS includes cellular organization (3D telomeric and centrosome organization)[64], DNA biomarkers ($MYD88^{L265P}$)[65], RNA biomarkers (miRNA signature)[66], MALDI-TOF MS assays for detection and monitoring[67], and next generation sequencing for better investigations of the genetic landscape of individual patients.

1.2.4 Smoldering multiple myeloma (SMM)

SMM is the intermediate stage of MM progression prior to patients progressing to symptomatic MM. Like MGUS, SMM is also an asymptomatic clonal plasma cell disorder, however it has a much higher risk of progression to MM (10% per year)[68]. Based on IMWG recommendations, any patient with a M protein serum concentration of ≥3 g/dL and/or a clonal bone marrow PCs infiltration of 10%-60% is diagnosed with SMM[57]. Even though SMM patients present with characteristics of both MGUS and MM, they do not present with any end organ damage or myeloma defining events (MDEs)[57]. Due to disease heterogeneity and variable rates of progression, the typical age of SMM diagnosis is quite vast from ~50-70 years old. Interestingly, SMM patients who do not progress to MM within those first 5 years are considered to have stable MGUS disease with SMM clinical features again demonstrating the broad spectrum of myeloma diagnosis[69]. The standard of care for SMM is similar to MGUS with observation until the development of symptomatic MM as the therapeutic strategy. However, there are some caveats in the treatment paradigm. If patients are deemed at high risk of progression based on M-protein serum concentration and PC infiltration in the BM[68], even without end-organ damage, physicians can now initiate therapy and uses sensitive imaging (MRI and PET-CT) to assess the severity of the disease[70]. Various trials are now being evaluated to determine if there is increased therapeutic benefit to an earlier treatment of SMM patients as opposed to treatment upon disease progression[71].

1.2.5 Symptomatic multiple myeloma (MM)

The defining features of symptomatic multiple myeloma are the development of end organ damage or CRAB symptoms (Hypercalcemia, Renal failure, Anemia and Bone lesions)[72]. The

most striking symptom is bone lesions which are readily observable via PET-CT and MRI scans[70, 73]. The IMWG has now revised the MM diagnostic criteria to include any patients with >10% clonal plasma cells and at least one of three myeloma defining events (MDEs) with or without CRAB symptoms[57]. The MDEs include 60% or greater clonal plasma cells on bone marrow examination, serum involved/uninvolved free light chain ratio of 100, or greater and more than one focal lesion on MRI that is at least 5mm or greater. The 5-year survival of patients with MM is 54% and the majority of patients are diagnosed after the disease has spread to distant parts of the body including the spleen, spinal cord and cranial bones[5]. Once patients present with CRAB symptoms or MDEs, they are eligible to begin current standard of care immediately to treat the disease.

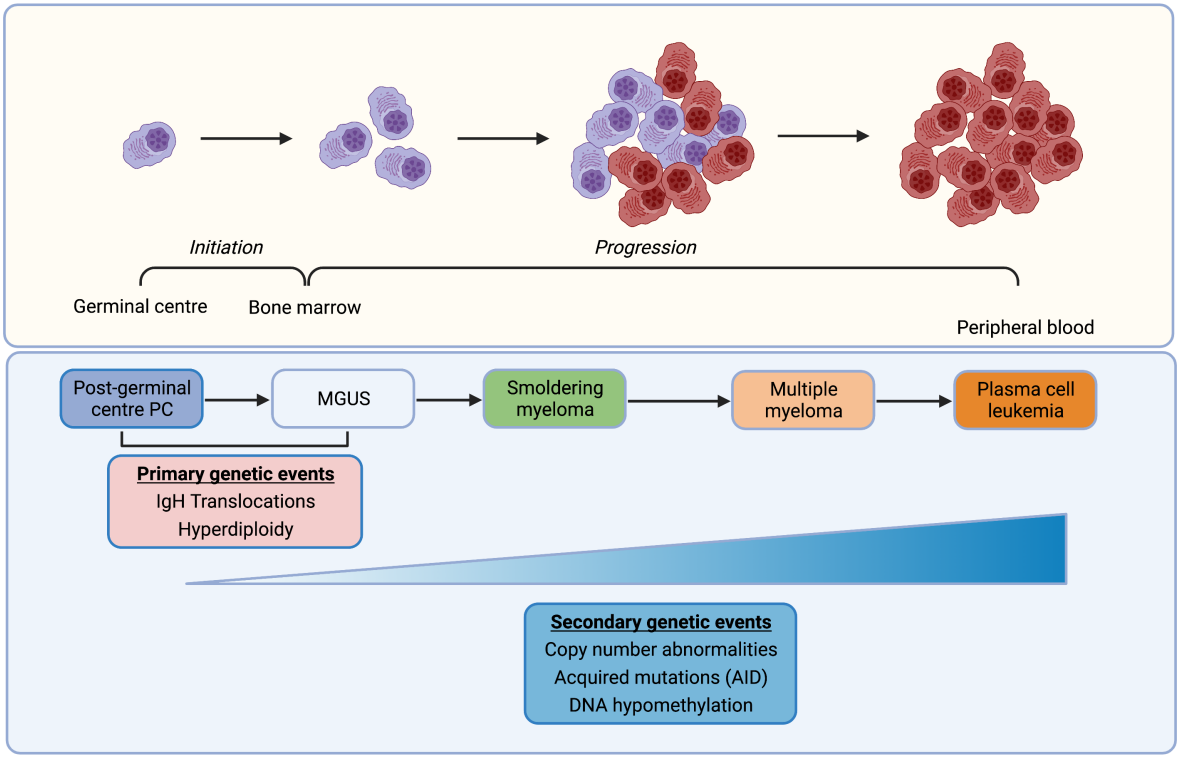

Figure 1.1 Multiple Myeloma Development

(Adapted from Kumar et al. *[Created via biorender]*)[74]

1.2.5.1 International staging system (ISS)

In 2005, the introduction of the ISS provided reliable guidelines for the classification and stratification of symptomatic MM patients on a global scale. The goal of the ISS is to address and mitigate the variability in outcome of MM patients. Using acquired knowledge of tumor and host prognostic factors, the staging system helps to better predict disease outcome by identifying risk groups and optimizing patient treatments based on known risk factors[75] (Figure 1.2). The ISS built upon a previous staging system introduced by Durie and Salmon (D/S) in 1975, which was heavily based on biological readouts of end organ damage in the serum (Ex: serum calcium and creatinine)[76]. Since the introduction of the D/S system, novel prognostic factors along with cytogenetics via fluorescent in situ hybridization (FISH) warranted an updated staging system. The ISS now includes the use of serum β2-microglogulin (a readout of renal function) and serum albumin caused by inflammatory cytokines (IL-6 and TNFα) in the microenvironment as easy clinically inexpensive prognostic factors[77] (Figure 1.2). More recently, the staging system was further updated to include more recent prognostic factors such as chromosomal aberrations and lactate dehydrogenase levels which has shown to correlate with a poor overall survival[78]. The revised ISS (R-ISS) was developed in parallel to other stratification metrics including the IMWG which recommended the addition of increased FISH analysis to the ISS in order to further stratify patients in the high risk (<2 year survival) and low risk (>10 year survival). The Mayo Clinic also designed its own stratification criteria used to adapt treatment approaches of MM patients based on risk. mSMART (Stratification for Myeloma and Risk-Adapted Therapy) guidelines were designed to combat the heterogeneity of MM patients. Using mSMART, researchers were able to show that MM can be subdivided into 6 myeloma types using genetic abnormalities, renal function, PC cell cycle rates and gene expression signatures[79]. New stratification models under current investigation include MASS (The Mayo Additive Staging System) which provides weight to prognostic factors and groups patients based on the number of risk factors rather than the bimodal R-ISS approach[80]. Furthermore, circulating tumor cells (CTCs) in peripheral blood has become an important readout of tumor progression and treatment response in numerous cancers including lung and breast cancer[81, 82]. Recent work in MM has shown that CTCs were detected in 92% of newly diagnosed MM patients and were associated with worse progression-free survival. Furthermore, when combined with the R-ISS, patient risk stratification was significantly improved based on minimal residual

disease status and progression-free survival[83]. It remains clear that the R-ISS and mSMART criteria have provided a strong foundation for patient stratification, however these systems require new clinical criteria such as CTCs and increased genetic risk factors in the MASS model to ameliorate stratification, improve the sensitivity of risk-adapted treatments, and improve patient outcomes.

Prognostic Factor	Criteria
ISS stage:	
I	Serum B2-microglobulin <3.5mg/L, serum albumin>= 3.5 g/dL
II	Not ISS stage I or III
III	Serum B2-microglobulin >= 5.5 mg/L
CA by iFISH	
High risk	Presence of del(17p) and/or translocation t(4;14), and/or t(14;16)
Standard risk	No high risk CA
LDH	
Normal	Serum LDH < normal upper limit (280-330 IU/L)
High	Serum LDH > normal upper limit (280-330 IU/L)
Revised-ISS stage	
I	ISS stage I and standard CA risk (iFISH) and normal LDH
II	Not revised ISS stage I or III
III	ISS stage III and either high risk CA (iFISH) or high LDH

Figure 1.2 Revised international staging system (R-ISS) for multiple myeloma

(Adapted from Palumbo et al.)[77]

1.3 Multiple myeloma bone marrow microenvironment

The BM microenvironment is well organized and composed of various cell types that can protect and support the growth of MM cells. These include osteoblasts, osteoclasts, BM endothelial cells, fibroblasts, and adipocytes. The BM niche aids in the growth and spreading of MM cells through a complex interplay of cytokines, chemokines, adhesion molecules, proteolytic enzymes, among other components of the ECM[84]. The BM microenvironment was

shown to confer survival and chemoresistance to current therapies and remains a critical determinant of MM patient survival[85].

1.3.1 Osteoblasts/osteoclasts

Focal bone lesions observed in MM patients are caused by a dysregulation of bone formation (osteoblasts) and bone resorption (osteoclasts) mechanisms[86, 87]. Under steady state conditions, osteoblasts line the bone surface producing mineralized bone osteoid at a similar rate to chemical induced bone resorption of osteoclasts. Osteoblasts line the bone surface and produce and mineralize bone osteoid as osteoclasts resorb bone. In healthy conditions, once activated, osteoblasts will mineralize and rebuild healthy bone matrices. In MM patients, bone homeostasis is disrupted by significant repression of osteoblast mediated bone growth and maintained activity of osteoclasts resulting in abnormal bone turnover[88]. The presence of lytic bone lesions manifests with severe bone pain, pathological fractures, and increased serum markers of bone resorption (hypercalcemia)[89].

In MM, osteoblast growth is significantly repressed resulting in unbalanced osteoclast bone resorption and abnormal bone turnover[88, 90]. Several mechanisms have been proposed to explain how osteoblasts influence tumor progression and drug resistance, the prevailing theory is through paracrine signaling. Osteoprotegerin is a soluble decoy receptor that binds RANKL and prevents the stimulation of osteoclast formation and bone resorption[91]. DKK1 a soluble extracellular antagonist of Wnt signaling has also demonstrated to inhibit bone formation in osteoblasts *in vitro* and is elevated in the peripheral blood of MM patients[92, 93].

Pathways influencing the homeostasis of the bone marrow microenvironment such as the RANK/RANKL, Wnt[94] and RUNX2[95] pathways will influence both osteoclasts and osteoblasts. However, additional pathways have been shown to primarily research osteoclast activity. VEGF[96], cell-cell interactions with MM cells[97, 98] and CD38 expression on MM cells[99]. Osteoclast activity resulting in the ongoing release of calcium, growth factors and ECM proteins enhance tumor growth and survival[100]. Osteoclasts can reactivate dormant MM cells by remodeling the endosteal niche, releasing MM cells from their physical and temporal hibernation[101]. Furthermore, osteoclasts have also been shown to protect MM cells from dexamethasone-induced apoptosis and support angiogenesis. Interestingly, BTZ treatment is

known to influence osteoblast/osteoclast homeostasis. BTZ increased markers in bone formation, alkaline phosphatase and osteocalcin[102], and a reduction in Dkk1 and RANKL[103]. Bisphosphonates are the most commonly used and effective treatment of myeloma bone disease. They are specific inhibitors of osteoclastic activity that reduce vertebral fractures and pain in MM patients[104]. This treatment is commonly used in conjunction with PIs or chemotherapies to limit bone destruction whilst targeting MM cells.

1.3.2 Hypoxic bone marrow

Hypoxia is an imbalance between oxygen (O_2) supply and O_2 consumption depriving cells or tissues of sufficient oxygen for respiration. The BM has long been accepted to be a naturally hypoxic organ, however there is an O_2 spatial distribution within the bone marrow that is heterogeneous[105, 106]. Depending on the location of the central vascular niche, certain portions of the BM are closer to oxygenated blood than others, creating a gradient of hypoxic niches. Decreases in oxygen levels are regulated via hypoxia inducible factors (HIFs). The HIFs are heterodimeric complexes composed of an inducible α-subunit (HIF-1α, HIF-2α or HIF-3α) and constitutively expressed β-subunit. Of the three HIF family members, HIF-1 and HIF-2 are the main regulators of oxygen homeostasis since their stability is dependent on O_2 levels[107]. In MM, exposure to high levels of hypoxia in the bone marrow microenvironment activates HIF-1 and HIF-2 to stimulate the production of angiogenic factors such as VEGF and bFGF[108]. Under oxygenated conditions, HIF-1α can interact with the von Hippel Lindau (VHL) complex resulting in ubiquitylation of HIF-1α and subsequent proteasome-dependent degradation[109]. In hypoxic conditions, the rate of asparagine and proline hydroxylation decreases and the rate of VHL binding and HIF-1α ubiquitylation causing an accumulation of HIF-1α. HIF-1α will then translocate into the nucleus, interact with HIF-1β and p300-CBP to activate transcription of target genes that respond to hypoxia. Building on this knowledge, targeting of the HIF-1α/p300 complex via chetomin, has antitumor activity on MM cells *in vitro*[110].

1.4 MM therapeutic options:

Standard-of-care for MM patients, in the early 2000s was almost exclusively composed of a chemotherapeutic coupled with autologous stem cell transplantation (ASCT), in the hope that the transplanted cells could reconstitute a normal PC physiology[111]. Problematically, a significant proportion of patients are diagnosed with MM above the age of 65, increasing the likelihood that patients are ineligible for ASCT and prone to experience adverse chemotherapy-related toxicity. Despite multiple myeloma incidence increasing since 1990[5], newly approved therapies over the last 20 years have substantially improved patient quality of life and survival rates[112, 113] (Figure 1.3). The overhaul of MM therapeutic options began in 2005, with the first FDA approved proteasome inhibitor Bortezomib (BTZ). From then, renewed scientific interest in MM treatment resulted in an inundation of new molecular biomarkers and drug targets[114, 115]. MM physicians are now equipped with an arsenal of treatments that can be used as first, second, third and even fourth lines of therapy either alone or in combination with other MM treatment options: proteasome inhibitors (PI; BTZ, Carfilzomib (CFZ), Ixazomib), immunomodulatory agents (IMiDs; Lenalidomide, Thalidomide, Pomalidomide)[71, 116, 117], chemotherapies (Melphalan, Doxorubicin)[118-120] and ASCT as well as new/upcoming single agent therapies including Bcl-2 inhibitors[121], XPO1 inhibition (Selinexor)[122], and CAR-T cell therapy of the B-cell maturation antigen (BCMA) and. CD-138[123](Figure 1.3). Despite the surge in the number of therapeutic alternatives that are offered to MM patients, relapse remains inevitable, highlighting the need for: *(i)* predictive biomarkers of PI efficacy; and *(ii)* novel therapeutic targets to improve MM patient survival.

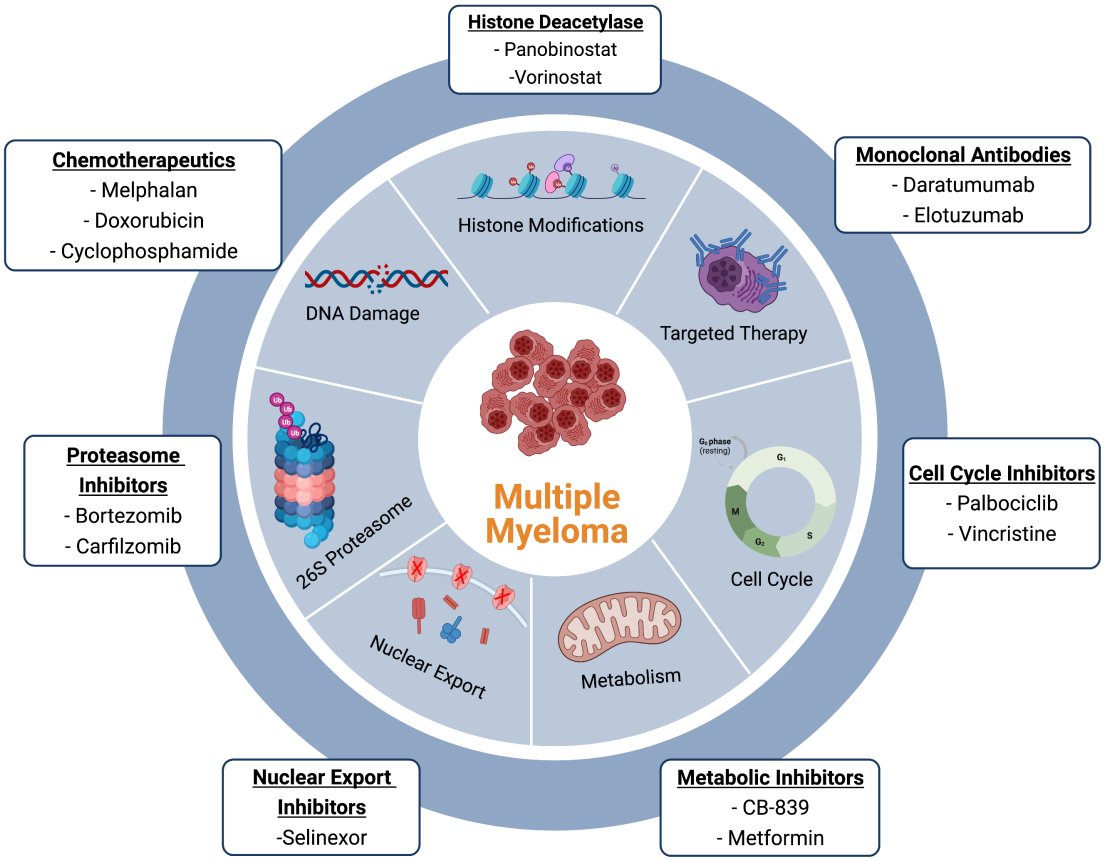

Figure 1.3 Multiple Myeloma Treatment Options

(Created with biorender)

1.4.1 Chemotherapy and DNA damage

The classical paradigm of MM treatment involved the use of chemotherapeutics to target and destroy rapidly dividing cancer cells. Common chemotherapeutics used in MM include: melphalan[118, 119]/ cyclophosphamide (intercalating agents)[124, 125], vincristine (anti-microtubule agent)[126] and doxorubicin (topoisomerase inhibitor)[120]. As of 1970, the combination of melphalan and prednisone became standard of care for elderly MM patients[127]. Unfortunately, in the years following this discovery, combinations of other novel alkylating agents failed to yield any significant results which stymied the research community. Additionally, chemotherapeutic options were not beneficial for asymptomatic or smoldering MM patients which validated the watch and wait paradigm that was initially adopted to treat MM patients. As of 2005, and the advent of BTZ, the IMWG now recommends MPT (Melphalan-

Prednisone-Thalidomide) as a therapeutic option for patients above the age of 65 and who are ineligible for ASCT[57]. Melphalan ASCT can be used in younger patients to reduce the toxicity of the ASCT procedure[119, 128]. While melphalan therapy still exists for MM patients, its usage has been limited with the advent of novel therapies. The combination of chemotherapy with ASCT has been shown to increase the PFS and OS of MM patients and can be used in cases of newly diagnosed, and relapse/refractory MM[129]. Apart from melphalan, doxorubicin has been shown that when combined with BTZ it improves the treatment of patients with refractory MM when compared to bortezomib alone[120, 130].

Vincristine inhibits microtubule formation in mitotic spindle preventing cell division and is inherently toxic to dividing cancer cells. Initially positioned as first line therapy in MM patients, vincristine in combination with doxorubicin and dexamethasone (VAD) resulted in an 84% response rate for 18 months[131]. Following improved therapies, the usage of VAD was relegated to induction therapy prior to ASCT. However, the VAD regimen was rapidly replaced by thalidomide and dexamethasone (thal-dex) which showed increased efficacy and comparable safety profiles[126].

Cyclophosphamide is an DNA alkylating agent that is cytotoxic by cross linking strands of DNA and RNA, as well as inhibit protein synthesis. Initially utilized in the treatment of newly diagnosed MM patients[132], its usage was then expanded to induction therapy for ASCT which yielded mixed results[133, 134]. Cyclophosphamide is now used as an additional component to PI based combination therapies both in newly diagnosed MM and relapsed/refractory MM[124, 125, 135].

1.4.2 DNA damage and genomic instability

Cells are constantly exposed to both exogenous and endogenous stressors that threaten the integrity of our genomic DNA sequence and cellular viability. While DNA mutations have played a critical role in evolution, it also plays a role in human pathologies such as cancer and aging. To ensure the transfer of accurate and undamaged DNA during cellular division, cells are equipped with protective mechanisms such as DNA repair, cell cycle checkpoints and cellular death pathways to minimize the consequences of DNA damage. The tens of thousands of DNA lesions experienced by the body each day can be broadly segregated into endogenous and exogenous DNA damage. Exogenous DNA damage occurs when environmental, chemical, and physical agents

damage the DNA. This includes natural damage from exposure to ultraviolet light all the way to DNA damaging agents used in oncology such as cisplatin, doxorubicin, and melphalan. On the other hand, endogenous damage occurs due to normal metabolic and cellular processes that constantly interfere with DNA integrity. Processes that produce such damage include DNA replication/synthesis[136, 137], activation induced deaminase (AID) activity during B-cell development[138] and reactive oxygen species (ROS)[139, 140]. To deal with the constant barrage of DNA damage, the DNA damage response (DDR) acts to remove and repair damaged DNA that threatens the survival of both normal and cancerous cells. Since unrepaired DNA damage is toxic to cancer cells, including MM, inhibition of these repair processes is critical to improving the efficacy of these chemotherapeutics.

1.4.2.1 DNA damage response

Upon DNA damage, lesion specific pathways are initiated to signal the presence of the damage and promote its subsequent repair. The DDR is a controlled process with factors regulated both spatially and temporally in concordance with chromatin remodelers that allow for access to the DNA damage[141]. The assembly of these factors around the sites of damage provides an umbrella of coverage that can effectively process and repair most DNA lesions. The most cytotoxic of DNA lesions is DNA double strand breaks (DSB) and thus DNA repair mechanisms must detect, signal their presence, and promote their repair. While there are many DNA repair processes that exist to repair different types of DNA damage (Base excision repair, nucleotide excision repair, mismatch repair, interstrand crosslinking repair), for the purpose of this thesis we will focus on the two major double strand break repair pathways homologous recombination (HR) and non-homologous end joining (NHEJ). The process of DNA repair broadly occurs via four main categories: DNA damage sensors, recruitment of mediators, transducers, and effectors. and cellular responses. In response to DSBs, cell signaling processes activate cell cycle checkpoints that inhibit the propagation of DNA damage until the DNA is repaired and this process begins with the recognition of DNA DSBs.

1.4.2.2 DSB recognition

Upon generation of a DSB, free DNA ends are recognized by the MRE11/RAD50/NBS1 (MRN) and KU70/KU80 complexes functioning as sensors of DSBs for HR and NHEJ

respectively[142-144]. Subsequent signaling of DSB recognition occurs via member of a family of kinases known as the phosphatidylinositol-3 kinase-related kinases (PIKK family). Ataxia-telangiectasia-mutated (ATM) and DNA-dependent protein kinase catalytic subunit (DNA-PKcs) as well as Ataxia telangiectasia and rad3 related (ATR) primarily functioning in the signaling of DSBs and single strand breaks (SSBs) respectively[145]. The MRN complex recruits ATM, while KU70/KU80 recruits DNA-PKcs to sites of DSBs. ATM is activated via autophosphorylation on serine 1981, 367 and 1893 and phosphorylates a histone H2A variant on its serine 139 residue (γ-H2A.X)[146]. DNA-PKcs bound to KU70/KU80 complex and ATR/ATRIP (ATR interacting protein) bound to RPA also phosphorylate serine 139 to generate (γ-H2A.X). MDC1 (Mediator Of DNA Damage Checkpoint 1) will then bind to γ-H2A.X, stabilize the MRN-ATM complex, and recruit the E3 ligase RNF8 to sites of DSB. In conjunction with other post-translational modification enzymes (RNF168 and UBC13) RNF8 mediates K-63-polyubiquitylation to modulate local chromatin structure and recruit additional factors for repair[147-149]. Serine/threonine protein phosphatases PP2A, PP5 and WIP1 regulate the autophosphorylation of ATM and PP2A and PP4 resolve γ-H2A.X phosphorylation to attenuate DNA repair signalling[150].

1.4.2.3 Homologous recombination

Following the recognition and signaling of DNA DSBs, recruitment of HR repair factors enables efficient repair of DNA lesions with limited errors. HR DNA repair is imperative during meiosis to ensure maintenance of genomic information in germ cells[151, 152], however it is also prevalent during mitosis when homologous templates are present in S and G2 phases of the cell cycle[153, 154]. DNA damage signaling continues after RNF8, RNF168 and UBC13 mediated polyubiquitylation surrounding the DNA lesion. Receptor-associated protein 80 (RAP80) recruits the BRCA1-A complex containing BRCA1, BARD1, BRCC3, BRE and NBA1 to sites of DNA damage[155, 156].

Resection of the broken 5'-end of the DNA strand is the primary commitment to HR mediated DNA repair via HR by generating 3'-single strand DNA ends. Because of the 3'-ssDNA overhangs, repairs factors within the NHEJ pathway have difficulty binding and promoting NHEJ mediated DSB repair. The primary mediator of DNA strand resection is CtIP (CtBP-interacting protein) which is phosphorylated by cyclin dependent kinases and binds BRCA1 to

be recruited to sites of damage[157]. The CtIP-BRCA1 complex recruitment antagonizes the accumulation of 53BP1 and RIF1 of the NHEJ pathway. CtIP in concert with the MRN complex nicks the 5' terminated DNA strand and utilizes the endonuclease activity of the MRN complex to degrade the nicked strand and generate the 3' overhang.

1.4.2.3.1 RAD51 recombinase nucleofilaments, homology search and invasion

Exposure of a 3' overhang of ssDNA acts as a platform to recruit recombinases such as RAD51 or DMC1 which polymerize to form a presynaptic filament that promotes the binding of accessory factors. The binding of RAD51 to ssDNA is hindered by replication protein A (RPA) which is an abundant protein binding ssDNA to protect it from nuclease degradation[158, 159]. For this reason, RAD52 functions as a chaperone to facilitate the binding of a limited amount of RAD51 on ssDNA and displacement of the more abundant RPA. This complex interacts with Rad51 and has a ssDNA-binding activity and is suggested to stabilize the Rad51 preassembled filament. BRCA2 is a critical component required for efficient HR due to its physical interaction with RAD51 and ssDNA binding capacity. Without BRCA2, cells ability to form RAD51 foci at sites of DNA damage is markedly hindered[160].

Once formed, the RAD51 strand filament actively samples adjacent dsDNA for sequence homology. When the DNA repair template is identified, RAD51 mediates strand invasion through base pairing evicting the noncomplementary DNA strand to form a D-loop composed of three strands of DNA[161]. This whole process is proximity dependent and facilitated during normal cell cycling and alignment. Upon strand invasion, DNA repair synthesis is primed by the invading 3' end to recover the lost DNA sequence from the donor molecule. First the sequence primer extension is conducted by recruited DNA pol η and ν[162]. From there resolution can occur via various pathways.

1.4.2.4 Non-homologous end-joining

Non-homologous end joining (NHEJ) is the primary pathway for DSB repair throughout cell cycle including S and G2 phases where HR is also present[163] (Figure 1.4). One of the major components of the NHEJ pathway is the Ku heterodimer consisting of Ku70 and Ku80 with positively charged residues that can interact with exposed double stranded DNA ends. The high abundance of Ku in mammalian cells allows it to bind and protect broken DNA ends from resection

favoring NHEJ mediated repair[164]. The DNA damage response protein p53-binding protein 1 (53BP1) and replication timing regulatory factor (RIF1)[165] are recruited via several histone modifications and act as antagonists to HR mediated repair.

1.4.2.4.1 Blunt end ligation

DSBs do not always result in blunt ended DNA strands, therefore various additional pathways within NHEJ work with microhomology overhangs[166] (Figure 1.4). As interstrand microhomology becomes greater, Ku protein plays a less essential role in the repair process[167]. Direct ligations of DNA blunt ends are prefered over additional processing in the NHEJ pathway. Therefore, blunt end ligation is heavily reliant on Ku mediated binding. Ku promotes the recruitment of two core components X-ray repair-cross complementing protein (XRCC4) and DNA ligase IV[168]. XRCC4 associates with DNA ligase IV at a 2:1 ratio, and bridges the DNA duplex structure by binding to Ku on each of the protected DNA ends[169, 170]. During NHEJ, processing of 5' or 3' ends via exonuclease or endonuclease activity, regions of microhomology (<4 nucleotides) are generated. This process is mediated by DNA-PKcs and the endonuclease Artemis which are recruited to Ku protected DNA breaks[171]. DNA-PKcs autophosphorylation activates Artemis (metallo-B-lactamase) to allow for its endo and exonuclease activity on both 5' and 3' strands and form blunt ends for repair[172]. The formation of microhomology regions promotes repair via alternative NHEJ repair pathways.

1.4.2.4.2 Polymerase-dependent pathway and alternative end joining

Two DNA polymerases, Pol μ and Pol λ, can be recruited to DNA ends via Ku-DNA complex binding[171]. Pol μ primarily functions by promoting the ligation of incompatible overhangs by adding nucleotides to generate regions of microhomology. On the other hand, Pol λ primarily functions on compatible overhangs where it can use the pre-existing template to synthesize the DNA gap[173].

As the amount of microhomology increases, classical blunt end NHEJ is dramatically reduced in favor of alt-EJ. Utilizing machinery that functions within HR, alt-EJ uses Pol θ[174], PARP1, CtIP and the MRN complex to execute repair[175]. Pol θ has been shown to stabilize the annealing of two long DNA overhangs with minimal sequence homology, allowing DNA ligase I or III to seal the missing sequences[176]. The limited role of the MRN complex and CtIP to generate these

long regions of resection, prime the binding and function of Pol θ mediated repair. When DNA ligase IV is not present, alt-EJ can compensate for NHEJ, however it is tenfold slower than its counterpart[175](Figure 1.4).

1.4.3 Genomic instability and multiple myeloma

Based on the high prevalence of cytogenetic abnormalities and genomic instability as a defining feature of MM cells, it is conceivable that the primarily cause is deficiencies in faithful DNA repair. This abnormal DNA repair may also explain the aneuploidy, chromosomal rearrangements, microsatellite instability, and increased mutational frequency that plague MM patients. Aneuploidy distinguishes most cancers from their normal tissue counterpart and is present in about 70% of MM cases[177]. Recent studies on whole-genome and exon sequencing of MM and SMM samples have shown that copy number alterations (CNAs) do not occur as one catastrophic event but rather represent a serial acquisition of these CNAs over time[178]. Some CNAs occur earlier than others. Additional alterations including 1q21 gain, 13q deletion and 17p deletion are some of the most common events observed in MM. 1q21 gain and 1p deletion are observed in 40% and 23% of MM patients respectively[179]. 13q deletion or monosomy of 13 is found in 45-50% of patients with MM and leads to the deletion of several tumor suppressor genes including RB1[180]. This alteration has more of an effect on MGUS progression than MM prognosis. Finally, 17p deletion leads to the loss of the TP53 gene (10% of patients)[181]. This can lead to a more instable genome of malignant plasma cells and leads to an unfavorable prognosis.

Instability can occur through several mechanisms including dysregulated genes governing the mitotic phase (cyclins and cyclin dependent kinases) of the cell cycle[182], aberrant centrosome duplication[183], defects in microtubule attachments[184], pre-mitotic replication stress[185] and mitotic DNA damage[186]. The “Intergroupe Francophone du Myeloma” had a 15 gene signature for worse overall survival in MM which includes genes implicated in mitosis, DNA replication and DNA repair as well as transcriptional regulation[187]. Overall, this paints a complex interplay between various pathways that are known to influence DNA repair.

On a cellular level, MM cells have persistent DNA damage evident by the high number of nuclear γ-H2A.X under steady state conditions[188]. High levels of DNA damage were shown to make tumor cells dependent on a proper DDR making repair pathways a promising target for

treatment of MM. For these reasons, DNA damaging agents such as melphalan, cyclophosphamide and doxorubicin have been used to treat MM[120, 125, 189]. ATR inhibition and the checkpoint inhibitor AZD7762 have been shown to synergize with melphalan and induce apoptosis of p53 mutated MM cells respectively[190]. Furthermore, patients treated with melphalan and ASCT, polymorphisms in DNA repair genes (PARP, RAD51, PCNA, OGG1, XPC, BRCA1, ERCC1, BARD1 and TP53BP1 were associated with overall survival[191].

Despite proteasome inhibition primarily targeting the unfolded protein response and proteotoxic stress, some groups have described a role for proteasome inhibition in maintaining faithful DNA repair. For example, proteasome inhibition led to depletion of the free ubiquitin pool that is critical at the DNA repair foci for protein recruitment[192]. Another critical factor influencing DNA repair is the temporal relaxation of chromatin to allowing DNA repair proteins to access sites of damage[193]. Epigenetic modulating agents, specifically histone deacetylases, have been therapeutically investigated in the treatment of MM[51, 54]. Additionally, the stability of c-Myc is dependent on the activity of the histone acetyltransferase p300, such that p300 dependent acetylation of c-Myc results in its proteasomal degradation[194]. C-Myc has been repeatedly implicated in DNA repair[195, 196], MM growth and survival[197, 198] suggesting a bi-modal mechanism of action of HDAC inhibitors.

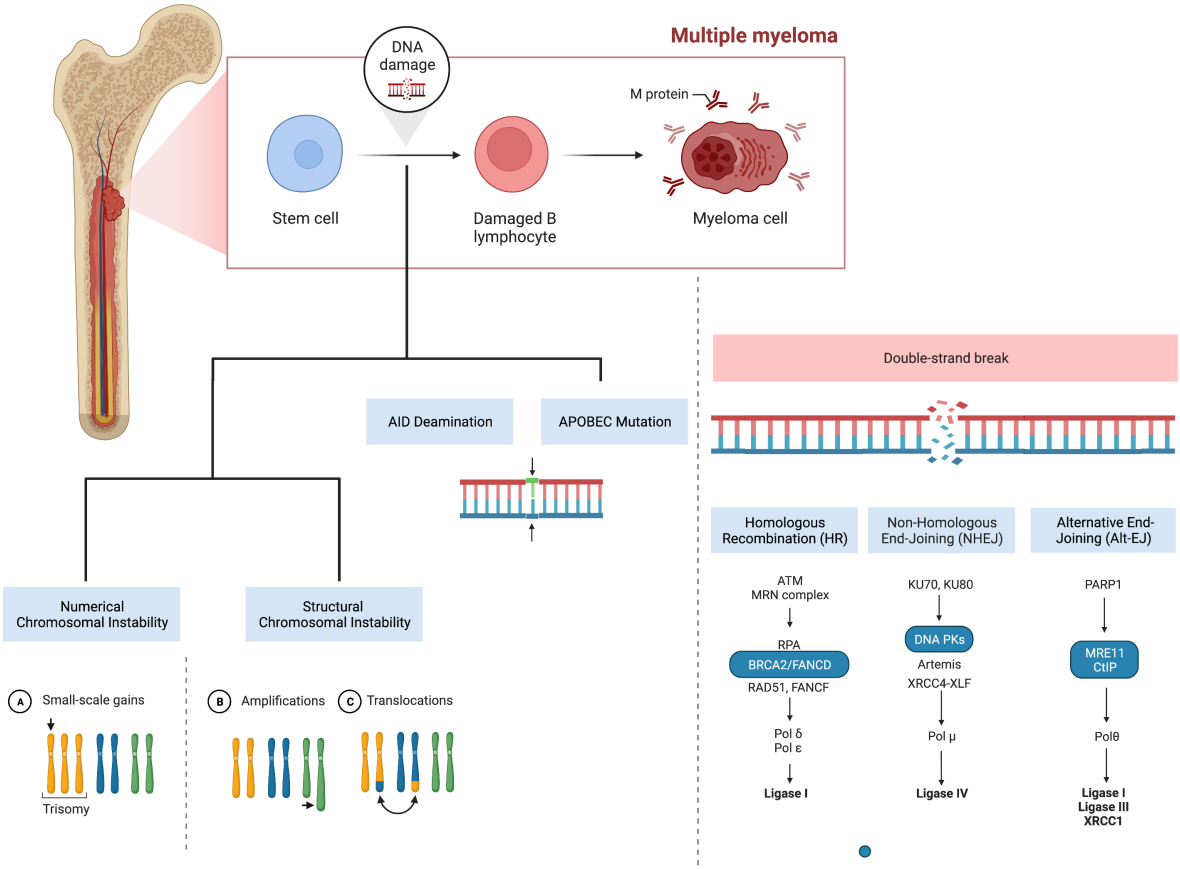

Figure 1.4 Genomic instability and DNA repair in MM

(Created with biorender)

1.4.4 Proteasome Inhibitors (PIs)

In 2005, the 26S proteasome was identified as a biological vulnerability in MM and fueled the discovery of numerous PIs over the last 15 years including BTZ[114], CFZ[199], Ixazomib[200]. The 26S proteasome is a multi-catalytic protease complex that is responsible for the ubiquitin-dependent turnover of cellular proteins. It is composed of a 20S catalytic subunit and two 19S regulatory caps (Figure 1.5). Within the 20S catalytic core, there are three major proteolytic activities: chymotrypsin-like activity (β5 subunit), a trypsin-like activity (β2 subunit) and a caspase-like activity (β1 subunit)[201]. The chymotrypsin-like subunit is known to be the rate-limiting step in proteasome dependent proteolysis and therefore the β5 subunit has been the primary target for PIs[202, 203]. MM cells produce large amounts of misfolded proteins, similar

to their cell of origin the PCs, and have a higher dependency on the proteasome to alleviate proteotoxic stress and maintain cellular homeostasis[204, 205] (Figure 1.5). Therefore, inhibition of proteasome activity would be inherently toxic to these cells. PI related toxicities are thought to be due to the non-specific inhibition of the other catalytic domains of the proteasome, therefore it is imperative that PIs be designed to allow part of the proteasome to continue to function and limit toxicity in normal cells.

Apart from BTZs proteotoxic role, 17 years of research has uncovered additional therapeutic effects. These include apoptosis of osteoclasts, induction of osteoblast differentiation[206], decreased NF-κB signaling[207] and decreased DNA repair (Figure 1.4). It has been shown to enhance the activity of other concurrent therapies including lenalidomide and dexamethasone[208]. Currently the preferred treatment option for transplant ineligible MM patients is a three-drug regimen including BTZ, lenalidomide and dexamethasone (VRd) which has shown to be effective in improving survival at a cost of increasing toxicities such as peripheral neuropathy, cytopenia, fatigue and gastrointestinal distress[209]. If VRd is unavailable or a patient has acute renal failure, BTZ, cyclophosphamide and dexamethasone (VCd) or BTZ, thalidomide and dexamethasone (VTD) can be used[209]. Although the substitution of CFZ for BTZ results in a similar efficacy in the ENDURANCE E1A11[210] and CLARION[211] phase III clinical trials, CFZ's toxicity profile includes more heart failure and hypertension than BTZ. For these reasons CFZ's primary utilization is to treat BTZ resistant MM patients in second line therapy[212]. Finally, Ixazomib in combination with lenalidomide and dexamethasone (IRd) is less effective than VRd based on initial data, however it is an oral formulation that can improve patient adherence and quality of life[213]. To complement ongoing clinical trials evaluating new combinations of MM treatments, a third generation of PIs including Oprozomib [214], Marizomib [215] and Delanzomib [216] are also being tested in clinical trials to improve efficacy and toxicity profiles of PIs.

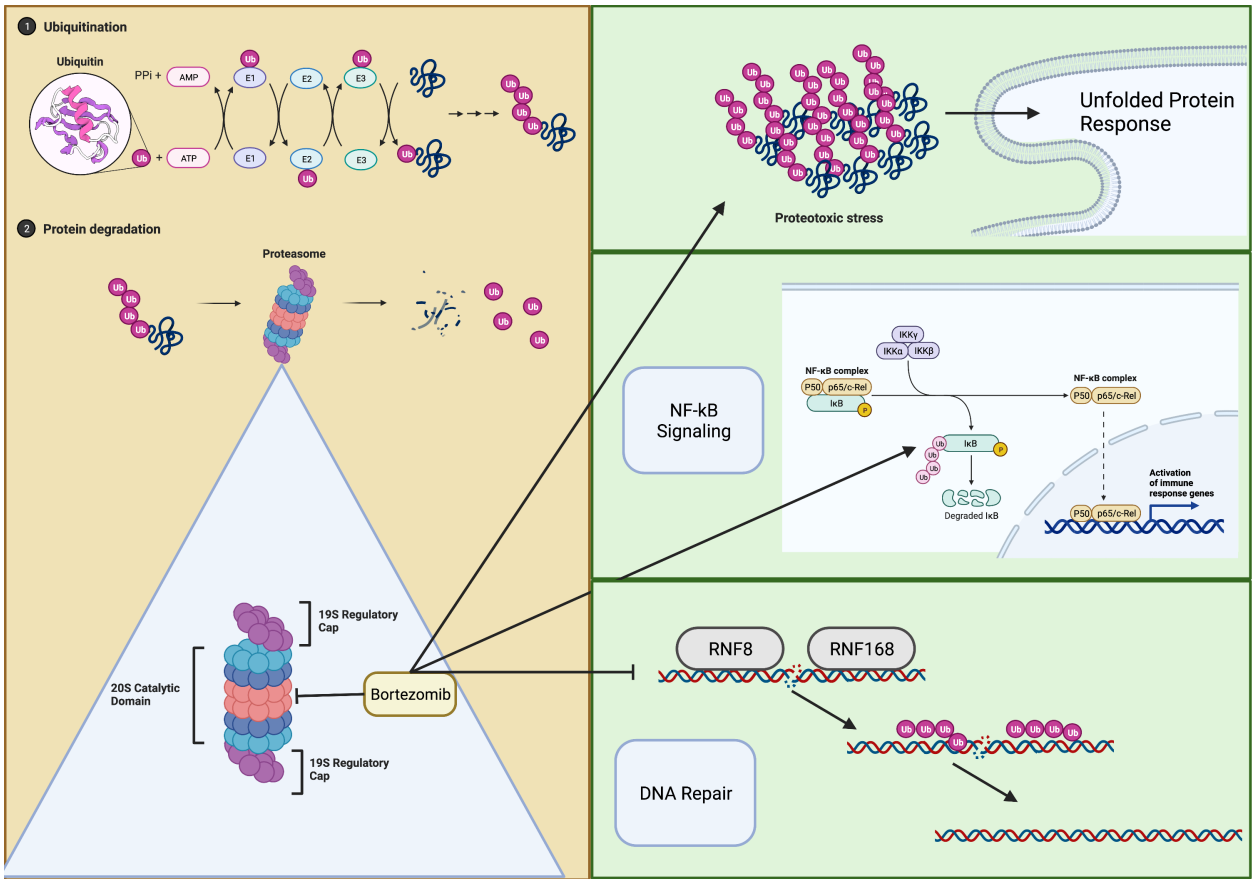

Figure 1.5 Biological consequences of BTZ treatment in MM

(Created with biorender)

1.4.5 Immunomodulatory drugs and monoclonal antibodies

Immunomodulatory drugs (IMiDs) are widely used in the treatment of MM and have been reported to have a multitude of activities including anti-angiogenic, cytotoxic and immunomodulatory functions. This class of drugs include thalidomide, lenalidomide and pomalidomide which enhance the sensitivity of MM cells to various treatments including PIs, chemotherapeutics and dexamethasone[116, 117, 217-219]. IMiD Specific cytotoxicity in MM cells has been attributed to NF-κB inhibition, decreases in IRF4 production, increased expression of pro-apoptotic factors and disruption of the PI3K/Akt pathway (Figure 1.5). Apart from MM specific action, IMiDs are also known to influence the bone marrow microenvironment. IMiD dependent decreased IL-6 production and expression of cell adhesion molecules disrupts myeloma cell-bone marrow stromal interaction[220, 221]. Lenalidomide has been shown to

downregulate osteoclast activity and inhibit secretion of osteoclastogenic factors (BAFF, APRIL, RANK-L)[222].

To add more complexity to the mechanism of action, IMiDs, as per their name, have immunomodulatory effects. MM tumor cells can induce pronounced immunosuppression both systematically and locally in the bone marrow microenvironment. Immunodeficiency in the BM microenvironment is characterized by an increase in immunosuppressive cell populations, including regulatory T cells and myeloid derived suppressor cells (MDSCs)[223]. In MM, MSDCs are unable to differentiate into immune-protective macrophages and granulocytes. Lenalidomide has been shown to decrease TNF-a, IL-6 and IL-12 production while increasing IL-2 and IFN-y synthesis[224]. IMiDs have also been shown to increase T-cell priming, enhance tumor antigen uptake by dendritic cells for antigen presentation, and enhance the activity of NK and NK T cells[225].

The immune modulating properties have also potentiated the effects of monoclonal antibodies (mAb) that are currently being used in MM treatment. Originally, lenalidomide and pomalidomide were both shown to improve the effect of rituximab in lymphoma. Now numerous mAbs including elotuzumab (SLAMF-7), daratumumab and isatuximab (CD38)[226] have been approved for treatment of relapsed/refractory MM patients. Immune therapy has now shifted into CAR-T cell therapy for MM patients and several ongoing trials are assessing their safety and efficacy profiles in MM patients.

1.5 CRISPR Technology and Screening Strategies

Clustered regularly interspaced short palindromic repeats (CRISPR/Cas) was identified as a bacterial defence mechanism against viruses and foreign nucleic acids[227]. The incorporation of short viral sequences into the host CRISPR locus and subsequent transcription results in small RNAs that guide the destruction of invading nucleic acids[228]. This knowledge provided the foundation for the generation of CRISPR targeted technology that allowed for targeted disruption of DNA targets[229] and targeted genome editing in eukaryotic cells[230]. Throughout the past decade, CRISPR technology has not only become a staple in molecular biology laboratories, but it has also expanded its repertoire with targeted transcriptional activation (CRISPRa)[231], gene inhibition (CRISPRi)[232], epigenome editing via histone modification enzymes[233], and targeted base editing[234]. As the CRISPR toolkit has grown throughout the last 20 years, it has

also revolutionized large scale genetic manipulation strategies from traditional shRNA and siRNA screens to genome wide CRISPR genetic KO screens.

RNA interference (RNAi) is an effective screen in identifying genes that are functionally responsible for a phenotype using loss or gain-of function screens. RNAi techniques have been used in the past to find essential genes that are responsible for MM cell survival, however some limitations include off-target effects, insufficient knockdown efficiency in highly expressed genes and when done in cell lines they don't fully replicate the heterogeneity of MM[235, 236]. Using CRISPR/Cas9 genome editing techniques paired with next generation sequencing, the opportunity to produce highly specific knockouts with improved off target cell cytotoxicity encourages and a more elaborate genome-wide approach to researching MM.

1.6 Cellular Metabolism and Energetics

Cells require energy to run biological reactions that maintain their viability, growth and homeostasis. Many metabolic pathways influence cellular energetics, however, there are two major pathways that influence the production of adenosine triphosphate (ATP), the dominant compound of chemical energy. Cytosolic glycolysis and mitochondrial oxidative phosphorylation are critical in the production of ATP. Normal cells rely primarily on mitochondrial oxidative phosphorylation (OXPHOS), which is efficient at generating more ATP than glycolysis. Historically, glycolysis is preferentially utilized under anaerobic conditions, converting a glucose molecule into pyruvate whilst generating two molecules of ATP. Pyruvate can then reduced to lactate by lactate dehydrogenase A (LDHA) in the cytoplasm and excreted into the extracellular space through monocarboxylate transporters (MCTs)[237, 238]. Under aerobic conditions, pyruvate is further oxidized into acetyl-CoA[239] in the mitochondria to fuel the citric acid (TCA) cycle which generates reduced intermediates NADH and $FADH_2$, as well as two ATP (Figure 1.6). Reoxidation of NADH and FADH2 via the electron transport chain (ETC) in the mitochondria generates an additional 30-32 ATP/glucose through OXPHOS. The ETC is a series of five complexes that transfer electron from electron donors to electron acceptors whilst transferring protons (H^+) into the mitochondrial intermembrane space[240]. The established proton gradient drives the synthesis of ATP via the ATP synthase (Complex V) (Figure 1.6). Energy production in response to cellular demand varies depending on cellular conditions and the microenvironment[241, 242]. The preferential utilization of glycolysis and OXPHOS under

various environmental conditions enables cells to rapid adapt their energetic production to meet cellular demands. Therefore, there is a cooperation between OXPHOS and glycolysis to maintain a balance of energy.

1.6.1 Mitochondria Pyruvate Carrier:

After glycolysis, pyruvate is transported from the cytosol into the mitochondria to be converted to acetyl-CoA and supply the TCA cycle and OXPHOS with metabolic intermediates. To compartmentalize mitochondrial machinery and function, metabolites must traverse the outer mitochondrial membrane (OMM) and the inner mitochondrial membrane (IMM). The OMM utilizes voltage dependent anion channels (VDAC) or porins to allow the permeability of small molecules[243-245]. However, the IMM is much more selective and contains specific carriers to allow the selective flow of metabolites between compartments. Most of these specified carriers belong to the SLC25 family of mitochondrial carriers that is highly conserved between species[246, 247]. One exception, that eluded scientists up until 2012 was the mitochondrial pyruvate carrier (MPC). Even though the fundamental function of the mitochondrial pyruvate carrier had been described in early studies using isolated mitochondria, the molecular identity of the proteins involved remained a mystery[248]. In 2012, two studies simultaneously reported the identification of the MPC accidently while trying to characterize two paralogous proteins of unknown function, BRP44L (MPC1) and BRP44 (MPC2), in yeast, drosophila, and murine models[249, 250]. Both groups concluded that these two genes encode the subunits of the MPC with a third subunit in yeast. The MPC, composed of MPC1 and MPC2, is a heterodimeric complex that is responsible for the transport of pyruvate into the mitochondrial matrix[249, 250]. The conversion of pyruvate to Acetyl-CoA is facilitated by the pyruvate dehydrogenase complex (PDH) composed of three enzymes: pyruvate dehydrogenase (E1), dihydrolipoly transacetylase (E2) and dihydrolipoyl dehydrogenase (E3)[251, 252]. Pyruvate can also be carboxylated by pyruvate carboxylase to oxaloacetate which can replenish the TCA cycle as well or be utilized to make amino acids such as aspartate[253]. Metabolic pathways are not always linear and certain metabolites can have multiple fates, such is the case with pyruvate. The decision of whether or not pyruvate is transported to the mitochondria is a critical determinant for metabolic homeostasis.

1.6.2 Cancer Metabolism:

Within a tissue microenvironment, there is constant competition between resident cells for a limited amount of resources. Such competition is only heightened in cancerous tissue where cancer cells exhibit greater metabolic flexibility to adapt to microenvironmental changes and ultimately obtain a survival advantage especially in unfavorable environments. Apart for tumor growth, metabolism also plays a critical role in treatment response and relapse throughout cancer progression[254, 255]. To make matters worse, different cancers have different metabolic signatures making a pan-cancerous metabolic treatment difficult to achieve[256]. This heterogeneity allows the cancer to escape treatment and clonally expand to reconstitute a resistant cancer[48]. Generally, cancer cells have increased energetic requirements and have metabolically adapted to favor fast, but inefficient, aerobic glycolysis[257].

Otto Warburg was the first to describe how some cancers have a preferential adaptation to use glycolysis as opposed to OXPHOS under aerobic conditions due to dysfunctional mitochondria[258]. The "Warburg Effect" was rapidly identified as a hallmark of cancer, however, contrary to his hypothesis, OXPHOS remains functional, but is suppressed by increased glycolysis ([259]. For example, glycolysis inhibition indirectly via LDHA suppression or directly via 2-DG administration enhanced OXPHOS function to compensate for reduced ATP production[260, 261]. It is more likely that the metabolic switch to glycolysis is a consequence of oncogene activation[262], loss of tumor suppressors, hypoxic microenvironment[263] and mitochondrial DNA mutation than mitochondrial dysfunction. Despite metabolically switching, glycolytic contribution to total ATP production does not generally exceed 50-60%, OXPHOS still substantially contributes to ATP production in tumor cells[259]. Due to increased rates of glycolysis and subsequent suppression of OXPHOS, cancer cells increasingly depend on glucose and glutamine to fuel energetic metabolism.

Apart from generating ATP, cancer cells also require metabolic intermediates and precursors that are critical for the biosynthesis of macromolecules. The accumulation of glycolytic intermediates is known to promote the pentose phosphate pathway (PPP) resulting in the generation of NADPH and ribose-5-phosphate[264]. Both are essential for the biosynthesis of lipids and nucleic acids. NADPH also enables cancer cells to maintain adequate levels of reduced forms of glutathione (GSH), a key non-enzymatic antioxidant[265]. GSH plays a pivotal role in protecting cancer cells against antineoplastic agents by maintaining the redox status and preventing

oxidative induced DNA damage[266]. Therefore, aerobic glycolysis in conjunction with pentose shunt pathway provide multiple benefits to cancer cells.

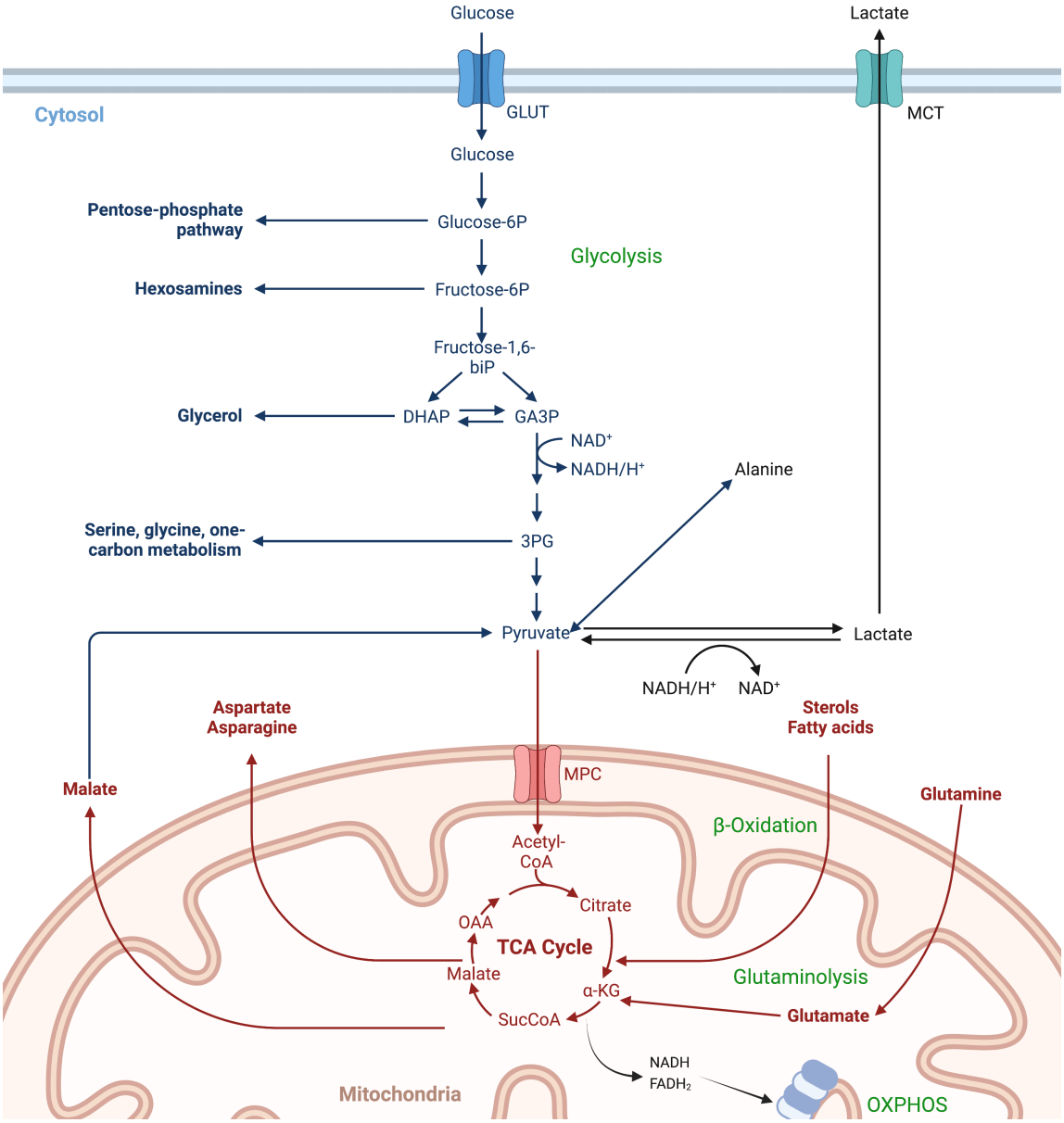

Figure 1.6 Mitochondrial Metabolism Overview

(Created with biorender)

1.6.3 Glutamine Metabolism:

Research into cancer metabolism has expanded beyond the Warburg effect to look at other nutrients and metabolic intermediates that may play a critical role in cancer biology. Circulating glutamine is the most abundant amino acid representing more than 20% of amino acids in the blood and 40% amino acids in the muscle[267]. It is primarily obtained via dietary retention in the endothelium, however it can also be synthesized in the lungs, liver, brain, skeletal muscles and adipose tissue. Under nutrient deprivation conditions, glutamine can also be acquired through the breakdown of macromolecules called macropinocytosis[268]. Glutamine provides a ready source of carbon and nitrogen to support biosynthesis, energetic and cellular homeostasis pathways which cancer cells can exploit to drive tumor growth in compensation for glucose depletion[269, 270]. Glutamine enters the cell via the SLC1A5 (ASCT2) transporter and can immediately be used to generate nucleotides or transported into the mitochondria for further processing[271, 272]. Mitochondrial glutaminases (GLS and GLS2) and alanine and aspartate aminotransferases convert glutamine into glutamate which can be utilized for various metabolic functions[273, 274]. Glutamate can further processed into α-ketoglutarate via glutamate dehydrogenase (GLUD1/GLUD2), glutamate-pyruvate transaminase (GPT1/GPT2) or glutamate oxaloacetate transaminase (GOT1/GOT2) respectively.[275] α-ketoglutarate is known to be an important metabolic intermediate in the TCA cycle which can be used as an alternative carbon source for TCA cycle respiration, also known as anaplerosis, and indirectly replenish citrate levels that are reduced due to increased lactate excretion, depleted acetyl-CoA and MPC inhibition[276] Figure1.6). Proliferating cells including cancer cells and activated lymphocytes use glutamine as an energy generating substrate[277].

The expression of glutamine metabolism enzymes is heterogenous, especially when taking into consideration the tissue of origin. However, GLS and GLS2 activity are dependent on the concentrations of inorganic phosphate, acetyl-CoA and succinyl-CoA, all of which are affected by nutrient uptake and metabolism[267]. Furthermore, glutamate dehydrogenase is activated by leucine, ADP and mTOR suggesting it might be induced when cells are in a low energetic state. Altogether, glutamine metabolism enzymes are responsive to the metabolic state of the cells, positioning them as sensors to maintain metabolic homeostasis.

Glutamine also plays an important role in supporting amino acid biosynthesis, since at least 50% of non-essential amino acids used in protein synthesis are derived from glutamine[278]. For

example in MYC oncogene driven cancers such as MM, there is a preferential synthesis of proline from glutamate[269, 279]. Elevation of glutamine consumption in cancer cells is closely related to MYC activation, such that when MYC expression is disrupted, cells reduce their dependency on glutamine[280, 281]. Glutamine is also important in the generation of purine and pyrimidines to support cell division as well as fatty acid synthesis under hypoxic conditions[282]. Since glutamine metabolism supports biosynthetic pathways resulting in protein synthesis, it also suppresses the integrated stress response (ISR) which is activated under amino acid depletion. Under glutamine deprivation, the amino acid sensing kinase (GCN2) activates a signalling cascade including ATF4 which acts as a transcription factor to increase transcription of amino acid synthesis genes[283]. It can also activate, apoptotic, autophagosome and ER stress pathways during infection to generate local inflammation[284, 285]. The pleiotropic role of glutamine in cellular functions such as energy production, macromolecular synthesis and ROS homeostasis make glutamine metabolism an attractive candidate for combination therapy.

1.6.4 Reactive Oxygen Species:

Reactive oxygen species are by products primarily generated via the ETC in OXPHOS that require homeostatic mechanisms to maintain a balance of ROS levels. Limited amounts of ROS can be pro-tumorigenic and promote tumor heterogeneity[286, 287], however when levels are in excess, ROS can be highly damaging to macromolecules and have an anti-tumorigenic role[288, 289]. The primary molecule involved in ROS homeostasis is glutathione. Glutathione is a tripeptide antioxidant that serves to neutralize peroxide, free radicals, lipid peroxides, as well as heavy metals and is highly conserved in plants, animals, fungi and bacteria[266]. Glutamine input is the rate-limiting step of glutathione synthesis and levels of glutathione are known to correlate with tumorigenesis and drug resistance in cancer[290-292]. Several publications have shown that administration of glutamine to cancer patients receiving chemotherapy reduces treatment toxicity through glutathione synthesis[293]. Glutamate combines with cysteine and glycine to form reduced glutathione (GSH) which is found in all human cells and is involved in regulating the redox state and is a major antioxidant in cells. This conversion of GSSG to GSH and is facilitated by oxidation of NADPH which can be produced when malate is converted to pyruvate in the cytoplasm.

As with other cancers, the production of reactive oxygen species (ROS) paradoxically is both a threat to and creates growth signals for MM cells. Overproduction of ROS is toxic to MM cells, however healthy plasma cells already have relatively high levels of ROS production as a result of their role as antibody producing factories[294, 295]. As a result, MM cells produce large amounts of ROS that need to be dealt with in order to prevent cell death and this is achieved through the oxidative stress response. This includes the expression of superoxide dismutase (SOD), peroxidase, glutathione (GSH) and vitamin E, which quench ROS[296]. ROS can also promote tumor growth by acting as signals for proliferation. For example, the release of H_2O_2 from mitochondria activates the transcription factor NF-κB, which is activated in myeloma cells in order to increase proliferation and survival[297]. Interestingly, ROS dependent oxidation of cysteine-62 of p50 inhibits NF-κB s DNA binding ability and therefore reducing NF-κB dependent transcriptional activity [298] . ROS has also been shown to directly activate PI3K and inactivate PTEN resulting in Akt inhibition[299], as well as ERK activation resulting in downstream signalling to JNK translocation into the nucleus regulating transcriptional activity which can also promote tumorigenesis[300].

Therefore, with increased glutamine oxidation, there can be increased ROS production, however, at the same time glutamine is critical for maintaining cellular ROS homeostasis. The most readily known pathway is through glutathione which is a tripeptide that serves to neutralize peroxide free radicals.

1.6.5 Energetic Stress:

The ability to rapidly adapt cellular bioenergetic capabilities to account for changing environmental conditions is mandatory for both normal cellular function and cancer progression. Any loss or disruptions of this adaptive response has the potential to compromise cellular function and render the cell more susceptible to external and endogenous stressors. The mitochondria not only plays a role in the bioenergetic pathways, but also the biosynthetic pathways to adjust for the metabolic needs of the cell. Increased demand is met by mitochondrial biogenesis and fusion of individual mitochondria, whereas a decrease in demand results in the removal of excess mitochondria through fission and mitophagy[301]. Energetically poor conditions are detected by an elevated AMP to ATP ratio which is sensed by the AMP-activated protein kinase (AMPK). At

high AMP:ATP ratios, AMP binds to the regulatory γ subunit of AMPK and allosterically activates the protein kinase to be phosphorylated by other kinases such as LKB1[302]. Activated AMPK regulates many proteins involved in restoring the energy balance of a cell including enzymes and transporters involved in glucose catabolism and oxidative phosphorylation[302]. One direct target is the coactivator PGC1α (peroxisome proliferator-activated receptor γ coactivator 1a)[303]. While PGC1α can undergo a variety of post-translational modifications including acetylation, ubiquitination, methylation and phosphorylation, the regulation through AMPK remains essential for regulating energy status of the genome. Activated PGC1α stimulates the transcription of many genes associated with mitochondrial biogenesis including NRF1 (Nuclear respiratory factor 1) which regulates genes that are crucial for the expression and function of the respiratory chain[304].

1.6.6 Mitochondria and Multiple Myeloma

Multiple myeloma cells reside in the hypoxic niche of the bone marrow which has been shown to promote resistance to current therapeutic options. In a hypoxic environment, hypoxia inducible factors (HIFs) are the master regulators of gene expression changes influencing cell cycle arrest, angiogenesis, glycolysis, and glucose transport induction[305]. In MM cells, HIF1α activation increases glycolytic pathway activity and subsequent inactivation of the tricarboxylic acid cycle[306]. Furthermore, under hypoxic conditions, MM cells are dependent on LDH, which reduces pyruvate to lactate, to maintain the intracellular balance of NADH/NAD+[306]. This allows cells to use glycolytic intermediates for anabolic processes and escape the effects of high ROS levels at the expense of additional OXPHOS energy. A prospective analysis comparing healthy and MM patients identified large differences in amino acid, lipid and energetic profiles[307]. Specifically, 2-hydroxyglutarate (2-HG), which is proposed to be an oncometabolite that influences epigenetic alterations through its inhibition of KDMs such as KDM4A[308]. 2-HG levels within the blood was shown to be higher in MM patients when compared to MGUS patients and it could predict SMM patients with higher risk of progression[309].

Apart from metabolic changes influencing MM progression, it is also known to play a role in treatment response and subsequent relapse. When comparing melphalan resistant and sensitive cell lines, MM cells switch to favor aerobic glycolysis promoting resistance[310]. Adaptive metabolic

changes in MM cells are emerging as the basis for PI resistance and this is driven primarily by the mitochondria. In particular, altered glucose metabolism resulted in increased TCA flux and increased antioxidant activity to sustain the resistance to BTZ in MM cells[306, 311, 312]. Paradoxically, others have reported an increase in both mitochondrial biomass and reliance on mitochondrial respiration as opposed to glycolysis. Additionally, cells become highly dependent on glutamine metabolism, not only as an energy source, but also to promote the formation of GSH[307]. Depletion of glutathione can potentiate the effect of PIs in multiple myeloma cells[290, 313] and GSH is known to be an important buffering agent that maintains redox homeostasis and is associated with increased cancer development[314]. One of the major regulators of cellular stress response is NFE2L2 or NRF2. In response to various stress stimuli, NRF2 translocates into the nucleus and activates stress-protective genes such as NQO1, HMOX1, P62, SLC7A11[315]. Proteomic analysis of PI resistant cell lines identified massive alterations in cellular metabolism and high oxidative phosphorylation[311]. Particularly pathways that fuel synthesis and regeneration of glutathione, NAD(P)H and tricarboxylic acid cycle. These changes led to an increased antioxidant capacity and preferential oxidative phosphorylation. Furthermore, changes in malate/aspartate shuttle, metabolism of purines/pyrimidines, alanine/aspartate/glutamate, with significant changes in the TCA cycle.

Chapter 2: The mitochondrial pyruvate carrier complex potentiates the efficacy of proteasome inhibitors in multiple myeloma

Steven Findlay, Zafir Kaiser, Alexandre Cajelot, Zahra Aryanpour, John Heath, Catherine St-Louis, David Papadopoli, Ivan Toposirovic, Julie St-Pierre, Michael Sebag, Laura Hulea, and Alexandre Orthwein

Manuscript under revision: Blood Advances November 2022.

2.1 Abstract

Multiple myeloma (MM) is a hematological malignancy that emerges from antibody-producing plasma B cells. Proteasome inhibitors, including the FDA-approved bortezomib (BTZ) and carfilzomib (CFZ), are frequently used for the treatment of MM patients. Still, a significant proportion of MM patients are refractory or develop resistance to this class of inhibitors, which represents a significant challenge in the clinic. Thus, identifying factors that determine the potency of proteasome inhibitors in MM is of paramount importance to bolster their efficacy in the clinic. Using genome-wide CRISPR-based screening, we identified a subunit of the mitochondrial pyruvate carrier (MPC) complex, MPC1, as a common modulator of BTZ response in two distinct human MM cell lines *in vitro*. We noticed that CRISPR-mediated deletion or pharmacological inhibition of the MPC complex enhanced BTZ/CFZ-induced MM cell death with minimal impact on cell cycle progression. In fact, targeting the MPC complex compromised the bioenergetic capacity of MM cells, which is accompanied by a reduced proteasomal activity, thereby exacerbating BTZ-induced cytotoxicity *in vitro*. Importantly, we observed that the RNA expression levels of several players in pyruvate metabolism were altered in advanced stages of MM wherein they correlated with poor prognosis for MM patients. Collectively, this study highlights the importance of the MPC complex for the survival of MM cells and their responses to proteasome inhibitors. These findings establish mitochondrial pyruvate metabolism as a potential target for the treatment of MM, and an unappreciated strategy to increase the efficacy of proteasome inhibitors in the clinic.

2.2 Introduction

Multiple myeloma (MM) is the second most common hematological malignancy, accounting for about 13% of all blood cancers [1]. MM is a genetically heterogenous disease, characterized by the accumulation of malignant plasma cells in the bone marrow that display a high number of chromosomal alterations and gene mutations [2]. Newly diagnosed MM patients, who are typically provided with a proteasome inhibitor, such as bortezomib (BTZ), an immunomodulatory drug, like lenalidomide, and a glucocorticoid (e.g. dexamethasone), respond well to this intensive therapeutic regimen [2]; however, long-term remission and cure are extremely rare, and a significant proportion of people diagnosed with MM relapse or become resistance to these drugs [3]. Still, the genetic landscape that determines the response of MM patients to the front-line proteasome inhibitor therapies remains obscure.

Targeted and genome-wide mapping by RNA interference (RNAi) or CRISPR technology have identified several genetic vulnerabilities that influence the response of MM cells to proteasome inhibitors *in vitro*, including ribosomal function, DNA damage pathways, mRNA translation initiation, and proteasomal subunits [4-8]. More recently, metabolic rewiring of MM cells in response to proteasome inhibitors has emerged as an additional critical element in the development of relapsed/resistant cases [9-14]. To this end, MM cells that developed resistance to proteasome inhibitors are characterized by perturbations in cellular metabolism, including glycolysis, oxidative phosphorylation, citric acid cycle (TCA), pentose phosphate pathway, and serine synthesis [9-11]. Interestingly, BTZ-resistant MM cells appear to rely heavily on mitochondrial respiration as their principal energy source [15]; however, the factors that drive the metabolic rewiring of proteasome inhibitor resistance in MM cells remains elusive.

In this present study, we performed *in vitro* CRISPR-based genome-wide dropout screens in two human MM cell lines, using BTZ as selective agent. This approach identified the mitochondrial pyruvate carrier 1 (MPC1), a key metabolic protein that regulates the transport of pyruvate into the mitochondrial matrix, as a common modulator of BTZ response in MM cells *in vitro*. Genetic ablation or pharmacological inhibition of the MPC complex induces a metabolic rewiring that compromises the proteasomal activity and increases proteasome inhibitor-induced MM cell death in *vitro.* Importantly, several pivotal players in pyruvate metabolism exhibit altered expression in late stages of MM and correlate with poor prognosis in a cohort of MM patients

(n=771). Altogether, our findings unravel the previously unrecognized importance of mitochondrial pyruvate import in MM cells and their responses to proteasome inhibitors.

2.3 Materials and Methods

Cell lines and transfection

JJN3, RPMI-8226, U266B1, KMS-12BM, and 5TGM1 MM cells were cultured in RPMI-1640 medium (Wisent) supplemented with 10% fetal bovine serum (FBS, Sigma) and 1% Penicillin-Streptomycin (P/S, Wisent). The 5TGM1 cell line was a kind gift of Dr. Michael Tomasson (University of Iowa, IA) and Greg Mundy (Vanderbilt University, TN) . All cell lines were regularly tested for mycoplasma contamination and STR DNA authenticated. Lentivirus was produced in HEK293T cells using calcium-phosphate transfection with psPAX2 (a lentiviral packaging plasmid), VSV-g (an envelope plasmid) and 25μM chloroquine (inhibitor of lysosomal degradation). HEK293T supernatant was collected and concentrated using 23% PEG (50%), 8% NaCl (5M) and 7% PBS 1X. Viral infection was done in the presence of 8μg/ml polybrene (lentiviral transduction enhancer) and 1000μg/ml F108 to improve cellular transduction. Transduced cells were incubated at 37°C and selected 48 hours later.

CRISPR/Cas9 genome-wide screen

For the genome-wide CRISPR/Cas9-based screen, 270 million U266/Cas9 and JJN3/Cas9 cells were transduced with TKOv1 concentrated library virus at MOI = 0.2 as described previously [16], ensuring a coverage of at least 600-fold for each individual sgRNA represented in the cell population. Two days later, puromycin was added to the media at a final concentration of 5 μg/ml and incubated for 4 days to allow for the emergence of resistant cells with fully repaired sgRNA library targeted loci. Cells were then split into two pools each in triplicate at a cell density of 54 million cells/replicate and treated with either vehicle (DMSO) or Bortezomib at 3 nM (IC_{25}) and cultured for 2 weeks with puromycin at a concentration of 1.5 μg/ml. Cells were passaged every 3 days keeping a minimum cell concentration of 54 million cells per replicate to ensure that a 600-fold library coverage was maintained over the duration of selection. At each time point cell pellets were collected and frozen prior to genomic DNA extraction. Cell pellets were resuspended in 6 ml DNA lysis buffer (10 mM Tris–Cl, 10 mM EDTA, 0.5% SDS, pH 8.0) with 100 μg/ml RNase A, followed by incubation at 37°C for 60 min. Proteinase K was subsequently added (400 μg/ml final), and lysates were further incubated at 55°C for 2 h. Samples were then briefly homogenized by passing them three times through a 18G needle followed by three times through a 22G needle.

Sheared samples were transferred into pre-spun 15 ml Maxtract tubes (Qiagen) mixed with an equal volume of neutral phenol:chloroform:isoamyl alcohol (25:24:1) solution, shook, and centrifuged at 1,500 *g* for 5 min at RT. The aqueous phase was extracted and precipitated with two volumes of ethanol and 0.2 M NaCl. Air-dried pellets were resuspended in water and quantitated via UV absorbance spectrometry.

Two-color CRISPR competitive growth assay

20,000 cells were infected at an MOI of ~ 1.2 to ensure 100% transduction efficiency with either virus particles of NLS-mCherry LacZ-sgRNA or NLS-BFP GOI-sgRNA. 96 h following transduction, mCherry- and BFP-expressing cells were mixed 1:1 and plated with or without bortezomib (4nM) in 12-well format. The cells were sub-cultured when near-confluency was reached and BTZ containing medium was replaced every 3 days. Cells were imaged for BFP and mCherry signal the day of initial plating (t=0) and on days 4, 8, 12 and 16. Data were acquired using FACS Fortessa cytofluorimeter and processed with FACSDiva 8.0 software (BD Biosciences).

Immunoblotting

Selected cell lines were treated as indicated prior to trypsinization, collection and PBS washes. Cells were placed in 1x LDS loading buffer (10mM Tris-HCL, 140mM Tris-base, 0.5mM EDTA, 1% lithium dodecyl sylphate, 10% glycerol) with 1x protease (Roche) and phosphatase (Sigma) inhibitors. Following sonication, cell lysates were cleared by centrifugation at a maximum speed for 15 min at 4°C. After the addition of loading dye and 2-mercaptoethanol, cleared lysate was placed at 70°C for 10 min. Protein lysates were subjected to immunoblotting as previously described (Findlay et al, 2018). Membranes were blocked with BSA 5% in Tween 20 (0.015%)-TBS for 3h at 4°C and probed overnight with primary antibody at a dilution of 1:1000 in T-TBS. Secondary antibodies were used at a dilution 1:10,000 in T-TBS. Signal was detected using Immobilon Western Chemiluminescent HRP substrate (GE Healthcare) and Azure 400 machine (Azure Biosystems).

Proliferation assay

Cells were incubated with various drugs and/or with media for the times indicated in the figure legends. Cells were trypsinized and resuspended in media and live cells were quantified by trypan blue exclusion using a hemocytometer daily for 4 days.

Apoptosis and cell cycle

Apoptosis was measured by flow cytometry with Annexin V-647 and propidium iodide staining. Briefly the cells were washed 2x in wash buffer (0.01M Hepes, 0.14M NaCl and 2.5mM CaCl2), stained with Annexin V-647 for 15 mins at RT, followed by a final wash and the addition of 2ug/ul of propidium iodide (PI). Viability of cells was assessed by gating PI^+ vs PI^- cells.
Cell cycle was measured flow cytometry using PI. Briefly, cells were washed in PBS and fixed in 70% Ethanol at 4°C overnight. The following day the cells were washed 3x with PBS and incubated with PI (1:2000). Data were acquired using FACSCanto II cytofluorimeter and processed with FACSDiva 8.0 software (BD Biosciences).

Drug preparation and treatment

Bortezomib, Carfilzomib, and UK-5099 (Selleck Chemicals) powder was dissolved in DMSO, filter sterilized and stored at -20°C. For in vitro experiments, Bortezomib and Carfilzomib were used at a final concentration of 3 to 4nM, UK-5099 was used at a final concentration of 10μM.

LC-MS

All LC-MS grade solvents and salts were purchased from Fisher (Ottawa, Ontario Canada: water, acetonitrile (ACN), Methanol (MeOH), formic acid, ammonium acetate and ammonium formate. The authentic metabolite standards and N-ethylmaleimide were purchased from Sigma-Aldrich Co. (Oakville, Ontario, Canada).

Nucleotide detection and analysis was performed using LC-MS/MS at the Metabolomics Core Facility of the Goodman Cancer Research Centre. Cultured cells were treated with bortezomib and UK-5099 for 16 hours and 24 hours respectively. Cells were washed in ammonium formate three times, then quenched in cold 50% methanol (v/v) with acetonitrile and NEM supplementation at 1mg/ml. Cells were lysed and homogenized by bead-beating for 30 seconds at 50 Hz using 4 ceramic beads (2 mm) per sample (SpeedMill Plus, Jena Analytik). Cellular extracts were

partitioned into aqueous and organic layers following dimethyl chloride treatment and centrifugation. The aqueous supernatants were dried by vacuum centrifugation with sample temperature maintained at -4°C (Labconco, Kansas City MO, USA). Dried extracts were subsequently re-suspended in 50 µL of chilled H_2O and clarified by centrifugation at 1°C. Sample injection volumes for analyses were 5 µL per injection.

For targeted metabolite analysis, samples were injected onto an Agilent 6470 Triple Quadrupole (QQQ)–LC–MS/MS (Agilent Technologies). Chromatographic separation of metabolites was achieved by using a 1290 Infinity ultra-performance quaternary pump liquid chromatography system (Agilent Technologies). The mass spectrometer was equipped with a Jet Stream™ electrospray ionization source, and samples were analyzed in negative mode. The source-gas temperature and flow were set at 150°C and 13 L min^{-1}, respectively, the nebulizer pressure was set at 45 psi, and capillary voltage was set at 2,000 V. Multiple reaction monitoring parameters (qualifier/quantifier ions and retention times) were either obtained optimized using authentic metabolite standards.

Chromatographic separation of the isomers and other metabolites was achieved by using a Zorbax Extend C18 column 1.8 µm, 2.1 × 150mm^2 with guard column 1.8 µm, 2.1 × 5mm^2 (Agilent Technologies). The chromatographic gradient started at 100% mobile phase A (97% water, 3% methanol, 10 mM tributylamine, 15 mM acetic acid, 5 µM medronic acid) for 2.5 min, followed with a 5-min gradient to 20% mobile phase C (methanol, 10 mM tributylamine, 15 mM acetic acid, 5 µM medronic acid), a 5.5-min gradient to 45% C and a 7-min gradient to 99% C at a flow rate of 0.25 mL min^{-1}. This was followed by a 4-min hold time at 100% mobile phase C. The column was restored by back-washing with 99% mobile phase D (90% ACN) for 3 min at 0.25 mL min^{-1}, followed by increase of the flow rate to 0.8mL min^{-1} over 0.5 min and a 3.85-min hold, after which the flow rate was decreased to 0.6mL min^{-1} over 0.15 min. The column was then re-equilibrated at 100% A over 0.75 min, during which the flow rate was decreased to 0.4mL min^{-1}, and held for 7.65 min. One minute before the next injection, the flow was brought back to forward flow at 0.25 mL min^{-1}. For all LC–MS analyses, 5µL of sample was injected. The column temperature was maintained at 35°C.

Seahorse XF96 respirometry assay

The Oxygen Consumption Rate (OCR) and Extracellular Acidification Rate (ECAR) were measured using a Mito Stress Test Kit and XF96 Extracellular Flux Analyzer (Seahorse Bioscience) according to the manufacturer's protocol. In brief, 96 well dishes were coated with CellTak at a concentration of 22.5μg/μl as per manufacturer's protocol and left at 4°C overnight. The day of measurement, cells were washed with XF base media supplemented with 10mM Glucose, 2mM Glutamine and 1mM Sodium Pyruvate (Wisent) and incubated for 1 hour to equilibrate prior to reading. ECAR and OCAR measurements were taken before and after the addition of oligomycin (1uM), FCCP (0.25μM) and Rotenone/Antimycin (1μM) and used to calculate ATP production, bioenergetic capacity and supply flexibility index as previously described [17].

Metabolic assays

Lactate and glucose concentrations were measured as previously described [18]. Briefly, 100k cells were plated and grown in 6-well dishes (35mm), incubated with fresh growth medium in the presence or absence of bortezomib and/or UK5099 for 48 hours prior to sample collection. Analysis of glucose consumption and lactate production was performed on the extracted media samples using the Nova BioProfile Analyzer 400 (Nova Biomedical) and normalized to cell number.

Proteasome activity

100,000 cells were plated in a 96 well dish and cultured for 24 hours prior to collection. Proteasomal-mediated degradation was evaluated using a 20S proteasome assay kit from Cayman Chemical according to the manufacturer's protocol and normalized to cell count.

Patient dataset analysis

The IA18 Release of CoMMpass data was downloaded from the MMRF researcher gateway portal (https://research.themmrf.org), which consists of 903 RNA sequencing data of baseline CD138+ plasma cell bone marrow samples from newly diagnosed MM patients. Among them, overall survival or progression-free survival information was available for 771 patients which were included in our analysis. Genes involved in pyruvate metabolism were incorporated into a multivariate Cox regression analysis (R-Studio) to generate a pyruvate metabolism gene signature.

The gene signature and patient survival data was organized via quartiles with the high pyruvate signature and low pyruvate signature plotted via Kaplan Meier (Prism).

Two other RNA-seq studies evaluating expression throughout MM development were retrieved from the Gene Expression Omnibus (GEO). Data of bone marrow-derived CD138+ plasma cells from 7 MGUS patients, 39 MM patients and 6 PCL patients were obtained from GSE2113. Data of bone marrow-derived CD138+ plasma cells from 15 normal donors, 22 MGUS patients, 17 smoldering MM patients, 69 MM patients and 32 relapsed MM patients were obtained from GSE6477. Expression was plotted based on the disease state.

Statistical analyses

All quantitative experiments are graphed with mean +/- SEM with data from the independent number of experiments in the figure legend. All data sets were tested for normal distribution by Shapiro-Wilk Test. Statistical significance was determined using the test indicated in the legend. All statistical analyses were performed in Prism v9 (Graphpad Software).

2.4 Results

CRISPR screening identifies MPC1 as a modulator of BTZ response in MM cells

To identify the factors that modulate BTZ response in MM cells, we employed two different human MM lines that recapitulate some of the cytogenetic heterogeneity observed in MM patients [2]: the U266 cell line is characterized by deletions in chromosome 13 and 17p, involving, *RB1* and *TP53* genes respectively [19], while the JJN3 cell line harbors an amplification of chromosome arm 1q21, which is a frequent chromosomal aberration in MM [20]. To ensure high genome editing capacity, we stably expressed Cas9 in both cell lines by lentiviral transduction (Fig.S2.1 A), while genome editing efficiency was confirmed by targeting FAM83G (Fig.S2.1 B).

Next, we performed CRISPR-based genome-wide screening in both human MM cell lines by transducing them with the TKO v1 sgRNA library [21], and selecting them with puromycin (Fig. 2.1 A). Both U266 and JJN3 transduced cell lines were subsequently treated with either BTZ IC_{25} or with vehicle (DMSO) for 21 days before being processed for next-generation sequencing (NGS) analysis. MaGECK algorithm was used to determine the relative abundance of a given sgRNA and identify genes whose knockout confers either resistance or sensitivity to BTZ (-0.2<β-score<0.2) [22]. In both cell lines, gene set enrichment analysis (GSEA) identified the proteasome core complex as significantly enriched in the sensitizing arm of both screens (Fig.S2.1 C). In fact, several subunits of the 20S proteasome (*PSMB1, PSMB4-6,* and *PSMB8)* sensitize to BTZ in both MM cell lines (Fig.2.1 B, Fig.S2.1 D), as previously shown [7, 8]. Similarly, pathway enrichment analysis identified several processes that have been described to modulate the response to proteasome inhibitors (Fig.S2.1 C) [8], including homologous recombination [23-25], cell cycle (reviewed in [26]), and RNA-mediated processes [8, 27, 28]. Collectively, these findings confirmed the validity of our CRISPR-based screening approach.

Taking into consideration the high heterogeneity of MM, we focused our attention on hits that increased sensitivity to BTZ in both U266 and JJN3 cell lines (-0.2<β-score; Fig.2.1 C). This analysis revealed 75 overlapping genes that scored highly in both screens, including the transcriptional factor *IRF4* (U266: β-score=-0.42358, JJN3: β-score=-0.3689; Fig. 2.1 D), which has been previously implicated in the response to BTZ (reviewed in [29]). To infer clinical relevance in our analysis, we examined their RNA expression using the multiple myeloma research

foundation (MMRF) CoMMpass database (n=921) [30]. Interestingly, the mitochondrial pyruvate carrier 1 (*MPC1)*, which encodes for a subunit of the MPC complex, scored as a top gene (Fig. 2.1 E). Of note, this complex was identified a decade ago [31, 32] but remains to be characterized in MM cells. In fact, our CRISPR-based approach identified several factors involved in pyruvate metabolism in at least one MM cell line (Fig.S2.1 C-D), including the other subunit of the MPC complex *MPC2* (U266: β-score=-0.14864) as well as the pyruvate dehydrogenase complex composed of *PDHA* (U266: β-score=-0.16121) and *PDHB* (U266: β-score=-0.19437, JJN3: β-score=-0.13871). These data suggest that pyruvate metabolism may play an important role in the response of MM cells to BTZ *in vitro*. Thus, we focused our attention on the role of mitochondrial pyruvate import and validated this hit using a CRISPR-based two-color competition assay (Fig.2.1 F) [33]. We targeted *MPC1* with three unique sgRNAs (sgMPC1-1, -2 and -3) coupled to BFP in U266 cells and used a sgRNA targeting LacZ (sgCtrl) coupled to mCherry as control. While targeting *MPC1* only modestly affected cell proliferation at steady state (DMSO, ~25%; Fig.2.1 G), it strongly sensitized U266 cells to BTZ (3nM) in this assay (~55%). Altogether, these data point towards an important contribution of MPC1 in the response of MM cells to BTZ *in vitro*.

Targeting the MPC complex exacerbates BTZ-induced MM cell death

MPC is a 150kDa complex composed of both MPC1 and MPC2, which transports pyruvate across the inner mitochondrial membrane (reviewed in [34]). To better understand how the MPC complex influences BTZ response in MM cells *in vitro*, we generated *MPC1* knockout clones (sgMPC1-1 and -2) in both JJN3 and U266 cells by CRISPR technology (Fig.S2.2 A-B). Interestingly, loss of MPC1 correlated with a drastic reduction in endogenous MPC2 protein levels (Fig.S2.2 B), highlighting the interdependent relationship between both MPC subunits [35]. First, we monitored the proliferative capacity of these clones and their respective cycle distribution, and we confirmed that *MPC1* deletion has limited impact on untreated MM cells (Fig.S2.2 C-D). Next, we measured clone viability by propidium iodide (PI) staining in presence of BTZ (4nM, 48hrs) or vehicle control. As expected, MPC1-deficient JJN3 and U266 clones display significantly higher levels of PI-positive cells upon exposure to BTZ (Fig.2.2 A). Coupling our PI analysis with annexin V staining, we observed a significant increase in the proportion on *MPC1* knock-out cells in late apoptosis upon BTZ treatment (Fig.2.2 B-C). We made similar observation using the

second-generation proteasome inhibitor CFZ (4nM, 48hrs; Fig.2.2 D), highlighting that MPC1 abrogation potentiates the effect of proteasome inhibitors in MM cells.

The MPC complex can be targeted by a series of inhibitors [36], including acyano-1-phenylindol-3-yl-acrylate, which specifically modifies a thiol group on the carrier (Fig.2.2 E). We took advantage of this drug to further characterize the link between the MPC complex and the response to proteasome inhibitors in MM cells. In this set of experiments, we tested a panel of both human (JJN3, U266, RPMI-8266, KMS-12-BM) and mouse (5TMG1) MM cell lines exposed to a sub-optimal dose of BTZ that, when applied alone, had limited effect on cell viability as monitored by PI staining (Fig.2.2 F). Of note, UK-5099 treatment alone did not cause any significant increase in the proportion of PI-positive cells in the MM cell lines tested (Fig.2.2 F). However, UK-5099 potentiated the effect of BTZ, whereby their combination significantly reduced MM cell viability *in vitro* (Fig.2.2 F). Importantly, combining UK-5099 to BTZ rapidly affected MM cell viability, peaking at 48hrs post-treatment relatively to each inhibitor alone (Fig.S2.2 F). Another surrogate method to monitor cell death relies on the presence of cells with fractional DNA content, designated as sub-G1 population [37]. The analysis of our cell cycle data revealed a more dramatic induction of sub-G1 population upon treatment with both BTZ and UK-5099 as compared to each single treatment (Fig.S2.2 G). Consistent with these data, annexin V/PI staining showed a significant increase in the proportion of early and/or late apoptotic cells upon exposure to both UK-5099 and a proteasome inhibitor (BTZ or CFZ) relative to vehicle controls (Fig.2.2 G-H, Fig.S2.2 H-I). Altogether, these data suggest that genetic or pharmacological targeting of the MPC complex enhances proteasome inhibitor-induced cell death in MM cells *in vitro*.

The MPC complex is required for bioenergetic capacity of MM cells under stress

To better understand the role of the MPC complex in MM cells, we analyzed the bioenergetic profiles of both JJN3 and U266 MM cell lines using the Seahorse bioanalyzer. Abrogation of MPC1 resulted in a decrease in both basal and maximal respiration rates as well as a reduced spare respiratory capacity (SPR) as compared to MPC1-proficient JJN3 and U266 controls (Fig.2.3 A-B). In turn, extracellular acidification rate (ECAR) measurement under mitochondrial stress showed a significant increase under basal conditions between *MPC1* knockout and control clones (Fig.2.3 C, Fig.S2.3 A). These data correlated with a rapid depletion of glucose and a significant

enrichment of lactate in the media of MPC1-deficient vs. -proficient JJN3 and U266 cells (Fig.2.3 D, Fig.S2.3 B), suggesting that abrogation of MPC1 results in increased glycolysis as a compensatory mechanism for the respiratory defects that we observed (Fig.2.3 A-B). Next, we quantified the effect of targeting MPC1 on maximal theoretical ATP production from oxidative phosphorylation (JATP(Ox)) and glycolysis (JATP(Glyc)) [17]. Consistent with these experiments, we noticed that MPC1 abrogation decreased JATP(Ox) (Fig.2.3 E-F). Albeit a concomitant increase in JATP(Glyc), MPC1 loss strongly impaired total cellular bioenergetic capacity (JATP(Ox) + JATP(Glyc)) (Fig.2.3 E-F). Altogether, these data indicate MPC1 plays a key role in the bioenergetic capacity of MM cells *in vitro*.

Targeting the MPC complex alters glutamine metabolism in MM cells

To better understand how mitochondrial pyruvate import enhances the response of MM cells to BTZ, we extended our metabolic analysis to the pharmacological inhibition of both pathways. Consistent with our genetic study, inhibiting the MPC complex with UK-5099 significantly impaired both basal and maximal respiration of U266 cells (Fig.2.4 A), which was accompanied by an increased glucose uptake and lactate secretion in the media (Fig.S2.4 A). In turn, BTZ only minimally affected basal respiration and maximal respiration capacity of U266 cells (Fig.2.4 A), with no significant changes in the levels of both glucose and lactate in the media as compared to vehicle treated controls (Fig.S2.4 B).

To further investigate whether metabolic perturbations could explain how MPC1 loss potentiates the cytotoxic effect of proteasome inhibitors, we performed a systematic liquid chromatography-tandem mass spectrometry (LC-MS)-based metabolomic profiling. As expected, we observed a significant accumulation of intracellular pyruvate in U266 cells treated with UK-5099 in presence or absence of BTZ, with a concomitant decrease in tricarboxylic acid (TCA) cycle intermediates, such as citric acid/isocitrate, cis-aconitic acid, α-ketoglutarate (α -KG) or 2-hydroxyglutaric acid (Fig.2.4 B-C, Fig.S2.4 C). Inhibition of the MPC complex and subsequent reduction in mitochondrial pyruvate import is known to induce to glutamine anaplerosis into the TCA cycle [38]. Inversely, proteasome inhibition has been shown to downregulate glutaminases [39], thereby suggesting that combinatorial targeting may simultaneously reduce mitochondrial pyruvate import and glutaminolysis. We therefore explored the impact of combining both UK-5099 with BTZ on glutamine intermediates by LC-MS. Strikingly, inhibiting both the MPC

complex and the proteasome resulted in a significant alteration of glutamine metabolism marked by a depletion of glutamine and N-Ethylmaleimide (NEM)-glutathione (Fig.2.4 D, Fig.S2.4 D). Altogether, these data highlight the critical role of glutamine anaplerosis for the survival of MM cells to both metabolic and proteolytic stresses.

Previous work has shown that glutamine starvation inhibits the proteolytic activity of the ubiquitin-proteasome in monocytes [40]. Thus, we wondered whether the underlining metabolic rewiring caused by the lack of mitochondrial pyruvate import may indirectly impair proteasomal activity in MM cells. As predicted, we observed a significant reduction in the 20S proteasomal activity of *MPC1* knock-out vs. control U266 cells (Fig.2.4 E), which is further exacerbated by the addition of BTZ. In line with these findings, we noted that the pharmacological inhibition of the MPC complex in combination with a sub-optimal dose of BTZ (4nM) further inhibits the proteolytic activity of U266 cells compared to monotherapy (Fig.2.4 F). These data suggest that the inhibition of mitochondrial pyruvate import impairs proteasomal activity of MM cells, thereby potentiating BTZ-induced cell death.

Pyruvate metabolism has prognostic potential for the survival of MM patients

To investigate the clinical relevance of our findings, we utilized two distinct cohorts of MM patients (GSE6477; GSE2113) where transcriptomic analysis was performed in early and late stages of the disease (Fig.S2.5 A) and focused our attention on the expression of genes involved in pyruvate metabolism. Interestingly, several regulators of pyruvate metabolism (Fig.2.5 A), including *MPC1*, *LDHB* and *DLAT*, were differently expressed between monoclonal gammopathy of undetermined significance (MGUS) and naïve or relapsed MM in the first cohort of patients (GSE6477, Fig.2.5 B). We made similar observations in an independent cohort of patients between MGUS, MM and a more aggressive stage of MM, plasma cell leukemia (PCL) (GSE2113, Fig.S2.5 B), suggestive of a transcriptionally driven metabolic rewiring of MM cells during the course of this disease.

We extended our analysis to the MMRF CoMMpass database (n=921), where the majority of patients have been treated with proteasome inhibitor-based regimen and investigated the prognostic potential of pyruvate metabolism on patient outcome. Strikingly, high expression of our pyruvate metabolic signature correlated with a significantly poorer overall survival of MM patients (median, $p<0.0001$; Fig.2.5 C). Moreover, high expressors of this pyruvate metabolic

signature display a significantly poorer progression-free survival (median, $p<0.0001$; Fig.2.5 C). Altogether, these data highlight the importance of pyruvate metabolism in the pathobiology of MM, delineating it as a potential prognostic biomarker for MM patients.

2.5 Discussion

Over the past two decades, proteasome inhibitors have revolutionized the treatment of MM patients by using the heightened dependency of MM cells on the protein quality control pathway as a therapeutic target [2]. Problematically, MM cells can acquire resistance to proteasome inhibitors through both genetic and non-genetic mechanisms [41], highlighting our knowledge gap on the biological pathways that influence the clinical effectiveness of this class of drugs. Previous studies have endeavoured to map the genetic dependencies of MM cells in response to proteasome inhibitors using RNA interference technology [4, 6, 7]. Here, we developed a high-throughput approach that utilizes the CRISPR technology to systematically interrogate the factors that influence the response of MM cells to BTZ *in vitro*, allowing the identification of a restricted number of novel modulators of proteasome inhibitors [5].

As expected, our pipeline showed that targeting subunits of the 19S proteasome, including PSMC5, PSMD5 and PSMD7, protect MM cells from proteasome inhibitors, as previously described [6, 42]. In turn, loss of a functional 20S proteasome further sensitizes MM cells to BTZ *in vitro,* highlighting the opposing effects of the catalytic core and the regulatory subunits of the proteasome on the response to proteasome inhibitors [6]. Our approach identified additional MM specific dependencies, including the transcriptional factor IRF4 (reviewed in [29] Previous work has described the addiction of MM cells toward this transcription factor and its associated regulatory network [43], and analysis of BTZ resistance in blood cancer lines correlated with an increased expression of IRF4 [44], in line with our findings that loss of IRF4 sensitize MM cells to proteasome inhibitors. Of interest to this study, we noticed that a series of genes linked to mitochondrial metabolism potentiates the efficacy of BTZ in at least one MM cell line, including the NADH dehydrogenase NDUFA7 alongside the pyruvate kinase PKM, both subunits of the pyruvate dehydrogenase complex, PDHA and PDHB, and both subunits of the MPC complex, highlighting the critical contribution of mitochondrial metabolism in the response to proteasome inhibitors [12].

After decades of research on mitochondrial pyruvate metabolism, the recent identification of the molecular components that form the mitochondrial pyruvate carrier (e.g. MPC1 and MPC2) revolutionized this research area. In-depth analysis of this complex has suggested that MPC1 is critical for the stability of MPC2 protein [35], an observation that we confirmed in our MPC1 knock-out MM cell lines. Rather than identifying the sole contribution of MPC1 in MM cells, our

study characterized the global contribution of the MPC complex in this subset of hematological malignancies. Not surprisingly, our findings are in line with previous reports, which described the central role of the MPC complex in the bioenergetic capacities of both normal and cancerous cells [45-48]. More importantly, our study highlights the importance of glutaminolysis as alternative energy source in response to impaired mitochondrial pyruvate transport, which was initially observed in glioma cells [38]. Glutamine is considered the most abundant amino acid in the blood [49], and could therefore be a critical energy supply for the maintenance of MM cell and their survival in response to proteasome inhibitors [13, 50].

Proteasome inhibition has been shown to act through multiple mechanisms to induce cell death, including the activation of the unfolded protein response, the inhibition of the NF-κB pathway and the induction of apoptosis through JNK and p53 [51]. However, it remains largely unexplored how proteasome inhibitors may influence the metabolism of MM cells and indirectly compromise their survival. Proteasome activity has been shown to regulate T lymphocyte metabolism and cell fate [52], while proteasome inhibitors, through the modulation of c-myc levels, have been demonstrated to affect glutamine metabolism in renal cell carcinoma [39]. In turn, work in monocytes has pointed towards a direct link between glutaminolysis and proteasome activity [40]. Our data suggest that the efficacy of proteasome inhibitors may be linked to the bioenergetic state of MM cells and their ability to induce a metabolic rewiring toward glutamine metabolism.

Altogether our study defines mitochondrial pyruvate transport as a novel modulator of proteasome inhibitors in MM cells, thereby providing a rational for the targeting of this metabolic pathway in the treatment of this hematological malignancy. Importantly, our findings delineate potential resistance mechanisms, including metabolic rewiring towards glutaminolysis, as potential compensatory pathways to consider in the therapeutic evaluation of MPC inhibitors.

Acknowledgments

We are grateful to Josie Ursini Siegel, Eric B. Taylor, Melissa Bates and Michael Tomasson for providing insightful suggestions on that project and useful reagents. We thank Dr. Daina Avizonis and the metabolomics core facility at McGill University which is supported by the Canada Foundation for Innovation, The Dr. John R. and Clara M. Fraser Memorial Trust, the Terry Fox Foundation (TFF Oncometabolism Team Grant; TFF-242122) and McGill University. SF is a recipient of a Cole Foundation doctoral scholarship. IT is supported by Fonds de Recherche du Québec-Santé (FRQS) Senior Investigator award and his lab is supported by Terry Fox Foundation (TFF) Oncometabolism Team Grant TFF-242122. LH is supported by Fonds de Recherche du Québec-Santé (FRQS) Senior Investigator award and her lab is supported by a Transition Grant from the Cole Foundation and an internal Operating Fund from the Hôpital Maisonneuve-Rosemont Foundation. AO is the Canada Research Chair Tier 2 in genome stability and haematological malignancies. Work in the AO laboratory was supported by a CIHR Project Grant (#376245), a Transition Grant from the Cole Foundation and an internal Operating Fund from the Sir Mortimer B. Davis Foundation of the Jewish General Hospital.

Author Contributions

SF designed and completed all the experiments presented in this manuscript, analyzed all the data and helped in the writing of the manuscript. ZK, AC, ZA, and JH under the supervision of SF helped in the generation of reagents necessary for the experiments presented in this manuscript. CST, under the supervision of JST, and DP, under the supervision of IT, helped in the optimization of the Seahorse assay. MS helped in the analysis of patient data. LH helped in the analysis of the metabolomic profiling by LC-MS. AO conceived the study, designed the research, provided supervision, and wrote the manuscript with input from all the other authors.

Conflict of Interest

The authors declare that they have no conflict of interest.

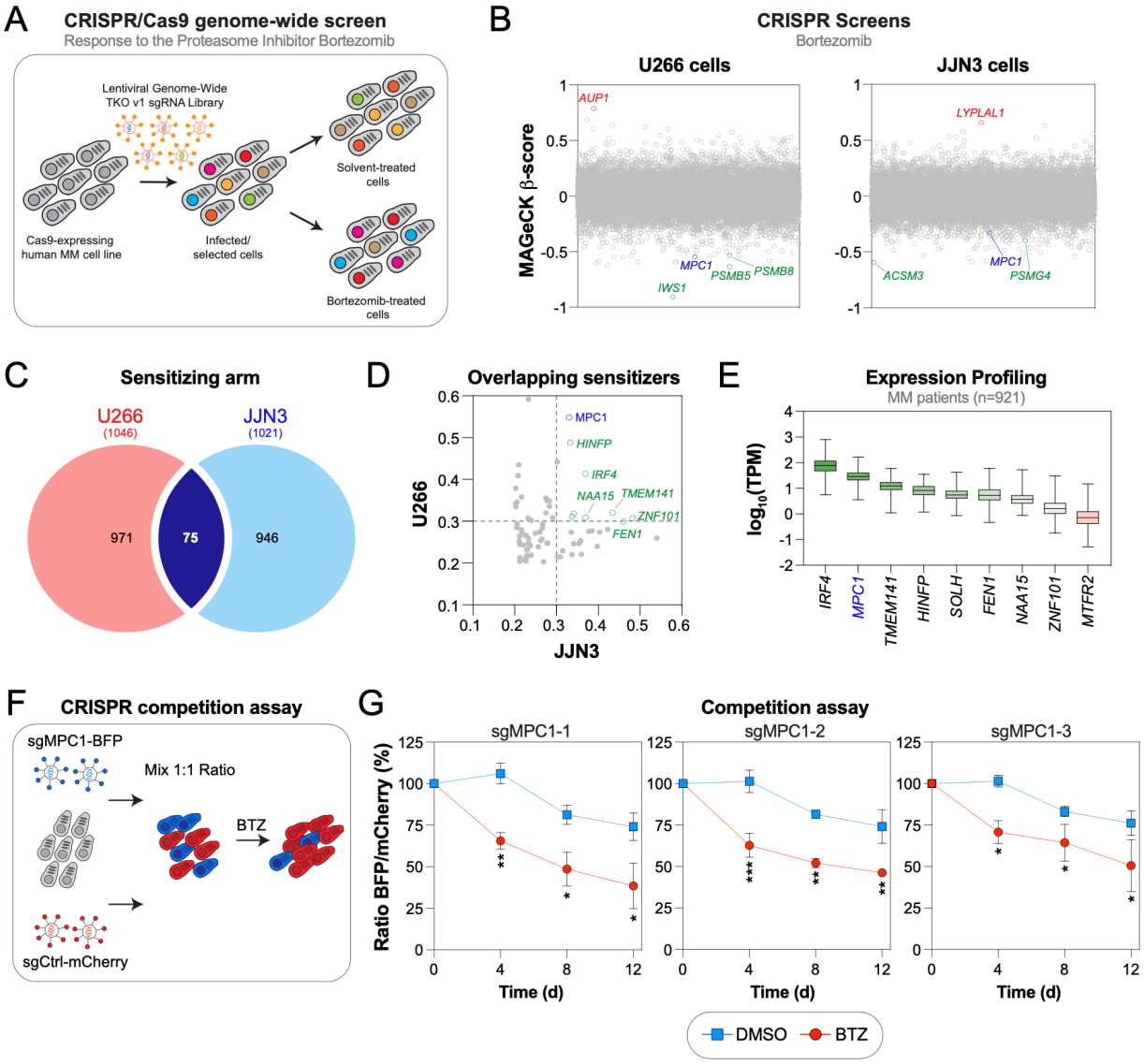

Figure 2.1 CRISPR screening identifies MPC1 as a modulator of BTZ response in MM cells.

(A) Schematic of our CRISPR-based genome-wide screening pipeline developed in MM cells.

(B) Representation of the CRISPR-based dropout screen performed in U266 and JJN3 cells in presence of BTZ (IC_{25}). Genes are represented in alphabetically order with their respective MAGeCK β-score.

(C) Overlapping genes from U266 and JJN3 sensitizing arms (MAGeCK β-score ≤ -0.2).

(D) Representation of the overlapping sensitizers identified in (C) with their respective MAGeCK β-score in x- (JJN3 cell line) and x-axis (U266 cell line).

(E) Expression analysis of the 75 overlapping sensitizers in the MMRF CoMMpass database (*n=921*). The top 9 most expressed genes are represented in this panel.

(F) Competitive growth assay ± BTZ (3nM) or DMSO (vehicle) in U266 cells. Data are represented as the ratio of BFP:mCherry positive cells ± SEM, normalized to day 0 (three different sgRNAs; *n=3*). Significance was determined by two-way ANOVA followed by a Sidak's test. *$P \leq 0.05$, **$P \leq 0.01$, ***$P \leq 0.005$.

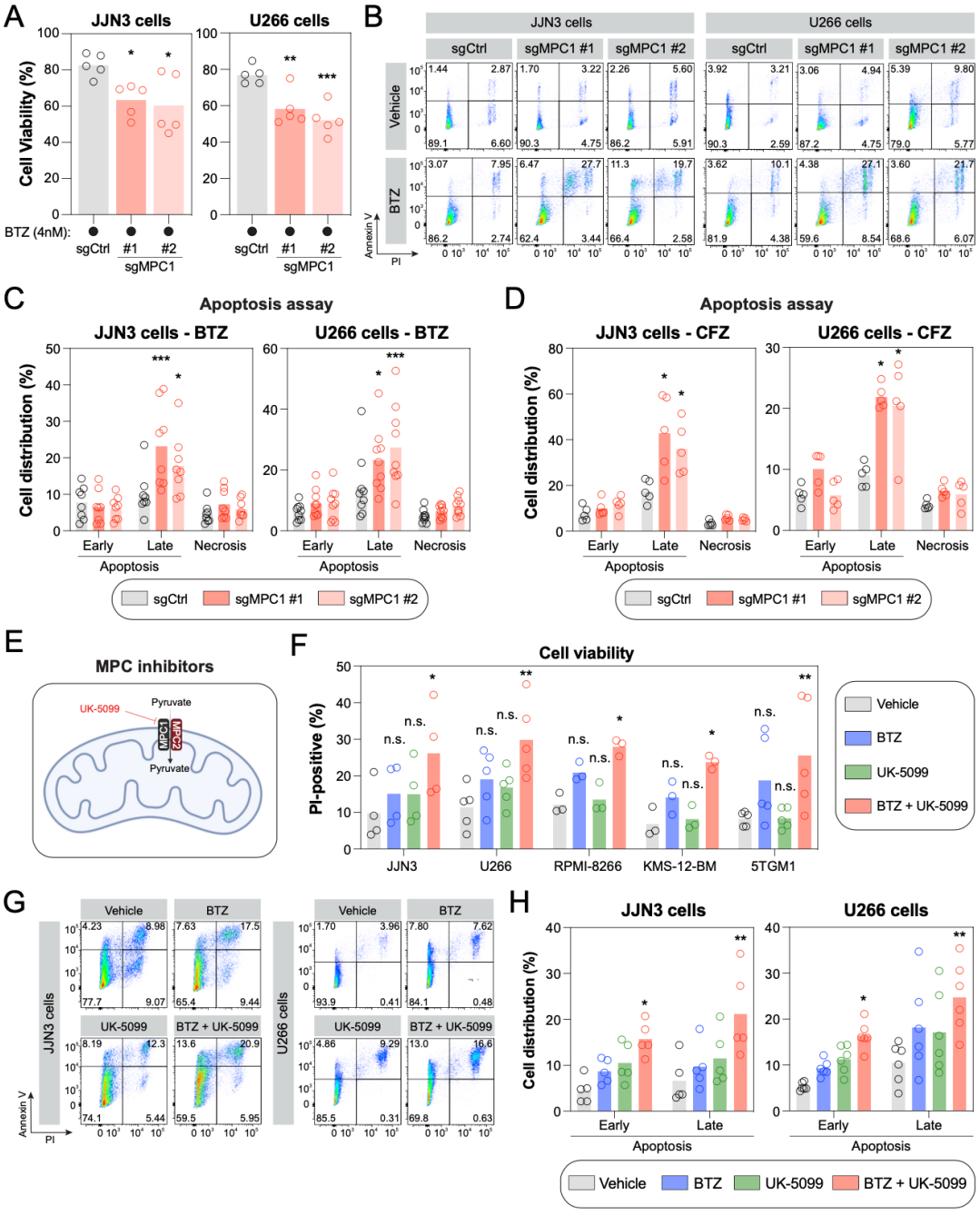

Figure 2.2 Targeting the MPC complex exacerbates BTZ-induced apoptosis of MM cells.

(A) JJN3 and U266 cells were treated with indicated concentrations of BTZ for 48 h, followed by an assessment of cell viability via PI staining (*n*=5). Significance was determined by one-way ANOVA followed by a Dunnett's test. *$P \leq 0.05$, **$P \leq 0.005$, ***$P \leq 0.005$.

(B) Representative flow cytometry analysis of JJN3 and U266 cells treated with either DMSO or BTZ (4nM) for 48 h and stained with Annexin V/PI.

(C) Representation of our Annexin V/PI analysis displayed in (B) for both JJN3 (n=8) and U266 cells (*n=9*). Significance was determined by two-way ANOVA followed by a Dunnett's test. **P≤0.05, ***P<0.0001.*

(D) Similar to (C), except that BTZ was replaced by CFZ for both JJN3 (*n=5*) and U266 cells (*n=5*). Significance was determined by two-way ANOVA followed by a Dunnett's test. **P≤0.0005.*

(E) Schematic representing UK-5099 inhibiting pyruvate entry into the mitochondrial matrix via MPC1 and MPC2.

(F) JJN3 (n=4), U266 (n=5), RPMI-8266 (n=3), KMS-12-BM (n=3) and 5TGM1 cells (n=5) were treated with BTZ (3nM) and UK-5099 (10μM) for 48 h, followed by an assessment of cell viability via PI. Significance was determined by two-way ANOVA followed by a Dunnett's test. **P≤0.05, **P≤0.005.*

(G) Representative flow cytometry analysis of JJN3 and U266 cells treated with either BTZ (3nM) and UK-5099 (10μM) for 48 h and stained with Annexin V/PI.

(H) Representation of our Annexin V/PI analysis displayed in (G) for both JJN3 (*n=5*) and U266 cells (*n=6*). Significance was determined by two-way ANOVA followed by a Dunnett's test. **P≤0.05, **P≤0.005.*

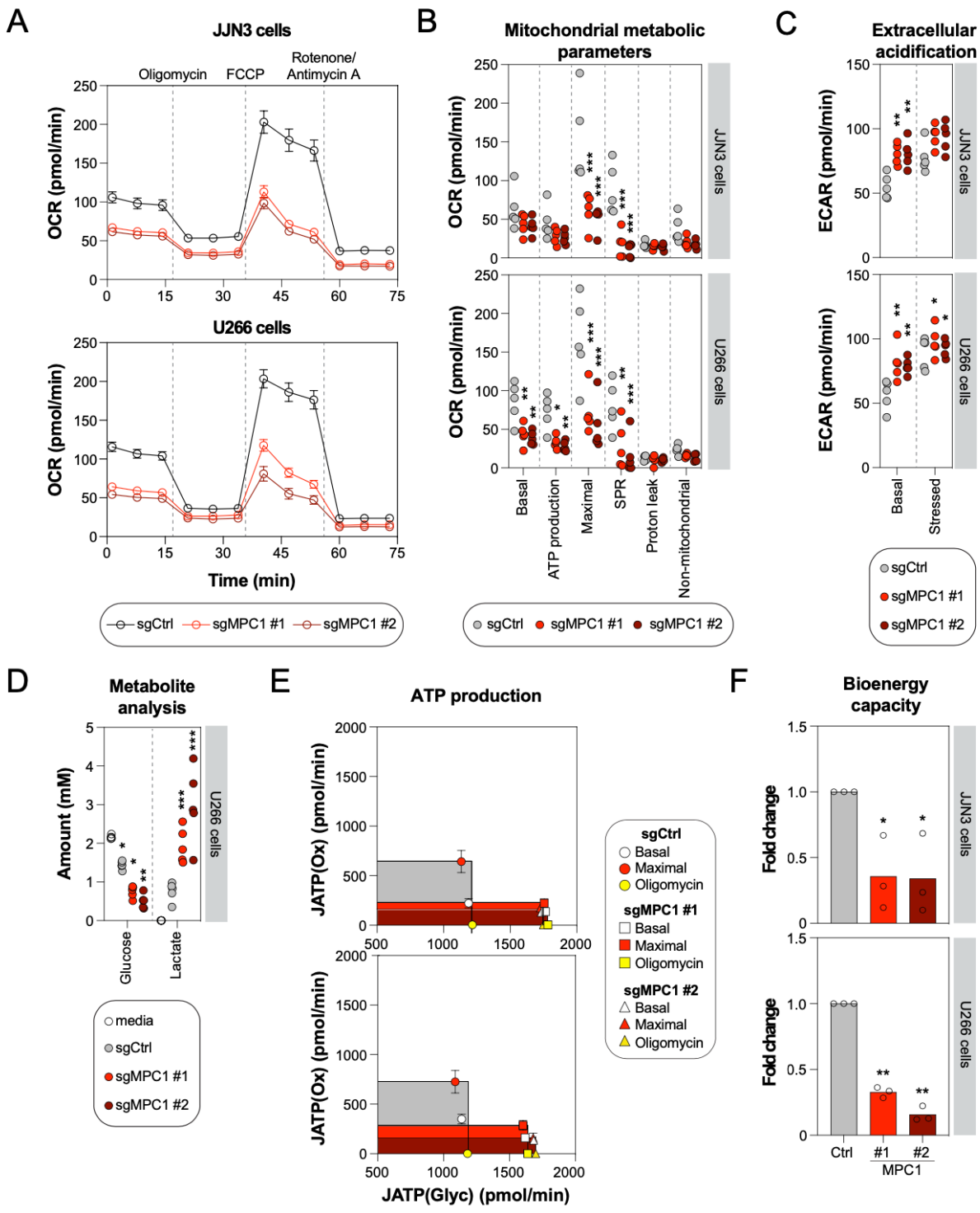

Figure 2.3 The MPC complex is required for bioenergetic capacity of MM cells.

(A) Oxygen consumption rate (OCR) monitored by the Seahorse XF96 Extracellular Flux Analyzer in JJN3 and U266 cells (*n*=*5*).

(B) Analysis of the different mitochondrial metabolic parameters obtained from the OCR in (A). Significance was determined by two-way ANOVA followed by a Dunnett's test. *$P \leq 0.05$, **$P \leq 0.005$, ***$P < 0.0001$.

(C) Quantification of basal ECAR and stressed ECAR in JJN3 and U266 cells ($n=5$). Significance was determined by two-way ANOVA followed by a Dunnett's test. *$P \leq 0.05$, **$P \leq 0.005$.

(D) Media metabolite analysis of U266 cells with a focus on extracellular glucose and lactate ($n=5$). Significance was determined by two-way ANOVA followed by a Dunnett's test. *$P \leq 0.05$, **$P \leq 0.005$, ***$P < 0.0001$.

(E) The metabolic capacity and flexibility of cells were represented by plotting the basal, oligomycin treated and maximal rates of ATP production from glycolysis (J_{ATP} gly) and oxidative phosphorylation (J_{ATP} ox), upon MPC1 knock-out ($n=5$).

Fold change in the bioenergetic capacity and of cells described in (A) ($n=5$). Significance was determined by two-way ANOVA followed by a Dunnett's test. *$P \leq 0.05$.

(F) Fold change in the bioenergetic capacity and of cells described in (A) ($n=5$). Significance was determined by two-way ANOVA followed by a Dunnett's test. *$P \leq 0.05$.

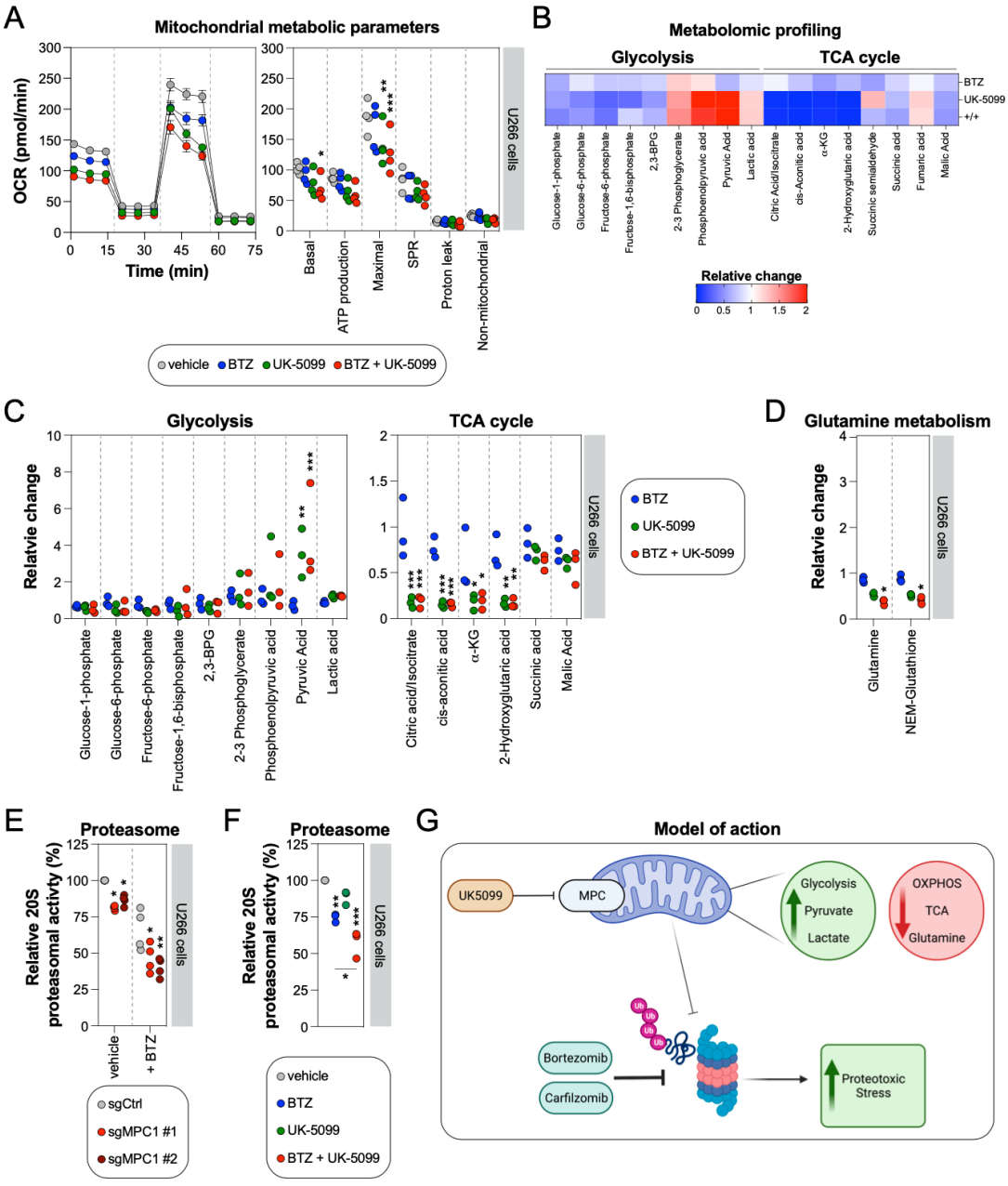

Figure 2.4 Lack of mitochondrial pyruvate import alters glutamine metabolism and BTZ-driven proteasomal inhibition in MM cells.

(A) OCR plot and metabolic parameters of U266 cells treated with the indicated drugs. Significance was determined by two-way ANOVA followed by a Dunnett's test. *$P \leq 0.05$, **$P \leq 0.005$, ***$P < 0.0001$.

(B) LC-MS results of glycolysis and the TCA cycle of mono- and combinatorial therapies relative to vehicle control U266 cells ($n=3$).

(C) Representation of data shown in (B). Significance was determined by two-way ANOVA followed by a Dunnett's test. *$P \leq 0.05$, **$P \leq 0.005$, ***$P < 0.0001$.

(D) Representation of LC-MS data presented in (B) with a focus on glutamine metabolism. Significance was determined by two-way ANOVA followed by a Dunnett's test. *$P \leq 0.05$, **$P \leq 0.005$, ***$P < 0.0001$.

(E) Chymotrypsin-like proteasome activity was monitored in control (sgCtrl) or MPC1 knock-out (sgMPC1 #1 and #2) U266 cells in presence or absence (vehicle) of BTZ (3nM) ($n=3$). Significance was determined by two-way ANOVA followed by a Dunnett's test. *$P \leq 0.05$, **$P \leq 0.005$.

(F) Similar as in (E), except that U266 cells were treated with either vehicle, BTZ (3nM), UK-5099 (10μM) or the combination ($n=3$). Significance was determined by two-way ANOVA followed by a Dunnett's test. *$P \leq 0.05$, **$P \leq 0.005$, ***$P < 0.0001$.

(G) Schematic representing link between the mitochondrial pyruvate carrier complex, the metabolic rewiring induced its inhibition, and the proteasomal capacity of MM cells.

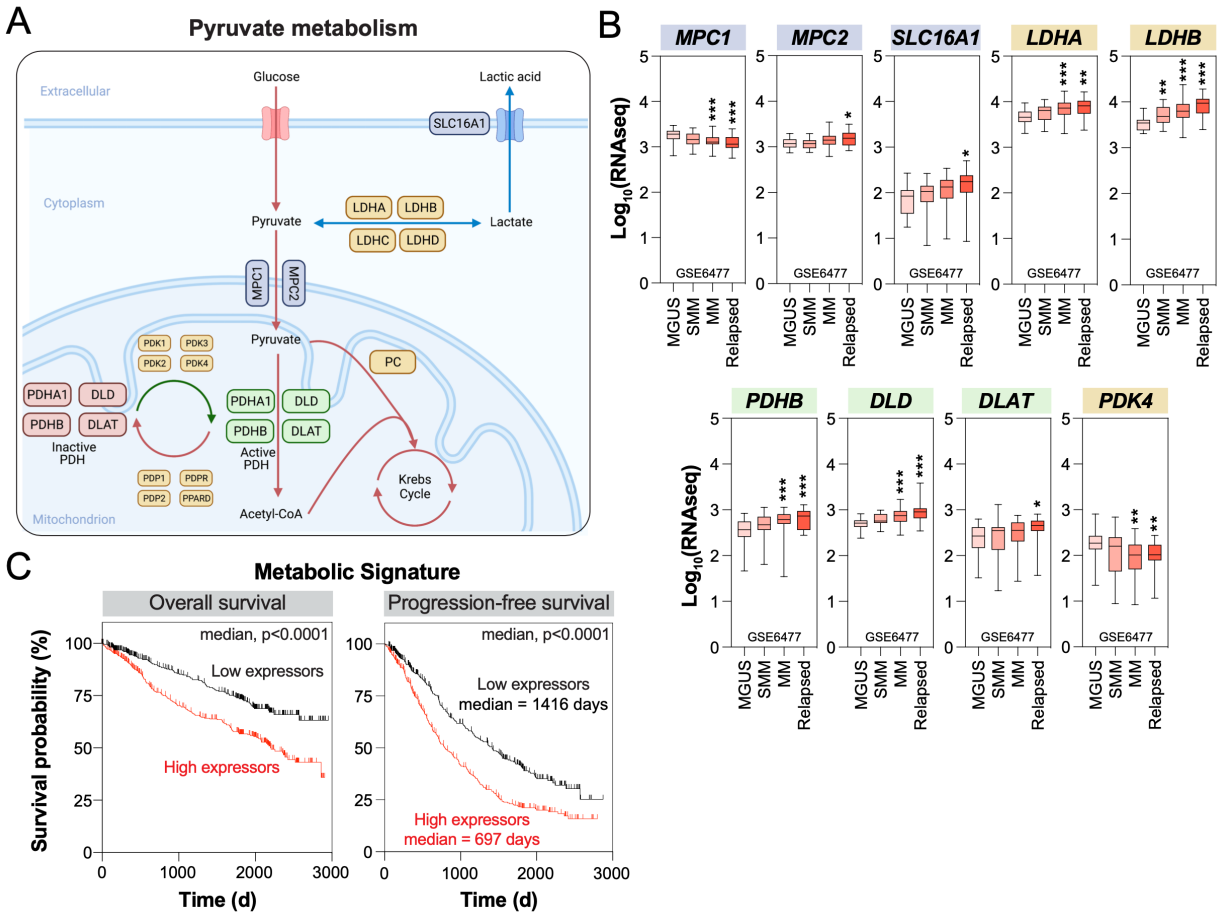

Figure 2.5 Pyruvate metabolism has prognostic potential for MM patients.

(A) Schematic representation of pyruvate metabolism and its molecular components.

(B) Expression profiling of genes related to pyruvate metabolism at different stages of MM: monoclonal gammopathy of undetermined significance (MGUS) (*n=22*), smoldering multiple myeloma (SMM) (*n=24*), MM (*n=73*) and relapsed MM (*n=28*). Significance was determined by two-way ANOVA followed by a Dunnett's test. *$P \leq 0.05$, **$P \leq 0.005$, ***$P < 0.0001$.

(C) The X-axis represents the survival time (days) while the Y-axis represents survival probability (left panel) and progression free survival (right panel). The survival analysis of OS and PFS in pyruvate metabolism^{high} and pyruvate metabolism^{low} groups of 772 MM patients in the MMRF database. Significance was determined by Gehan-Breslow-Wilcoxon test.

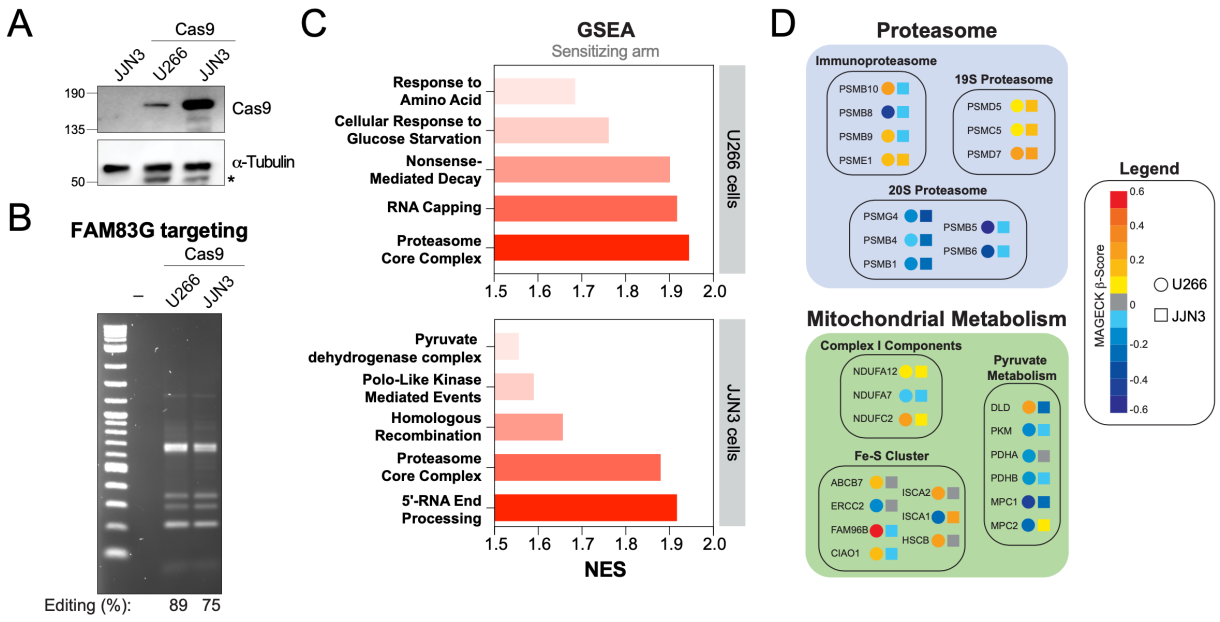

Supplemental Figure 2.1 CRISPR-based genome-wide screen analysis of BTZ-treated MM cells.

(A) Immunoblot of U266 and JJN3 cell lines infected with lentiviral Cas9 constructs. α-tubulin was used as a loading control.

(B) Gel electrophoresis depicting genome editing efficiency at the FAM83G locus in both U266 and JJN3 cell lines.

(C) GSEA profiling of JJN3 and U266 sensitizing arms.

(D) Bubble plot of proteasomal and mitochondrial metabolic genes and their scores (blue-sensitive; red-resistant) in both U266 (circle) and JJN3 (square) genome-wide CRISPR screens.

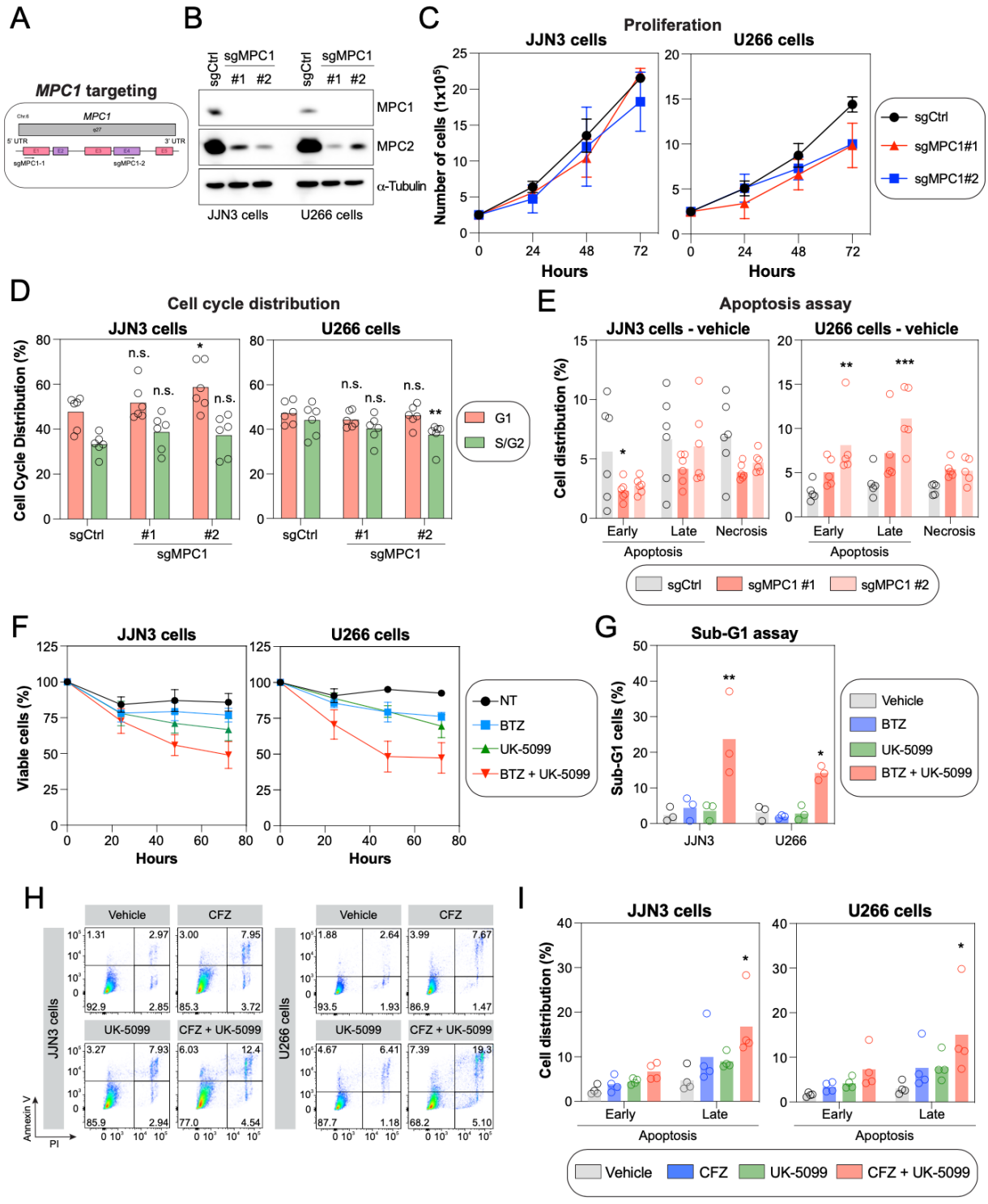

Supplemental Figure 2.2 Characterization of MPC1-deficient MM cells.

(A) Schematic depicting the exons targeted by each MPC1 sgRNA.

(B) Immunoblot of both JJN3 and U266 sub-clones obtained after stable integration of sgCtrl and sgMPC1 #1 and #2. α-tubulin was used as a loading control.

(C) Proliferation of MM cell lines from (B) via trypan blue staining and counting via hemocytometer (*n=3)*.

(D) Cell cycle distribution of the indicated cell lines via PI staining and flow cytometry (*n=6*).

(E) Apoptosis via annexin V/PI staining of the indicated MM cell lines at steady state (*n=6*).

(F) Cell viability of JJN3 (left) and U266 (right) under treatment with BTZ and/or UK-5099 assessed via trypan blue staining and hemocytometer counting (*n=3*).

(G) Sub-G1 population of the indicated MM cells treated with BTZ and/or UK-5099 for 48hrs (*n=3*).

(H) Representative flow cytometry analysis of JJN3 and U266 cells treated with either DMSO, CFZ and/or UK-5099 for 48 h and stained with Annexin V/PI.

(I) Apoptosis of MM cells treated with CFZ and/or UK-5099 for 48hrs via annexin V/PI staining(*n=4*).

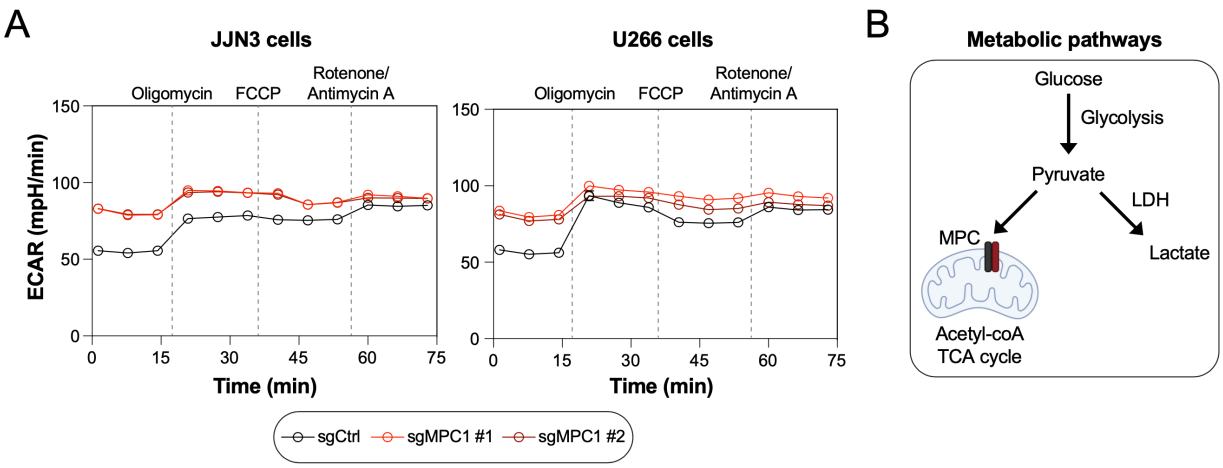

Supplemental Figure 2.3 Impact of MPC1 depletion on ECAR and OCR.

(A) Extracellular acidification rate of JJN3 and U266 cell lines with sgCtrl or sgMPC1 (*n=5*).

(B) Simplified schematic of pyruvate fate in the cytosol.

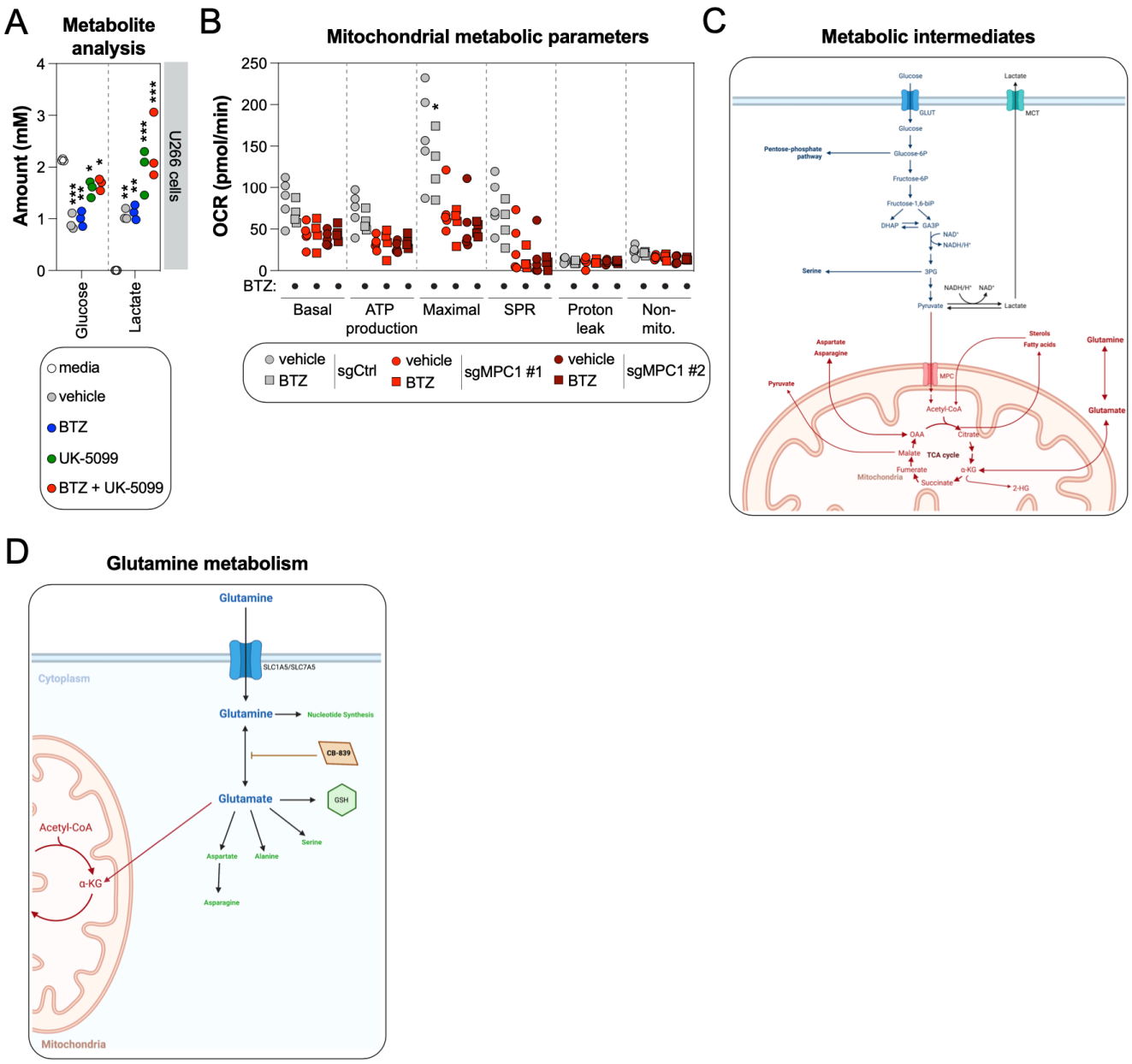

Supplemental Figure 2.4 Loss of MPC1 alters glutaminolysis.

(A) Extracellular metabolite levels in media containing U266 cells after 24 h of treatment with BTZ and/or UK-5099 ($n = 3$).

(B) Mitochondrial metabolic parameters of sgMPC1 U266 cells treated with BTZ (3nM) or DMSO for 24 hrs ($n=5$).

(C) Schematic of glycolysis and the TCA cycle with glutamine supplementation.

(D) Schematic representing glutamine metabolism.

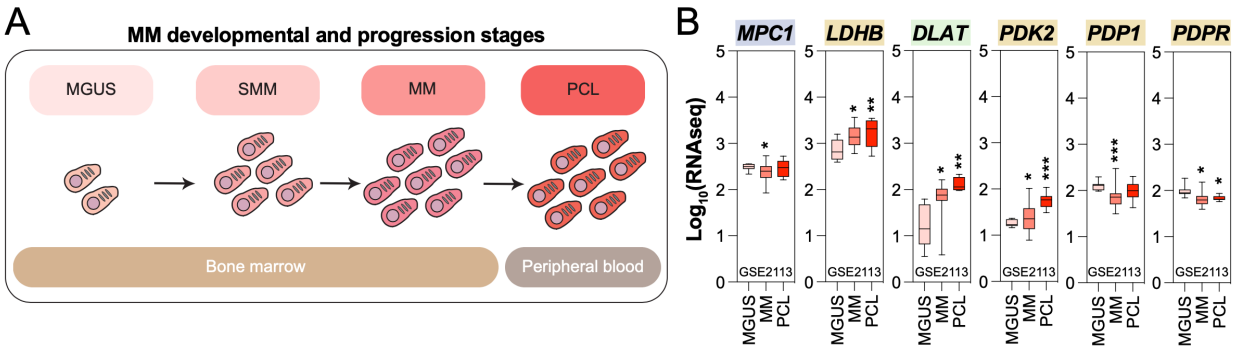

Supplemental Figure 2.5 Pyruvate metabolism expression in MM development

(A) Schematic representing the different stages of MM: monoclonal gammopathy of undetermined significance (MGUS), smoldering multiple myeloma (SMM), multiple myeloma (MM), and plasma cell leukemia (PCL).

(B) Expression profiling of genes related to pyruvate metabolism at different stages of MM in the GSE2113 dataset: MGUS (*n=6*), MM (*n=20*), and PCL (*n=5)*. Significance was determined by two-way ANOVA followed by a Dunnett's test. *$P \leq 0.05$, **$P \leq 0.005$, ***$P < 0.0001$.

2.6 Reference

1. Padala, S.A., et al., *Epidemiology, Staging, and Management of Multiple Myeloma.* Med Sci (Basel), 2021. **9**(1).
2. Gulla, A. and K.C. Anderson, *Multiple myeloma: the (r)evolution of current therapy and a glance into future.* Haematologica, 2020. **105**(10): p. 2358-2367.
3. Bazarbachi, A.H., et al., *Relapsed refractory multiple myeloma: a comprehensive overview.* Leukemia, 2019. **33**(10): p. 2343-2357.
4. Zhu, Y.X., et al., *RNAi screen of the druggable genome identifies modulators of proteasome inhibitor sensitivity in myeloma including CDK5.* Blood, 2011. **117**(14): p. 3847-57.
5. Shi, C.X., et al., *CRISPR Genome-Wide Screening Identifies Dependence on the Proteasome Subunit PSMC6 for Bortezomib Sensitivity in Multiple Myeloma.* Mol Cancer Ther, 2017. **16**(12): p. 2862-2870.
6. Acosta-Alvear, D., et al., *Paradoxical resistance of multiple myeloma to proteasome inhibitors by decreased levels of 19S proteasomal subunits.* Elife, 2015. **4**: p. e08153.
7. Chen, S., et al., *Genome-wide siRNA screen for modulators of cell death induced by proteasome inhibitor bortezomib.* Cancer Res, 2010. **70**(11): p. 4318-26.
8. Tiedemann, R.E., et al., *Identification of molecular vulnerabilities in human multiple myeloma cells by RNA interference lethality screening of the druggable genome.* Cancer Res, 2012. **72**(3): p. 757-68.
9. Maiso, P., et al., *Metabolic signature identifies novel targets for drug resistance in multiple myeloma.* Cancer Res, 2015. **75**(10): p. 2071-82.
10. Zaal, E.A., et al., *Bortezomib resistance in multiple myeloma is associated with increased serine synthesis.* Cancer Metab, 2017. **5**: p. 7.
11. Soriano, G.P., et al., *Proteasome inhibitor-adapted myeloma cells are largely independent from proteasome activity and show complex proteomic changes, in particular in redox and energy metabolism.* Leukemia, 2016. **30**(11): p. 2198-2207.
12. Besse, L., et al., *A metabolic switch in proteasome inhibitor-resistant multiple myeloma ensures higher mitochondrial metabolism, protein folding and sphingomyelin synthesis.* Haematologica, 2019. **104**(9): p. e415-e419.

13. Thompson, R.M., et al., *Glutaminase inhibitor CB-839 synergizes with carfilzomib in resistant multiple myeloma cells.* Oncotarget, 2017. **8**(22): p. 35863-35876.
14. Riz, I., et al., *Noncanonical SQSTM1/p62-Nrf2 pathway activation mediates proteasome inhibitor resistance in multiple myeloma cells via redox, metabolic and translational reprogramming.* Oncotarget, 2016. **7**(41): p. 66360-66385.
15. Ortiz-Ruiz, A., et al., *Myc-Related Mitochondrial Activity as a Novel Target for Multiple Myeloma.* Cancers (Basel), 2021. **13**(7).
16. Findlay, S., et al., *SHLD2/FAM35A co-operates with REV7 to coordinate DNA double-strand break repair pathway choice.* EMBO J, 2018. **37**(18).
17. Mookerjee, S.A., et al., *Quantifying intracellular rates of glycolytic and oxidative ATP production and consumption using extracellular flux measurements.* J Biol Chem, 2017. **292**(17): p. 7189-7207.
18. Andrzejewski, S., et al., *PGC-1alpha Promotes Breast Cancer Metastasis and Confers Bioenergetic Flexibility against Metabolic Drugs.* Cell Metab, 2017. **26**(5): p. 778-787 e5.
19. Fernando, R.C., et al., *Multiple myeloma cell lines and primary tumors proteoma: protein biosynthesis and immune system as potential therapeutic targets.* Genes Cancer, 2015. **6**(11-12): p. 462-471.
20. Hanamura, I., *Gain/Amplification of Chromosome Arm 1q21 in Multiple Myeloma.* Cancers (Basel), 2021. **13**(2).
21. Hart, T., et al., *High-Resolution CRISPR Screens Reveal Fitness Genes and Genotype-Specific Cancer Liabilities.* Cell, 2015. **163**(6): p. 1515-26.
22. Li, W., et al., *MAGeCK enables robust identification of essential genes from genome-scale CRISPR/Cas9 knockout screens.* Genome Biol, 2014. **15**(12): p. 554.
23. Yarde, D.N., et al., *Targeting the Fanconi anemia/BRCA pathway circumvents drug resistance in multiple myeloma.* Cancer Res, 2009. **69**(24): p. 9367-75.
24. Murakawa, Y., et al., *Inhibitors of the proteasome suppress homologous DNA recombination in mammalian cells.* Cancer Res, 2007. **67**(18): p. 8536-43.
25. Jacquemont, C. and T. Taniguchi, *Proteasome function is required for DNA damage response and fanconi anemia pathway activation.* Cancer Res, 2007. **67**(15): p. 7395-405.

26. Maes, A., et al., *The therapeutic potential of cell cycle targeting in multiple myeloma.* Oncotarget, 2017. **8**(52): p. 90501-90520.
27. Zismanov, V., et al., *Multiple myeloma proteostasis can be targeted via translation initiation factor eIF4E.* Int J Oncol, 2015. **46**(2): p. 860-70.
28. Mancino, M., et al., *Cap dependent translation contributes to resistance of myeloma cells to bortezomib.* Translation (Austin), 2013. **1**(2): p. e27245.
29. Agnarelli, A., T. Chevassut, and E.J. Mancini, *IRF4 in multiple myeloma-Biology, disease and therapeutic target.* Leuk Res, 2018. **72**: p. 52-58.
30. Settino, M. and M. Cannataro, *Using MMRFBiolinks R-Package for Discovering Prognostic Markers in Multiple Myeloma.* Methods Mol Biol, 2022. **2401**: p. 289-314.
31. Bricker, D.K., et al., *A mitochondrial pyruvate carrier required for pyruvate uptake in yeast, Drosophila, and humans.* Science, 2012. **337**(6090): p. 96-100.
32. Herzig, S., et al., *Identification and functional expression of the mitochondrial pyruvate carrier.* Science, 2012. **337**(6090): p. 93-6.
33. Girish, V. and J.M. Sheltzer, *A CRISPR Competition Assay to Identify Cancer Genetic Dependencies.* Bio Protoc, 2020. **10**(14): p. e3682.
34. Ruiz-Iglesias, A. and S. Manes, *The Importance of Mitochondrial Pyruvate Carrier in Cancer Cell Metabolism and Tumorigenesis.* Cancers (Basel), 2021. **13**(7).
35. Oonthonpan, L., et al., *Two human patient mitochondrial pyruvate carrier mutations reveal distinct molecular mechanisms of dysfunction.* JCI Insight, 2019. **5**.
36. Tavoulari, S., et al., *Key features of inhibitor binding to the human mitochondrial pyruvate carrier hetero-dimer.* Mol Metab, 2022. **60**: p. 101469.
37. Plesca, D., S. Mazumder, and A. Almasan, *DNA damage response and apoptosis.* Methods Enzymol, 2008. **446**: p. 107-22.
38. Yang, C., et al., *Glutamine oxidation maintains the TCA cycle and cell survival during impaired mitochondrial pyruvate transport.* Mol Cell, 2014. **56**(3): p. 414-424.
39. Sourbier, C., et al., *Proteasome inhibition disrupts the metabolism of fumarate hydratase-deficient tumors by downregulating p62 and c-Myc.* Sci Rep, 2019. **9**(1): p. 18409.
40. Zellner, M., et al., *Glutamine starvation of monocytes inhibits the ubiquitin-proteasome proteolytic pathway.* Biochim Biophys Acta, 2003. **1638**(2): p. 138-48.

41. Gandolfi, S., et al., *The proteasome and proteasome inhibitors in multiple myeloma.* Cancer Metastasis Rev, 2017. **36**(4): p. 561-584.
42. Tsvetkov, P., et al., *Compromising the 19S proteasome complex protects cells from reduced flux through the proteasome.* Elife, 2015. **4**.
43. Shaffer, A.L., et al., *IRF4 addiction in multiple myeloma.* Nature, 2008. **454**(7201): p. 226-31.
44. Perez-Galan, P., et al., *Bortezomib resistance in mantle cell lymphoma is associated with plasmacytic differentiation.* Blood, 2011. **117**(2): p. 542-52.
45. Ramstead, A.G., et al., *Mitochondrial Pyruvate Carrier 1 Promotes Peripheral T Cell Homeostasis through Metabolic Regulation of Thymic Development.* Cell Rep, 2020. **30**(9): p. 2889-2899 e6.
46. Schell, J.C., et al., *A role for the mitochondrial pyruvate carrier as a repressor of the Warburg effect and colon cancer cell growth.* Mol Cell, 2014. **56**(3): p. 400-413.
47. Koh, E., et al., *MPC1 is essential for PGC-1alpha-induced mitochondrial respiration and biogenesis.* Biochem J, 2018. **475**(10): p. 1687-1699.
48. Rossi, A., et al., *Defective Mitochondrial Pyruvate Flux Affects Cell Bioenergetics in Alzheimer's Disease-Related Models.* Cell Rep, 2020. **30**(7): p. 2332-2348 e10.
49. Xi, P., et al., *Regulation of protein metabolism by glutamine: implications for nutrition and health.* Front Biosci (Landmark Ed), 2011. **16**(2): p. 578-97.
50. Effenberger, M., et al., *Glutaminase inhibition in multiple myeloma induces apoptosis via MYC degradation.* Oncotarget, 2017. **8**(49): p. 85858-85867.
51. Nunes, A.T. and C.M. Annunziata, *Proteasome inhibitors: structure and function.* Semin Oncol, 2017. **44**(6): p. 377-380.
52. Widjaja, C.E., et al., *Proteasome activity regulates CD8+ T lymphocyte metabolism and fate specification.* J Clin Invest, 2017. **127**(10): p. 3609-3623.

Chapter 3: SHLD2/FAM35A co-operates with REV7 to coordinate DNA double-strand break repair pathway choice

*Published in "*Steven Findlay*, John Heath*, Vincent M Luo, Abba Malina, Théo Morin, Yan Coulombe, Billel Djerir, Zhigang Li, Arash Samiei, Estelle Simo-Cheyou, Martin Karam, Halil Bagci, Dolev Rahat, Damien Grapton, Elise G Lavoie, Christian Dove, Husam Khaled, Hellen Kuasne, Koren K Mann, Kathleen Oros Klein, Celia M Greenwood, Yuval Tabach, Morag Park, Jean-Francois Côté, Jean-Yves Masson, Alexandre Maréchal and Alexandre Orthwein

Manuscript published: (2018) *EMBO J.* **37**(18)

3.1 Preface to the manuscript

In Chapter 2, we identified the MPC complex and pyruvate metabolism as a novel vulnerabilities that enhanced the cytotoxic effects of proteasome inhibitors, including bortezomib. Our data show that genetic disruption or pharmacological inhibition of the MPC complex potentiates the efficacy of proteasome inhibitors by increasing MM cell death. Furthermore, we show a metabolic re-wiring of MM cells upon MPC disruption favoring a glycolytic/glutaminolysis state with limited bioenergetic capacities and impaired proteasomal activity. Our data positions mitochondrial pyruvate metabolism as a potential prognostic marker for the outcome of MM patients and their responsiveness to proteasome inhibitors.

Proteasome inhibition has been shown to act through multiple mechanisms to induce cell death, including the activation of the unfolded protein response[1], the inhibition of the NF-κB pathway[2], the induction of apoptosis through JNK and p53[3] and disruption of DNA repair [4]. Proteasome inhibitors prevent the normal recycling of the limited pool of ubiquitin moieties leaving them trapped on residues in the cytosol. The depletion of free ubiquitin moieties has been shown to compromise the DNA damage response[5, 6] and several reports have demonstrated that proteasome inhibitors block the repair of DNA double-strand breaks[4, 7, 8]. Still, the landscape of DNA repair factors influencing the response of proteasome inhibitors in MM cells remains poorly understood.

The use of DNA damaging agents, such as melphalan, cyclophosphamide and doxorubicin, were a staple in the treatment of MM patients and is still used in combination with BTZ to treat some MM patients. Many believe that DNA repair proteins remain a logical target to further improve the efficacy of the combination therapy[9]. Despite the identification of several DNA repair proteins as prognostic marks in MM patient outcome[9, 10], investigation of other DNA alkylating agents and pharmacological disruption of repair components has had limited therapeutic success. For these reasons, it remains imperative to identify novel DNA repair proteins that could be therapeutically targeted in the future.

One of the top sensitizers of our genome-wide screen was a component of the Shieldin complex, SHLD1 (Fig. 3.1 A,B), and expression of both Shieldin components (SHLD1, SHLD2) are shown to correlate with the progression free and overall survival of MM patients. (Fig. 3.1 D). The impact on patient outcome was similar to that of other DNA repair factors including REV7 suggesting a

potential role in DNA repair. Our goal in chapter 3, was to investigate the role of the Shieldin complex in the DNA repair pathway. Using established DNA repair experimental procedures as well as mass spectrometry, we evaluated the impact of SHLD1 and SHLD2 depletion, overexpression and targeted mutation on DNA damage resolution, recruitment, and signaling.

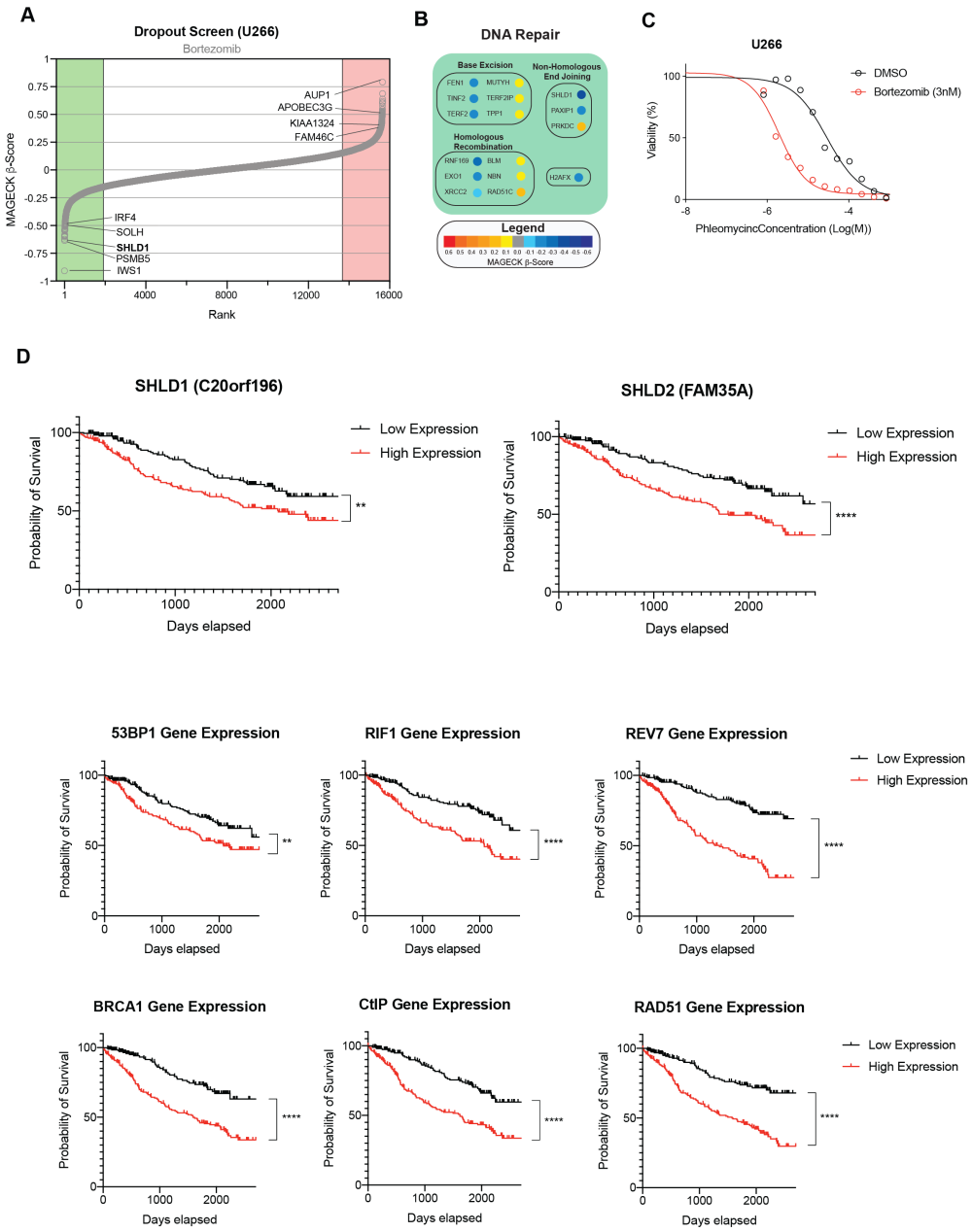

Figure 3.1 The Shieldin complex is a prognostic mark of bortezomib treatment efficacy in MM patients.

(A) Representation of the CRISPR-based dropout screen performed in U266 cells in presence of BTZ (IC_{25}). Genes are ranked based on their respective MAGeCK β-score.

(B) Bubble plot of DNA BER, HR and NHEJ genes and their scores (blue-sensitive; red-resistant) in the U266 genome-wide CRISPR screen.

(C) IC_{50} phleomycin drug sensitivity of U266 cells with and without bortezomib treatment.

(D) The X-axis represents the survival time (days) while the Y-axis represents survival probability. The survival analysis of OS in relation to high and low expression of Shieldin components and other HR and NHEJ factors of 772 MM patients in the MMRF database. Significance was determined by Gehan-Breslow-Wilcoxon test.

3.2 Abstract

DNA double-strand breaks (DSBs) can be repaired by two major pathways: non-homologous end-joining (NHEJ) and homologous recombination (HR). DNA repair pathway choice is governed by the opposing activities of 53BP1, in complex with its effectors RIF1 and REV7, and BRCA1. However, it remains unknown how the 53BP1/RIF1/REV7 complex stimulates NHEJ and restricts HR to the S/G2 phases of the cell cycle. Using a mass spectrometry (MS)-based approach, we identify 11 high-confidence REV7 interactors and elucidate the role of SHLD2 (previously annotated as FAM35A and RINN2) as an effector of REV7 in the NHEJ pathway. FAM35A depletion impairs NHEJ-mediated DNA repair and compromises antibody diversification by class switch recombination (CSR) in B-cells. FAM35A accumulates at DSBs in a 53BP1-, RIF1- and REV7-dependent manner and antagonizes HR by limiting DNA end resection. In fact, FAM35A is part of a larger complex composed of REV7 and SHLD1 (previously annotated as C20orf196 and RINN3), which promotes NHEJ and limits HR. Together, these results establish SHLD2 as a novel effector of REV7 in controlling the decision-making process during DSB repair.

3.3 Introduction

Due to their highly recombinogenic and pro-apoptotic potentials, DNA double-strand breaks (DSBs) are one of the most cytotoxic DNA lesions. Their inaccurate resolution can result in point mutations, small deletions/insertions, chromosomal rearrangements or loss of gross genetic information that drive genomic instability, carcinogenesis and cell death (reviewed in [11]). To avoid these deleterious outcomes, cells have deployed a complex network of proteins to signal and repair DSBs. One critical step during the DSB response consists in the choice between two mutually exclusive DNA repair pathways: Non-Homologous End Joining (NHEJ) and Homologous Recombination (HR) (reviewed in [12]). This decision process, named DNA repair pathway choice, integrates several elements including the cell cycle status, the complexity of the DNA end and the epigenetic context. Importantly, DNA repair pathway choice is under the control of two antagonizing factors, 53BP1 and BRCA1 (reviewed in [13]).

NHEJ is predominantly involved in the repair of DSBs during the G1 phase of the cell cycle. It is characterized by a limited processing of the DNA ends catalyzed by the nuclease Artemis and their subsequent ligation by DNA ligase IV (reviewed in [14]). Importantly, NHEJ is promoted by the recruitment of 53BP1 at DSBs, along with its effectors RIF1, REV7 and PTIP [15-23]. These latter factors play a central in several additional biological processes, including the establishment of a protective immunity during class switch recombination (CSR), a programmed DSB-dependent process that specifically occurs in B-cells [15, 17, 18, 20, 21, 24, 25].

In S/G2 phases of the cell cycle (when sister chromatids are available as templates), HR is activated and can alternatively repair DSBs. One of the key features of HR is the formation of long stretches of single-stranded DNA (ssDNA), a process called DNA end resection (reviewed in [26]). The resulting ssDNA stretches are rapidly coated by RPA, which is subsequently replaced by the recombinase RAD51 to form nucleofilaments that are a pre-requisite for the subsequent search of homology, strand invasion and strand exchange before the resolution of the DSB by the HR machinery. Critically, BRCA1 promotes the initiation of DNA end resection and HR-mediated DSB repair by preventing the recruitment of 53BP1 and its downstream effectors to sites of DNA damage in S/G2 phases [15, 16, 21, 23], thereby antagonizing 53BP1 function in NHEJ.

While the opposing role of 53BP1 and BRCA1 in DNA repair pathway choice has been extensively scrutinized over the past years, it remains largely unclear how the 53BP1 downstream effectors, namely REV7, promote NHEJ and antagonize BRCA1-mediated HR in G1 phase of the

cell cycle [17, 18]. REV7 is an adaptor protein that has been described for its role in mitotic progression through the control of both the activity of the spindle assembly checkpoint (SAC) and the formation of a functional anaphase-promoting complex/cyclosome-Cdc20 (APC/C) [27-29]. In parallel, REV7 is a well-defined player in DNA translesion synthesis (TLS) (reviewed in [30]) as well as DSB repair by HR as part of a complex composed of the deoxycytidyl (dCMP) transferase REV1 and the catalytic subunit of the DNA polymerase ζ, REV3L [31]. The recent discovery that REV7 participates in the NHEJ pathway in a TLS-independent manner raised fundamental questions about how this adaptor protein promotes DSB repair and controls DNA repair pathway choice.

In this present study, we sought to get insight into the decision-making process underpinning DNA repair pathway choice by deciphering the interactome of REV7. Using a mass spectrometry (MS)-based approach, we identified SHLD2 (previously known as FAM35A/RINN2) as an effector of REV7 in the NHEJ pathway. FAM35A accumulates at DSBs through its N-terminal domain in a 53BP1-, RIF1- and REV7-dependent manner. Importantly, depletion of FAM35A impairs both NHEJ and CSR, while promoting DNA end resection and HR. In fact, FAM35A acts in concert with SHLD1 (previously known as C20orf196/RINN3) in promoting both NHEJ and CSR while antagonizing HR. Altogether, our results provide a better insight into the molecular events that control DNA repair pathway choice.

3.4 Results

3.4.1 Mapping of REV7 proximal/interacting partners relevant for DNA repair pathway choice

To get better insight into the interactome of REV7, we performed a standard affinity purification (AP) followed by MS (AP-MS) (Fig S3.1 A), where REV7 was tagged with the Flag epitope and stably expressed in the human embryonic kidney 293 (HEK293) cell line using the Flp-In/T-REX system (Fig S3.1.B). As a complementary approach, we used a proximity-based biotin labelling technique (BioID), which allows the monitoring of proximal/transient interactions (Fig S3.1.A) [32, 33]. Briefly, REV7 was fused to a mutant of an *E.coli* biotin-conjugating enzyme (BirA*) and stably expressed in HEK293 as previously described [34]. This fusion protein is capable of biotinylating proteins that come in close proximity or directly interact with REV7 (Fig S3.1.C). Labelled proteins were subsequently purified by streptavidin affinity and identified by MS. Both approaches were carried out in triplicate using extracts of cells treated in the absence or presence of the radiomimetic DNA damaging drug Neocarzinostatin (NCS). We identified 140 high-confidence REV7 interactors that were either common to the four experimental conditions or found in both the AP-MS and the BioID following NCS treatment (Fig.3.2 A). As expected, pathways critical for mitosis and DNA repair were enriched in our list of REV7 partners (Fig S3.1 D). To further refine REV7 interactors, we intersected our data with previously reported proteomic profiling of REV7 [28], Rolland, Tasan [35], [36-47]. Using this methodology, we obtained 11 high-confidence REV7 interactors (Fig.3.2 B and Fig S3.1 E), including the chromosome alignment-maintaining phosphoprotein (CHAMP1), a kinetochore-microtubule attachment protein that has been recently linked to REV7 and its role during mitotic progression [48], as well as the cell-division cycle protein 20 (CDC20), a critical activator of the anaphase promoting complex (APC/C) that allows chromatid separation and entrance into anaphase [27, 28, 40]. However, whether these high-confidence REV7 interactors play any role in the DSB response remains unresolved.

To ascertain the relevance of these interactors for NHEJ, we used a well-established GFP-based reporter assay that monitors total NHEJ events [49], the EJ5-GFP assay, and targeted each candidate using small interfering RNA (siRNA) pools (Fig.3.2 C). As positive controls, we incorporated both RIF1 and REV7, which have been previously shown to impair this assay [15,

18, 21]. Out of the 11 candidates tested, downregulation of seven REV7 interactors significantly impaired the restoration of the GFP signal following DSB induction and subsequent repair by NHEJ (Fig.3.2 C), without impacting drastically cell cycle progression (Fig S3.1 F). SHLD2 emerged as our strongest hit, with a reduction of more than 60% of the GFP signal compared to the control condition in this assay (Fig.3.2 C). Therefore, we concentrated our efforts on this factor to better define its involvement in DNA repair pathway choice.

3.4.2 SHLD2 promotes DSB repair in human cells

To get an evolutionary perspective and determine whether SHLD2 may be relevant for DNA repair, we used a novel phylogenetic profiling (PP) approach and defined the landscape of genes that co-evolved with SHLD2 among mammals and vertebrates [50]. Importantly, this PP method has been previously shown to successfully predict protein function by analyzing the genes that co-evolved with a given factor of interest [50, 51]. Gene ontology analysis for biological process enrichment identified DNA repair, IL-1 signaling, Nucleotide Excision repair (NER) and the APC/C-CDC20 pathway as the most significant biological functions associated to genes that co-evolved with SHLD2 (Fig.3.3 A). Strikingly, SHLD2 co-evolves with RIF1 in both mammalians and vertebrates, which further suggests a putative role of SHLD2 in the maintenance of genome stability.

To explore this hypothesis, we first assessed the ability of SHLD2 to promote DSB repair using the neutral comet assay. We depleted SHLD2 in the osteosarcoma U2OS cell line using a short hairpin RNA (shRNA) (Fig S3.2 A) and we observed that loss of SHLD2 resulted in in the persistence of comet tails (time points 1, 2 and 3 hours), following exposure to ionizing radiation (IR; 10Gy), compared to control cells (Fig.3.3 B). For comparison, we depleted REV7 by shRNA (Fig S3.2 A) and obtained similar results. In a second assay, we depleted SHLD2 in U2OS cells using a deconvoluted siRNA (Fig. S3.2 C) and monitored the phosphorylation of the histone variant H2AX (γ-H2AX), a marker of DSBs, over time by flow cytometry following treatment with NCS. Again, the kinetics of γ-H2AX resolution was delayed in SHLD2-depleted U2OS cells compared to control conditions (Fig.3.3 C and Fig S3.2 D), suggesting a role of SHLD2 in DSB repair.

Next, we employed the breast cancer MCF-7 cell line to study the impact of SHLD2 depletion on survival following DSB induction by IR. We observed that SHLD2 depletion hypersensitizes MCF-7 cells to IR, in a manner similar to REV7 (Fig.3.3 D and Fig S3.2 A). Loss or depletion of REV7 has been previously linked to a hypersensitivity to UV in line with its TLS function [52], raising the question of whether SHLD2 is associated with a similar phenotype. Strikingly, SHLD2 depletion did not sensitize MCF-7 cells to increased doses of UV (Fig.3.3 E), suggesting that SHLD2 is dispensable for TLS. From these results, we conclude that SHLD2 is critical for DNA repair in a TLS-independent manner.

3.4.3 SHLD2 is recruited to DSBs through its N-terminal domain

SHLD2 is a 904-amino-acid protein with very limited structural information available (Fig.3.4 A). By performing structure prediction analyses on SHLD2 protein sequence using Motif Scan (MyHits, SIB, Switzerland) and InterProScan5 [53], we identified a putative N-terminal DNA binding-domain (NUMOD3 domain) and a structural motif in its C-terminus that we labelled PFAM (Fig.3.4 A). Recently, structural prediction analyses of SHLD2 also defined a N-terminal motif promoting protein-protein as well as three putative OB-fold like domains at its C-terminus [54-58]. Finally, previous phospho-proteomic analysis identified a S/Q substrate of ATM/ATR following DNA damage at position 339 [59].

To gain better insight into how SHLD2 promotes DSB repair, we tested whether it accumulates at DNA damage sites. Indeed, we observed that HA-tagged SHLD2, similar to REV7, is rapidly recruited to laser micro-irradiation-induced DNA damage in U2OS cells, co-localizing with γ-H2AX (Fig.3.4 B). As laser micro-irradiation elicits high levels of both single-strand breaks (SSBs) and DSBs, we complemented this approach by using the previously described mCherry-LacR-FokI-induced DSB reporter system [60]. Here, GFP-tagged SHLD2 is readily recruited to localized FokI-induced DSBs 30 min post-induction (Fig.3.4 C) and the majority of cells displays a GFP-SHLD2-positive signal at the mCherry dot 2 hours post-DSB induction (Fig.3.4 D). Furthermore, GFP-SHLD2 accumulation at DSBs is significantly distinct from empty vector 2 hours following the induction of DNA damage (Fig.3.4 E). We therefore used this experimental approach for our subsequent FokI-based experiments. As an orthogonal validation of the recruitment of SHLD2 to DNA damage, we sought to use a well-established system where the

induction of targeted DSBs is triggered by the controlled expression of the *Asi*SI restriction enzyme fused to a modified oestrogen receptor hormone-binding domain [61]. This model has been used to monitor the recruitment of DNA repair factors in the vicinity of DSBs and we confirmed by chromatin immunoprecipitation (ChIP) that induction of a DSB at chromosome 22 following addition of 4-hydroxy tamoxifen (4-OHT) triggers the formation of γ-H2AX proximally (3.7kb), but not distally (2Mb) from the site of damage (Fig.3.4 F). Importantly, we observed that Flag-tagged SHLD2 displays a similar distribution around the *Asi*SI-induced DSB. Altogether, these data indicate that SHLD2 is persistently recruited at DSBs, confirming its role in DNA repair.

We further characterized the role of SHLD2 during DSB repair by examining which domains of SHLD2 are critical for its recruitment to sites of DNA damage. We first evaluated the contribution of SHLD2 C-terminal PFAM/OB3 domain (SHLD2Δ720−904), its S/Q motif (S339) and most of SHLD2 N-terminus (SHLD2Δ1−680) for its recruitment to laser micro-irradiation-induced DNA lesions. We observed that both SHLD2Δ720−904 and S339A mutants are still recruited to DNA damage sites (Fig.3.4 G and Fig S3.3 A). However, deletion of the first 680 amino acids of SHLD2 (SHLD2Δ1−680) impairs its recruitment to laser micro-irradiation-induced DNA damage sites, suggesting a putative contribution of SHLD2 N-terminus for its accumulation at DSBs. To more quantitatively ascertain the importance of the different domains of SHLD2, we complemented this approach by monitoring the accumulation of different GFP-SHLD2 constructs in the FokI system. We observed that deletion of the first 60 amino acids of SHLD2 (SHLD2Δ1−60) totally abrogates its accumulations to DSBs, while the localization of the SHLD2 S/Q mutant (S339A) remained unaltered (Fig S3.3 B). Indeed, most of SHLD2 N-terminus (SHLD2Δ61−904) retained its ability to accumulate to DSBs, suggesting a limited contribution of SHLD2 C-terminus to DNA damage sites. From the data, we conclude that the N-terminal domain of SHLD2 is critical for its recruitment to DSBs.

These observations suggest that SHLD2 may have the capacity to directly bind DNA. To test this hypothesis, we purified recombinant full-length SHLD2 (SHLD2-FL) from Sf9 insect cells (Fig S3.3 C) and monitored its capacity to bind *in vitro* single-stranded (SS) and double-stranded (DS) radiolabeled DNA probes. Interestingly, we found that SHLD2 is proficient in binding both substrate *in vitro* (Fig S3.3 D). Furthermore, we observed that deleting a large portion of SHLD2 C-terminus (SHLD2Δ130−904) greatly impairs its DNA binding capacity, while the N-terminus of SHLD2 (SHLD2Δ1−129) is largely dispensable for interacting with both substrates *in vitro* (Fig

S3.3 D). Altogether, these data suggest that SHLD2 is composed of a DSB-recruitment motif at its N-terminus and a DNA-binding domain at its C-terminus.

3.4.4 SHLD2 associates with REV7 to promote NHEJ and limit HR

To decipher the link between SHLD2 and REV7, we tested the genetic requirements for the recruitment of SHLD2 to DSBs using the FokI system. Depletion of 53BP1, RIF1 or REV7 by siRNA impaired its recruitment to a localized site of DNA damage (Fig.3.5 A and Fig S3.4 A). However, we did not observe any impact on the recruitment of SHLD2 to the FokI site following BRCA1 depletion (Fig.3.5 A and Fig S3.4 A). Importantly, depletion of SHLD2 did not significantly impact the recruitment of 53BP1, RIF1 or REV7 to DSBs (Fig S3.4 B). These data indicate that SHLD2 is acting in concert with REV7 in the NHEJ pathway.

We reasoned that if SHLD2 is a direct effector of REV7, its recruitment to DSBs should be mediated through a physical interaction with REV7. Indeed, we confirmed the REV7-SHLD2 interaction in co-immunoprecipitation experiments where tagged versions of both REV7 and SHLD2 were expressed in 293T cells (Fig.3.5 B). Exposure to IR did not stimulate the REV7-SHLD2 interaction and pharmacological inhibition of ATM did not abrogate it (Fig.3.5 B), suggesting that this interaction is constitutive and stable in 293T cells, which is consistent with our MS data.

Our data point towards a role of SHLD2 in NHEJ downstream of REV7. Therefore, we confirmed that SHLD2 depletion impairs NHEJ in the EJ5-GFP assay using two distinct siRNAs (Fig.3.5 C and Fig S3.4 C). Next, we tested whether SHLD2 and REV7 act epistatically to promote NHEJ. As expected, co-depletion of REV7 with SHLD2 did not alter further the EJ5-GFP assay compared to the individual depletion (Fig.3.5 C and Fig S3.4 C). We further defined the similarities between REV7 and SHLD2 in the NHEJ pathway by testing the role of SHLD2 in CSR. REV7 depletion has been previously shown to cause a profound defect in CSR in CH12F3-2 B-cells that switch from IgM to IgA following the addition of a cocktail of cytokines (IL-4/TGF-β/anti-CD40; CIT), which induces the expression of the cytidine deaminase AID [62], and we confirmed these data (Fig.3.5 D and Fig S3.4 D) [17, 18]. Using two distinct shRNAs targeting SHLD2, we observed that its depletion impairs significantly CSR at both 24h and 48h post-activation (Fig.3.5 D and Fig S3.4 D). Importantly, this phenotype is not due to a defect in AID expression (Fig S3.4

D) or in cell proliferation (Fig S3.4 E). Together, these data suggest that SHLD2 regulates CSR at the level of DNA repair, which is consistent with its role as a REV7 effector.

53BP1 and its effectors have emerged as strong inhibitors of the HR pathway as well as the single-strand annealing (SSA) pathway [15-18, 20-23]. Therefore, we tested whether depletion of SHLD2 alters both DNA repair pathways using the DR- and the SA-GFP reporter assays, respectively (Fig S3.4 F) [63, 64]. In both U2OS and HeLa DR-GFP cells (Fig.3.5 E and Fig S3.5 A), SHLD2 depletion leads to a significant increase in HR using two distinct siRNAs, similar to what we observed with RIF1. Additionally, depletion of SHLD2, like RIF1, promotes SSA (Fig S3.4 B) [21]. This anti-HR role of 53BP1 and its effectors was attributed to a putative function in limiting DNA end resection, a key step in initiating DSB repair by HR. To define whether SHLD2 controls DNA end resection, we carried out a modified version of the DNA combing assay, where a dual-pulse labelling of the replicating DNA was performed using two distinct nucleotides analogs (IdU and CldU) before addition of NCS (Fig.3.5 F). While the length of the IdU-labeled DNA should not be altered by DNA end resection, we hypothesized that any increase in the processing of the DNA end should result in a shorter CldU-labeled DNA track and therefore a reduced ratio of CldU/IdU track length. Indeed, depletion of SHLD2 in U2OS cells resulted in a significant reduction of the CldU/IdU ratio compared to control cells (Fig.3.5 F and Fig S3.5 C), suggesting that SHLD2 limits DNA end resection. To support this hypothesis, we monitored by immunoblot the levels of phosphorylated RPA2 at position S4 and S8, which is widely used as a marker of DNA end resection, following treatment with NCS. We observed that depletion of SHLD2 in U2OS cells increased p-RPA2 levels upon NCS treatment compared to control cells (Fig S3.4 D), confirming that SHLD2 opposes HR by limiting DNA end resection.

Loss of REV7 in BRCA1-deficient cells has also been shown to restore partially HR [17]. We sought to examine whether depletion of SHLD2 could result in a similar phenotype. Therefore, we co-depleted both BRCA1 and SHLD2 in HeLa DR-GFP cells and we found a partial and significant restoration of HR in co-depleted vs. BRCA1-depleted cells (Fig S3.4 E). Altogether, these results are consistent with a model where SHLD2, like 53BP1, RIF1 and REV7, promotes DSB repair by NHEJ and antagonizes HR by inhibiting DNA end resection.

3.4.5 SHLD2 associates with SHLD1 to promote NHEJ

It remains largely unclear how SHLD2 promote NHEJ and limit HR, similar to 53BP1, RIF1 and REV7. Therefore, we determined the interactome of SHLD2 using the BioID approach in presence or absence of DNA damage (+/-NCS; Fig S3.6 A and B). Using this methodology, we identified previously described SHLD2 interactors, including REV7, the RNA-binding protein HNRNPA1 and the E3 Ubiquitin ligase TRIM25 (Fig S3.6 B) [65-67]. Interestingly, several members of the COP9 signalosome (COPS4 and COPS6) and the Cullin-RING E3 Ubiquitin ligase family (CUL3, CUL4B, CUL5, DDB1) emerged as high-confidence proximal interactors of SHLD2. However, by comparing both REV7 and SHLD2 BioID datasets, we did not identify any common complex of relevance for DNA repair. Therefore, we sought to undertake a more systematical and unbiased approach to identify novel DNA repair factors using the CRISPR/Cas9 technology (Fig.3.6 A). We employed the previously described TKO.v1 sgRNA library that contains 91,320 sequences and targets 17,232 genes and applied it to an hTERT immortalized retinal pigment epithelial RPE1 cell line stably expressing Cas9 [68]. To identify genes that are relevant for DNA repair, we used the chemotherapy drug doxorubicin as a selective agent (Fig.3.6 A). TP53, along with CHK1 and TOP2A emerged as our strongest hits providing resistance to doxorubicin (Fig.3.6 B). Their depletion was previously shown to elicit doxorubicin resistance [69], thereby validating our approach (Fig.3.6 B). We subsequently focused our analysis on doxorubicin-sensitizers, as they are likely to play a key role in DNA repair. Interestingly, SHLD1 scored as one of our most depleted genes (Fig.3.6 B). This factor is of particular interest as it has been previously identified in the proteomic analysis of two of our high-confidence SHLD2 interactors, REV7 [70] and CUL3 [71]. We therefore concentrated our efforts on this factor to define its link with FAM35A during DNA repair.

First, we confirmed that REV7 and SHLD1 interact together by co-immunoprecipitation experiments where tagged versions of both REV7 and SHLD1 were expressed in 293T cells (Fig.3.6 C). Next, we tested whether SHLD2 interacts with SHLD1 using a similar approach (Fig.3.6 C). Importantly, both REV7-SHLD1 and SHLD2-SHLD1 interactions did not increase upon IR treatment, neither did the pharmacological inhibition of ATM abrogates them (Fig.3.6 C), similar to what we observed previously with the REV7- SHLD2 interaction. If SHLD1 is part of a complex composed of REV7 and SHLD2, we would expect SHLD1 to accumulate at sites of damages, recapitulating the observations we made with both REV7 and SHLD2. Therefore, we carried out laser stripe micro-irradiation experiments and observed that HA-tagged SHLD1 co-

localizes with γ-H2AX at DNA damages sites (Fig S3.6 C), suggesting a role of SHLD1 in DNA repair.

We further investigated this hypothesis by evaluating the contribution of SHLD1 in the NHEJ and in CSR. Indeed, we observed that depletion of SHLD1 in U2OS EJ5-GFP cells resulted in a significant reduction of DSB repair by NHEJ (Fig.3.6 D and Fig S3.6 D), as previously observed with SHLD2 and REV7. Furthermore, depleting SHLD1 in CH12F3-2 B-cells using two distinct shRNAs impaired significantly CSR at both 24h and 48h post-activation (Fig.3.6 E), suggesting a potential role of SHLD1 in DNA repair during CSR. Finally, depletion of SHLD1 in the U2OS DR-GFP cells led to a significant increase in HR (Fig.3.6 F). Altogether, these data suggest that SHLD2 functions as part of a large multi-protein complex, composed of at least REV7 and SHLD1, to promote NHEJ and CSR while restricting HR.

3.4.6 SHLD2 levels correlate with a poorer prognosis in a subset of breast cancer patients

Dysregulation of DSB repair pathways has been frequently observed in several types of cancer and extensively documented for its role in the pathobiology of breast cancer (BC). We sought to determine whether SHLD2 may contribute to the outcome of BC by interrogating two distinct patient-based cohorts of triple negative breast cancer (TNBC) and basal-like BC. Interestingly, high levels of SHLD2 correlates with a poorer survival probability in a well annotated cohort of 24 TNBC patients (Fig.3.7 A). We confirmed this observation in the publicly available TCGA database where we focused our analysis of basal-like BC patients. Again, high expressers of SHLD2 have significantly lower relapse-free survival in this cohort (Fig.3.7 B), suggesting a putative role of SHLD2 in the pathobiology of a BC subset. Altogether, our data are consistent with a model where SHLD2 needs to be tightly regulated to control DNA repair pathway choice where it acts in concert with SHLD1 as a downstream effector of REV7 in the NHEJ pathway and restricts DNA end resection, thereby antagonizing HR (Fig.3.7 C).

3.5 Discussion

Two main DNA repair pathways, NHEJ and HR, are typically mobilized to repair cytotoxic DSBs and optimal pathway selection is central in preserving genome integrity. Several factors including 53BP1, RIF1 and REV7, emerged recently as key players in DNA repair pathway choice [15-18, 20-23]. However, it remains largely unclear how they modulate the proper balance between NHEJ and HR. Several recent studies have recently tackled to decipher the effectors of the 53BP1-RIF1-REV7 axis [54-58, 72, 73], and our work contributes to this effort by providing further insight into the role of REV7 in DNA repair pathway choice.

Using a mass spectrometry-based approach, we identified SHLD2 as a high-confidence interactor of REV7. While this association has been previously reported [65], it is only recently that its biological relevance has been further investigated [54-58, 73]. Up to now, SHLD2 remained an enigma in regard to its physiological functions. The first indication of a potential involvement of SHLD2 in the response to DSBs emerged from a comprehensive interactome mapping of key DNA repair factors, including 53BP1 and BRCA1 [58]. Here we provide further insight into the role of SHLD2 in DNA repair and show that SHLD2 acts as a downstream effector of REV7 in the NHEJ pathway. Through its N-terminal domain, SHLD2 is mobilized to and accumulates at sites of DNA damage in a 53BP1-, RIF1- and REV7-dependent manner, in accordance with several recent studies describing the role of SHLD2 in the DNA damage response [54-58, 72, 73]. Importantly, we show that the N-terminus of SHLD2 has very limited DNA binding capacity, which support a model where the recruitment of SHDL2 to DSBs is promoted by protein-protein interactions [56]. This finding corroborates the initial observation made by Gupta *et al.*, showing that the N-terminal domain of SHLD2 is critical for its association with REV7 [58]. In a series of functional studies, we show that SHLD2 is critical during both antibody diversification and DSB repair by the NHEJ pathway. Our data suggest that SHLD2 and REV7 act together in an epistatic manner, which is corroborated by several studies that described SHLD2 as a novel DNA repair factor [54-58, 72, 73]. We further show that, similar to 53BP1 and RIF1 [15, 16, 20-23], SHLD2 opposes HR by limiting DNA end resection. However, whether this anti-HR function of SHLD2 is related to a steric hindrance of the DNA ends or an active process of preventing CtIP and its associated nucleases to initiate DNA end resection remains an avenue of investigation.

Second, our genome-wide screening approach identified novel players in DNA repair, including SHLD1. Our data point toward a more complex model where REV7, SHLD2 and SHLD1

cooperate together to promote NHEJ and limit HR, as described by several other groups [54-58, 72, 73]. Indeed, we show that SHLD1 co-immunoprecipitates with both REV7 (as previously described [70]) but also SHLD2. Surprisingly though, we did not identify SHLD1 as a high confidence interactor of SHLD2 in our BioID approach, likely due to the low abundance of this factor and in accordance with a previous report [58]. Still, our genetic dissection of SHLD1 recapitulates the striking data that we observe with SHLD2: (i) SHLD1 is recruited to and accumulates at sites of DNA damage; (ii) its depletion impairs both NHEJ and CSR while promoting HR. Why REV7 requires several factors to promote NHEJ and inhibit DNA end resection is unclear; our model suggests that, alike the Shelterin complex at telomeres [74], which lacks any catalytic activity *per se*, REV7 forms a large multi-protein complex at DSBs to protect DNA ends from extensive processing and promote their rapid joining by the NHEJ machinery. This model, described elegantly in Noordermeer et al. [56], has driven the nomenclatural renaming of the SHLD proteins as the Shieldin complex.

Finally, our observation that SHLD2 levels correlate with a poor prognosis in a subset of BC has profound implications for the diagnosis and treatment of these patients. Imbalance in DSB repair pathways has been well documented to predispose and promote the development of BC; in the majority of the cases, inactivation of HR factors is the cause of this predisposition with a very limited understanding of the molecular mechanisms underlining this phenomenon. Our study points toward an expressional dysregulation of SHLD2 as a potential predisposing factor to TNBC/Basal-like BC outcome, which may point toward a direct contribution of this novel NHEJ component in the pathobiology of BC. It will be of great importance to further define the role of SHLD2 in BC as it may be a relevant biomarker for its diagnosis.

Altogether, the work presented here not only describes the role of two DNA repair factors in controlling DNA repair pathway choice but it also provides the first evidence that SHLD2 could benefit clinicians as a relevant biomarker for a subset of BC. Our data points toward a more complex model for DNA repair pathway choice where REV7 mobilizes additional factors to DSBs to catalyze NHEJ and limit the processing of DNA ends, thereby restricting HR to the S/G2 phases of the cell cycle.

3.6 Materials and Methods

Cell culture and plasmid transfection

HEK293-T, Flp-In T-REx, -XT, and HeLa cells were cultured in Dulbecco's Modified Eagle medium (DMEM; Wisent) and were supplemented with 10 % fetal bovine serum (FBS) and 1% Penicillin-Streptavidin (P/S). CH12F3-2 cells were cultured in RPMI 1640 (Wisent) supplemented with 10% FBS, 5% NCTC-109 media (Thermo Fisher), 50μM 2-mercaptoethanol and 1% P/S. U2OS cells were cultured in McCoy's 5A Modified medium (Wisent) and was supplemented with 10 % FSB and 1% P/S. All cell lines were tested for mycoplasma contamination and STR DNA authenticated. Plasmid transfections were carried out using Lipofectamine 2000 Transfection Reagent (Invitrogen) following the manufacturer's protocol. Lentiviral infections were done as previously described [21], with modifications listed below.

To generate the ER-AsiSI-expressing HEK293T cell line, retroviral particles were produced using pBABE HA-AsiSI-ER (kind gift of Dr. Michael Witcher, McGill University), the packaging plasmid pUMVC (addgene 8449), and the envelope plasmid VSV-g (Addgene #8454) co-transfected into HEK293T cells. To produce U2OS stable cell lines for microirradiation, lentiviral particles were produced by polyethyleneimine-mediated transfection of pHAGE-EF1α plasmid-cDNA with psPAX2 and pMD2.G packaging and envelope plasmids in 293 XT packaging cells. U2OS cells were infected with lentiviruses for 24h in media containing 8 μg/mL polybrene and 1μg/mL puromycin selection was applied. To generate a HEK293-TREx Flp-in cells were co-transfected with pOG44 and pcDNA5 FRT/TO FLAG-FAM35A and selected in with 200 μg/ml hygromycin B and 5 μg/ml blasticidin. The U2OS-LacI-FokI-mCherry cell line was a kind gift of R. Greenberg (University of Pennsylvania). The DNA-repair reporter cell lines DR-GFP, EJ5-GFP, and SA-GFP were a kind gift of Dr. Jeremy Stark (City of Hope National Medical Center, California).

Plasmids

The cDNAs of human SHLD2, SHLD1 and REV7 were obtained from Sidong Huang (McGill University). Quikchange site directed mutagenesis (Agilent) was performed as per manufacturers guidelines to obtain the different SHLD2 mutants. All these constructs were transferred from ENTRY vectors into lentiviral pHAGE-EF1α vectors in frame with N-terminal 3XHA epitopes,

GFP-construct, BirA-construct and Flag-tagged constructs using LR Clonase II according to manufacturer's instructions (ThermoFisher). Plasmids encoding, I-SceI or pDEST-FRT-FLAG (EV) for the different GFP reporter assays, were kindly provided by Dr. Daniel Durocher (Lunenfeld-Tanenbaum Research Institute). The following pLKO-puro shRNA lentiviruses obtained from Mission library clones (Sigma) against mouse genes: Negative control (scramble); *Mad2l2* 45 (TRCN0000012845); *Aicda* (TRCN00000112033); *Fam35a (Shld2)* (TRCN0000183111) and *Fam35a (Shld2) (*TRCN0000183379); *C20orf196* (*Shld1)* (TRCN0000092993) and *C20orf196* (*Shld1)* (TRCN0000092995)

RNA interference

All siRNAs employed in this study were single duplex siRNAs purchased from Dharmacon (GE Healthcare, Colorado, US). RNAi transfections were performed using Lipofectamine RNAiMax (Invitrogen) in a forward transfection mode. Except when stated otherwise, siRNAs were transfected 48 h prior to cell processing. The individual siRNA duplexes used are: Control (D-001810-03); RIF1 (D-027983-02); CBX1 (L-009716-00); CDC20 (L-021601-02); CHAMP1 (L-021601-02); EHMT2 (L-006937-00); GTF21 (L-013686-00); POGZ (J-006953-10/12); REV1 (D-008234-01/02/0/3/04); REV3L (D-006302-01/02/03/04); REV7 (J-003272-14); SRPRB (L-013646-00); SSR4 (L-012264-00); ZMFM4 (L-019932-02); ZNF644 (L-007085-02); SHLD2 (D-013761-01/02/03/04); SHLD1 (D-018767-01/02/03/04); BRCA1 (D-003461-05); CTIP (M-011376-00). In most of the experiments, SHLD2 siRNAs D-013761-01and D-013761-03 were used except during the validation screen.

Immunofluorescence microscopy

In most cases, cells were grown on glass coverslips. All steps were carried out at room temperature. Cells grown on coverslips were fixed in freshly prepared 2% paraformaldehyde for 10 minutes. Fixed cells were then incubated for 10 minutes with a combination of permeabilization/blocking buffer (0.1% Triton X-100 and 1% bovine serum albumin (BSA)). Next, primary antibodies were added for 1.5 hours in phosphate-buffered saline (PBS) + 1% BSA followed by three washes with PBS. Secondary antibody was next added in the same buffer for a period of one hour. Nuclei were stained with DAPI (1 μg/ml) for 5 min and subjected to a set of final washes with PBS and subsequently sterile water. After this, coverslips were mounted onto

glass slides using a ProLong Diamond antifade reagent (Life Technologies). Images were acquired using a Zeiss LSM800 confocal microscope. Images were analyzed and quantified using ImageJ software [75]. For the FokI system, DSBs were induced by adding Shield-1 and 4-OHT for two hours prior to immunofluorescence sample preparation.

Clonogenic Assay

Clonogenic assays was performed as described [76]. Briefly, cells were allowed to reach ~50% confluence prior to genotoxic insult. Culture plates were then exposed to the indicated dose of IR or 254 nM ultraviolet (UV) light and allowed to recover overnight. Cells were then trypsinized and re-seeded into 60 cm dishes at 400 cells (or 800 cells for the highest dose) per dish. Colonies were allowed to form over the duration of 2 weeks and then fixed in 100% methanol and stained with 0.4% crystal violet (in 20% methanol). Colony number was manually tabulated with only colonies of >50 cells included in the total count.

Co-Immunoprecipitation

HEK293T cells were co-transfected with pDEST-FRT-TO-Flag and pDEST-FRT-TO-GFP tagged vectors. Twenty four hour post-transfection all cells were exposed to irradiation (10 Gy). ATMi-treated cells were exposed to 10 μM KU-60019 one hour prior to irradiation. Cells recovered at 37°C for one hour before being harvested and lysed in a high salt lysis buffer (50 mM Tris, 300 mM NaCl, 1mM EDTA, 1% Triton), supplemented with 1x Protease Inhibitor Cocktail (Roche)/Phosphate Inhibitor cocktail (Sigma) and gently rotated for 30 minutes at 4°C. Nuclear fractions were extracted with 0.25M $CaCl_2$ and 250U benzonase and homogenized on an orbital shaker for 15 minutes at 30°C. The resulting solution was pelleted at 4°C at 18000g for 15 minutes and the supernatant was applied to an anti-Flag (M2) resin (Sigma) and equilibrated at 4°C for two hours. The anti-Flag resin was then washed once with the high salt lysis buffer and twice with the immunoprecipitation (IP) buffer (50mM Tris, pH 7.6, 150mM NaCl, 1mM EDTA). The immunoprecipitated proteins were eluted from the resin with 1x LDS NuPage sample buffer (10mM Tris-HCl, 140 mM Tris-base, 0.5 mM EDTA, 1% lithium dodecyl sulfate, 10% glycerol).

Biotin labelling and sample preparation for MS

Samples for BioID were processed as previously described [34]. Briefly, HEK293-T cells were either transiently transfected with FLAG-BirA*-SHLD2 or stably expressed using the T-REX system (FLAG-BirA*-REV7). Media was supplemented, 24 hours post-transfection, with 50μM biotin and cells were incubated for an additional 24 hrs with neocarzinostatin (NCS, 150 ng/ml). Cells were then harvested, washed twice with PBS, and dried. Pellets were subsequently resuspended in cold RIPA buffer containing: 50 mM Tris-HCl pH 7.4, 150 mM NaCl, 1 mM EDTA, 1% NP-40, 0.1% SDS, 0.5% sodium deoxycholate, 1mM PMSF, 1mM dithiothreitol, 1:500 Sigma-Aldrich protease inhibitor cocktail P8340. Cell homogenates were sonicated, followed by the addition of 250 U benzonase and centrifuged (12,000 g, 30 min). Supernatants were incubated with pre-washed Streptavidin-sepharose beads (GE, #17-5113-01) at 4°C with rotation for three hours. Beads were collected by centrifugation (2,000 rpm, 1 min), washed twice with RIPA buffer, three times with 50 mM ammonium bicarbonate (ABC, pH 8.2). Beads were resuspended in 50 mM ABC and treated with 1 μg trypsin (Sigma-Aldrich T6567) overnight at 37 °C with rotation. Digestion was continued by adding an additional 1 ug of trypsin for an additional 2 hrs at 37 °C with rotation. Supernatant containing peptides, and supernatants from two following washes with HPLC-grade H_2O, was collected and pooled. Digestion was ended with the addition of formic acid to a final concentration of 5 %. Samples were centrifuged (13200rpm for 10 min) and the supernatants were dried in a SpeedVac for three hours at high rate. Peptides were resuspended in 5 % formic acid and kept at −80 °C for mass spectrometric analysis. MS processing and protein analysis were carried out as previously described.

Mass spectrometry data generated by the Regional Mass Spectrometry Centre (Université de Montréal) or the IRCM Proteomics Discovery Platform were stored, accessed, searched and analyzed using the ProHits laboratory information management system (LIMS) platform. Significance Analysis of INTeractome (SAINT)express (v3.6.1) was the statistical tool utilized to calculate the probability of protein-protein interaction from background, non-specific interactions [77]. These results were evaluated with the Trans-Proteomic Pipeline (TPP v5.1) via the iProphet search engine integrated in the ProHits software [78, 79]. A minimum of two unique peptide ions, an iProphet probability of >0.95, a Bait False Discovery Rate (BFDR) of <0.05, and a ≥10 peptide count were the criteria required for protein consideration. Biofilters were applied against albumin, artifact protein, cytoskeleton, and keratin. Resultant proteins from AP-MS (FLAG-REV7) and BioID (BirA-REV7; BirA-SHLD2) experiments were tabulated and analyzed for common

potential interactors between the AP-MS and BioID groups, respectively. Common candidates were then sorted according to largest peptide counts. This analysis yielded 140 mutual candidates for the NCS+ group and 170 for the NCS- group. By way of literature review and the use of the Biological General Repository for Interaction Datasets (BioGRID), promising candidates were selected for targeted experimentation. Selected prey proteins were used for dot-plot heat map generation. Plots were generated using the ProHits Visualization Suite (ProHits-viz) [80].

GFP-based DNA repair assays

For DR-, EJ5-, EJ2-, SA-GFP reporter assays, U2OS or HeLa cells carrying the respective GFP expression cassette were transfected with indicated siRNA. Twenty-four hours after transfection, cells were transfected with empty vector (EV, pDEST-FRT-FLAG) or I-SceI plasmids. After 48 hours, cells were trypsinized, harvested, washed and re-suspended in PBS. The percentage of GFP-positive cells were determined by flow cytometry. The data was analyzed using the FlowJo software.

Class Switch Recombination Assay

Immunoglobulin (Ig) M (IgM) to IgA switching was assayed in CH12F3-2 cells with integrated shRNA for REV7, AID, SHLD2 or SHLD1. Cells were activated in 1 mL complete CH12F3-2 media with 1.25 ng transforming growth factor beta 1 (TGF-β1, PeproTech), 5 ng interleukin (IL) 4 (IL-4, PeproTech) and 0.5 μg anti-cluster of differentiation (CD) 40 (CD40, eBioscience). IgA expression was measured by flow-cytometry using primary conjugated anti-mouse IgA-PE (Southern Biotech) at 24h and 48h after activation. Proliferation of the different transduced CH12F3-2 cell lines was monitored using carboxyfluoroscein succinimidyl ester (CFSE, Invitrogen) following the manufacturer's guidelines. Class switching assays were done in triplicate for every independent experiment.

Comet assay

U2OS cells were exposed to IR (10 Gy) and processed according to manufacturer's recommendations (Trevigen). Cells were trypsinized at the indicated time points and re-suspended at 10^5 cells/mL in PBS. Cells were combined with low melting agarose at 1:10 ratio and spread over the CometSlide. Slides were allowed to dry at 4ºC for ten minutes then immersed in lysis buffer (Trevigen) overnight. The next day the slides were immersed neutral electrophoresis buffer

(two 15-minute washes) followed by electrophoresis at 31V for 45 minutes. Subsequently the slides were incubated for 30 minutes in DNA precipitation solution followed by 30 minutes in 70% ethanol. Slides were dried and stained with SYBR Gold (Invitrogen). Images were taken using the EVOS FL Cell Imaging System microscope and the tail moment was quantified using the CaspLab software. For each condition, at least 50 cells were analyzed.

Immunoblot

Cells were washed with cold PBS (2X) and whole cell lysates were collected using: 50 mM HEPES, KOH (pH 8.0), 100 mM KCl, 2 mM EDTA, 0.1% NP-40, 10% glycerol, and protease/phosphatase inhibitors (Tkac, 2016). The following antibodies were used for the immunoblot analysis: rabbit anti-pRPA2 S4/S8 (A300-245A, Bethyl), and mouse anti-α-tubulin (ab7291, Abcam).

Laser Micro-irradiation

U2OS stable cell populations expressing the various constructs were transferred to a 96-well plate with 170 μm glass bottom (Ibidi), presensitized with 10 μg/mL Hoescht 33342 and microirradiated using a FV-3000 Olympus confocal microscope equipped with a 405nm laser line as described previously [81]. Immunofluorescence was performed as described previously [81]. Briefly, following microirradiation, cells were allowed to recover before pre-extraction in 1X PBS containing 0.5 % Triton X-100 on ice for five minutes. Following washes with 1X PBS, cells were fixed for 15 min in 3 % paraformaldehyde 2 % sucrose 1X PBS solution, permeabilized in 1X PBS containing 0.5 % Triton X-100 for five min, blocked in 1X PBS containing 3% BSA and 0.05% Tween-20 and stained with the following primary antibodies 1:500 RPA32 mouse (Santa Cruz, sc-56770) or 1:500 γ-H2A.X mouse (abcam, ab26350) and 1:500 HA-tag rabbit (Bethyl, A190-108A). After extensive washing, samples were incubated with 1:250 each of goat anti-mouse Alexa 488-conjugated and goat anti-rabbit Alexa 647-conjugated antibodies (Cell Signaling 4408S and 4414S). DAPI staining was performed and samples were imaged on a FV-3000 Olympus confocal microscope.

ChIP Quantitive PCR

Stable 293T cell lines expressing ER-AsiSI cells were transfected with Flag-SHLD2 and treated with 1 μM of 4-OHT (4-Hydroxytamoxifen) for 6 hours. Cells were collected for ChIP assay as per previously [61]. Briefly, cells were crosslinked using 1.5 mM EGS (ethylene glycol bis(succinimidyl succinate), Thermo Fisher # 21565), followed by 1 % of formaldehyde. Cell nuclei was isolated and lysed. Chromatin was sonicated for 15 min using a water bath sonicator/bioruptor. Fragmented chromatin bound to SHLD2 and γ-H2AX was immunoprecipitated using Anti-FLAG Magnetic Beads (Sigma, M8823), and anti-γ-H2AX (JBW301, EMD-Millipore, Massachusetts, US) in combination with protein A/G magnetic Beads, respectively. Antibody/protein/DNA complexes were then eluted and reverse crosslinked. DNA was purified using QIAquick Kit (Qiagen #28106) and used for qPCR detection with the following oligonucleotides: AsiSI22-distF 5'-CCCATCTCAACCTCCACACT-3'; AsiSI22-distR 5'-CTTGTCCAGATTCGCTGTGA-3'; AsiSI22-ProxF 5'-CCTTCTTTCCCAGTGGTTCA-3'; AsiSI22-ProxR 5'-GTGGTCTGACCCAGAGTGGT-3'. IP efficiency was calculated as percentage of input DNA immunoprecipitated.

DNA Fiber Combing

U2OS cells were transfected with the indicated siRNA in a 6-well cell culture plate. After 48 hours, cells were treated with indicated schedules and concentrations of thymidine analogue pulses (chlorodeoxyuridine (CldU; C6891); iododeoxyuridine (IdU; I7125); Sigma, Missouri, US) with and without neocarzinostatin (NCS, Sigma) treatment to measure replication fork kinetics and extent of DNA end-resection. Cells were trypsinized, agarose plug embedded, and subjected to DNA extraction as per the Fibreprep protocol (Genomic Vision, Bagneux, FR). Vinylsilane coated coverslips (Genomic Vision) were combed through prepared DNA solution using FibreComb Molecular Combing system (Genomic Vision). Combed DNA was dehydrated, denatured, blocked with BlockAid blocking solution (Invitrogen, California, US) and stained with mouse anti-BrdU (B44, BD, New Jersey, US), rat anti-BrdU (BU1/75, Abcam, Cambridge, UK) and rabbit anti-ssDNA (18731, Immuno-Biological Materials, Gunma, Japan) antibodies. Slides were subsequently washed and stained with secondary antibodies: Goat anti-rabbit IgG conjugated Alexa Fluor 480 (BD Horizon) goat anti-mouse IgG conjugated Alexa Fluor 555 (Invitrogen), goat anti-rat conjugated Cy5 (Abcam). Slides were dehydrated, mounted, and visualized using FibreScan services (Genomic Vision).

Phospho-H2AX Flow Cytometry

U2OS cells were transfected with indicated siRNA in a 6-well cell culture plate. After 48 hours, cells were treated with NCS for 30 mins and after indicated time intervals, cells were trypsinized, washed, and fixed with 1% para-formaldehyde, washed and subsequently permeabilized in 70% ethanol at -20ºC. Cells were washed twice with intracellular wash buffer (1% BSA, 0.05% Tween-20, PBS) and re-suspended in 1.0 ug/mL mouse anti-γ-H2AX (JBW301, EMD-Millipore, Massachusetts, US) for one hour at RT. Cells were then washed and re-suspended in 2.0 ug/mL goat anti-mouse Alexa Fluor 647 (Invitrogen) for one hour at RT. Cells were washed and re-suspended in a propidium iodide (PI) solution (20 ug/mL PI, 300ug/mL RNase, PBS), incubated at RT for 30 minutes. Events were acquired on a LSRFortessa (BD). Events were analyzed on FlowJo v10 (Treestar, Oregon, US).

CRISPR/Cas9 genome-wide screen

For the genome-wide CRISPR/Cas9-based screen, 270 million RPE-hTERT/Cas9 cells were transduced as described previously [68] with TKOv1 concentrated library virus at MOI = 0.2, ensuring a coverage of at least 600-fold for each individual sgRNA represented in the cell population. Two days later, puromycin was added to the media at a final concentration of 15 ug/ml and incubated for four days to allow for the emergence of resistant cells with fully repaired sgRNA library targeted loci. Cells were then split into 2 pools each in triplicate at a cell density of 54 million cells/replicate and treated with either vehicle (H_20) or doxorubicin at its IC25 (3 nM) and cultured for two weeks with puromycin at a concentration of 7.5 ug/mL. Cells were passaged every three days keeping a minimum cell concentration of 54 million cells per replicate to ensure that a 600-fold library coverage was maintained over the duration of selection. At each time point, cell pellets were collected and frozen prior to genomic DNA extraction. Cell pellets were resuspended in 6 mL DNA lysis buffer (10 mM Tris-Cl, 10mM EDTA, 0.5% SDS, pH 8.0) with 100 ug/mL RNase A, followed by incubation at 37 ºC for 60 min. Proteinase K was subsequently added (400 ug/mL final) and lysates were further incubated at 55 ºC for two hours. Samples were then briefly homogenized by passing them three times through a 18G needle followed by three times through a 22G needle. Sheared samples were transferred into pre-spun 15 mL MaXtract tubes (Qiagen) mixed with an equal volume of neutral phenol:chlorophorm:isoamyl alcohol (25:24:1) solution,

shook and centrifuged at 1,500g for five min at RT. The aqueous phase was extracted and precipitated with two volumes of ethanol and 0.2M NaCl. Air-dried pellets were resuspended in water and quantitated via UV absorbance spectrometry.

For next-generation sequencing (NGS), sgRNA integrated loci were amplified from 330 ug of total genomic DNA per replicate using two rounds of nested PCR. The initial outer PCR consisted of 25 cycles with an annealing temperature of 65 ºC using Hot start Q5 polymerase (NEB) using primers Outer Primer Forward (AGGGCCTATTTCCCATGATTCCTT) and Outer Primer Reverse (TCAAAAAAGCACCGACTCGG). PCR reactions were pooled and ~2% of the input was amplified a further 12 cycles for the addition of Illumina HiSeq adapter sequences. The resulting ~200bp product from each pooled sample was further purified following separation in a 6% 0.5XTBE polyacrylamide gel. The amplicon library NGS-ready final product was quantified using qPCR and submitted for deep-sequencing on the HiSeq 2500 Illumina platform using standard Single-Read (SR) 50-cycle chemistry with dual-indexing with Rapid Run reagents. The first 20 cycles of sequencing were "dark cycles", or base additions without imaging. The actual 26bp read begins after the dark cycles and contains two index reads, reading the i7 first, followed by i5 sequences. Prior to analysis, FastQ NGS read files were initially processed using FastQC software to assess uniformity and quality. Reads were trimmed of NGS adapter sequences using the Cutadapt tool. Reads were aligned to the sgRNA library index file using Bowtie to assign a matching gene-specific sgRNA, and total read count tables were subsequently generated using Samtools. A pseudocount of 1 was added to each sgRNA read count, and reads were normalized to the total read count per experimental replicate. Any sgRNA that had fewer than 25 total reads in any replicate or which were represented by less than 3 unique sgRNA for a given gene were dropped from the analysis. Average log2 fold-change was calculated for a given gene between the initial and final abundances for all sgRNAs targeting it across the replicates.

Phylogenetic profiling analysis

To identify genes co-evolved with SHLD2 we used normalized phylogenetic profiling as previously described [50, 51]. Briefly, we have generated the phylogenetic profile of 42 mammalian species and calculated the Pearson correlation coefficients between the phylogenetic profile of SHLD2 and the phylogenetic profiles of 19520 human protein coding genes, and defined the 200 genes with the highest correlation coefficients as co-evolved with SHLD2 in mammalians.

In a similar manner, we identified the top 200 genes that co-evolved with SHLD2 in 63 vertebrate species. The intersection between these two lists yielded 159 genes that were subsequently considered as co-evolving with SHLD2 with high confidence and further processed for pathway enrichment analysis.

Patient Cohort analysis

TNBC patient data was collected in accordance with the McGill University Health Center research ethics board (SUR-99-780). Informed consent was obtained from all subjects and the experiments performed are conformed to the principles set out in the WMA Declaration of Helsinki and the Department of Health and Human Services Belmont Report. Total RNA was isolated from TNBC primary tissues using Qiagen AllPrep DNA/RNA Mini Kit. RNA quality was assessed using a Bioanalyser (Agilent). RNA-Seq library was generated using the Illumina TruSeq RNA Library Prep Kit and sequencing was performed on the Illumina HiSeq 2500 platform using 75 base-pair paired-end reads. Reads were mapped to human genome version hg19 using STAR (Spliced Transcripts Alignment to a Reference). The data were mean-centered, log-transformed and the expression values for *SHLD2* was extracted for further analysis. Survival analysis was performed using the coxph function in the R package 'survival'. Expression was classified as either low or high using the top quartile as the threshold.

Protein Purification

Recombinant SHLD2 proteins fused with a with a cleavable N-terminal GST tag and a C-terminal histidine tag were purified from baculovirus-infected Sf9 cells. Recombinant baculoviruses were produced by the Bac-to-Bac expression system (Invitrogen), Sf9 insect cells were infected with the different baculoviruses for 3 days at 27°C. The cells were harvested by centrifugation and the cell pellet was resuspended in 40 ml GST buffer (PBS 1×, 150 mM KCl, 1% Triton X-100, 0,5 mM DTT, 0.019 UIT/ml Aprotinin, 1 µg/ml Leupeptin). The suspension was sonicated and insoluble material was removed by centrifugation. Glutathione sepharose beads (GE Healthcare) were added to the supernatant and incubated for 2 h at 4°C. The beads were washed four times with GST buffer and two times with PreScission washing buffer (50 mM Tris–HCl pH 7.4, 150 mM NaCl, 1 mM EDTA, 1 mM DTT, 0.05% (v/v) Tween 20). The proteins were eluted by cleavage with PreScission protease (80 U/ml, GE Healthcare) overnight at 4°C. The

supernatant was dialyzed against Talon buffer (50 mM $NaHPO_4$ pH 7, 500 mM NaCl, 10% (v/v) glycerol, 0.05% (v/v) Triton X-100, 5 mM imidazole). Talon beads (Clontech) were added to the supernatant and incubated for 60 min at 4°C. The resin was washed three times with Talon washing buffer (50 mM NaHPO4 pH 7, 500 mM NaCl, 10% glycerol, 0.05% Triton X-100, 30 mM imidazole). SHLD2 proteins were eluted in Talon buffer containing 500 mM imidazole and dialyzed in storage buffer (20 mM Tris–HCl pH 7.5, 10% glycerol, 0.05% Tween 20, 200 mM NaCl, 1 mM DTT).

DNA substrates and DNA binding assays

DNA substrates used were generated with purified oligonucleotides (JYM696 GGGCGAATTGGGCCCGACGTCGCATGCTCCTCTAGACTCGAGGAATTCGGTACCCCG GGTTCGAAATCGATAAGCTTACAGTCTCCATTTAAAGGACAAG and JYM698 CTTGTCCTTTAAATGGAGACTGTAAGCTTATCGATTTCGAACCCGGGGTACCGAATT CCTCGAGTCTAGAGGAGCATGCGACGTCGGGCCCAATTCGCCC). Briefly, double-strand DNA were prepared by annealing reaction carried out by slowly cooling from 95 to 12°C. The DNA binding reactions (10 µl) contained ^{32}P-labeled DNA oligonucleotides (50 nM nucleotides of each substrate) and the indicated concentrations of SHLD2 full-length or fragments in MOPS buffer (25 mM MOPS at pH 7.0, 60mM KCl, 0.2% Tween 20, 2 mM DTT and 5 mM $MgCl_2$). Reaction mixtures were incubated at 37°C for 20 min and then protein–DNA complexes were fixed with 0.2% (v/v) glutaraldehyde for 20 min. The reactions were subjected to electrophoresis on an 8% TBE1X-acrylamide gel and ^{32}P-labeled DNA was visualized by autoradiography.

DATA AVAILABILITY

The mass spectrometry data from this publication have been deposited to the ProteomeXchange Consortium50 database (http://proteomecentral.proteomexchange.org/) via the MassIVE partner repository and assigned the identifier PXD010648 (MassIVE code: MSV000082676).

ACKNOWLEDGMENTS

We are grateful to Amelie Fradet-Turcotte, Michael Witcher, Josie Ursini-Siegel, Chantal Autexier and William Foulkes for critical reading of the manuscript; to Daniel Durocher, Anne-

Claude Gingras, Jeremy Stark, Michael Witcher and Roger Greenberg for plasmids and other reagents. We would like to specifically thank Roderick McInnes, Josie Ursini-Siegel and Koren Mann for their constant support. JH, VL and MK received a doctoral fellowship from the Cole Foundation. AM was supported by a post-doctoral fellowship from the Cole Foundation. ESC received a FRQS postdoctoral training scholarship. HB was supported by a doctoral training award from the FRQS (#33603). JFC is the recipient of the TRANSAT chair in Breast Cancer Research. JYM is a FRQS Chair in Genome Stability. AO is the Canada Research Chair (Tier 2) in Genome Stability and Hematological Malignancies. Work in the AO laboratory was supported by a CIHR Project Grant (#376245), a CRS Operating Grant (#21038), a Transition Grant from the Cole Foundation and an internal Operating Fund from the Sir Mortimer B. Davis Foundation of the Jewish General Hospital. Work in the JFC laboratory was supported by a NSERC Discovery Grant (RGPIN-2016-04808). Work in the AM laboratory was supported by a NSERC Discovery Grant (#5026) and a CIHR Project Grant (#376288). “Life always offers you a second chance. It is called tomorrow!”. Work in the JYM laboratory was supported by a CIHR Foundation grant.

AUTHOR CONTRIBUTIONS

SF and JH designed, performed most of the experiments presented in this manuscript and analyzed the data. VL designed and performed the CSR experiments and analyzed the data. AbM designed, performed the CRISPR/Cas9-based genome-wide screen and the clonogenic experiments and analyzed the data. TM and BD performed the laser stripe micro-irradiation and AM designed the experiments and analyzed the data. YC purified recombinant SHLD2 and performed the in vitro DNA binding assays under the supervision of JYM. ZL generated most of the constructs used in this manuscript, designed and performed the ChIP experiments and analyzed the data. AS designed and performed the comet assay experiments and analyzed the data. ESC, HB, DG, CD and HuK and EGL performed the MS experiments and analyzed the data under the supervision of JFC. MK performed the initial characterization of SHDL2 in the FokI system. DR performed the phylogenetic analysis profiling under the supervision of YT. KM performed the pathway analysis of SHLD2. HK and KK performed the RNA-seq analysis and the patient cohort analysis under the supervision of CMG. MP provided the RNA-seq data and the related patient outcome of the TNBC cohort. AO conceived the study, designed the research, provided supervision and wrote the manuscript with input from all the other authors.

CONFLICT OF INTEREST

The authors declare that they have no conflict of interest.

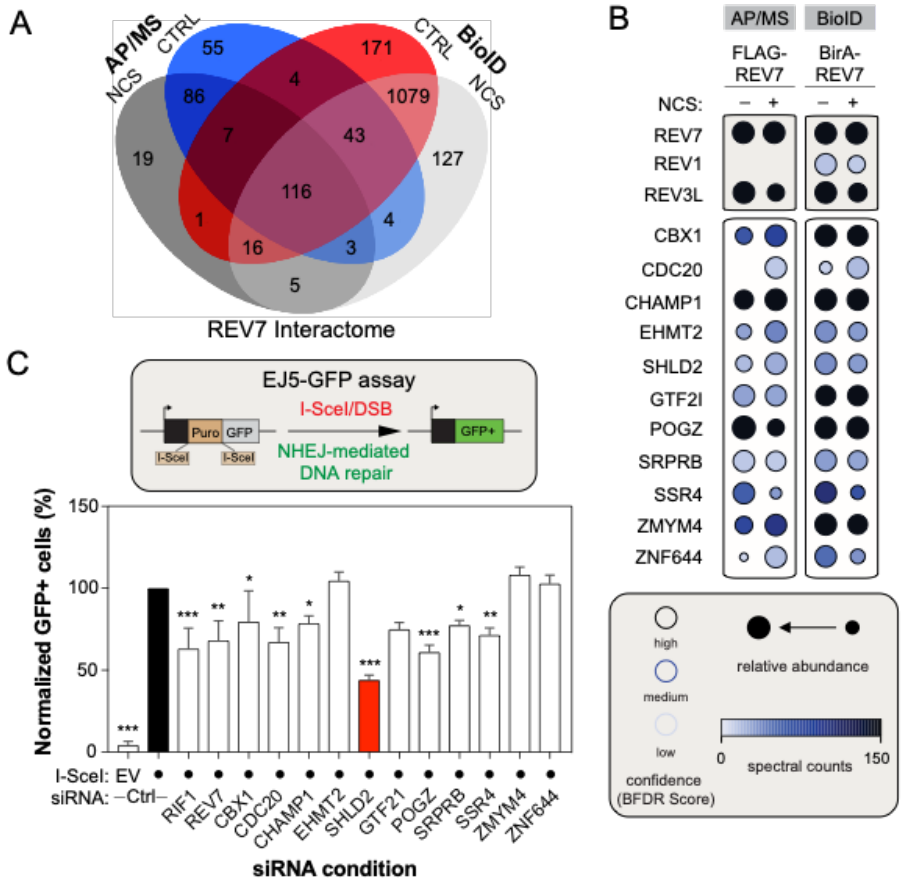

Figure 3.2 Identification of novel REV7 interactors relevant for the NHEJ pathway.

(A) Venn Diagram representing the distribution of proteins identified by both the BioID and the standard AP/MS of REV7, with or without DNA damage (NCS).

(B) Selected BioID REV7 results, shown as dot plots. The spectral counts for each indicated prey protein are shown as AvgSpec. Proteins were selected based on and iProphet probability of >0.95, BFDR of <0.05 and ≥10 peptide count. The circle size represents the relative abundance of preys over baits.

(C) U2OS EJ5-GFP cells were transfected with the indicated siRNAs. At 24hr post-transfection, cells were transfected with the I-SceI expression plasmid, and the GFP^+ population was analyzed 48 hr post-plasmid transfection. The percentage of GFP^+ cells was determined for each individual condition and subsequently normalized to the non-targeting condition (siCTRL). Data is presented as the mean ± SD (n=3). Significance was determined by one-way ANOVA followed by a Dunnett test. *$p<0.05$, **$p<0.005$, ***$p<0.0005$

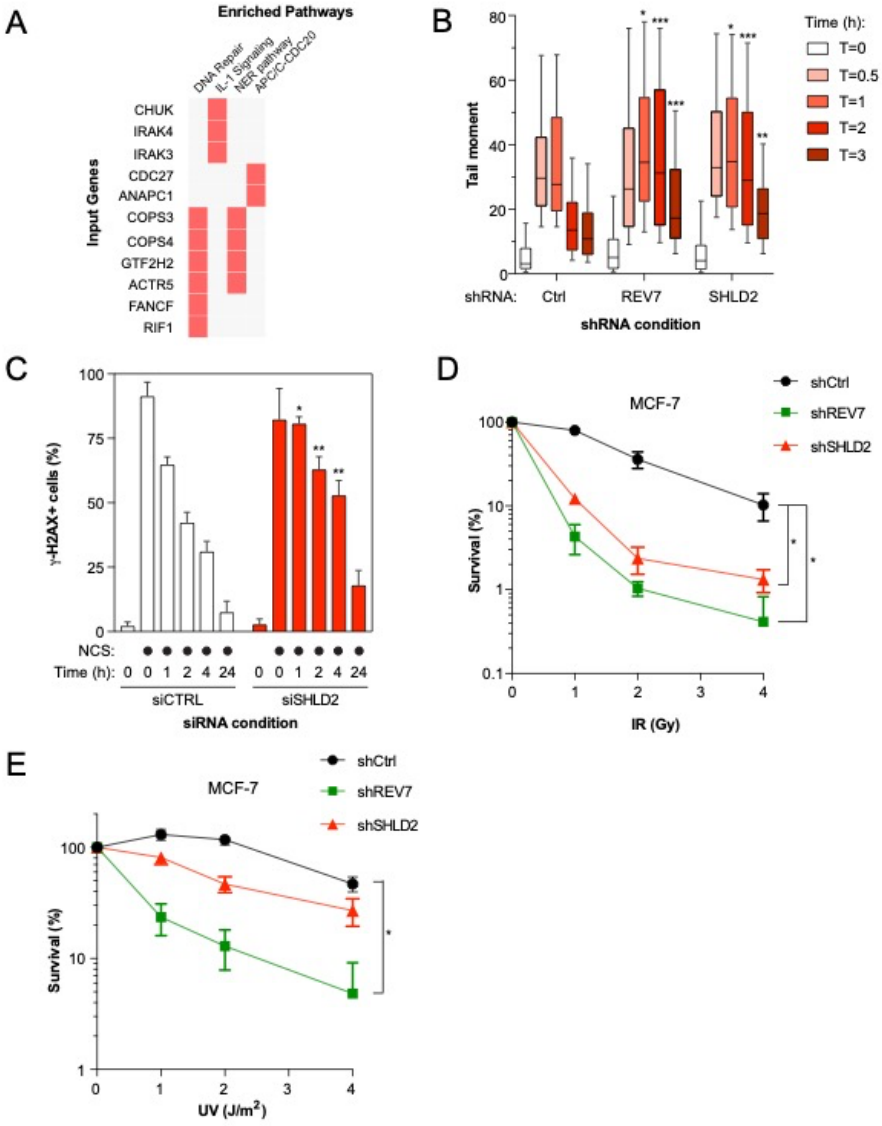

Figure 3.3 SHLD2 plays a critical in DNA repair.

(A) Pathway enrichment analysis on genes co-evolving with SHLD2 in mammalians and vertebrates using a phylogenetic profiling approach followed by an Enrichr-based analysis.

(B) Quantification of the Neutral Comet assay. U2OS cells stably expressing shCtrl, shREV7 or shSHLD2 were exposed to IR (10 Gy) and run in low melting agarose under neutral conditions. Immunofluorescence against DNA stained with SYBR Gold was performed to measure the tail moment. Data are represented as a box and whiskers graph where the box tends from the 25th to the 75th percentiles while the whiskers are drawn down to the 10th percentile and up to the

90^{th}. Significance was determined by one-way ANOVA followed by a Dunnett test. *p<0.05, **p<0.005, ***p<0.0005**.**

(C) U2OS cells were transfected with the indicated siRNA. 48h post-transfection the cells were treated with NCS to induce DNA damage and the cells were harvested at 0, 1, 2, 4 and 24 hr post NCS treatment. Flow Cytometry analysis of phosphorylated-H2AX signal was used to measure γ-H2AX endogenous signal. Data are represented as a bar graph showing the mean +/- SD. Significance was determined by two-way ANOVA followed by a Bonferroni test. *p<0.05, **p<0.005.

(D) Sensitivity to IR monitored by Colony formation assay. MCF-7 cells stably expressing the the indicated shRNAs were exposed to increasing doses of IR. 24 h post-irradiation, the cells were re-seeded to allow colony formation, fixed and stained with 0.4% crystal violet. Shown is the quantification of colonies per condition which possessed more than 50 colonies. Significance was determined by one-way ANOVA followed by a Dunnett test. *p<0.05.

(E) Similar to (D), except that cells were exposed to increasing doses of UV radiation. Significance was determined by one-way ANOVA followed by a Dunnett test. *p<0.05.

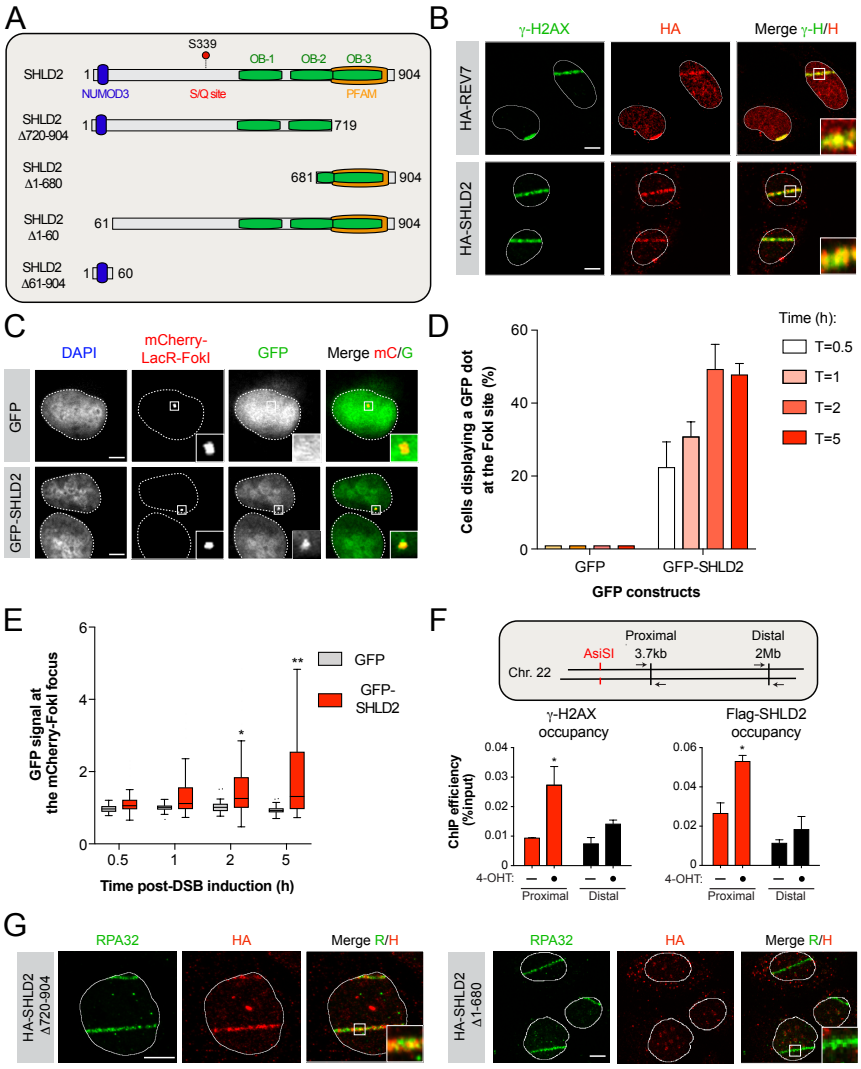

Figure 3.4 SHLD2 is recruited and accumulates at DNA damage sites.

(A) Schematic representation of SHLD2 and the different mutants used in this study. Each putative structural domain of SHLD2 is represented.

(B) U2OS cells stably expressing HA-REV7 (Top) or HA-SHLD2 (Bottom) were pre-sensitized with 10ug/mL Hoescht 33342 before exposed to UV micro-irradiation. Immunofluorescence against endogenous HA and γ-H2AX epitope was subsequently performed to monitor REV7 and SHLD2 accumulation at sites of damage. Shown are representative micrographs. Scale bar = 5μm.

(C) U2OS LacR-Fok1 cells were transfected with GFP or GFP-SHLD2 and 24 h later DNA damage was induced using Shield-1 and 4-OHT. The cells were then processed for GFP and mCherry immunofluorescence. Shown are representative micrographs. Scale bar = 5μm.

(D) Quantification of the experiments shown in (C). Data are represented as the mean ± SD (n=3). At least 100 cells per condition were counted.

(E) Quantification of the experiments shown in (C). Shown is the quantification of the GFP signal at the mCherry-LacR-Fok1 focus. Data are represented as a box-and-whisker plot in the style of Tukey. At least 100 cells per condition were counted. Significance was determined by non-parametric test followed by a Kruskal-Wallis test. *$p<0.005$, **$p<0.0005$.

(F) Schematic representation of the site-directed generation of DSB by the restriction enzyme *AsiSI* (Top). 293T cell lines expressing ER-*AsiSI* with Flag-SHLD2 and treated with 1 μM of 4-OHT. 6h later the cells were processed and immunoprecipitated with Anti-FLAG Magnetic Beads and anti-γ-H2AX.x/Protein A/G magnetic beads. DNA was purified and subjected to qPCR detection. Shown is the quantification of IP efficiency as the percentage of DNA precipitated from input (Bottom). Data is presented as the mean ± SEM (n=3). Significance was determined by two-way ANOVA followed by a Sidak test. *$p<0.05$.

(G) U2OS cells stably expressing HA-SHLD2Δ720-904 (Left) or HA-SHLD2Δ1-680 (Right) were processed as in (B). Immunofluorescence against endogenous HA and RPA32 epitope was subsequently performed to monitor RPA32 and SHLD2 accumulation at sites of damage. Shown are representative micrographs. Scale bar = 5μm.

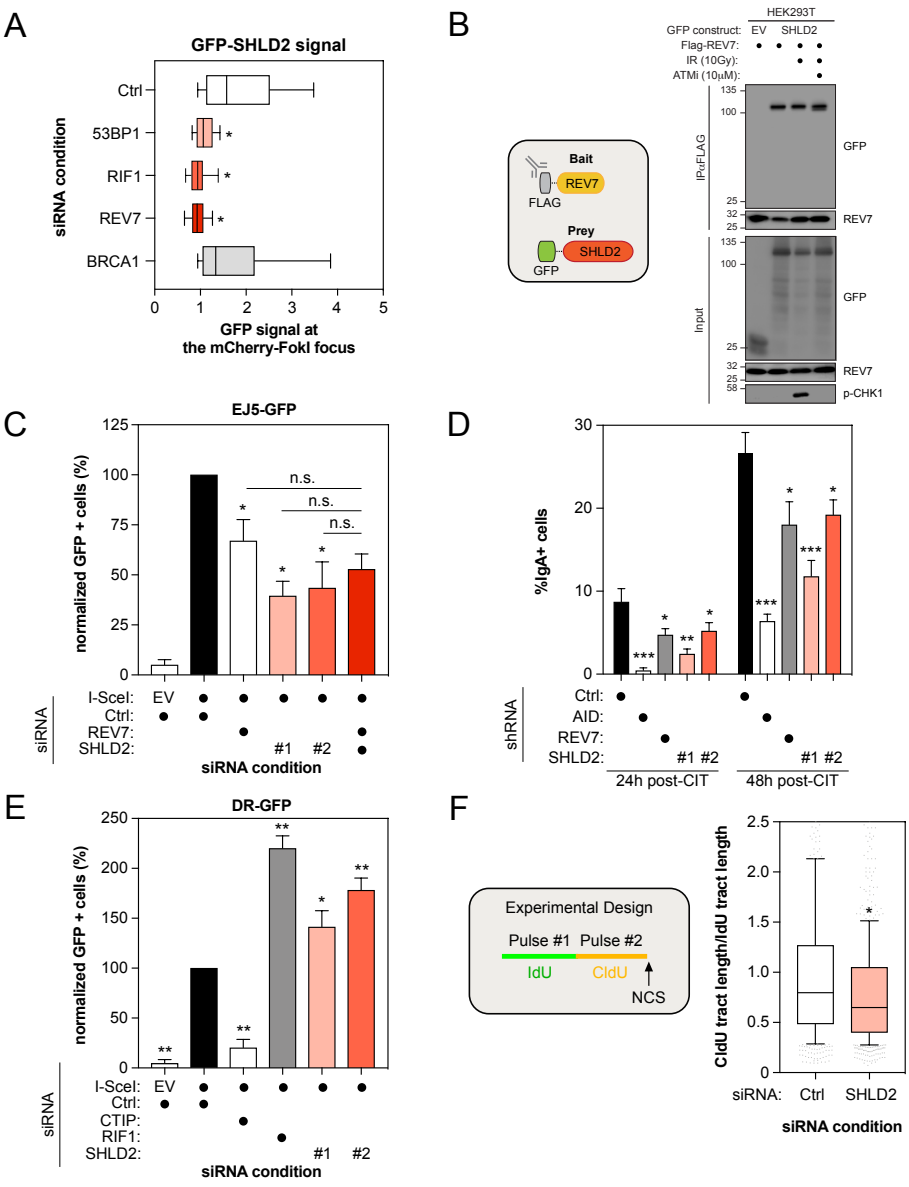

Figure 3.5 SHLD2 is an effector of REV7 in promoting NHEJ and antagonizing HR.

(A) U2OS mCherry-LacR-Fok1 cells were treated with the indicated siRNA and subsequently transfected with a GFP-SHLD2 construct. 24 h post-transfection DNA damage was induced using Shield-1 and 4-OHT. The cells were then fixed and analyzed for the intensity of the GFP-SHLD2 signal at mCherry-LacR-Fok1 focus. Shown is the quantification of the GFP-SHLD2 signal at the Fok1 focus. Data are represented as a box-and-whisker plot where the whiskers represent the 10-90 percentile. At least 75 cells were counted per condition. Significance was determined by one-way ANOVA followed by a Dunnett test. *p<0.05.

(B) 293T cells were transfected with Flag-REV7 and GFP-SHLD2 expression vectors as indicated. 24h post-transfection cells were treated with DMSO or with 10uM of ATM inhibitor KU-60019 for 1 h prior to irradiation. 1h post-irradiation (10 Gy) nuclear extracts were prepared and REV7 complexes were immunoprecipitated using anti-Flag (M2) Resin and then analyzed by immunoblotting using GFP, REV7 and p-Chk1 antibodies.

(C) U2OS EJ5-GFP cells were transfected with the indicated siRNAs. At 24hr post-transfection, cells were transfected with the I-SceI expression plasmid, and the GFP^+ population was analyzed 48 hr post-plasmid transfection. The percentage of GFP^+ cells was determined for each individual condition and subsequently normalized to the non-targeting condition (siCTRL). Data are presented as the mean ± SD (n=3*).* Significance was determined by one-way ANOVA followed by a Dunnett test using Ctrl+SceI as a comparison (*p<0.0005) or the indicated reference (n.s.= non-significant).

(D) CH12F3-2 cells stably expressing the indicated shRNAs were stimulated with a cocktail of cytokines (CIT) to induce class switching to IgA. The percentage of IgA^+ cells was monitored 24 and 48h post-stimulation by staining with an anti-IgA antibody followed by flow cytometry analysis. Data are presented as the mean ± SD (n=3*).* Significance was determined by one-way ANOVA followed by a Dunnett test. *p<0.05, **p<0.005, ***p<0.0005**.**

(E) U2OS DR-GFP cells were transfected with the indicated siRNAs. At 24hr post-transfection, cells were transfected with the I-SceI expression plasmid, and the GFP^+ population was analyzed 48 hr post-plasmid transfection. The percentage of GFP^+ cells was determined for each individual condition and subsequently normalized to the non-targeting condition (siCTRL). Data are presented as the mean ± SD (n=3). Significance was determined by one-way ANOVA followed by a Dunnett test. *p<0.005, **p<0.0005**.**

(F) Schematic representation of the DNA fiber assay experimental design (Left). U2OS cells were transfected with the indicated siRNAs and then treated with CldU, IdU and NCS 48h post-transfection as indicated. The slides were stained, dehydrated, mounted and visualized and shown is the quantification of CldU/IdU tract length in order to visualize DNA end-resection (Right). At least 500 DNA tracks were measured per condition. Data are represented as a box-and-whisker plot where the whiskers represent the 10-90 percentile. Significance was determined by one-way ANOVA followed by a Dunnett test. *p<0.0005**.**

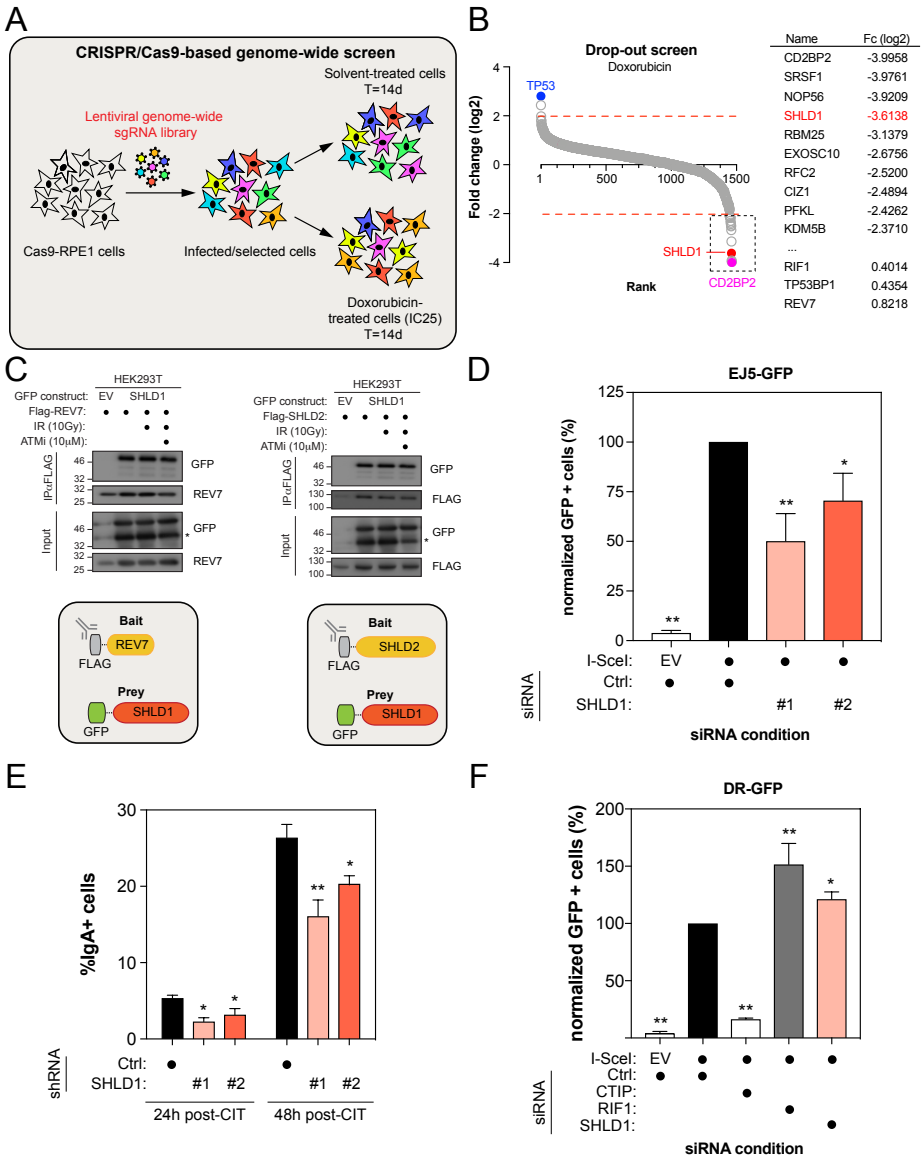

Figure 3.6 SHLD1 cooperates with SHLD2 and REV7 to promote NHEJ and restrict HR.

(A) Schematic Representation of CRISPR/Cas9-based Genome-Wide Screen under Doxorubicin treatment.

(B) Genes significantly enriched or dropped out after a 14-day treatment with Doxorubicin were identified by plotting as a Log2 fold change compared to untreated. Ranking was determined based on the Log2 fold score (Left). The top ten Doxorubicin sensitizers are indicated on the right with their respective fold change (Fc) in Log2.

(C) 293T cells were transfected with Flag-REV7 and GFP-SHLD1 (Left) or Flag-SHLD2 and GFP-SHLD1 (Right) expression vectors as indicated. 24h post-transfection cells were treated with DMSO or with 10uM of ATM inhibitor KU-60019 for 1 h prior to irradiation. 1h post-irradiation (10 Gy) nuclear extracts were prepared and REV7 or SHLD2 complexes were immunoprecipitated using anti-Flag (M2) Resin and then analyzed by immunoblotting using GFP and REV7 antibodies.

(D) U2OS EJ5-GFP cells were transfected with either siCTRL, siSHLD1 #1 or siSHLD1 #2. At 24hr post-transfection, cells were transfected with the I-SceI expression plasmid, and the GFP^+ population was analyzed 48 hr post-plasmid transfection. The percentage of GFP^+ cells was determined for each individual condition and subsequently normalized to the non-targeting condition (siCTRL). Data is presented as the mean ± SD (n=3). Significance was determined by one-way ANOVA followed by a Dunnett test. *p<0.005, **p<0.0005.

(E) CH12F3-2 cells stably expressing either shCTRL, shSHLD1#1 or shSHLD1#2 were stimulated with a cocktail of cytokines (CIT) to induce class switching to IgA. The percentage of IgA^+ cells was monitored 24 and 48h post-stimulation by staining with an anti-IgA antibody followed by flow cytometry analysis. Data are presented as the mean ± SD (n=3*).* Significance was determined by one-way ANOVA followed by a Dunnett test. *p<0.05, **p<0.005.

(F) U2OS DR-GFP cells were transfected with the indicated siRNAs. At 24hr post-transfection, cells were transfected with the I-SceI expression plasmid, and the GFP^+ population was analyzed 48 hr post-plasmid transfection. The percentage of GFP^+ cells was determined for each individual condition and subsequently normalized to the non-targeting condition (siCTRL). Data are presented as the mean ± SD (n=3). Significance was determined by one-way ANOVA followed by a Dunnett test. *p<0.005, **p<0.0005.

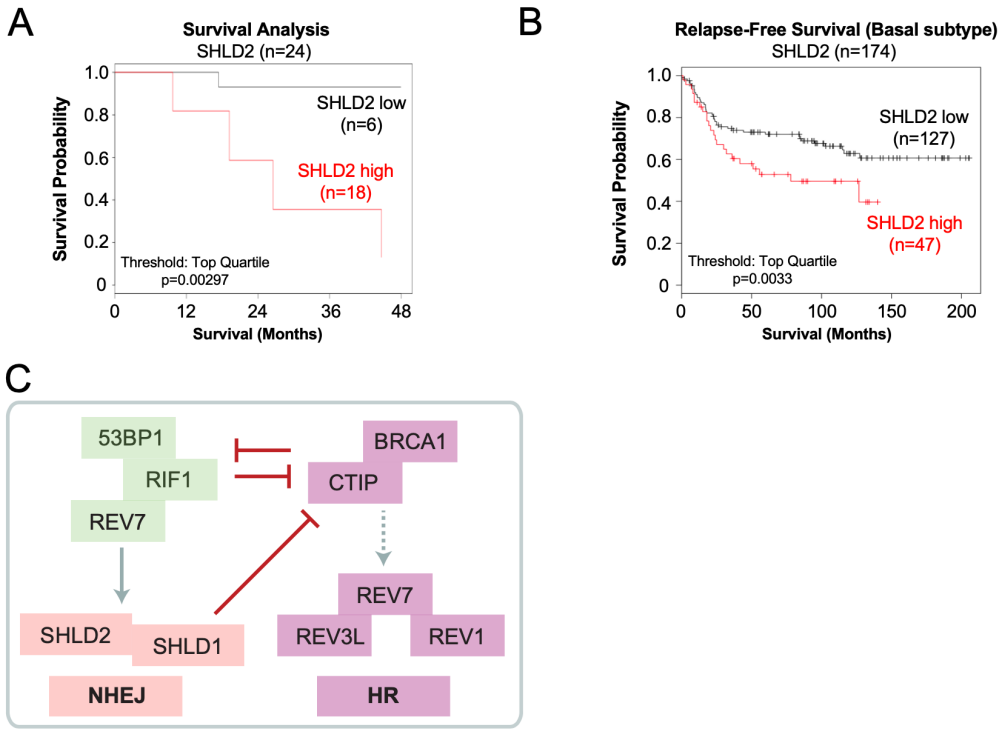

Figure 3.7 SHLD2 levels are candidate marker for the prognosis of subset of breast cancer.

(A) Survival analysis of low and high expressers of SHLD2 in a cohort of 24 patients affected by Triple Negative Breast cancer (TNBC). Data are represented as Kaplan-Meyer curves with expression classified as low and high. Threshold for high cut-off is the top quartile. Significance was determined by calculating the hazard ratio with 95% confidence and the logrank P value.

(B) Relapse-free Survival (Basal Subtype) of low and high expressers of SHLD2 obtained from the KM-plotter database. Data are represented as Kaplan-Meyer curves with expression classified as low and high. Threshold for high cut-off is the top quartile. Significance was determined by calculating the hazard ratio with 95% confidence and the logrank P value.

(C) Schematic incorporating SHLD2 and SHLD1 as REV7 effectors in the NHEJ pathway and modulators of DNA repair pathway choice.

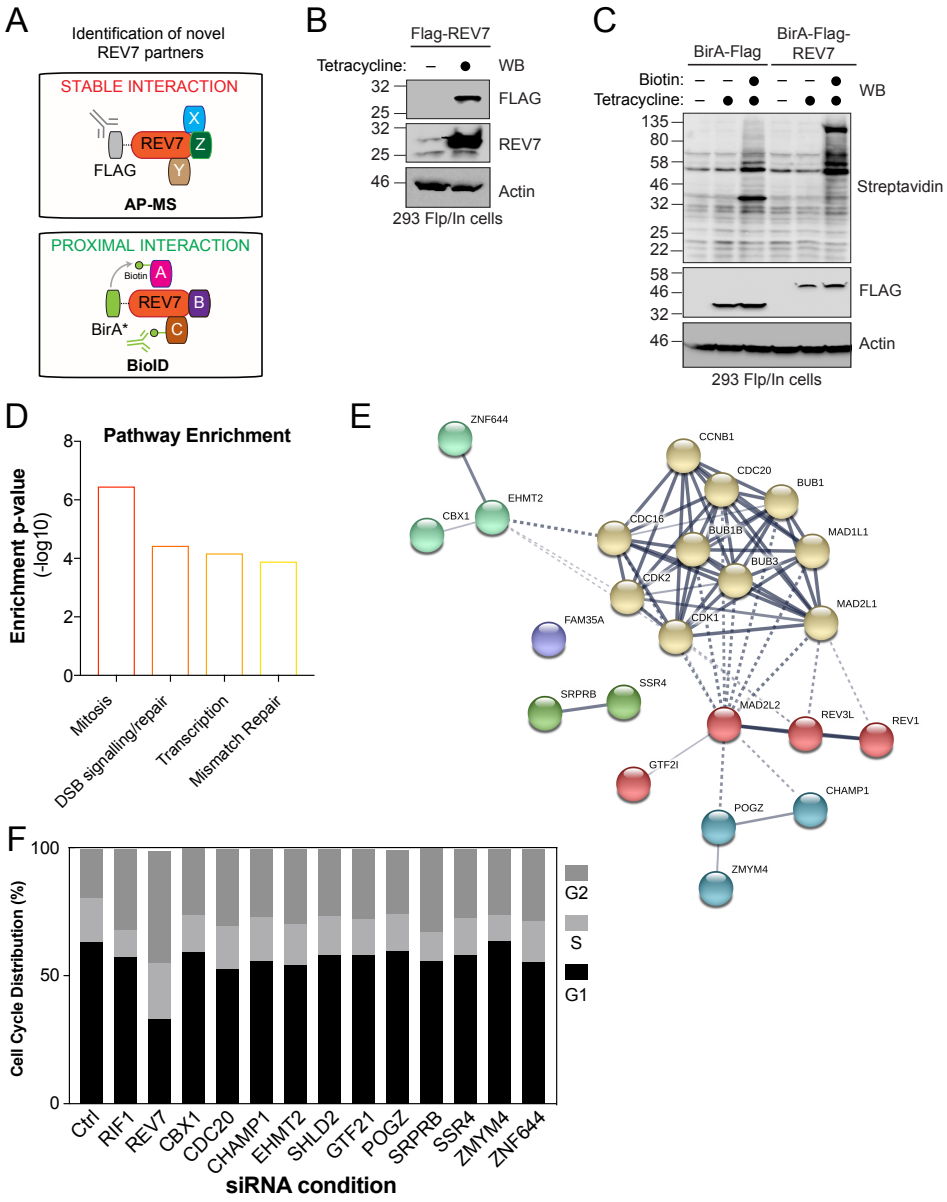

Supplemental Figure 3.1 Analysis of REV7 interactome.

(A) Schematic representation of AP-MS stable interaction Flag-REV7 pulldown and the BioID BirA*-REV7 biotinylation of proximal interactors.

(B) HEK293-TREx cells stably expressing an inducible Flag-REV7 construct were tested for expression following induction with tetracycline as indicated. After lysis, samples were immunoblotted for FLAG and REV7. Actin was used as a loading control.

(C) HEK293-TREx cells stably expressing an inducible BirA-Flag or BirA-Flag-REV7 construct were tested for expression and biotinylation following induction with tetracycline and incubation with biotin as indicated. After lysis, samples were immunoblotted for FLAG and Streptavidin. Actin was used as a loading control.

(D) The interactome of REV7 obtained from both the AP-MS and the BioID approaches were analyzed for pathway enrichment using EnrichR. The y-axis represents the ratio of the number of genes from the dataset that map to the pathway and the number of all known genes ascribed to the pathway and is defined as enrichment of p-value(-log10).

(E) Network representation of the selected 11 high-confidence interactors of REV7 (annotated as MAD2L2 in this figure) and their previously described interactors. Proteins are represented following the k-means clustering through STRING v10.5.

(F) Cell cycle distribution of U2OS EJ5-GFP cells transfected with the indicated siRNAs and subsequently for Propidium iodide (PI) staining and flow cytometry analysis. Data are presented as the mean (n=2).

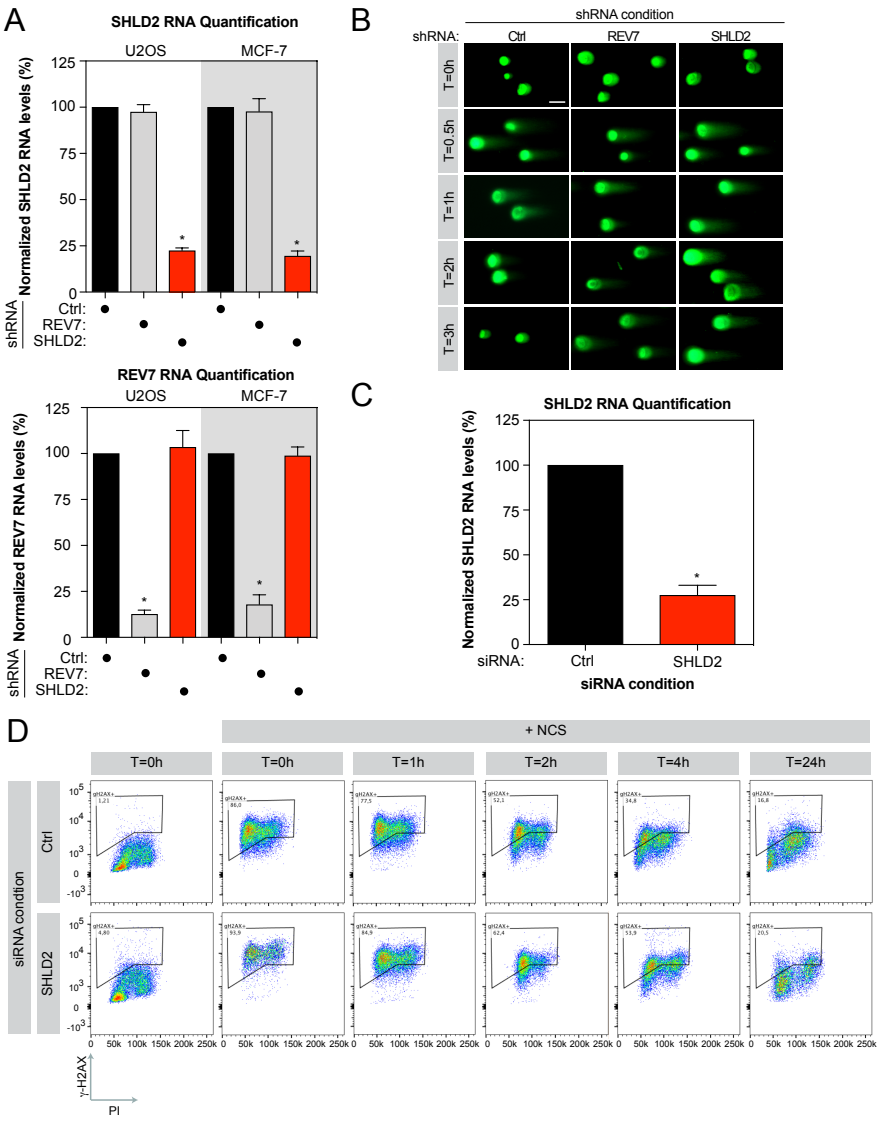

Supplemental Figure 3.2 Evaluation of the impact of SHLD2 on DNA repair.

(A) U2OS and MCF-7 cells were subjected to lentiviral-mediated short hairpin RNA knockdown for REV7 or SHLD2, selected with puromycin for 48 hours then harvested. Total RNA was isolated, cDNA was generated and levels of REV7 and SHLD2 were identified by qPCR. mRNA levels were normalized to mRNA levels of GAPDH. Data are presented as the mean ± SEM (n=3*)*. Significance was determined by one-way ANOVA followed by a Dunnett test. *p<0.0005**.**

(B) Representative images of Comet Assay Tail Moment quantified in Figure 2. U2OS cells stably expressing shCtrl, shREV7 or shSHLD2 were exposed to irradiation (10Gy) and run in low

melting agarose under neutral conditions. Immunofluorescence against DNA stained with SYBR Gold was performed to measure the tail moment. Scale bar = 10μm.

(C) U2OS cells were transfected with small interfering RNA against REV7 or SHLD2 for 48 hours, Total RNA was isolated, cDNA was generated and levels of REV7 and SHLD2 were identified by qPCR. mRNA levels were normalized to mRNA levels of GAPDH. Data are presented as the mean ± SEM (n=3*)*. Significance was determined by one-way ANOVA followed by a Dunnett test. *$p<0.0005$**.**

(D) Representative flow cytometry profiles of U2OS cells transfected with the indicated siRNA and subsequently treated with NCS for 30 mins before being trypsinized and processed for anti-γ-H2AX (y axis) and PI (x axis) staining.

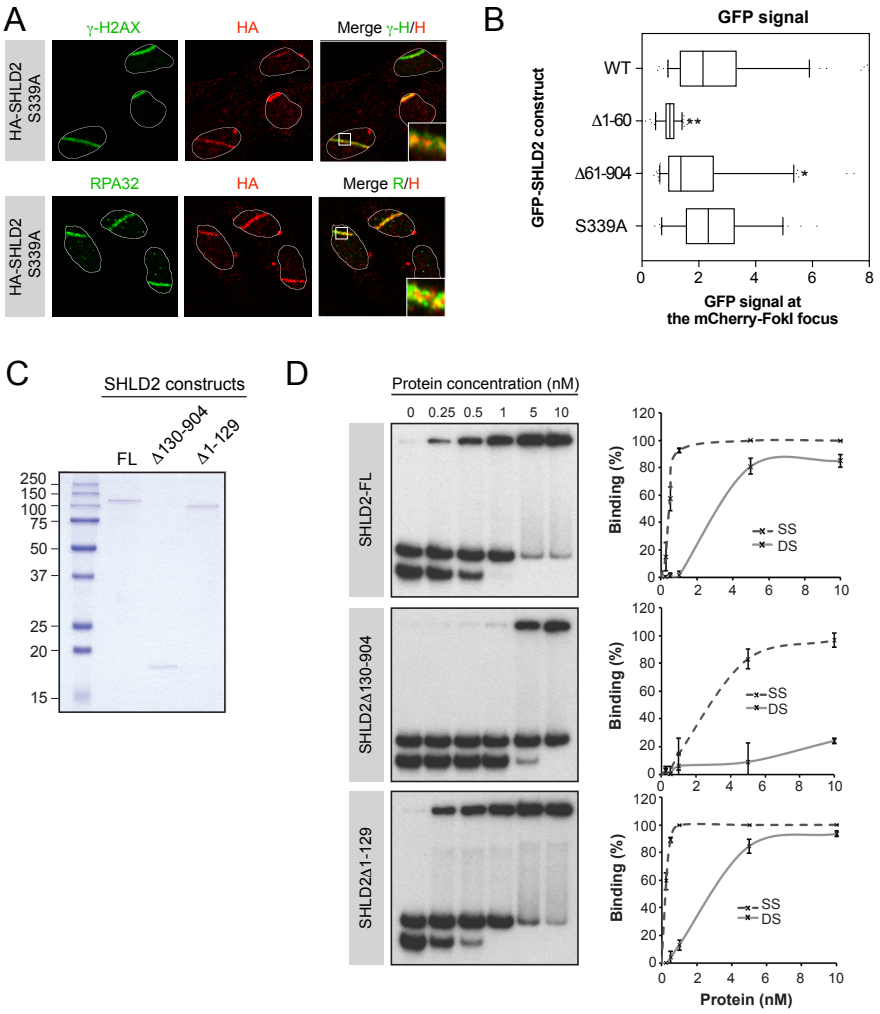

Supplemental Figure 3.3 Structure-Function analysis of SHLD2.

(A) U2OS cells stably expressing HA-SHLD2-S399A were processed as previously described Immunofluorescence against endogenous HA, γ-H2AX (Top) and RPA32 (Bottom) epitope was subsequently performed to monitor their accumulation at sites of damage. Shown are representative micrographs.

(B) U2OS LacR-Fok1 cells were transfected with GFP-SHLD2, GFP-SHLD2-S339A, GFP-SHLD2-Δ1-60, or GFP-SHLD2-Δ61-904 mutant, and 24 h later DNA damage was induced using Shield-1 and 4-OHT. The cells were then processed for GFP and mCherry

immunofluorescence. Shown is the quantification of cells expression GFP at Fok1 sites. Data are represented as a box-and-whisker plot where the whiskers represent the 10-90 percentile. At least 75 cells were counted per condition. Significance was determined by one-way ANOVA followed by a Dunnett test. *$p<0.005$, **$p<0.0005$

(C) Recombinant SHLD2 constructs were purified from Sf9 insect infected and protein purity was assessed by Coomassie Blue stain. Shown are the protein samples used for the DNA binding assay.

(D) *In vitro* DNA binding assay was performed using a purified recombinant SHLD2 or SHLD2-mutants (concentration range: 0–10nM) with ^{32}P labelled DNA oligonucleotide substrates. Protein-DNA complexes were subjected to electrophoresis and visualized by autoradiography. Representative binding experiments (left panel; n=3) and quantification of the binding efficiency (right panel) are shown.

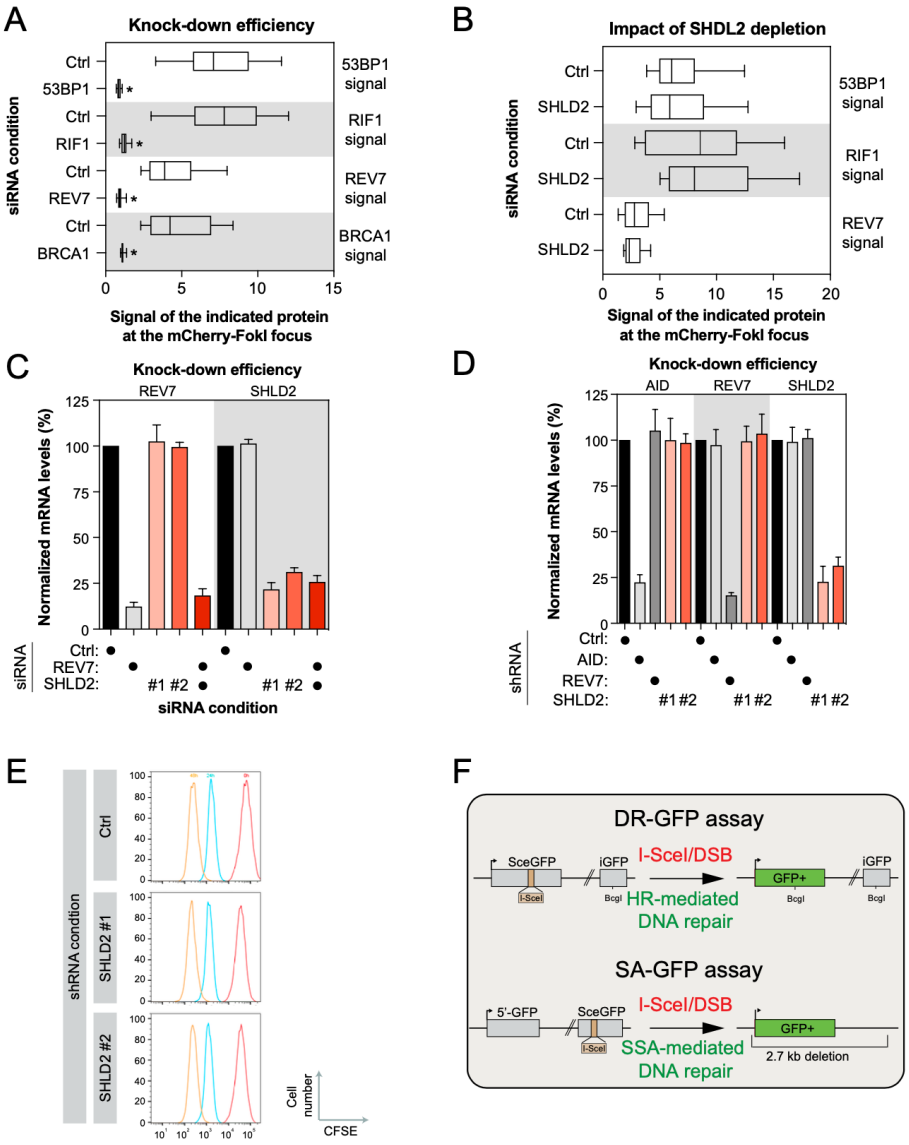

Supplemental Figure 3.4 Characterization of the role of SHLD2 in the NHEJ pathway.

(A) U2OS LacR-Fok1 cells were transfected with small interfering RNA directed against 53BP1, RIF1, REV7 or BRCA1. Forty-eight hours later the cells were then processed for AF647 and mCherry immunofluorescence. Shown is the ratio of fluorescence of AF647 at Fok1 focus compared to background. Data are represented as a box-and-whisker plot where the whiskers represent the 10-90 percentile. At least 75 cells were counted per condition. Significance was determined by one-way ANOVA followed by a Dunnett test. *$p<0.005$, **$p<0.0005$

(B) U2OS LacR-Fok1 cells were transfected with small interfering RNA directed against SHLD2. 48 hours later DNA damage was induced using Shield-1 and 4-OHT, followed by staining to identify 53BP1, RIF1, REV7 or BRCA1 protein localization by indirect AF647 fluorescence.

The cells were then processed for AF647 and mCherry immunofluorescence. Shown is the quantification of cells expression GFP at Fok1 sites. Data are represented as a box-and-whisker plot where the whiskers represent the 10-90 percentile. At least 75 cells were counted per condition. Significance was determined by one-way ANOVA followed by a Dunnett test. *p<0.005, **p<0.0005.

(C) EJ5-2OS cells were transfected with small interfering RNA against REV7 or SHLD2 for 48 hours, Total RNA was isolated, cDNA was generated and levels of REV7 and SHLD2 were identified by qPCR. mRNA levels were normalized to mRNA levels of GAPDH. Data are presented as the mean ± SEM (n=3*).* Significance was determined by one-way ANOVA followed by a Dunnett test. *p<0.0005.

(D) CH12F2-3 cells were subjected to lentiviral-mediated short hairpin RNA knockdown for REV7 or SHLD2, selected with puromycin for 48 hours then harvested. Total RNA was isolated, cDNA was generated and levels of REV7 and SHLD2 were identified by qPCR. mRNA levels were normalized to mRNA levels of GAPDH. Data are presented as the mean ± SEM (n=3*).* Significance was determined by one-way ANOVA followed by a Dunnett test. *p<0.0005.

(E) Proliferation of the different transduced CH12F3-2 cell lines was monitored using CFSE dilution. FACS profiles are representative of 3 independent experiments.

(F) Schematic diagram of both the DR-GFP reporter assay (Top) and the SA-GFP reporter assay showing (Bottom).

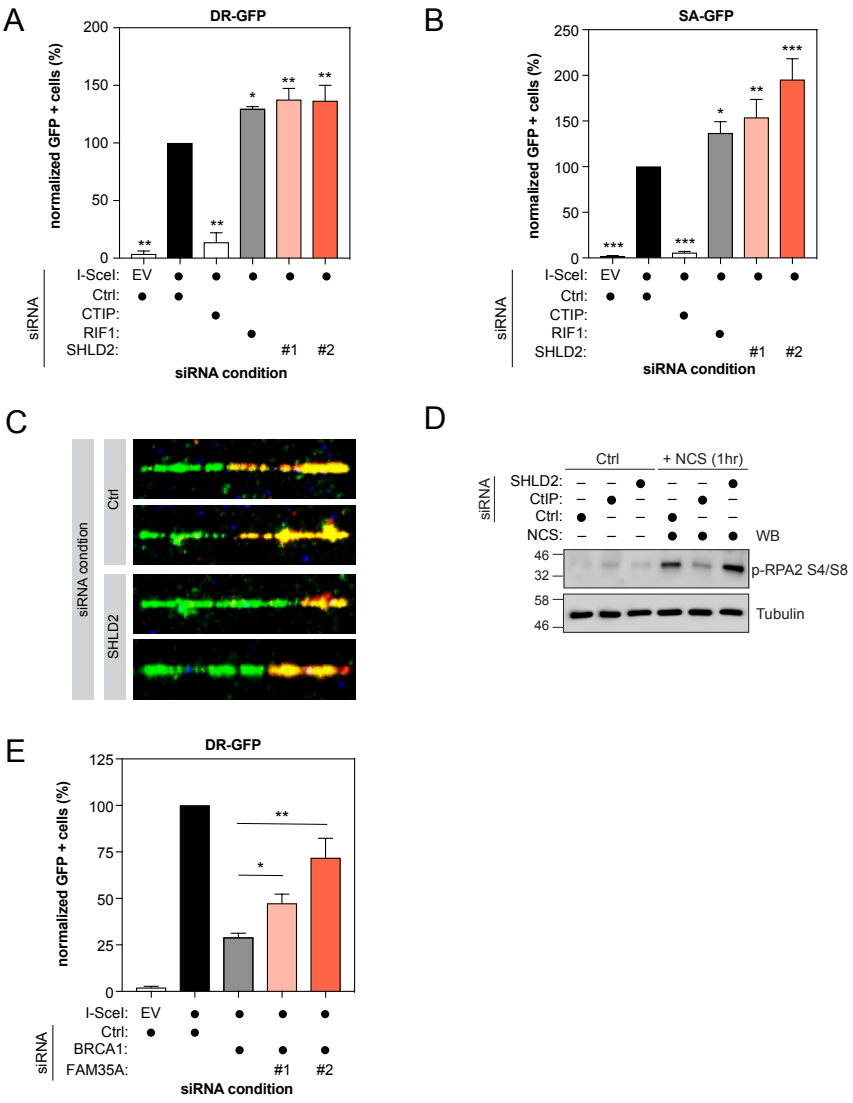

Supplemental Figure 3.5 Characterization of the role of SHLD2 in the HR pathway.

(A) HeLa DR-GFP cells were transfected with the indicated siRNAs. At 24hr post-transfection, cells were transfected with the I-SceI expression plasmid, and the GFP^+ population was analyzed 48 hr post-plasmid transfection. The percentage of GFP^+ cells was determined for each individual condition and subsequently normalized to the non-targeting condition (siCTRL). Data is presented as the mean ± SD (n=3). Significance was determined by one-way ANOVA followed by a Dunnett test. *p<0.0005, **p=0.0001.

(B) U2OS SA-GFP cells were transfected with the indicated siRNAs. At 24hr post-transfection, cells were transfected with the I-SceI expression plasmid, and the GFP^+ population was

analyzed 48 hr post-plasmid transfection. The percentage of GFP^+ cells was determined for each individual condition and subsequently normalized to the non-targeting condition (siCTRL). Data is presented as the mean ± SD (n=3). Significance was determined by one-way ANOVA followed by a Dunnett test. *p<0.05, **p<0.005, ***p<0.0005.

(C) Representative images of the DNA fiber assay obtained from U2OS cells which were transfected with the indicated siRNAs and then treated with CldU, IdU and NCS 48h post-transfection as indicated. The slides were stained, dehydrated, mounted and visualized and shown is the quantification of CldU/IdU tract length in order to visualize DNA end-resection.

(D) U2OS cells were transfected with the indicated siRNA's. The DNA damage experimental condition was performed using 500ng/ml of neocarzinostatin (NCS) for 1 hour. Cells were washed in D-PBS and harvested with a lysis buffer (50 mM HEPES, KOH (pH 8.0), 100 mM KCl, 2 mM EDTA, 0.1% NP-40, 10% glycerol) supplemented with protease/phosphatase inhibitors. The resulting whole cell lysates were analyzed by immunoblotting using p-RPA and α-tubulin then analyzed by immunoblotting using GFP, REV7 and p-Chk1 antibodies.

(E) HeLa DR-GFP cells were co-transfected with siBRCA1 and the indicated siRNAs. At 24hr post-transfection, cells were transfected with the I-SceI expression plasmid, and the GFP^+ population was analyzed 48 hr post-plasmid transfection. The percentage of GFP^+ cells was determined for each individual condition and subsequently normalized to the non-targeting condition (siCTRL). Data is presented as the mean ± SD (n=3). Significance was determined by one-way ANOVA followed by a Dunnett test. *p<0.05, **p<0.0005.

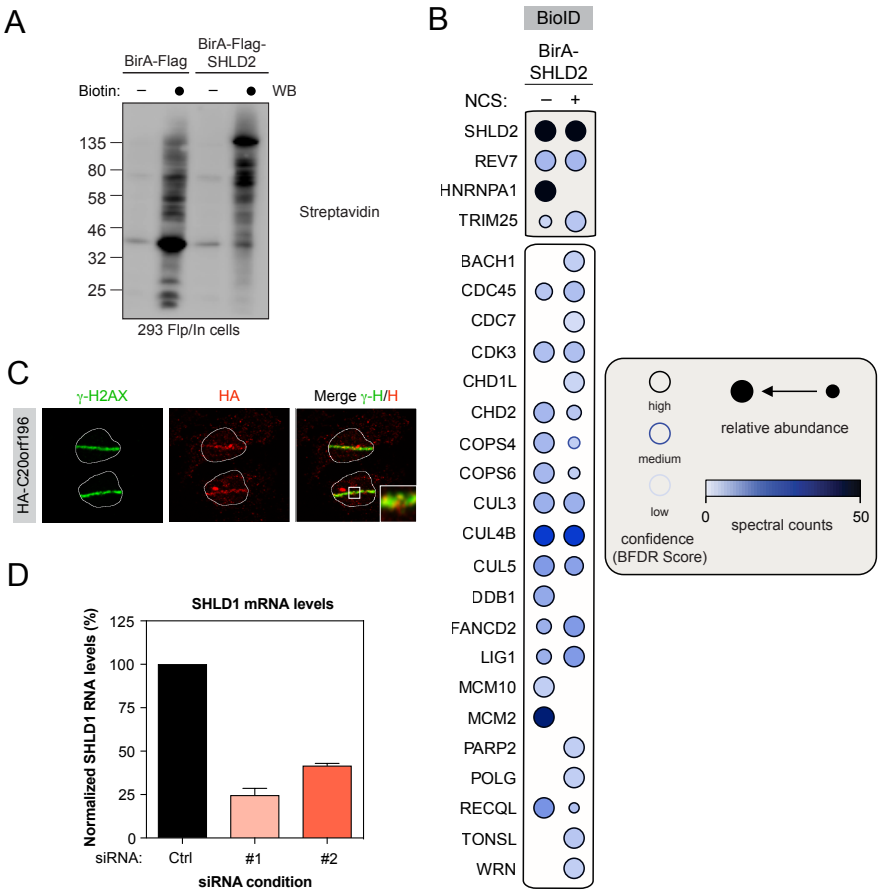

Supplemental Figure 3.6 Identification of SHLD2 interactome.

(A) HEK293-TREx cells transfected with a BirA-Flag or BirA-Flag-SHLD2 construct were tested for biotinylation following incubation with biotin as indicated. After lysis, samples were immunoblotted for Streptavidin.

(B) Selected BioID SHLD2 results, shown as dot plots. The spectral counts for each indicated prey protein are shown as AvgSpec. Proteins were selected based on and iProphet probability of >0.95, BFDR of <0.05 and ≥10 peptide count. The circle size represents the relative abundance of preys over baits.

(C) U2OS cells stably expressing HA-SHLD1 were processed as previously described Immunofluorescence against endogenous HA and γ-H2AX epitope was subsequently performed to monitor their accumulation at sites of damage. Shown are representative micrographs.

(D) EJ5-2OS cells were transfected with small interfering RNA against SHLD1 for 48 hours, Total RNA was isolated, cDNA was generated and levels of SHLD1 were identified by qPCR. mRNA levels were normalized to mRNA levels of GAPDH.

3.7 References

1. Obeng, E.A., et al., *Proteasome inhibitors induce a terminal unfolded protein response in multiple myeloma cells.* Blood, 2006. **107**(12): p. 4907-16.
2. Sung, M.H., et al., *Dynamic effect of bortezomib on nuclear factor-kappaB activity and gene expression in tumor cells.* Mol Pharmacol, 2008. **74**(5): p. 1215-22.
3. Lauricella, M., et al., *JNK and AP-1 mediate apoptosis induced by bortezomib in HepG2 cells via FasL/caspase-8 and mitochondria-dependent pathways.* Apoptosis, 2006. **11**(4): p. 607-25.
4. Neri, P., et al., *Bortezomib-induced "BRCAness" sensitizes multiple myeloma cells to PARP inhibitors.* Blood, 2011. **118**(24): p. 6368-6379.
5. Dantuma, N.P., et al., *A dynamic ubiquitin equilibrium couples proteasomal activity to chromatin remodeling.* J Cell Biol, 2006. **173**(1): p. 19-26.
6. Mailand, N., et al., *RNF8 ubiquitylates histones at DNA double-strand breaks and promotes assembly of repair proteins.* Cell, 2007. **131**(5): p. 887-900.
7. Takeshita, T., et al., *Perturbation of DNA repair pathways by proteasome inhibitors corresponds to enhanced chemosensitivity of cells to DNA damage-inducing agents.* Cancer Chemotherapy and Pharmacology, 2009. **64**(5): p. 1039-1046.
8. Cron, K.R., et al., *Proteasome inhibitors block DNA repair and radiosensitize non-small cell lung cancer.* PLoS One, 2013. **8**(9): p. e73710.
9. Gourzones-Dmitriev, C., et al., *DNA repair pathways in human multiple myeloma: role in oncogenesis and potential targets for treatment.* Cell cycle, 2013. **12**(17): p. 2760-2773.
10. Vangsted, A., et al., *Polymorphisms in the genes ERCC2, XRCC3 and CD3EAP influence treatment outcome in multiple myeloma patients undergoing autologous bone marrow transplantation.* International Journal of Cancer, 2007. **120**(5): p. 1036-1045.
11. Tubbs, A. and A. Nussenzweig, *Endogenous DNA Damage as a Source of Genomic Instability in Cancer.* Cell, 2017. **168**(4): p. 644-656.
12. Ceccaldi, R., B. Rondinelli, and A.D. D'Andrea, *Repair Pathway Choices and Consequences at the Double-Strand Break.* Trends Cell Biol, 2016. **26**(1): p. 52-64.

13. Hustedt, N. and D. Durocher, *The control of DNA repair by the cell cycle.* Nat Cell Biol, 2016. **19**(1): p. 1-9.
14. Betermier, M., P. Bertrand, and B.S. Lopez, *Is non-homologous end-joining really an inherently error-prone process?* PLoS Genet, 2014. **10**(1): p. e1004086.
15. Chapman, J.R., et al., *RIF1 is essential for 53BP1-dependent nonhomologous end joining and suppression of DNA double-strand break resection.* Mol Cell, 2013. **49**(5): p. 858-71.
16. Chapman, J.R., et al., *BRCA1-associated exclusion of 53BP1 from DNA damage sites underlies temporal control of DNA repair.* J Cell Sci, 2012. **125**(Pt 15): p. 3529-34.
17. Xu, G., et al., *REV7 counteracts DNA double-strand break resection and affects PARP inhibition.* Nature, 2015. **521**(7553): p. 541-544.
18. Boersma, V., et al., *MAD2L2 controls DNA repair at telomeres and DNA breaks by inhibiting 5' end resection.* Nature, 2015. **521**(7553): p. 537-540.
19. Callen, E., et al., *53BP1 mediates productive and mutagenic DNA repair through distinct phosphoprotein interactions.* Cell, 2013. **153**(6): p. 1266-80.
20. Di Virgilio, M., et al., *Rif1 prevents resection of DNA breaks and promotes immunoglobulin class switching.* Science, 2013. **339**(6120): p. 711-5.
21. Escribano-Diaz, C., et al., *A cell cycle-dependent regulatory circuit composed of 53BP1-RIF1 and BRCA1-CtIP controls DNA repair pathway choice.* Mol Cell, 2013. **49**(5): p. 872-83.
22. Zimmermann, M., et al., *53BP1 regulates DSB repair using Rif1 to control 5' end resection.* Science, 2013. **339**(6120): p. 700-4.
23. Feng, L., et al., *RIF1 counteracts BRCA1-mediated end resection during DNA repair.* J Biol Chem, 2013. **288**(16): p. 11135-43.
24. Manis, J.P., et al., *53BP1 links DNA damage-response pathways to immunoglobulin heavy chain class-switch recombination.* Nat Immunol, 2004. **5**(5): p. 481-7.
25. Ward, I.M., et al., *53BP1 is required for class switch recombination.* J Cell Biol, 2004. **165**(4): p. 459-64.
26. Fradet-Turcotte, A., et al., *BRCA2 functions: from DNA repair to replication fork stabilization.* Endocr Relat Cancer, 2016. **23**(10): p. T1-T17.
27. Bhat, A., et al., *Rev7/Mad2B plays a critical role in the assembly of a functional mitotic spindle.* Cell Cycle, 2015. **14**(24): p. 3929-38.

28. Listovsky, T. and J.E. Sale, *Sequestration of CDH1 by MAD2L2 prevents premature APC/C activation prior to anaphase onset.* J Cell Biol, 2013. **203**(1): p. 87-100.
29. Cahill, D.P., et al., *Characterization of MAD2B and other mitotic spindle checkpoint genes.* Genomics, 1999. **58**(2): p. 181-7.
30. Waters, L.S., et al., *Eukaryotic translesion polymerases and their roles and regulation in DNA damage tolerance.* Microbiol Mol Biol Rev, 2009. **73**(1): p. 134-54.
31. Sharma, S., et al., *REV1 and polymerase zeta facilitate homologous recombination repair.* Nucleic Acids Res, 2012. **40**(2): p. 682-91.
32. Roux, K.J., D.I. Kim, and B. Burke, *BioID: a screen for protein-protein interactions.* Curr Protoc Protein Sci, 2013. **74**: p. Unit 19 23.
33. Roux, K.J., et al., *A promiscuous biotin ligase fusion protein identifies proximal and interacting proteins in mammalian cells.* J Cell Biol, 2012. **196**(6): p. 801-10.
34. Lambert, J.P., et al., *Proximity biotinylation and affinity purification are complementary approaches for the interactome mapping of chromatin-associated protein complexes.* J Proteomics, 2015. **118**: p. 81-94.
35. Rolland, T., et al., *A proteome-scale map of the human interactome network.* Cell, 2014. **159**(5): p. 1212-1226.
36. Guo, C., et al., *Mouse Rev1 protein interacts with multiple DNA polymerases involved in translesion DNA synthesis.* EMBO J, 2003. **22**(24): p. 6621-30.
37. Tissier, A., et al., *Crosstalk between replicative and translesional DNA polymerases: PDIP38 interacts directly with Poleta.* DNA Repair (Amst), 2010. **9**(8): p. 922-8.
38. Zhang, L., S.H. Yang, and A.D. Sharrocks, *Rev7/MAD2B links c-Jun N-terminal protein kinase pathway signaling to activation of the transcription factor Elk-1.* Mol Cell Biol, 2007. **27**(8): p. 2861-9.
39. Vermeulen, M., et al., *Quantitative interaction proteomics and genome-wide profiling of epigenetic histone marks and their readers.* Cell, 2010. **142**(6): p. 967-80.
40. Chen, J. and G. Fang, *MAD2B is an inhibitor of the anaphase-promoting complex.* Genes Dev, 2001. **15**(14): p. 1765-70.
41. Hong, C.F., et al., *MAD2B, a novel TCF4-binding protein, modulates TCF4-mediated epithelial-mesenchymal transdifferentiation.* J Biol Chem, 2009. **284**(29): p. 19613-22.

42. Iwai, H., et al., *A bacterial effector targets Mad2L2, an APC inhibitor, to modulate host cell cycling.* Cell, 2007. **130**(4): p. 611-23.
43. Medendorp, K., et al., *The mitotic arrest deficient protein MAD2B interacts with the small GTPase RAN throughout the cell cycle.* PLoS One, 2009. **4**(9): p. e7020.
44. Nelson, K.K., J. Schlondorff, and C.P. Blobel, *Evidence for an interaction of the metalloprotease-disintegrin tumour necrosis factor alpha convertase (TACE) with mitotic arrest deficient 2 (MAD2), and of the metalloprotease-disintegrin MDC9 with a novel MAD2-related protein, MAD2beta.* Biochem J, 1999. **343 Pt 3**: p. 673-80.
45. Weterman, M.A., et al., *Impairment of MAD2B-PRCC interaction in mitotic checkpoint defective t(X;1)-positive renal cell carcinomas.* Proc Natl Acad Sci U S A, 2001. **98**(24): p. 13808-13.
46. Huttlin, E.L., et al., *The BioPlex Network: A Systematic Exploration of the Human Interactome.* Cell, 2015. **162**(2): p. 425-440.
47. Huttlin, E.L., et al., *Architecture of the human interactome defines protein communities and disease networks.* Nature, 2017. **545**(7655): p. 505-509.
48. Itoh, G., et al., *CAMP (C13orf8, ZNF828) is a novel regulator of kinetochore-microtubule attachment.* EMBO J, 2011. **30**(1): p. 130-44.
49. Bennardo, N., et al., *Alternative-NHEJ is a mechanistically distinct pathway of mammalian chromosome break repair.* PLoS Genet, 2008. **4**(6): p. e1000110.
50. Tabach, Y., et al., *Identification of small RNA pathway genes using patterns of phylogenetic conservation and divergence.* Nature, 2013. **493**(7434): p. 694-8.
51. Tabach, Y., et al., *Human disease locus discovery and mapping to molecular pathways through phylogenetic profiling.* Mol Syst Biol, 2013. **9**: p. 692.
52. Lawrence, C.W., G. Das, and R.B. Christensen, *REV7, a new gene concerned with UV mutagenesis in yeast.* Mol Gen Genet, 1985. **200**(1): p. 80-5.
53. Jones, P., et al., *InterProScan 5: genome-scale protein function classification.* Bioinformatics, 2014. **30**(9): p. 1236-40.
54. Dev, H., et al., *Shieldin complex promotes DNA end-joining and counters homologous recombination in BRCA1-null cells.* Nat Cell Biol, 2018. **20**(8): p. 954-965.
55. Ghezraoui, H., et al., *53BP1 cooperation with the REV7-shieldin complex underpins DNA structure-specific NHEJ.* Nature, 2018.

56. Noordermeer, S.M., et al., *The shieldin complex mediates 53BP1-dependent DNA repair.* Nature, 2018.
57. Tomida, J., et al., *FAM35A associates with REV7 and modulates DNA damage responses of normal and BRCA1-defective cells.* EMBO J, 2018. **37**(12).
58. Gupta, R., et al., *DNA Repair Network Analysis Reveals Shieldin as a Key Regulator of NHEJ and PARP Inhibitor Sensitivity.* Cell, 2018. **173**(4): p. 972-988 e23.
59. Matsuoka, S., et al., *ATM and ATR substrate analysis reveals extensive protein networks responsive to DNA damage.* Science, 2007. **316**(5828): p. 1160-6.
60. Tang, J., et al., *Acetylation limits 53BP1 association with damaged chromatin to promote homologous recombination.* Nat Struct Mol Biol, 2013. **20**(3): p. 317-25.
61. Iacovoni, J.S., et al., *High-resolution profiling of gammaH2AX around DNA double strand breaks in the mammalian genome.* EMBO J, 2010. **29**(8): p. 1446-57.
62. Nakamura, M., et al., *High frequency class switching of an IgM+ B lymphoma clone CH12F3 to IgA+ cells.* Int Immunol, 1996. **8**(2): p. 193-201.
63. Pierce, A.J., et al., *XRCC3 promotes homology-directed repair of DNA damage in mammalian cells.* Genes Dev, 1999. **13**(20): p. 2633-8.
64. Stark, J.M., et al., *Genetic steps of mammalian homologous repair with distinct mutagenic consequences.* Mol Cell Biol, 2004. **24**(21): p. 9305-16.
65. Hein, M.Y., et al., *A human interactome in three quantitative dimensions organized by stoichiometries and abundances.* Cell, 2015. **163**(3): p. 712-23.
66. Choudhury, N.R., et al., *RNA-binding activity of TRIM25 is mediated by its PRY/SPRY domain and is required for ubiquitination.* BMC Biol, 2017. **15**(1): p. 105.
67. Roy, R., et al., *hnRNPA1 couples nuclear export and translation of specific mRNAs downstream of FGF-2/S6K2 signalling.* Nucleic Acids Res, 2014. **42**(20): p. 12483-97.
68. Hart, T., et al., *High-Resolution CRISPR Screens Reveal Fitness Genes and Genotype-Specific Cancer Liabilities.* Cell, 2015. **163**(6): p. 1515-26.
69. Burgess, D.J., et al., *Topoisomerase levels determine chemotherapy response in vitro and in vivo.* Proc Natl Acad Sci U S A, 2008. **105**(26): p. 9053-8.
70. Hutchins, J.R., et al., *Systematic analysis of human protein complexes identifies chromosome segregation proteins.* Science, 2010. **328**(5978): p. 593-9.

71. Bennett, E.J., et al., *Dynamics of cullin-RING ubiquitin ligase network revealed by systematic quantitative proteomics.* Cell, 2010. **143**(6): p. 951-65.
72. Barazas, M., et al., *The CST Complex Mediates End Protection at Double-Strand Breaks and Promotes PARP Inhibitor Sensitivity in BRCA1-Deficient Cells.* Cell Rep, 2018. **23**(7): p. 2107-2118.
73. Mirman, Z., et al., *53BP1-RIF1-shieldin counteracts DSB resection through CST- and Polalpha-dependent fill-in.* Nature, 2018.
74. Schmutz, I. and T. de Lange, *Shelterin.* Curr Biol, 2016. **26**(10): p. R397-9.
75. Suliman-Lavie, R., et al., *Pogz deficiency leads to transcription dysregulation and impaired cerebellar activity underlying autism-like behavior in mice.* Nat Commun, 2020. **11**(1): p. 5836.
76. Orthwein, A., et al., *Mitosis inhibits DNA double-strand break repair to guard against telomere fusions.* Science, 2014. **344**(6180): p. 189-93.
77. Choi, H., et al., *SAINT: probabilistic scoring of affinity purification-mass spectrometry data.* Nat Methods, 2011. **8**(1): p. 70-3.
78. Shteynberg, D., et al., *iProphet: multi-level integrative analysis of shotgun proteomic data improves peptide and protein identification rates and error estimates.* Mol Cell Proteomics, 2011. **10**(12): p. M111 007690.
79. Liu, G., et al., *ProHits: integrated software for mass spectrometry-based interaction proteomics.* Nat Biotechnol, 2010. **28**(10): p. 1015-7.
80. Knight, J.D.R., et al., *ProHits-viz: a suite of web tools for visualizing interaction proteomics data.* Nat Methods, 2017. **14**(7): p. 645-646.
81. Gaudreau-Lapierre, A., et al., *Investigation of Protein Recruitment to DNA Lesions Using 405 Nm Laser Micro-irradiation.* J Vis Exp, 2018(133).

Chapter 4: Discussion and Future Directions

Multiple myeloma remains a difficult disease to treat due to its heterogeneity, which drives, at least in part, the risk of relapse/resistance from current standard of care regimens, including PIs. The overarching aim of my thesis is to identify new biological targets that, when manipulated, synergize with PIs and improve treatment efficacy. These novel therapeutic targets could also serve as prognostic markers and be used to improve MM patient survival. Utilizing CRISPR-Cas9 genome-wide screens, we are amongst the first groups to publish a comprehensive investigation of both MM essential genes and genes that influence PI treatment response [316]. While our *in vitro* MM CRIPSR Cas9 genome-wide screens were incredibly informative, they are not without their limitations. Using cell lines in cell culture, our screen was unable to accurately incorporate factors from the BMM which are known to have an impact on MM survival. This includes cytokines and chemokines such as IL-6, as well as cell surface adhesion stimulation of pathways in MM cells. Secondly, to ensure adequate dropout of sgRNAs the screens were conducted over a three weeks in culture adding additional stress on top of BTZ treatment to MM cells. Finally, due to the inherent heterogeneity of MM cells, genome-wide screens in numerous MM cell lines would be ideal to distinguish between cell line specific effects and pan-MM effects.

Despite these limitations, our screens also identified biological pathways that have yet to be fully characterized in MM, such as nonsense mediated mRNA decay (NMD), iron sulfur cluster metabolism, and dead(h) box helicases (DHX proteins). Unsurprisingly, two biological pathways that have been extensively studied in MM biology and treatment response, DNA repair and metabolism, were abundant in both the essential and BTZ treatment arms of our screens. Each chapter of this thesis provides the initial foundation of basic research implicating both the MPC and Shieldin complexes as potential predictive biomarkers and therapeutic targets in MM.

4.1 The MPC in MM biology and BTZ treatment

Oncogenic induced metabolic rewiring has been thoroughly studied in many cancer models including MM, whereby cells adapt by increasing nutritional demands via aerobic respiration to maintain survival, proliferation, and expansion. Although metabolic pathways such as glutamine metabolism, amino acid biosynthesis and OXPHOS have been studied in the context of MM[312,

317, 318], this research has yet to amount to viable therapeutic alternatives [319], particularly for high-risk MM patients and patients who must overcome drug resistance.

The first-generation PI, BTZ, induces significant gastrointestinal side effects, including nausea, vomiting, diarrhea, low platelets, anemia, and peripheral neuropathy[320]. Similarly, CFZ, the second generation PI, has side effects including anemia, low platelets, nausea, fever, trouble breathing, diarrhea, headache, some cardiotoxicity[212, 321]. These toxicities can be detrimental to elderly MM patients and limit the maximal tolerable dose of current combination therapies, thus hampering its therapeutic efficacy. I strived to identify a combination therapy that synergized with BTZ to not only improve PI efficacy, but also to limit pharmacological toxicity of combination therapies. Based on our CRISPR-based genome-wide screens, our findings suggest that MPC1 could be a strong candidate to improve PI efficacy and mitigate pharmacological toxicity in MM patients[322]. To our surprise, the other component of the MPC complex, MPC2, was not as robust at increasing cellular sensitivity in PI treatment as MPC1, only scoring as a sensitizing factor in the U266 cell line. However, upon characterization, we noted that sgRNA targeting of MPC1 decreased MPC2 protein expression. This phenomenon has been described by several other groups whereby targeted mutation[323] or deletion of MPC1 in both human and murine models lead to minimal protein expression of MPC2, while mRNA expression of MPC2 remains relatively unchanged [324-327]. Furthermore, both publications identifying MPC components, positioned MPC1 and not MPC2 as the driving factor influencing cell growth in both yeast and murine models[328, 329]. Despite our data conforming to these findings, further characterization of MPC2 disruption in MM would complement the data presented in this thesis. Understanding the stability of MPC1 upon MPC2 genetic disruption, PI sensitivity upon MPC2 KO, and rescue experiments re-expressing MPC1 or MPC2 in MPC KO cells would provide clarity on the interplay between MPC components. In addition to the MPC specifically, our data positions other proteins involved in pyruvate metabolism as a potential prognostic signature of MM patient survival. Overall mitochondrial metabolism in MM and PI treatment remains an exciting area of investigation.

Since its discovery in 2012[250, 329], the MPC has been extensively studied in various cancer models since disruption of this carrier favors a metabolic rewiring to aerobic glycolysis. The Warburg effect hypothesized that a glycolytic rewiring of cancerous tissue would outcompete normal tissue and evade cancer therapeutics[258]. Unsurprisingly, loss of MPC activity has been associated with tumor progression and poor patient outcome in numerous cancer models such as

prostate, colon, lung, and esophageal cancers. Research in each of these cancers have shown that decreased expression of MPC1 leads to increased migration, invasiveness and resistance to radiation/chemotherapy[330-333]. Additionally, low expression of MPC1 in patients with brain cancer is associated with a worse overall prognosis[334]. Interestingly, our data positions the MPC in a different light, such that MPC disruption induces a metabolic rewiring that does not influence MM tumor growth or progression *in vitro*, however it sensitizes the cells to subsequent PI treatment. We show that both knockout or pharmacological inhibition of MPC1 does not significantly affect cell cycle, cellular proliferation, or survival of MM cells without treatment. However, upon treatment, MPC1 knockout or UK5099 treated cells are significantly more sensitive to PIs and undergo apoptosis. The influence of pyruvate metabolism on cancer cells survival is becoming increasingly cancer and tissue dependent, whereby which cancers dependent on pyruvate utilization are negatively impacted by MPC disruption. For example, disruption of the MPC in androgen receptor-driven prostate cancer[335], hepatocellular tumorigenesis[336], gall bladder cancer[337], and cervical cancer[338] inhibits growth and is associated with a better overall survival. Furthermore, metabolic disruption *in vivo* is far more complex than *in vitro* phenotypes since it may also play a role in altering the hypoxic tissue microenvironment and neighboring cells known to influence MM survival[339]. Altogether, our research adds to the existing hypothesis that the consequences of MPC activity in cancer are context dependent, specifically influencing PI treatment efficacy and not growth or survival under steady state conditions. While our data *in vitro* positions the MPC as having a cell intrinsic effect on MM cells, I hypothesize that there will be additional cell extrinsic consequences *in vivo*. Future experiments should investigate growth of MPC1 disrupted cells *in vivo* and the pharmacokinetics and pharmacodynamics of UK5099 treatment.

Various hypothetical mechanisms of action have been proposed to explain the downstream consequences of MPC inhibition mentioned above. While we are the first group to investigate the therapeutic potential of the MPC in MM cells, it has been studied in its precursor, long lived plasma cells (LLPCs). It was postulated that LLPCs utilize additional metabolic pathways to their short lived counterparts to extend their survival[340]. This was evident in the maximal metabolic respiration of LLPCs which was reversed upon inhibition with UK5099 while SLPCs were only marginally affected. This was the first piece of evidence suggesting that LLPCs utilize pyruvate dependent respiration more readily than SLPCs. Furthermore, LLPCs that had been extracted and

cultured *in vitro* were able to persist longer than SLPCs or naïve B-cells. Interestingly, the survival advantage exhibited by LLPCs was attenuated by UK5099 treatment and it also disrupted LLPC function by altering the production of antibody specific titres[24]. Our extracellular flux analysis in MM cells treated with UK5099 or MPC1 KO cells showed a similar profile to that seen in LLPCs. Whereby the maximal respiration after FCCP treatment was attenuated in MPC disrupted MM cells when compared to untreated counterparts. Interestingly, the effect was not confounded by the addition of BTZ suggesting that the reduced cell viability was not exclusively dependent on mitochondrial respiration.

Glutamine is also known to play an essential role in PC survival and differentiation and this dependency has been observed in MM biology[90, 317, 341]. Without MPC1 expression and subsequent lack of pyruvate entry into the mitochondrial matrix, MM cells rely on the pentose phosphate pathway (PPP) and glutamine oxidation to maintain TCA cycle intermediates and NADPH levels to ensure normal metabolic function. Glutamine tracing experiments in hepatocellular carcinoma has shown that upon MPC disruption cells utilize glutamine to supplement the TCA cycle[342]. Our metabolomic analysis of UK5099 and the combination of UK5099 and BTZ treated MM cells identified a decrease in TCA intermediates prior to alpha-ketoglutarate (citrate and isocitrate) and reduced glutamine intermediates such as glutamine and NEM-glutathione. Two groups have targeted both the transport and enzymatic processing of glutamine in the mitochondria. Both conclude that disruption of glutamine metabolism synergizes with PI treatment in MM cells[313, 343]. While further experiments are required to deduce the exact consequence of depleted glutamine metabolites on MM cells, we hypothesized that due to their dependency on glutamine for survival, alterations in steady state homeostasis would be deleterious to the cells. Our hypothesis is that MPC disruption forces MM cells to utilize even more glutamine for survival, thus limiting available glutamine to sustain growth and produce glutathione to maintain redox homeostasis. Future glutamine tracing and ROS experiments in MPC1 KO cells are required to test this hypothesis.

Another interesting avenue of investigation is the connection between energetic stress and MPC biology. Specifically, how energetic stress signaling via peroxisome proliferator-activated receptor-gamma coactivator 1-alpha (PGC-1α) which has been shown to increase expression of MPC1 and MPC2. PGC-1α is a key regulator of energy metabolism that is stimulated by environmental stimulus and promotes mitochondrial biogenesis and promote OXPHOS while

regulating carbohydrate and lipid metabolism[344]. It is also a powerful regulator of ROS production increasing the amount of antioxidants to minimize the impact of ROS on cellular physiology[345]. Koh et al. had previously shown that in renal carcinoma, MPC1 expression is dependent on PGC-1α activity. They showed that overexpression of PGC-1α stimulated MPC1 transcription and PGC-1α siRNA suppressed MPC expression and therefore pyruvate dependent respiration[346]. Furthermore, Park et al. showed that PGC-1α and ERRα are required for the expression of MPC1. Under energetic stress, increased PGC-1α expression results to increased expression of MPC1 that promotes rapid generation of ATP via glycolysis and promote cellular survival[347]. Altogether, investigating the interplay between PGC-1α and MPC expression and function in MM cells would be an exciting avenue of research to pursue in the future.

Although our data identifies the MPC as novel therapeutic target in combination with PIs in vitro, a question remains about how the MPC and pyruvate metabolism influences proteasome activity. We have shown that in MM cells, MPC disruption, via genetic manipulation or pharmacological inhibition, exacerbates BTZ dependent proteasome inhibition. We show that MPC1 KO cells have a marked decrease in proteasome activity as compared to the non-targeting control. Additionally, the combination of UK5099 and BTZ reduce proteasome activity when compared to BTZ and UK5099 monotherapies. Although, we do not know the exact mechanism connecting proteasome activity and pyruvate metabolism, several hypotheses have been proposed. The most direct connection between the two pathways is ATP. Proteasomal degradation is an ATP dependent process that enables the 20S catalytic domain to breakdown proteins into amino acids. Disruption of the TCA cycle and OXPHOS is likely to affect ATP production in MM cells and we have shown that MPC disruption led to reduced maximal respiration and lower bioenergetic capacity. Altogether, ATP production could play a role in MM proliferation and survival under MPC disruption, however a more targeted experiment is required to assess the levels of ATP and AMP to confirm this hypothesis. Alternatively, others have proposed that glutamine utilization may also influence proteasome activity. It has been shown that in monocytes, glutamine led to a global reduction in proteasome activity, however there was a preferential degradation of some proteins over others[348]. Glutamine starvation caused a reduction of protein degradation, accumulation of ubiquitin-protein conjugates and a reduction of intracellular ATP. Interestingly, a study in T-lymphocytes has shown that disruption of proteasome activity via genetic manipulation and pharmacological inhibition altered cellular metabolism favoring glycolysis over

OXPHOS[349]. These authors speculated that the metabolic alterations were due in part to the regulation of MYC expression, however the results were limited and further investigation into the mechanism of action linking glutamine metabolism and proteasome activity is required. Our LC-MS metabolomics data provided a snapshot suggesting UK5099 and BTZ treatment resulted in depleted glutamine and NEM-glutathione, however to validate our findings glutamine tracing experiments of UK5099 and BTZ treated cells are required fully understand the dynamics of glutaminolysis. An additional pathway for further investigation is pyruvate anaplerosis via pyruvate carboxylase which converts pyruvate to oxaloacetate in the TCA. Initial analysis of the MMRF database showed that pyruvate carboxylase expression does not correlate with MM patient survival, however a more thorough investigation of this pathway is also required in the future. While the majority of our MPC1 research revolves around proteasome activity, it is conceivable that the combination of MPC1 inhibition and PI treatment impacts other cellular processes independent of proteasome activity to induce MM cell death. Future experiments understanding how MPC inhibition influences other pathways influenced by BTZ treatment such as NF-κB and the DNA damage response would be interesting to investigate.

Despite PIs drastically altering the landscape of MM treatment, resulting in triplicate and quadruplicate combination therapies, most patients relapse to the current standard of care. Therefore, recent MM research has focused on identifying how PI resistant tumors adapt to evade drug induced cytotoxicity and several groups have implicated metabolic rewiring as playing a central role. Zaal et al. were one of the first groups to systematically investigate the extent of metabolic rewiring in BTZ resistant MM cells. Using ^{13}C-glucose tracer experiments, they identified that BTZ resistant RPMI-8266 MM cells had enhanced glucose uptake and lactate secretion suggesting a higher glycolytic activity[311]. Furthermore, they observed minimal change in glucose flux to the TCA cycle intermediates and increased glucose flux to the pentose phosphate pathway (PPP) which functions to provide ribose for nucleotide synthesis and NADPH for intracellular redox balance. Additionally, they showed increased glucose flux via the serine synthesis pathway which is also involved in NADPH regeneration and GSH production. Increased GSH production and reduced glutathione provided increased antioxidant protection in BTZ resistant MM cells[290, 311]. Besse et al. then built upon this work and conducted targeted metabolomic profiling of BTZ and CFZ resistant MM cells. They identified glutathione metabolism, glutamate metabolism and the malate-aspartate shuttle as the most significant

metabolic changes in PI resistant cells when compared to their sensitive counterparts. This led to a higher antioxidant capacity, reduced cytosolic ATP/ADP ratio and increased size and morphological changes of PI resistant MM cells[312]. Soriano et al. confirmed the previous findings and identified high oxidative phosphorylation as another attributable characteristic of PI resistant cells. Additional pathways such as hexosamine biosynthetic pathway (HBP), increased protein glycosylation[350], coenzyme Q10, and the mevalonate pathway[351] have also been described in PI resistance models. Novel therapeutics against glucose transporters (compound 20 and ritonavir), hexokinases (3BP and 2DG supplementation), LDH inhibition (Oxamate) have been proposed in the treatment of MM.

Despite increasing research investigating the role glutaminolysis, oxidative phosphorylation, glycolysis and amino acid biosynthesis pathways in the development and treatment of MM, very little is known about the role of pyruvate metabolism in MM and the consequences of its inhibition. Our research not only identifies pyruvate metabolism components as a prognostic biomarker, but also identifies the MPC as a therapeutic target that improves PI treatment efficacy. With various known and hypothesized pharmacological inhibitors of the MPC (UK5099, pioglitazone, rosiglitazone), our data provides the foundation for future research into the clinical applicability of inhibiting the MPC and pyruvate metabolism in MM patients.

To build upon the existing foundation of our work with MPC1 and PIs, future experiments using primary patient samples and in vivo models remain critical to translate this basic research to the clinic. Firstly, primary BM aspirates from MM patients would be cultured *in vitro* for 24 hours and subjected to BTZ and UK5099 monotherapies as well as the combination of the two compounds to assess changes in cell viability, similar to what was done with our MM cell lines. This would provide the first line of pre-clinical evidence suggesting that this combination therapy could be effective in MM patients. Secondly, the utilization of physiologically relevant mouse models such as Vk*MYC[352] and 5TGM1[353] mouse models is important to assess the therapeutic impact of MPC1 inhibition and UK5099 treatment on MM in an intact BM microenvironment with a functioning immune system. The culmination of these future experiments along with pharmacodynamics and pharmacokinetics of UK5099 will be essential for the pre-clinical data package required to initiate a phase I clinical trial in the future.

4.2 The role of DNA repair and the Shieldin complex in MM biology.

Apart from metabolic alterations influencing MM therapeutic response, DNA repair pathways including NHEJ[354], HR[355, 356], BER[357], NER[358] and MMR[359] have emerged as important pathways implicated in both MM development, treatment response and relapse. As previously mentioned, MM is a heterogeneous malignancy that is characterized by its genomic instability from MM initiation throughout progression. Several groups have hypothesized that inappropriate repair resulting from AID and/or APOBEC induced damage is a critical step during MM development[360]. During CSR, DNA double strand breaks depend on DNA repair machinery, especially NHEJ to ensure faithful repair of immunoglobulin chains and if not repaired could lead to genomic instability. It has been shown that MM cells *in vitro*, under steady state conditions, have persistent γ-H2AX foci and constitutively phosphorylated ATR suggesting a persistence of DNA damage[188]. Various groups have attempted to correlate NHEJ and HR activity with radiosensitivity, however both publications had limited cell lines and MM patient samples to account for the heterogeneity of the disease[361].

In 2010, 53BP1 has emerged as a central component of the NHEJ pathway[362, 363] and several effectors including RIF1, PTIP and REV7 have been described[364-366]. However, it remained largely unclear how this multiprotein complex mediates NHEJ and DNA end protection. REV7 was initially described for its role in mitotic progression by controlling both the spindle assembly checkpoint (SAC), the anaphase promoting complex (APC) and translesion synthesis [367, 368]. More recent studies by Boersma et al and Xu et al identified REV7 as a counteracting DNA break end resection and favoring NHEJ mediated repair, affecting PARP inhibition and DNA repair of telomeres[369, 370]. Despite REV7 being described as a critical component of multiple complexes, REV7 has been characterized as an adapter protein with no catalytic activity, therefore it was believed that there were other downstream effectors from REV7. Prior to the publication of our manuscript, effectors of 53BP1 mediated shielding of DNA ends favoring NHEJ was unknown except for the adapter protein REV7 playing a role in pathway decision of NHEJ and HR.

Interestingly several groups used various strategies to identify the Shieldin complex as the downstream effectors of 53BP1. Our strategy utilized a proximity BirA biotin ligase mass-spectrometry (MS) based approach investigating REV7 interactors, whereas Gupta et al used an APEX2-53BP1 proximity labeling approach [371]. Another strategy involved CRISPR/Cas9 based pool screens identifying mutations conferring resistance to PARPi in BRCA1-mutated

cells[372, 373] and our genome-wide screen identified sensitizers to doxorubicin treatment in RPE1 cells where SHLD1 was identified as a top sensitizer. Each of these approaches identified previously uncharacterized proteins FAM35A (SHLD2) and C20orf196 (SHLD1). Interestingly, Noordermeer et al also identified SHLD3 (CTC-534A2.2) which is a protein encoded from an alternative transcript of the TRAPPC13 locus[373].

To validate our MS identification of SHLD1 and SHLD2, we investigated if each of these components form a stable complex with REV7. Our data supports similar findings surrounding the Shieldin complex, whereby we show that SHLD1 and SHLD2 have a strong interaction with REV7, forming a complex at steady state and during DNA damage[371-374]. Due to the hypothesized role of the complex promoting pathway decision towards NHEJ as opposed to HR repair, disruption of the Shieldin complex was extensively studied in the context of HR. Several groups identified that depletion of any Shieldin subunit in BRCA1-deficient cell lines suppressed PARPi sensitivity *in vitro*[371-373, 375, 376]. Shieldin dependent PARPi sensitivity in BRCA null tumors was also confirmed *in vivo* using allograft mammary tumors[373] and patient derived xenografts[372]. Additionally, using gene reporter assays and RAD51 IR induced foci formation, our data supports similar findings that loss of both BRCA1 and a Shieldin component restores HR suppression[371-374]. Our data also shows that siRNA mediated knockdown of RIF1, REV7 or 53BP1 prevents SHLD2 recruitment to sites of damage and knockdown of Shieldin components hinders NHEJ mediated repair in the EJ-5 reporter, positioning the Shieldin complex downstream of the aforementioned NHEJ components[371-374, 377]. Furthermore, we showed that loss of Shieldin components confers sensitivity to IR and UV damage, while other groups showed additional sensitivity to etoposide and bleomycin[371-374]. Finally, our data supports similar findings that depletion of Shieldin components including REV7 impairs CSR suggesting an important involvement in immune system development and antibody diversification[371-373, 375]. As previously mentioned, the decision point of DSB repair revolves around end resection and our data shows that knockdown of Shieldin subunits results in increased resection and RPA phosphorylation after the induction of DSBs[372, 373]. Additionally, other groups have noted increased numbers of RPA foci formation[371, 372], increased RPA bound to immunoglobulin switch regions[375] and increased ssDNA after camptothecin treatment[371, 372]. While our work identified the N-terminal domain of SHLD2 as critical for its recruitment to sites of damage, it is now known that two proline residues (P14 and P17) are essential for REV7 interaction[374].

Furthermore the third OB-fold domain in the C-terminus is important for the association of SHLD2 with SHLD1[372]. The Shieldin complex is now recognized as a critical complex involved in the DNA repair pathway decision-making process. Since the majority of our Shieldin data was done using U2OS, HeLa and RPE1 cell lines, future experiments using MM cell lines such as U266, JJN3 and RPMI-8226 are required to fully understand how SHLD1 and SHLD2 affect MM viability. This is especially true since SHLD2 is not found in the TKOv1 sgRNA library used for our genome-wide screens. Assessing cell viability in SHLD1 and SHLD2 KO MM cells with and without PI treatment will be important to distinguish their roles in MM cell survival vs treatment response. Additionally, treatment with DNA damaging agents commonly used in MM treatment such as cyclophosphamide, melphalan and doxorubicin with the disruption of the Shieldin complex can also be assessed. As with MPC1, the hope is that these initial experiments *in vitro* will stimulate future experiments using MM primary patient samples and MM *in vivo* mouse models.

While further research is required to identify the role of the Shieldin complex in the development and progression of MM, there is some evidence suggesting that disruption of the NHEJ pathway plays an important role in MM biology. A study by Roddam et al. investigated polymorphisms in NHEJ DNA ligase IV (LIG4) and found that both A3V and T9I amino acid substitutions were associated with a two-fold and 1.5-fold reduction in developing MM[378]. Furthermore, Herrero et al. investigated the activity of various DNA repair pathways between MM and normal control lymphoblastoid cell lines. They concluded that MM cell lines had persistent DNA damage despite increased activity of both HR and NHEJ pathways[361]. It was noted that the activity of the Alt-NHEJ pathway, which is known to be highly mutagenic and promote translocations, was also elevated in MM cell lines. Additionally, DNA ligase IIIa, which has been previously proposed to drive AML and CML progression was overexpressed in MM patient samples[379]. Our genome-wide screens in two MM cell lines identified several components of both NHEJ and HR pathways as essential genes, whereby upon CRISPR mediated KO of each of these genes resulted in a reduced overall cell survival. Analysis of patient data from the MMRF CoMMpass trial revealed that high expression of these genes in MM patients was associated with a worse overall survival. DNA repair, especially NHEJ mediated repair remains an evolving field of research in MM development and response to treatment.

Prior to the discovery of PIs, chemotherapeutics resulting in DNA damage, such as melphalan, were the standard of care in the treatment of newly diagnosed MM patients. Melphalan treatment

results in DNA interstrand crosslinking that is repaired by both BER and FA pathways, and if not repaired results in the generation of DNA DSBs[380, 381]. While melphalan is still used in ASCT eligible patients, its usage has been limited due to high relapse rates and inferior efficacy when compared to PIs. Despite plenty of research aimed to identify other effective intercalating agents in the treatment of MM, none could recapitulate the efficacy of melphalan. Researchers believed that melphalan induced DNA damage and subsequent repair within MM cells was far more complex than initially hypothesized, resulting in limited use of DNA damage therapeutics in the future. Since it was already known that activity of HR, NHEJ and Alt-NHEJ pathways were increased in MM cells, many hypothesized that the increased DNA repair capacity of these cells could contribute to the resistance of MM therapeutics[189]. Gkotzamanidou et al. investigated whether disruption of DNA repair pathways improved melphalan-induced toxicity in MM cells. They found that treatment with DNA repair inhibitors SCR7 (LigIV inhibitor) and RI-1 (RAD51 inhibitor) significantly increased the number of γ-H2AX foci and reduced the concentration of melphalan required to initiate apoptosis[382]. This positioned NHEJ and HR repair pathways as potential therapeutic targets to increase melphalan treatment sensitivity. Furthermore, melphalan-resistant cells have been shown to upregulate components of NHEJ (LigIV, XRCC4 and RPA2) and FA repair (FANCC, FANCL, RAD51) suggesting a compensation of DNA repair pathways[380, 381].

Although DNA repair pathways have been implicated as therapeutic targets for the improvement of melphalan therapeutics, our genome-wide screen data identifies SHLD1 (C20orf196) as a sensitizer to bortezomib treatment. Since SHLD2 was not part of our screen library, we extended our investigation of the Shieldin complex by examining the correlation of SHLD1 and SHLD2 expression with overall survival in MM patients using the MMRF CoMMpass dataset. Approximately 90% of patients in the MMRF dataset have received a treatment containing BTZ, therefore the progression free and overall survival analysis allowed us to gain insight into how expression of the Shieldin complex affects BTZ treatment response. Stratified by expression, we showed that high expression of SHLD1 or SHLD2 resulted in a worse overall survival and worse progression free survival than low expression of either component (Figure 3.1). Mitsiades et al. were the first group to investigate the potential synergistic effects of BTZ with conventional chemotherapeutic agents in MM[383]. At the time, BTZ was in clinical trials testing its efficacy as a monotherapy and in combination with chemotherapeutic DNA damaging agents (melphalan

and doxorubicin). They found that BTZ increased chemosensitivity of both drugs in drug sensitive and drug-resistant MM cell lines. Furthermore, these results were validated in primary MM cells isolated from patients, where the combination therapy significantly increased cell death in melphalan resistant patients[114]. Several groups built upon the successful combination of BTZ and melphalan/doxorubicin investigating other DNA damaging agents and their impact on MM cell survival with BTZ. Kiziltepe et al. showed that 5-azacytidine, a DNA methyltransferase inhibitor, known to induce DNA damage[384] in combination with BTZ led to synergistic toxicity and apoptosis in MM cells[385]. In a separate publication, they also showed that a prodrug designed to release nitric oxide, induce double strand breaks and activate the DNA damage response, synergized with BTZ[386]. Finally, Chen et al. described a novel phosphoramide compound, DCZ0847, which synergized with BTZ, promoting apoptosis, and inducing DNA damage in MM cells[387].

Despite several studies suggesting synergy between chemotherapy induced DNA damage and BTZ proteasome inhibition, very few publications have described a direct mechanism of action linking the two pathways. Neri et al. provide the most conclusive data suggesting that BTZ treatment induced a “BRCAness” phenotype that sensitizes MM cells to PARP inhibitors. They showed that treatment with PARP inhibitors alone had no effect on MM cell survival due to their ability to rapidly repair PARPi induced DNA double strand breaks[192]. In parallel, they noted that BTZ treatment transiently repressed the transcriptional expression of HR genes such as FANCD2, RAD51, BRCA2 and BRCA1 and inhibited HR mediated repair of DNA DSBs. The combination of BTZ with PARP inhibitors significantly reduced MM cell survival *in vitro* and *in vivo* using MM xenograft mouse models. Their most striking data was that BTZ treatment depleted the pool of nuclear ubiquitin that is necessary for downstream signaling of PARPi induced DNA damage. With most of the ubiquitin moieties attached to proteins targeted for degradation, they observed a lack of BRCA1 ubiquitylation and depletion of free nuclear ubiquitin pools via immunofluorescence. While HR was the predominant focus of the publication, it is well known that ubiquitin moieties are also involved in the NHEJ signaling process. Histone H2B and H2A monoubiquitylation results in the recruitment and initiation of NHEJ DNA repair[388, 389], suggesting it is feasible that BTZ induced depletion of free nuclear ubiquitin could also impact NHEJ mediated repair which would be exacerbated with dysregulation of the Shieldin complex.

Prior to our research, effectors of 53BP1 strand protection and NHEJ pathway decision was limited to the adapter protein REV7. Our research identified and characterized the Shieldin complex as the effector and described its role in promoting NHEJ mediated repair. Furthermore, we are the first to implicate the Shieldin complex as a prognostic biomarker in MM and that when disrupted improves PI treatment response based on our genome-wide screen data.

References

1. Siegel, R.L., K.D. Miller, and A. Jemal, *Cancer statistics, 2016.* CA Cancer J Clin, 2016. **66**(1): p. 7-30.
2. Teras, L.R., et al., *2016 US lymphoid malignancy statistics by World Health Organization subtypes.* CA Cancer J Clin, 2016. **66**(6): p. 443-459.
3. Zhou, L., et al., *Measuring the global, regional, and national burden of multiple myeloma from 1990 to 2019.* BMC Cancer, 2021. **21**(1): p. 606.
4. Cowan, A.J., et al., *Global Burden of Multiple Myeloma: A Systematic Analysis for the Global Burden of Disease Study 2016.* JAMA Oncol, 2018. **4**(9): p. 1221-1227.
5. Committee, C.C.S.A. *Canadian Cancer Statistics 2022*. 2022 May 2022 [cited 2022 June 21st]; Available from: https://cancer.ca/en/research/cancer-statistics.
6. Weiss, B.M., *Multiethnic myeloma.* Blood, 2013. **121**(16): p. 3062-4.
7. Fiala, M.A., et al., *Socioeconomic status is independently associated with overall survival in patients with multiple myeloma.* Leuk Lymphoma, 2015. **56**(9): p. 2643-9.
8. Kazandjian, D., et al., *Molecular underpinnings of clinical disparity patterns in African American vs. Caucasian American multiple myeloma patients.* Blood Cancer J, 2019. **9**(2): p. 15.
9. Manojlovic, Z., et al., *Comprehensive molecular profiling of 718 Multiple Myelomas reveals significant differences in mutation frequencies between African and European descent cases.* PLoS Genet, 2017. **13**(11): p. e1007087.
10. Kanapuru, B., et al., *Analysis of racial and ethnic disparities in multiple myeloma US FDA drug approval trials.* Blood Adv, 2022. **6**(6): p. 1684-1691.
11. Kyle, R.A., et al., *Review of 1027 patients with newly diagnosed multiple myeloma.* Mayo Clin Proc, 2003. **78**(1): p. 21-33.
12. Bhattacharya, K., et al., *Phase-Specific and Lifetime Costs of Multiple Myeloma Among Older Adults in the US.* JAMA Netw Open, 2021. **4**(7): p. e2116357.
13. Smol, T., et al., *Combination of t(4;14), del(17p13), del(1p32) and 1q21 gain FISH probes identifies clonal heterogeneity and enhances the detection of adverse cytogenetic profiles in 233 newly diagnosed multiple myeloma.* Mol Cytogenet, 2017. **10**: p. 26.

14. van Nieuwenhuijzen, N., et al., *From MGUS to Multiple Myeloma, a Paradigm for Clonal Evolution of Premalignant Cells.* Cancer Res, 2018. **78**(10): p. 2449-2456.
15. McHeyzer-Williams, L.J., D.J. Driver, and M.G. McHeyzer-Williams, *Germinal center reaction.* Curr Opin Hematol, 2001. **8**(1): p. 52-9.
16. Shapiro-Shelef, M. and K. Calame, *Regulation of plasma-cell development.* Nature Reviews Immunology, 2005. **5**(3): p. 230-242.
17. Klein, U., et al., *Transcription factor IRF4 controls plasma cell differentiation and class-switch recombination.* Nature Immunology, 2006. **7**(7): p. 773-782.
18. Shaffer, A.L., et al., *Blimp-1 Orchestrates Plasma Cell Differentiation by Extinguishing the Mature B Cell Gene Expression Program.* Immunity, 2002. **17**(1): p. 51-62.
19. Shaffer, A.L., et al., *XBP1, downstream of Blimp-1, expands the secretory apparatus and other organelles, and increases protein synthesis in plasma cell differentiation.* Immunity, 2004. **21**(1): p. 81-93.
20. Mei, H.E., et al., *Blood-borne human plasma cells in steady state are derived from mucosal immune responses.* Blood, 2009. **113**(11): p. 2461-2469.
21. Kawanishi, H., L.E. Saltzman, and W. Strober, *Mechanisms regulating IgA class-specific immunoglobulin production in murine gut-associated lymphoid tissues. I. T cells derived from Peyer's patches that switch sIgM B cells to sIgA B cells in vitro.* J Exp Med, 1983. **157**(2): p. 433-50.
22. Luger, E.O., et al., *Induction of long-lived allergen-specific plasma cells by mucosal allergen challenge.* J Allergy Clin Immunol, 2009. **124**(4): p. 819-26.e4.
23. Shi, W., et al., *Transcriptional profiling of mouse B cell terminal differentiation defines a signature for antibody-secreting plasma cells.* Nature Immunology, 2015. **16**(6): p. 663-673.
24. Lam, Wing Y., et al., *Mitochondrial Pyruvate Import Promotes Long-Term Survival of Antibody-Secreting Plasma Cells.* Immunity, 2016. **45**(1): p. 60-73.
25. Merz, M., et al., *Deciphering spatial genomic heterogeneity at a single cell resolution in multiple myeloma.* Nature Communications, 2022. **13**(1): p. 807.
26. Corre, J., et al., *Multiple myeloma clonal evolution in homogeneously treated patients.* Leukemia, 2018. **32**(12): p. 2636-2647.

27. Hallek, M., P.L. Bergsagel, and K.C. Anderson, *Multiple myeloma: increasing evidence for a multistep transformation process.* Blood, 1998. **91**(1): p. 3-21.
28. Chng, W.J., et al., *Prognostic factors for hyperdiploid-myeloma: effects of chromosome 13 deletions and IgH translocations.* Leukemia, 2006. **20**(5): p. 807-813.
29. Kuehl, W.M. and P.L. Bergsagel, *Early Genetic Events Provide the Basis for a Clinical Classification of Multiple Myeloma.* Hematology, 2005. **2005**(1): p. 346-352.
30. Chesi, M., et al., *The t(4;14) translocation in myeloma dysregulates both FGFR3 and a novel gene, MMSET, resulting in IgH/MMSET hybrid transcripts.* Blood, 1998. **92**(9): p. 3025-34.
31. Chesi, M., et al., *Activated fibroblast growth factor receptor 3 is an oncogene that contributes to tumor progression in multiple myeloma.* Blood, 2001. **97**(3): p. 729-736.
32. Bergsagel, P.L., et al., *Cyclin D dysregulation: an early and unifying pathogenic event in multiple myeloma.* Blood, 2005. **106**(1): p. 296-303.
33. Hurt, E.M., et al., *Overexpression of c-maf is a frequent oncogenic event in multiple myeloma that promotes proliferation and pathological interactions with bone marrow stroma.* Cancer Cell, 2004. **5**(2): p. 191-199.
34. Smadja, N.V., et al., *Chromosomal analysis in multiple myeloma: cytogenetic evidence of two different diseases.* Leukemia, 1998. **12**(6): p. 960-9.
35. Fonseca, R., M.M. Oken, and P.R. Greipp, *The t(4;14)(p16.3;q32) is strongly associated with chromosome 13 abnormalities in both multiple myeloma and monoclonal gammopathy of undetermined significance.* Blood, 2001. **98**(4): p. 1271-2.
36. Debes-Marun, C.S., et al., *Chromosome abnormalities clustering and its implications for pathogenesis and prognosis in myeloma.* Leukemia, 2003. **17**(2): p. 427-36.
37. Fonseca, R., et al., *The recurrent IgH translocations are highly associated with nonhyperdiploid variant multiple myeloma.* Blood, 2003. **102**(7): p. 2562-7.
38. Chng, W.J., et al., *Ploidy status rarely changes in myeloma patients at disease progression.* Leuk Res, 2006. **30**(3): p. 266-71.
39. Barilà, G., et al., *Identification of the true hyperdiploid multiple myeloma subset by combining conventional karyotyping and FISH analysis.* Blood Cancer Journal, 2020. **10**(2): p. 18.

40. Rajkumar, S.V., *Multiple myeloma: 2022 update on diagnosis, risk stratification, and management.* Am J Hematol, 2022.
41. Shaughnessy, J., Jr., et al., *Cyclin D3 at 6p21 is dysregulated by recurrent chromosomal translocations to immunoglobulin loci in multiple myeloma.* Blood, 2001. **98**(1): p. 217-23.
42. Chesi, M., et al., *Dysregulation of cyclin D1 by translocation into an IgH gamma switch region in two multiple myeloma cell lines.* Blood, 1996. **88**(2): p. 674-81.
43. Chapman, M.A., et al., *Initial genome sequencing and analysis of multiple myeloma.* Nature, 2011. **471**(7339): p. 467-472.
44. Koduru, S., et al., *Dendritic cell–mediated activation-induced cytidine deaminase (AID)–dependent induction of genomic instability in human myeloma.* Blood, The Journal of the American Society of Hematology, 2012. **119**(10): p. 2302-2309.
45. Rustad, E.H., et al., *Timing the initiation of multiple myeloma.* Nature Communications, 2020. **11**(1): p. 1917.
46. Maura, F., et al., *Biological and prognostic impact of APOBEC-induced mutations in the spectrum of plasma cell dyscrasias and multiple myeloma cell lines.* Leukemia, 2018. **32**(4): p. 1043-1047.
47. Magrangeas, F., et al., *Minor clone provides a reservoir for relapse in multiple myeloma.* Leukemia, 2013. **27**(2): p. 473-81.
48. Keats, J.J., et al., *Clonal competition with alternating dominance in multiple myeloma.* Blood, 2012. **120**(5): p. 1067-76.
49. Merlo, A., et al., *5′ CpG island methylation is associated with transcriptional silencing of the tumour suppressor p16/CDKN2/MTS1 in human cancers.* Nat Med, 1995. **1**(7): p. 686-92.
50. Kaiser, M.F., et al., *Global methylation analysis identifies prognostically important epigenetically inactivated tumor suppressor genes in multiple myeloma.* Blood, 2013. **122**(2): p. 219-26.
51. Harada, T., et al., *HDAC3 regulates DNMT1 expression in multiple myeloma: therapeutic implications.* Leukemia, 2017. **31**(12): p. 2670-2677.
52. Pawlyn, C., et al., *Overexpression of EZH2 in multiple myeloma is associated with poor prognosis and dysregulation of cell cycle control.* Blood Cancer J, 2017. **7**(3): p. e549.

53. Stec, I., et al., *WHSC1, a 90 kb SET domain-containing gene, expressed in early development and homologous to a Drosophila dysmorphy gene maps in the Wolf-Hirschhorn syndrome critical region and is fused to IgH in t(4;14) multiple myeloma.* Hum Mol Genet, 1998. **7**(7): p. 1071-82.
54. Maes, K., et al., *Epigenetic modulating agents as a new therapeutic approach in multiple myeloma.* Cancers (Basel), 2013. **5**(2): p. 430-61.
55. Kyle, R.A., et al., *Prevalence of monoclonal gammopathy of undetermined significance.* N Engl J Med, 2006. **354**(13): p. 1362-9.
56. Kyle, R.A., *Monoclonal gammopathy of undetermined significance. Natural history in 241 cases.* Am J Med, 1978. **64**(5): p. 814-26.
57. Rajkumar, S.V., et al., *International Myeloma Working Group updated criteria for the diagnosis of multiple myeloma.* Lancet Oncol, 2014. **15**(12): p. e538-48.
58. Melton, L.J., 3rd, et al., *Fracture risk in monoclonal gammopathy of undetermined significance.* J Bone Miner Res, 2004. **19**(1): p. 25-30.
59. Blade, J., et al., *Malignant transformation and life expectancy in monoclonal gammopathy of undetermined significance.* Br J Haematol, 1992. **81**(3): p. 391-4.
60. Cesana, C., et al., *Prognostic factors for malignant transformation in monoclonal gammopathy of undetermined significance and smoldering multiple myeloma.* J Clin Oncol, 2002. **20**(6): p. 1625-34.
61. Nowakowski, G.S., et al., *Circulating plasma cells detected by flow cytometry as a predictor of survival in 302 patients with newly diagnosed multiple myeloma.* Blood, 2005. **106**(7): p. 2276-9.
62. Kyle, R.A., et al., *A long-term study of prognosis in monoclonal gammopathy of undetermined significance.* N Engl J Med, 2002. **346**(8): p. 564-9.
63. Ho, M., et al., *Changing paradigms in diagnosis and treatment of monoclonal gammopathy of undetermined significance (MGUS) and smoldering multiple myeloma (SMM).* Leukemia, 2020. **34**(12): p. 3111-3125.
64. Yu, P.L.I., et al., *Distinct Nuclear Organization of Telomeresand Centromeres in Monoclonal Gammopathyof Undetermined Significance and Multiple Myeloma.* Cells, 2019. **8**(7).

65. Zapata, J.M., et al., *B-Cell-Specific Myd88 L252P Expression Causes a Premalignant Gammopathy Resembling IgM MGUS.* Mouse Models of B Cell Malignancies, 2021.
66. Avenoso, A., et al., *Quantitative polymerase Chain reaction profiling of microRNAs in peripheral lymph-monocytes from MGUS subjects.* Pathology - Research and Practice, 2021. **218**: p. 153317.
67. Fatica, E.M., et al., *MALDI-TOF mass spectrometry can distinguish immunofixation bands of the same isotype as monoclonal or biclonal proteins.* Clinical Biochemistry, 2021. **97**: p. 67-73.
68. Kyle, R.A., et al., *Clinical course and prognosis of smoldering (asymptomatic) multiple myeloma.* N Engl J Med, 2007. **356**(25): p. 2582-90.
69. Rosiñol, L., et al., *Smoldering multiple myeloma: natural history and recognition of an evolving type.* Br J Haematol, 2003. **123**(4): p. 631-6.
70. Sundaram, S., et al., *FDG PET imaging in multiple myeloma: implications for response assessments in clinical trials.* American journal of nuclear medicine and molecular imaging, 2018. **8**(6): p. 421-427.
71. Mateos, M.V., et al., *Lenalidomide plus dexamethasone for high-risk smoldering multiple myeloma.* N Engl J Med, 2013. **369**(5): p. 438-47.
72. Kyle, R.A. and S.V. Rajkumar, *Criteria for diagnosis, staging, risk stratification and response assessment of multiple myeloma.* Leukemia, 2009. **23**(1): p. 3-9.
73. Hillengass, J., et al., *Prognostic significance of focal lesions in whole-body magnetic resonance imaging in patients with asymptomatic multiple myeloma.* J Clin Oncol, 2010. **28**(9): p. 1606-10.
74. Kumar, S.K., et al., *Multiple myeloma.* Nature Reviews Disease Primers, 2017. **3**(1): p. 17046.
75. Greipp, P.R., et al., *International staging system for multiple myeloma.* J Clin Oncol, 2005. **23**(15): p. 3412-20.
76. Durie, B.G. and S.E. Salmon, *A clinical staging system for multiple myeloma. Correlation of measured myeloma cell mass with presenting clinical features, response to treatment, and survival.* Cancer, 1975. **36**(3): p. 842-54.

77. Palumbo, A., et al., *Revised International Staging System for Multiple Myeloma: A Report From International Myeloma Working Group.* J Clin Oncol, 2015. **33**(26): p. 2863-9.
78. D'Agostino, M., et al., *Second Revision of the International Staging System (R2-ISS) for Overall Survival in Multiple Myeloma: A European Myeloma Network (EMN) Report Within the HARMONY Project.* Journal of Clinical Oncology, 2022: p. JCO.21.02614.
79. Mikhael, J.R., et al., *Management of newly diagnosed symptomatic multiple myeloma: updated Mayo Stratification of Myeloma and Risk-Adapted Therapy (mSMART) consensus guidelines 2013.* Mayo Clin Proc, 2013. **88**(4): p. 360-76.
80. Abdallah, N.H., et al., *A simple additive staging system for newly diagnosed multiple myeloma.* Blood Cancer Journal, 2022. **12**(1).
81. Marquette, C.-H., et al., *Circulating tumour cells as a potential biomarker for lung cancer screening: a prospective cohort study.* The Lancet Respiratory Medicine, 2020. **8**(7): p. 709-716.
82. Lucci, A., et al., *Circulating tumour cells in non-metastatic breast cancer: a prospective study.* The Lancet Oncology, 2012. **13**(7): p. 688-695.
83. Garcés, J.-J., et al., *Circulating Tumor Cells for the Staging of Patients With Newly Diagnosed Transplant-Eligible Multiple Myeloma.* Journal of Clinical Oncology, 2022. **40**(27): p. 3151-3161.
84. Ribatti, D., M. Moschetta, and A. Vacca, *Microenvironment and multiple myeloma spread.* Thromb Res, 2014. **133 Suppl 2**: p. S102-6.
85. Nimmanapalli, R., et al., *HSP70 inhibition reverses cell adhesion mediated and acquired drug resistance in multiple myeloma.* British journal of haematology, 2008. **142**(4): p. 551-561.
86. Mundy, G., *Myeloma bone disease.* European Journal of Cancer, 1998. **34**(2): p. 246-251.
87. Mundy, G.R., et al., *Evidence for the secretion of an osteoclast stimulating factor in myeloma.* N Engl J Med, 1974. **291**(20): p. 1041-6.
88. Adamik, J., et al., *EZH2 or HDAC1 Inhibition Reverses Multiple Myeloma–Induced Epigenetic Suppression of Osteoblast DifferentiationMyeloma-Induced Runx2 Silencing Rescued by EZH2i or HDAC1i.* Molecular Cancer Research, 2017. **15**(4): p. 405-417.

89. Hameed, A., et al., *Bone disease in multiple myeloma: pathophysiology and management.* Cancer Growth Metastasis, 2014. **7**: p. 33-42.
90. Chiu, M., et al., *Myeloma cells deplete bone marrow glutamine and inhibit osteoblast differentiation limiting asparagine availability.* Cancers, 2020. **12**(11): p. 3267.
91. Simonet, W., et al., *Osteoprotegerin: a novel secreted protein involved in the regulation of bone density.* Cell, 1997. **89**(2): p. 309-319.
92. Rawadi, G., et al., *BMP-2 controls alkaline phosphatase expression and osteoblast mineralization by a Wnt autocrine loop.* Journal of Bone and Mineral Research, 2003. **18**(10): p. 1842-1853.
93. Tian, E., et al., *The role of the Wnt-signaling antagonist DKK1 in the development of osteolytic lesions in multiple myeloma.* New England Journal of Medicine, 2003. **349**(26): p. 2483-2494.
94. Jurczyszyn, A., et al., *The analysis of the relationship between multiple myeloma cells and their microenvironment.* Journal of Cancer, 2015. **6**(2): p. 160.
95. Giuliani, N., et al., *Myeloma cells block RUNX2/CBFA1 activity in human bone marrow osteoblast progenitors and inhibit osteoblast formation and differentiation.* Blood, 2005. **106**(7): p. 2472-2483.
96. Tanaka, Y., et al., *Myeloma cell-osteoclast interaction enhances angiogenesis together with bone resorption: a role for vascular endothelial cell growth factor and osteopontin.* Clinical Cancer Research, 2007. **13**(3): p. 816-823.
97. Oba, Y., et al., *MIP-1α utilizes both CCR1 and CCR5 to induce osteoclast formation and increase adhesion of myeloma cells to marrow stromal cells.* Experimental hematology, 2005. **33**(3): p. 272-278.
98. Tsirakis, G., et al., *Increased serum levels of MIP-1alpha correlate with bone disease and angiogenic cytokines in patients with multiple myeloma.* Medical Oncology, 2013. **31**(1): p. 778.
99. Sun, L., et al., *Disordered osteoclast formation and function in a CD38 (ADP-ribosyl cyclase)-deficient mouse establishes an essential role for CD38 in bone resorption.* The FASEB journal, 2003. **17**(3): p. 369-375.

100. Abe, M., et al., *Osteoclasts enhance myeloma cell growth and survival via cell-cell contact: a vicious cycle between bone destruction and myeloma expansion.* Blood, 2004. **104**(8): p. 2484-91.
101. Lawson, M.A., et al., *Osteoclasts control reactivation of dormant myeloma cells by remodelling the endosteal niche.* Nature Communications, 2015. **6**(1): p. 8983.
102. Zangari, M., et al., *Response to bortezomib is associated to osteoblastic activation in patients with multiple myeloma.* British journal of haematology, 2005. **131**(1): p. 71-73.
103. Terpos, E., et al., *Bortezomib reduces serum dickkopf-1 and receptor activator of nuclear factor-κB ligand concentrations and normalises indices of bone remodelling in patients with relapsed multiple myeloma.* British journal of haematology, 2006. **135**(5): p. 688-692.
104. Mhaskar, R., et al., *Bisphosphonates in multiple myeloma: a network meta-analysis.* Cochrane Database of Systematic Reviews, 2012(5).
105. Lassailly, F., et al., *Multimodal imaging reveals structural and functional heterogeneity in different bone marrow compartments: functional implications on hematopoietic stem cells.* Blood, The Journal of the American Society of Hematology, 2013. **122**(10): p. 1730-1740.
106. Fluegen, G., et al., *Phenotypic heterogeneity of disseminated tumour cells is preset by primary tumour hypoxic microenvironments.* Nature cell biology, 2017. **19**(2): p. 120-132.
107. Forristal, C.E., et al., *Hypoxia inducible factors regulate pluripotency and proliferation in human embryonic stem cells cultured at reduced oxygen tensions.* Reproduction (Cambridge, England), 2010. **139**(1): p. 85.
108. Yata, K., et al., *Expression of angiogenic factors including VEGFs and the effects of hypoxia and thalidomide on human myeloma cells.* International journal of oncology, 2003. **22**(1): p. 165-173.
109. Woelfle, U., et al., *Molecular signature associated with bone marrow micrometastasis in human breast cancer.* Cancer research, 2003. **63**(18): p. 5679-5684.
110. Viziteu, E., et al., *Chetomin, targeting HIF-1α/p300 complex, exhibits antitumour activity in multiple myeloma.* Br J Cancer, 2016. **114**(5): p. 519-23.

111. Ludwig, H., et al., *Myeloma in patients younger than age 50 years presents with more favorable features and shows better survival: an analysis of 10 549 patients from the International Myeloma Working Group.* Blood, The Journal of the American Society of Hematology, 2008. **111**(8): p. 4039-4047.
112. Kumar, S.K., et al., *Improved survival in multiple myeloma and the impact of novel therapies.* Blood, The Journal of the American Society of Hematology, 2008. **111**(5): p. 2516-2520.
113. Cavo, M., et al., *International Myeloma Working Group consensus approach to the treatment of multiple myeloma patients who are candidates for autologous stem cell transplantation.* Blood, 2011. **117**(23): p. 6063-73.
114. Mitsiades, N., et al., *The proteasome inhibitor PS-341 potentiates sensitivity of multiple myeloma cells to conventional chemotherapeutic agents: therapeutic applications.* Blood, 2003. **101**(6): p. 2377-80.
115. Richardson, P.G., et al., *Bortezomib or high-dose dexamethasone for relapsed multiple myeloma.* N Engl J Med, 2005. **352**(24): p. 2487-98.
116. Chanan-Khan, A.A., et al., *Pomalidomide: the new immunomodulatory agent for the treatment of multiple myeloma.* Blood Cancer Journal, 2013. **3**(9): p. e143-e143.
117. Dimopoulos, M., et al., *Lenalidomide plus dexamethasone for relapsed or refractory multiple myeloma.* New England Journal of Medicine, 2007. **357**(21): p. 2123-2132.
118. Hoogstraten, B., et al., *Melphalan in multiple myeloma.* Blood, 1967. **30**(1): p. 74-83.
119. Barlogie, B., et al., *High-dose melphalan with autologous bone marrow transplantation for multiple myeloma.* 1986.
120. Popat, R., et al., *Bortezomib, doxorubicin and dexamethasone (PAD) front-line treatment of multiple myeloma: updated results after long-term follow-up.* British journal of haematology, 2008. **141**(4): p. 512-516.
121. Punnoose, E.A., et al., *Expression Profile of BCL-2, BCL-XL, and MCL-1 Predicts Pharmacological Response to the BCL-2 Selective Antagonist Venetoclax in Multiple Myeloma ModelsPredictive Biomarkers of Venetoclax Efficacy in Myeloma.* Molecular cancer therapeutics, 2016. **15**(5): p. 1132-1144.

122. Schmidt, J., et al., *Genome-wide studies in multiple myeloma identify XPO1/CRM1 as a critical target validated using the selective nuclear export inhibitor KPT-276.* Leukemia, 2013. **27**(12): p. 2357-2365.
123. Gulla, A. and K.C. Anderson, *Multiple myeloma: the (r)evolution of current therapy and a glance into future.* Haematologica, 2020. **105**(10): p. 2358-2367.
124. Garcia-Sanz, R., et al., *The oral combination of thalidomide, cyclophosphamide and dexamethasone (ThaCyDex) is effective in relapsed/refractory multiple myeloma.* Leukemia, 2004. **18**(4): p. 856-863.
125. Reeder, C.B., et al., *Cyclophosphamide, bortezomib and dexamethasone induction for newly diagnosed multiple myeloma: high response rates in a phase II clinical trial.* Leukemia, 2009. **23**(7): p. 1337-1341.
126. Cavo, M., et al., *Superiority of thalidomide and dexamethasone over vincristine-doxorubicindexamethasone (VAD) as primary therapy in preparation for autologous transplantation for multiple myeloma.* Blood, 2005. **106**(1): p. 35-39.
127. Costa, G., et al., *Melphalan and prednisone: An effective combination for the treatment of multiple myeloma.* The American Journal of Medicine, 1973. **54**(5): p. 589-599.
128. Attal, M., et al., *Lenalidomide (LEN) maintenance (MNTC) after high-dose melphalan and autologous stem cell transplant (ASCT) in multiple myeloma (MM): A meta-analysis (MA) of overall survival (OS)*. 2016, American Society of Clinical Oncology.
129. Grövdal, M., et al., *Autologous stem cell transplantation versus novel drugs or conventional chemotherapy for patients with relapsed multiple myeloma after previous ASCT.* Bone marrow transplantation, 2015. **50**(6): p. 808-812.
130. Shah, J.J., R.Z. Orlowski, and S.K. Thomas, *Role of combination bortezomib and pegylated liposomal doxorubicin in the management of relapsed and/or refractory multiple myeloma.* Therapeutics and clinical risk management, 2009. **5**: p. 151.
131. Samson, D., et al., *INFUSION OF VINCRISTINE AND DOXORUBICIN WITH ORAL DEXAMETHASONE AS FIRST-LINE THERAPY FOR MULTIPLE MYELOMA.* The Lancet, 1989. **334**(8668): p. 882-885.
132. Korst, D.R., et al., *Multiple Myeloma: II. Analysis of Cyclophosphamide Therapy in 165 Patients.* JAMA, 1964. **189**(10): p. 758-762.

133. Dingli, D., et al., *Cyclophosphamide mobilization does not improve outcome in patients receiving stem cell transplantation for multiple myeloma.* Clinical Lymphoma and Myeloma, 2006. **6**(5): p. 384-388.
134. Ludwig, H., et al., *Randomized phase II study of bortezomib, thalidomide, and dexamethasone with or without cyclophosphamide as induction therapy in previously untreated multiple myeloma.* Journal of Clinical Oncology, 2013. **31**(2): p. 247-255.
135. Gay, F., et al., *Carfilzomib with cyclophosphamide and dexamethasone or lenalidomide and dexamethasone plus autologous transplantation or carfilzomib plus lenalidomide and dexamethasone, followed by maintenance with carfilzomib plus lenalidomide or lenalidomide alone for patients with newly diagnosed multiple myeloma (FORTE): a randomised, open-label, phase 2 trial.* The Lancet Oncology, 2021. **22**(12): p. 1705-1720.
136. Dale Rein, I., et al., *Replication-induced DNA damage after PARP inhibition causes G2 delay, and cell line-dependent apoptosis, necrosis and multinucleation.* Cell cycle, 2015. **14**(20): p. 3248-3260.
137. Jones, R.M. and E. Petermann, *Replication fork dynamics and the DNA damage response.* Biochem J, 2012. **443**(1): p. 13-26.
138. Hasham, M.G., et al., *Activation-induced cytidine deaminase-initiated off-target DNA breaks are detected and resolved during S phase.* J Immunol, 2012. **189**(5): p. 2374-82.
139. Ogrunc, M., et al., *Oncogene-induced reactive oxygen species fuel hyperproliferation and DNA damage response activation.* Cell Death & Differentiation, 2014. **21**(6): p. 998-1012.
140. Renaudin, X., *Reactive oxygen species and DNA damage response in cancer.* International Review of Cell and Molecular Biology, 2021. **364**: p. 139-161.
141. Hustedt, N. and D. Durocher, *The control of DNA repair by the cell cycle.* Nat Cell Biol, 2016. **19**(1): p. 1-9.
142. Uziel, T., *Requirement of the MRN complex for ATM activation by DNA damage.* The EMBO Journal, 2003. **22**(20): p. 5612-5621.
143. Boboila, C., et al., *Alternative end-joining catalyzes class switch recombination in the absence of both Ku70 and DNA ligase 4.* J Exp Med, 2010. **207**(2): p. 417-27.

144. Mari, P.O., et al., *Dynamic assembly of end-joining complexes requires interaction between Ku70/80 and XRCC4.* Proc Natl Acad Sci U S A, 2006. **103**(49): p. 18597-602.
145. Blackford, A.N. and S.P. Jackson, *ATM, ATR, and DNA-PK: The Trinity at the Heart of the DNA Damage Response.* Molecular Cell, 2017. **66**(6): p. 801-817.
146. Douglas, P., et al., *Protein phosphatase 6 interacts with the DNA-dependent protein kinase catalytic subunit and dephosphorylates gamma-H2AX.* Mol Cell Biol, 2010. **30**(6): p. 1368-81.
147. Wu, J., et al., *Histone ubiquitination associates with BRCA1-dependent DNA damage response.* Mol Cell Biol, 2009. **29**(3): p. 849-60.
148. Bohgaki, M., et al., *RNF168 ubiquitylates 53BP1 and controls its response to DNA double-strand breaks.* Proc Natl Acad Sci U S A, 2013. **110**(52): p. 20982-7.
149. Krais, J.J., et al., *RNF168-mediated localization of BARD1 recruits the BRCA1-PALB2 complex to DNA damage.* Nature Communications, 2021. **12**(1): p. 5016.
150. Harris, D.R. and F. Bunz, *Protein phosphatases and the dynamics of the DNA damage response.* Cell Cycle, 2010. **9**(5): p. 861.
151. Székvölgyi, L. and A. Nicolas, *From meiosis to postmeiotic events: homologous recombination is obligatory but flexible.* Febs j, 2010. **277**(3): p. 571-89.
152. Neumann, F.R., et al., *Targeted INO80 enhances subnuclear chromatin movement and ectopic homologous recombination.* Genes & Development, 2012. **26**(4): p. 369-383.
153. Beucher, A., et al., *ATM and Artemis promote homologous recombination of radiation-induced DNA double-strand breaks in G2.* The EMBO Journal, 2009. **28**(21): p. 3413-3427.
154. Rothkamm, K., et al., *Pathways of DNA double-strand break repair during the mammalian cell cycle.* Mol Cell Biol, 2003. **23**(16): p. 5706-15.
155. Wang, B., et al., *Abraxas and RAP80 form a BRCA1 protein complex required for the DNA damage response.* Science, 2007. **316**(5828): p. 1194-1198.
156. Sobhian, B., et al., *RAP80 targets BRCA1 to specific ubiquitin structures at DNA damage sites.* Science, 2007. **316**(5828): p. 1198-1202.
157. Sartori, A.A., et al., *Human CtIP promotes DNA end resection.* Nature, 2007. **450**(7169): p. 509-514.

158. Yates, L.A., et al., *A structural and dynamic model for the assembly of Replication Protein A on single-stranded DNA.* Nature Communications, 2018. **9**(1): p. 5447.
159. Golub, E.I., et al., *Interaction of human rad51 recombination protein with single-stranded DNA binding protein, RPA.* Nucleic acids research, 1998. **26**(23): p. 5388-5393.
160. Tarsounas, M., D. Davies, and S.C. West, *BRCA2-dependent and independent formation of RAD51 nuclear foci.* Oncogene, 2003. **22**(8): p. 1115-1123.
161. Shibata, T., W. Iwasaki, and K. Hirota, *The intrinsic ability of double-stranded DNA to carry out D-loop and R-loop formation.* Computational and Structural Biotechnology Journal, 2020. **18**: p. 3350-3360.
162. Moldovan, G.L., et al., *DNA polymerase POLN participates in cross-link repair and homologous recombination.* Mol Cell Biol, 2010. **30**(4): p. 1088-96.
163. Chang, H.H.Y., et al., *Non-homologous DNA end joining and alternative pathways to double-strand break repair.* Nature Reviews Molecular Cell Biology, 2017. **18**(8): p. 495-506.
164. Yaneva, M., T. Kowalewski, and M.R. Lieber, *Interaction of DNA-dependent protein kinase with DNA and with Ku: biochemical and atomic-force microscopy studies.* The EMBO journal, 1997. **16**(16): p. 5098-5112.
165. Zimmermann, M., et al., *53BP1 regulates DSB repair using Rif1 to control 5′ end resection.* Science, 2013. **339**(6120): p. 700-704.
166. Ceccaldi, R., B. Rondinelli, and A.D. D'Andrea, *Repair pathway choices and consequences at the double-strand break.* Trends in cell biology, 2016. **26**(1): p. 52-64.
167. Sfeir, A. and L.S. Symington, *Microhomology-Mediated End Joining: A Back-up Survival Mechanism or Dedicated Pathway?* Trends Biochem Sci, 2015. **40**(11): p. 701-714.
168. Costantini, S., et al., *Interaction of the Ku heterodimer with the DNA ligase IV/Xrcc4 complex and its regulation by DNA-PK.* DNA repair, 2007. **6**(6): p. 712-722.
169. Grawunder, U., et al., *Activity of DNA ligase IV stimulated by complex formation with XRCC4 protein in mammalian cells.* Nature, 1997. **388**(6641): p. 492-495.
170. Sibanda, B.L., et al., *Crystal structure of an Xrcc4–DNA ligase IV complex.* Nature structural biology, 2001. **8**(12): p. 1015-1019.

171. Ma, Y., et al., *A biochemically defined system for mammalian nonhomologous DNA end joining.* Molecular cell, 2004. **16**(5): p. 701-713.
172. Goodarzi, A.A., et al., *DNA-PK autophosphorylation facilitates Artemis endonuclease activity.* The EMBO journal, 2006. **25**(16): p. 3880-3889.
173. McElhinny, S.A.N., et al., *A gradient of template dependence defines distinct biological roles for family X polymerases in nonhomologous end joining.* Molecular cell, 2005. **19**(3): p. 357-366.
174. Koole, W., et al., *A Polymerase Theta-dependent repair pathway suppresses extensive genomic instability at endogenous G4 DNA sites.* Nature communications, 2014. **5**(1): p. 1-10.
175. Han, L. and K. Yu, *Altered kinetics of nonhomologous end joining and class switch recombination in ligase IV–deficient B cells.* The Journal of experimental medicine, 2008. **205**(12): p. 2745-2753.
176. Masani, S., et al., *Redundant function of DNA ligase 1 and 3 in alternative end-joining during immunoglobulin class switch recombination.* Proceedings of the National Academy of Sciences, 2016. **113**(5): p. 1261-1266.
177. Drach, J., et al., *Multiple myeloma: high incidence of chromosomal aneuploidy as detected by interphase fluorescence in situ hybridization.* Cancer research, 1995. **55**(17): p. 3854-3859.
178. Maura, F., et al., *Genomic landscape and chronological reconstruction of driver events in multiple myeloma.* Nature communications, 2019. **10**(1): p. 1-12.
179. Boyd, K.D., et al., *Mapping of chromosome 1p deletions in myeloma identifies FAM46C at 1p12 and CDKN2C at 1p32.3 as being genes in regions associated with adverse survival.* Clin Cancer Res, 2011. **17**(24): p. 7776-84.
180. Fonseca, R., et al., *Deletions of chromosome 13 in multiple myeloma identified by interphase FISH usually denote large deletions of the q arm or monosomy.* Leukemia, 2001. **15**(6): p. 981-6.
181. Boyd, K.D., et al., *The clinical impact and molecular biology of del(17p) in multiple myeloma treated with conventional or thalidomide-based therapy.* Genes, Chromosomes and Cancer, 2011. **50**(10): p. 765-774.

182. Uetake, Y. and G. Sluder, *Cell cycle progression after cleavage failure: mammalian somatic cells do not possess a "tetraploidy checkpoint".* The Journal of cell biology, 2004. **165**(5): p. 609-615.

183. Pihan, G.A., et al., *Centrosome defects and genetic instability in malignant tumors.* Cancer research, 1998. **58**(17): p. 3974-3985.

184. Bakhoum, S.F., G. Genovese, and D.A. Compton, *Deviant kinetochore microtubule dynamics underlie chromosomal instability.* Current Biology, 2009. **19**(22): p. 1937-1942.

185. Burrell, R.A., et al., *Replication stress links structural and numerical cancer chromosomal instability.* Nature, 2013. **494**(7438): p. 492-496.

186. Crasta, K., et al., *DNA breaks and chromosome pulverization from errors in mitosis.* Nature, 2012. **482**(7383): p. 53-58.

187. Decaux, O., et al., *Prediction of survival in multiple myeloma based on gene expression profiles reveals cell cycle and chromosomal instability signatures in high-risk patients and hyperdiploid signatures in low-risk patients: a study of the Intergroupe Francophone du Myelome.* Journal of clinical oncology, 2008. **26**(29): p. 4798-4805.

188. Walters, D.K., et al., *Evidence for ongoing DNA damage in multiple myeloma cells as revealed by constitutive phosphorylation of H2AX.* Leukemia, 2011. **25**(8): p. 1344-53.

189. Patel, P.R., et al., *Overcoming Melphalan Resistance By Targeting Crucial DNA Repair Pathways in Multiple Myeloma.* Biology of Blood and Marrow Transplantation, 2020. **26**(3, Supplement): p. S224-S225.

190. Landau, H.J., et al., *The checkpoint kinase inhibitor AZD7762 potentiates chemotherapy-induced apoptosis of p53-mutated multiple myeloma cells.* Mol Cancer Ther, 2012. **11**(8): p. 1781-8.

191. Vangsted, A., et al., *Polymorphisms in the genes ERCC2, XRCC3 and CD3EAP influence treatment outcome in multiple myeloma patients undergoing autologous bone marrow transplantation.* International Journal of Cancer, 2007. **120**(5): p. 1036-1045.

192. Neri, P., et al., *Bortezomib-induced "BRCAness" sensitizes multiple myeloma cells to PARP inhibitors.* Blood, 2011. **118**(24): p. 6368-6379.

193. Goodarzi, A.A., et al., *ATM signaling facilitates repair of DNA double-strand breaks associated with heterochromatin.* Mol Cell, 2008. **31**(2): p. 167-77.

194. Faiola, F., et al., *Dual regulation of c-Myc by p300 via acetylation-dependent control of Myc protein turnover and coactivation of Myc-induced transcription.* Molecular and cellular biology, 2005. **25**(23): p. 10220-10234.
195. Jin, Z., et al., *Bcl2 suppresses DNA repair by enhancing c-Myc transcriptional activity.* Journal of Biological Chemistry, 2006. **281**(20): p. 14446-14456.
196. Song, L., et al., *Up-regulation of miR-1245 by c-myc targets BRCA2 and impairs DNA repair.* Journal of molecular cell biology, 2012. **4**(2): p. 108-117.
197. Szabo, A.G., et al., *Overexpression of c-myc is associated with adverse clinical features and worse overall survival in multiple myeloma.* Leukemia & Lymphoma, 2016. **57**(11): p. 2526-2534.
198. Holien, T., et al., *Addiction to c-MYC in multiple myeloma.* Blood, 2012. **120**(12): p. 2450-2453.
199. Parlati, F., et al., *Carfilzomib can induce tumor cell death through selective inhibition of the chymotrypsin-like activity of the proteasome.* Blood, 2009. **114**(16): p. 3439-47.
200. Kupperman, E., et al., *Evaluation of the proteasome inhibitor MLN9708 in preclinical models of human cancer.* Cancer Res, 2010. **70**(5): p. 1970-80.
201. Orlowski, M. and S. Wilk, *Catalytic activities of the 20 S proteasome, a multicatalytic proteinase complex.* Arch Biochem Biophys, 2000. **383**(1): p. 1-16.
202. Naujokat, C., et al., *Proteasomal chymotrypsin-like peptidase activity is required for essential functions of human monocyte-derived dendritic cells.* Immunology, 2007. **120**(1): p. 120-32.
203. Franke, N.E., et al., *Impaired bortezomib binding to mutant β5 subunit of the proteasome is the underlying basis for bortezomib resistance in leukemia cells.* Leukemia, 2012. **26**(4): p. 757-68.
204. Goldfinger, M., et al., *Protein synthesis in plasma cells is regulated by crosstalk between endoplasmic reticulum stress and mTOR signaling.* European Journal of Immunology, 2011. **41**(2): p. 491-502.
205. Cenci, S. and R. Sitia, *Managing and exploiting stress in the antibody factory.* FEBS Letters, 2007. **581**(19): p. 3652-3657.

206. Kaiser, M.F., et al., *The proteasome inhibitor bortezomib stimulates osteoblastic differentiation of human osteoblast precursors via upregulation of vitamin D receptor signalling.* Eur J Haematol, 2013. **90**(4): p. 263-72.
207. Hideshima, T., et al., *Bortezomib induces canonical nuclear factor-κB activation in multiple myeloma cells.* Blood, 2009. **114**(5): p. 1046-1052.
208. Dimopoulos, M.A., et al., *Carfilzomib and dexamethasone versus bortezomib and dexamethasone for patients with relapsed or refractory multiple myeloma (ENDEAVOR): a randomised, phase 3, open-label, multicentre study.* Lancet Oncol, 2016. **17**(1): p. 27-38.
209. Moreau, P., E. Zamagni, and M.-V. Mateos, *Treatment of patients with multiple myeloma progressing on frontline-therapy with lenalidomide.* Blood Cancer Journal, 2019. **9**(4).
210. Kumar, S.K., et al., *Carfilzomib or bortezomib in combination with lenalidomide and dexamethasone for patients with newly diagnosed multiple myeloma without intention for immediate autologous stem-cell transplantation (ENDURANCE): a multicentre, open-label, phase 3, randomised, controlled trial.* Lancet Oncol, 2020. **21**(10): p. 1317-1330.
211. Facon, T., et al., *Carfilzomib or bortezomib with melphalan-prednisone for transplant-ineligible patients with newly diagnosed multiple myeloma.* Blood, 2019. **133**(18): p. 1953-1963.
212. Waxman, A.J., et al., *Carfilzomib-Associated Cardiovascular Adverse Events: A Systematic Review and Meta-analysis.* JAMA Oncology, 2018. **4**(3): p. e174519-e174519.
213. Li, J., et al., *Ixazomib-based frontline therapy in patients with newly diagnosed multiple myeloma in real-life practice showed comparable efficacy and safety profile with those reported in clinical trial: a multi-center study.* Ann Hematol, 2020. **99**(11): p. 2589-2598.
214. Ghobrial, I.M., et al., *A Phase Ib/II Study of Oprozomib in Patients with Advanced Multiple Myeloma and Waldenström Macroglobulinemia.* Clin Cancer Res, 2019. **25**(16): p. 4907-4916.
215. Levin, N., et al., *Marizomib irreversibly inhibits proteasome to overcome compensatory hyperactivation in multiple myeloma and solid tumour patients.* Br J Haematol, 2016. **174**(5): p. 711-20.

216. Vogl, D.T., et al., *Phase I/II study of the novel proteasome inhibitor delanzomib (CEP-18770) for relapsed and refractory multiple myeloma.* Leuk Lymphoma, 2017. **58**(8): p. 1872-1879.
217. Baz, R., et al., *Lenalidomide and pegylated liposomal doxorubicin-based chemotherapy for relapsed or refractory multiple myeloma: safety and efficacy.* Ann Oncol, 2006. **17**(12): p. 1766-71.
218. Richardson, P.G., et al., *Lenalidomide, bortezomib, and dexamethasone combination therapy in patients with newly diagnosed multiple myeloma.* Blood, 2010. **116**(5): p. 679-86.
219. Nijhof, I.S., et al., *Phase 1/2 study of lenalidomide combined with low-dose cyclophosphamide and prednisone in lenalidomide-refractory multiple myeloma.* Blood, 2016. **128**(19): p. 2297-2306.
220. Mitsiades, N., et al., *Apoptotic signaling induced by immunomodulatory thalidomide analogs in human multiple myeloma cells: therapeutic implications.* Blood, 2002. **99**(12): p. 4525-4530.
221. Vacca, A., et al., *Thalidomide Downregulates Angiogenic Genes in Bone Marrow Endothelial Cells of Patients With Active Multiple Myeloma.* Journal of Clinical Oncology, 2005. **23**(23): p. 5334-5346.
222. Breitkreutz, I., et al., *Lenalidomide inhibits osteoclastogenesis, survival factors and bone-remodeling markers in multiple myeloma.* Leukemia, 2008. **22**(10): p. 1925-32.
223. Van Valckenborgh, E., et al., *Multiple myeloma induces the immunosuppressive capacity of distinct myeloid-derived suppressor cell subpopulations in the bone marrow.* Leukemia, 2012. **26**(11): p. 2424-2428.
224. Kotla, V., et al., *Mechanism of action of lenalidomide in hematological malignancies.* J Hematol Oncol, 2009. **2**: p. 36.
225. Davies, F.E., et al., *Thalidomide and immunomodulatory derivatives augment natural killer cell cytotoxicity in multiple myeloma.* Blood, 2001. **98**(1): p. 210-216.
226. Lokhorst, H.M., et al., *Targeting CD38 with Daratumumab Monotherapy in Multiple Myeloma.* N Engl J Med, 2015. **373**(13): p. 1207-19.
227. Barrangou, R., et al., *CRISPR provides acquired resistance against viruses in prokaryotes.* Science, 2007. **315**(5819): p. 1709-12.

228. Charpentier, E. and L.A. Marraffini, *Harnessing CRISPR-Cas9 immunity for genetic engineering.* Curr Opin Microbiol, 2014. **19**: p. 114-119.
229. Garneau, J.E., et al., *The CRISPR/Cas bacterial immune system cleaves bacteriophage and plasmid DNA.* Nature, 2010. **468**(7320): p. 67-71.
230. Ran, F.A., et al., *Genome engineering using the CRISPR-Cas9 system.* Nat Protoc, 2013. **8**(11): p. 2281-2308.
231. Gilbert, L.A., et al., *CRISPR-mediated modular RNA-guided regulation of transcription in eukaryotes.* Cell, 2013. **154**(2): p. 442-51.
232. Larson, M.H., et al., *CRISPR interference (CRISPRi) for sequence-specific control of gene expression.* Nat Protoc, 2013. **8**(11): p. 2180-96.
233. Konermann, S., et al., *Optical control of mammalian endogenous transcription and epigenetic states.* Nature, 2013. **500**(7463): p. 472-476.
234. Komor, A.C., et al., *Programmable editing of a target base in genomic DNA without double-stranded DNA cleavage.* Nature, 2016. **533**(7603): p. 420-4.
235. Zhu, Y.X., et al., *RNA interference screening identifies lenalidomide sensitizers in multiple myeloma, including RSK2.* Blood, 2015. **125**(3): p. 483-491.
236. Tiedemann, R.E., et al., *Identification of molecular vulnerabilities in human multiple myeloma cells by RNA interference lethality screening of the druggable genome.* Cancer Res, 2012. **72**(3): p. 757-68.
237. Ferriero, R., et al., *Pyruvate dehydrogenase complex and lactate dehydrogenase are targets for therapy of acute liver failure.* J Hepatol, 2018. **69**(2): p. 325-335.
238. Gray, L.R., S.C. Tompkins, and E.B. Taylor, *Regulation of pyruvate metabolism and human disease.* Cell Mol Life Sci, 2014. **71**(14): p. 2577-604.
239. Hiltunen, J.K., et al., *Mitochondrial fatty acid synthesis--an adopted set of enzymes making a pathway of major importance for the cellular metabolism.* Prog Lipid Res, 2010. **49**(1): p. 27-45.
240. Zhao, R.Z., et al., *Mitochondrial electron transport chain, ROS generation and uncoupling (Review).* Int J Mol Med, 2019. **44**(1): p. 3-15.
241. Lyssiotis, C.A. and A.C. Kimmelman, *Metabolic Interactions in the Tumor Microenvironment.* Trends Cell Biol, 2017. **27**(11): p. 863-875.

242. Guillaumond, F., et al., *Strengthened glycolysis under hypoxia supports tumor symbiosis and hexosamine biosynthesis in pancreatic adenocarcinoma.* Proc Natl Acad Sci U S A, 2013. **110**(10): p. 3919-24.
243. Reina, S. and V. De Pinto, *Anti-cancer compounds targeted to VDAC: potential and perspectives.* Current Medicinal Chemistry, 2017. **24**(40): p. 4447-4469.
244. Zheng, Y., et al., *Essential role of the voltage-dependent anion channel (VDAC) in mitochondrial permeability transition pore opening and cytochrome c release induced by arsenic trioxide.* Oncogene, 2004. **23**(6): p. 1239-47.
245. Lemasters, J.J. and E. Holmuhamedov, *Voltage-dependent anion channel (VDAC) as mitochondrial governator--thinking outside the box.* Biochim Biophys Acta, 2006. **1762**(2): p. 181-90.
246. Palmieri, F., *The mitochondrial transporter family SLC25: identification, properties and physiopathology.* Mol Aspects Med, 2013. **34**(2-3): p. 465-84.
247. Ruprecht, J.J. and E.R.S. Kunji, *The SLC25 Mitochondrial Carrier Family: Structure and Mechanism.* Trends Biochem Sci, 2020. **45**(3): p. 244-258.
248. Halestrap, A.P., *The mitochondrial pyruvate carrier. Kinetics and specificity for substrates and inhibitors.* Biochem J, 1975. **148**(1): p. 85-96.
249. Herzig, S., et al., *Identification and Functional Expression of the Mitochondrial Pyruvate Carrier.* Science, 2012. **337**(6090): p. 93-96.
250. Bricker, D.K., et al., *A mitochondrial pyruvate carrier required for pyruvate uptake in yeast, Drosophila, and humans.* Science, 2012. **337**(6090): p. 96-100.
251. Patel, M.S. and T.E. Roche, *Molecular biology and biochemistry of pyruvate dehydrogenase complexes.* Faseb j, 1990. **4**(14): p. 3224-33.
252. Patel, M.S., et al., *The pyruvate dehydrogenase complexes: structure-based function and regulation.* J Biol Chem, 2014. **289**(24): p. 16615-23.
253. Cardaci, S., et al., *Pyruvate carboxylation enables growth of SDH-deficient cells by supporting aspartate biosynthesis.* Nat Cell Biol, 2015. **17**(10): p. 1317-26.
254. El Arfani, C., et al., *Metabolic Features of Multiple Myeloma.* International Journal of Molecular Sciences, 2018. **19**(4): p. 1200.
255. Desbats, M.A., et al., *Metabolic Plasticity in Chemotherapy Resistance.* Frontiers in Oncology, 2020. **10**.

256. Zheng, J., *Energy metabolism of cancer: Glycolysis versus oxidative phosphorylation (Review).* Oncol Lett, 2012. **4**(6): p. 1151-1157.
257. Jiang, B., *Aerobic glycolysis and high level of lactate in cancer metabolism and microenvironment.* Genes Dis, 2017. **4**(1): p. 25-27.
258. Warburg, O., F. Wind, and E. Negelein, *THE METABOLISM OF TUMORS IN THE BODY.* J Gen Physiol, 1927. **8**(6): p. 519-30.
259. Shiratori, R., et al., *Glycolytic suppression dramatically changes the intracellular metabolic profile of multiple cancer cell lines in a mitochondrial metabolism-dependent manner.* Scientific Reports, 2019. **9**(1): p. 18699.
260. Le, A., et al., *Inhibition of lactate dehydrogenase A induces oxidative stress and inhibits tumor progression.* Proceedings of the National Academy of Sciences, 2010. **107**(5): p. 2037-2042.
261. de Padua, M.C., et al., *Disrupting glucose-6-phosphate isomerase fully suppresses the "Warburg effect" and activates OXPHOS with minimal impact on tumor growth except in hypoxia.* Oncotarget, 2017. **8**(50): p. 87623-87637.
262. Levine, A.J. and A.M. Puzio-Kuter, *The control of the metabolic switch in cancers by oncogenes and tumor suppressor genes.* Science, 2010. **330**(6009): p. 1340-1344.
263. Vasseur, S., et al., *Hypoxia induced tumor metabolic switch contributes to pancreatic cancer aggressiveness.* Cancers, 2010. **2**(4): p. 2138-2152.
264. Patra, K.C. and N. Hay, *The pentose phosphate pathway and cancer.* Trends in biochemical sciences, 2014. **39**(8): p. 347-354.
265. Tribble, D.L. and D.P. Jones, *Oxygen dependence of oxidative stress: rate of NADPH supply for maintaining the GSH pool during hypoxia.* Biochemical pharmacology, 1990. **39**(4): p. 729-736.
266. Garcia, J., et al., *Regulation of mitochondrial glutathione redox status and protein glutathionylation by respiratory substrates.* Journal of Biological Chemistry, 2010. **285**(51): p. 39646-39654.
267. Labow, B.I., W.W. Souba, and S.F. Abcouwer, *Mechanisms governing the expression of the enzymes of glutamine metabolism--glutaminase and glutamine synthetase.* J Nutr, 2001. **131**(9 Suppl): p. 2467S-74S; discussion 2486S-7S.

268. Lee, S.W., et al., *EGFR-Pak Signaling Selectively Regulates Glutamine Deprivation-Induced Macropinocytosis.* Dev Cell, 2019. **50**(3): p. 381-392.e5.
269. Altman, B.J., Z.E. Stine, and C.V. Dang, *From Krebs to clinic: glutamine metabolism to cancer therapy.* Nat Rev Cancer, 2016. **16**(10): p. 619-34.
270. Jiang, L., et al., *Reductive carboxylation supports redox homeostasis during anchorage-independent growth.* Nature, 2016. **532**(7598): p. 255-8.
271. Zhang, Z., et al., *ASCT2 (SLC1A5)-dependent glutamine uptake is involved in the progression of head and neck squamous cell carcinoma.* British Journal of Cancer, 2020. **122**(1): p. 82-93.
272. Kanai, Y., et al., *The SLC1 high-affinity glutamate and neutral amino acid transporter family.* Mol Aspects Med, 2013. **34**(2-3): p. 108-20.
273. Davidson, S.M., et al., *Environment Impacts the Metabolic Dependencies of Ras-Driven Non-Small Cell Lung Cancer.* Cell Metab, 2016. **23**(3): p. 517-28.
274. Gross, M.I., et al., *Antitumor Activity of the Glutaminase Inhibitor CB-839 in Triple-Negative Breast CancerAntitumor Activity of the Glutaminase Inhibitor CB-839 in TNBC.* Molecular cancer therapeutics, 2014. **13**(4): p. 890-901.
275. Cluntun, A.A., et al., *Glutamine Metabolism in Cancer: Understanding the Heterogeneity.* Trends Cancer, 2017. **3**(3): p. 169-180.
276. Fendt, S.M., et al., *Reductive glutamine metabolism is a function of the α-ketoglutarate to citrate ratio in cells.* Nat Commun, 2013. **4**: p. 2236.
277. Chang, W.K., K.D. Yang, and M.F. Shaio, *Lymphocyte proliferation modulated by glutamine: involved in the endogenous redox reaction.* Clin Exp Immunol, 1999. **117**(3): p. 482-8.
278. Watford, M., *Glutamine and glutamate: Nonessential or essential amino acids?* Anim Nutr, 2015. **1**(3): p. 119-122.
279. Feist, M., et al., *Cooperative STAT/NF-κB signaling regulates lymphoma metabolic reprogramming and aberrant GOT2 expression.* Nat Commun, 2018. **9**(1): p. 1514.
280. Tambay, V., V.-A. Raymond, and M. Bilodeau, *Myc rules: Leading glutamine metabolism toward a distinct cancer cell phenotype.* Cancers, 2021. **13**(17): p. 4484.

281. Li, B. and M.C. Simon, *Molecular pathways: targeting MYC-induced metabolic reprogramming and oncogenic stress in cancer.* Clinical Cancer Research, 2013. **19**(21): p. 5835-5841.
282. Cory, J.G. and A.H. Cory, *Critical roles of glutamine as nitrogen donors in purine and pyrimidine nucleotide synthesis: asparaginase treatment in childhood acute lymphoblastic leukemia.* In Vivo, 2006. **20**(5): p. 587-9.
283. Harding, H.P., et al., *An Integrated Stress Response Regulates Amino Acid Metabolism and Resistance to Oxidative Stress.* Molecular Cell, 2003. **11**(3): p. 619-633.
284. Li, N., et al., *Glutamine decreases lipopolysaccharide-induced intestinal inflammation in infant rats.* American Journal of Physiology-Gastrointestinal and Liver Physiology, 2004. **286**(6): p. G914-G921.
285. Petrus, P., et al., *Glutamine Links Obesity to Inflammation in Human White Adipose Tissue.* Cell Metab, 2020. **31**(2): p. 375-390.e11.
286. Burdon, R.H., V. Gill, and C. Rice-Evans, *Oxidative stress and tumour cell proliferation.* Free Radic Res Commun, 1990. **11**(1-3): p. 65-76.
287. Storz, P., *Reactive oxygen species in tumor progression.* Front Biosci, 2005. **10**: p. 1881-96.
288. Chung, Y.M., Y.S. Bae, and S.Y. Lee, *Molecular ordering of ROS production, mitochondrial changes, and caspase activation during sodium salicylate-induced apoptosis.* Free Radic Biol Med, 2003. **34**(4): p. 434-42.
289. Simon, H.U., A. Haj-Yehia, and F. Levi-Schaffer, *Role of reactive oxygen species (ROS) in apoptosis induction.* Apoptosis, 2000. **5**(5): p. 415-8.
290. Starheim, K.K., et al., *Intracellular glutathione determines bortezomib cytotoxicity in multiple myeloma cells.* Blood Cancer Journal, 2016. **6**(7): p. e446-e446.
291. O'Dwyer, P.J., et al., *Phase I trial of buthionine sulfoximine in combination with melphalan in patients with cancer.* J Clin Oncol, 1996. **14**(1): p. 249-56.
292. Cichon, M.A. and D.C. Radisky, *ROS-induced epithelial-mesenchymal transition in mammary epithelial cells is mediated by NF-kB-dependent activation of Snail.* Oncotarget, 2014. **5**(9): p. 2827-38.
293. Fox, A.D., et al., *Effect of a glutamine-supplemented enteral diet on methotrexate-induced enterocolitis.* JPEN J Parenter Enteral Nutr, 1988. **12**(4): p. 325-31.

294. Caillot, M., et al., *Targeting Reactive Oxygen Species Metabolism to Induce Myeloma Cell Death.* Cancers (Basel), 2021. **13**(10).
295. Vené, R., et al., *Redox remodeling allows and controls B-cell activation and differentiation.* Antioxid Redox Signal, 2010. **13**(8): p. 1145-55.
296. Zuo, L., et al., *Biological and physiological role of reactive oxygen species--the good, the bad and the ugly.* Acta Physiol (Oxf), 2015. **214**(3): p. 329-48.
297. Takada, Y., et al., *Hydrogen peroxide activates NF-kappa B through tyrosine phosphorylation of I kappa B alpha and serine phosphorylation of p65: evidence for the involvement of I kappa B alpha kinase and Syk protein-tyrosine kinase.* J Biol Chem, 2003. **278**(26): p. 24233-41.
298. Toledano, M.B. and W.J. Leonard, *Modulation of transcription factor NF-kappa B binding activity by oxidation-reduction in vitro.* Proc Natl Acad Sci U S A, 1991. **88**(10): p. 4328-32.
299. Lee, S.R., et al., *Reversible inactivation of the tumor suppressor PTEN by H2O2.* J Biol Chem, 2002. **277**(23): p. 20336-42.
300. León-Buitimea, A., et al., *Ethanol-induced oxidative stress is associated with EGF receptor phosphorylation in MCF-10A cells overexpressing CYP2E1.* Toxicol Lett, 2012. **209**(2): p. 161-5.
301. Toyama, E.Q., et al., *AMP-activated protein kinase mediates mitochondrial fission in response to energy stress.* Science, 2016. **351**(6270): p. 275-281.
302. Kim, J., et al., *AMPK activators: mechanisms of action and physiological activities.* Exp Mol Med, 2016. **48**(4): p. e224.
303. Wu, Z., et al., *Mechanisms controlling mitochondrial biogenesis and respiration through the thermogenic coactivator PGC-1.* Cell, 1999. **98**(1): p. 115-24.
304. Patti, M.E., et al., *Coordinated reduction of genes of oxidative metabolism in humans with insulin resistance and diabetes: Potential role of PGC1 and NRF1.* Proc Natl Acad Sci U S A, 2003. **100**(14): p. 8466-71.
305. Gonzalez, F.J., C. Xie, and C. Jiang, *The role of hypoxia-inducible factors in metabolic diseases.* Nature Reviews Endocrinology, 2019. **15**(1): p. 21-32.
306. Maiso, P., et al., *Metabolic signature identifies novel targets for drug resistance in multiple myeloma.* Cancer Res, 2015. **75**(10): p. 2071-82.

307. Steiner, N., et al., *The metabolomic plasma profile of myeloma patients is considerably different from healthy subjects and reveals potential new therapeutic targets.* PLoS One, 2018. **13**(8): p. e0202045.
308. Chowdhury, R., et al., *The oncometabolite 2-hydroxyglutarate inhibits histone lysine demethylases.* EMBO Rep, 2011. **12**(5): p. 463-9.
309. Gonsalves, W.I., et al., *Glutamine-derived 2-hydroxyglutarate is associated with disease progression in plasma cell malignancies.* JCI Insight, 2018. **3**(1).
310. Zub, K.A., et al., *Modulation of cell metabolic pathways and oxidative stress signaling contribute to acquired melphalan resistance in multiple myeloma cells.* PLoS One, 2015. **10**(3): p. e0119857.
311. Zaal, E.A., et al., *Bortezomib resistance in multiple myeloma is associated with increased serine synthesis.* Cancer & Metabolism, 2017. **5**(1).
312. Besse, L., et al., *A metabolic switch in proteasome inhibitor-resistant multiple myeloma ensures higher mitochondrial metabolism, protein folding and sphingomyelin synthesis.* Haematologica, 2019. **104**(9): p. e415-e419.
313. Thompson, R.M., et al., *Glutaminase inhibitor CB-839 synergizes with carfilzomib in resistant multiple myeloma cells.* Oncotarget, 2017. **8**(22): p. 35863-35876.
314. Gourzones, C., et al., *Antioxidant Defenses Confer Resistance to High Dose Melphalan in Multiple Myeloma Cells.* Cancers (Basel), 2019. **11**(4).
315. Kaspar, J.W., S.K. Niture, and A.K. Jaiswal, *Nrf2:INrf2 (Keap1) signaling in oxidative stress.* Free Radic Biol Med, 2009. **47**(9): p. 1304-9.
316. Shi, C.X., et al., *CRISPR Genome-Wide Screening Identifies Dependence on the Proteasome Subunit PSMC6 for Bortezomib Sensitivity in Multiple Myeloma.* Mol Cancer Ther, 2017. **16**(12): p. 2862-2870.
317. Bolzoni, M., et al., *Dependence on glutamine uptake and glutamine addiction characterize myeloma cells: a new attractive target.* Blood, 2016. **128**(5): p. 667-679.
318. Xiang, Y., et al., *SR18292 exerts potent antitumor effects in multiple myeloma via inhibition of oxidative phosphorylation.* Life Sciences, 2020. **256**: p. 117971.
319. Lim, J.S.L., P.S.Y. Chong, and W.-J. Chng, *Metabolic Vulnerabilities in Multiple Myeloma.* Cancers, 2022. **14**(8): p. 1905.

320. Cengiz Seval, G. and M. Beksac, *The safety of bortezomib for the treatment of multiple myeloma.* Expert Opin Drug Saf, 2018. **17**(9): p. 953-962.
321. Del Giudice, M.L., et al., *Carfilzomib plus dexamethasone in patients with relapsed and refractory multiple myeloma: a retro-prospective observational study.* Eur J Haematol, 2022.
322. Tantawy, M., et al., *Lactate Dehydrogenase B and Pyruvate Oxidation Pathway Associated With Carfilzomib-Related Cardiotoxicity in Multiple Myeloma Patients: Result of a Multi-Omics Integrative Analysis.* Front Cardiovasc Med, 2021. **8**: p. 645122.
323. Oonthonpan, L., et al., *Two human patient mitochondrial pyruvate carrier mutations reveal distinct molecular mechanisms of dysfunction.* JCI Insight, 2019. **5**(13).
324. McCommis, K.S., et al., *Loss of Mitochondrial Pyruvate Carrier 2 in the Liver Leads to Defects in Gluconeogenesis and Compensation via Pyruvate-Alanine Cycling.* Cell metabolism, 2015. **22**(4): p. 682-694.
325. Vigueira, P.A., et al., *Mitochondrial pyruvate carrier 2 hypomorphism in mice leads to defects in glucose-stimulated insulin secretion.* Cell Rep, 2014. **7**(6): p. 2042-2053.
326. Colca, J.R., et al., *Identification of a mitochondrial target of thiazolidinedione insulin sensitizers (mTOT)--relationship to newly identified mitochondrial pyruvate carrier proteins.* PloS one, 2013. **8**(5): p. e61551-e61551.
327. Vanderperre, B., et al., *Embryonic Lethality of Mitochondrial Pyruvate Carrier 1 Deficient Mouse Can Be Rescued by a Ketogenic Diet.* PLoS genetics, 2016. **12**(5): p. e1006056-e1006056.
328. Bricker, D.K., et al., *A Mitochondrial Pyruvate Carrier Required for Pyruvate Uptake in Yeast, Drosophila , and Humans.* Science, 2012. **337**(6090): p. 96-100.
329. Herzig, S., et al., *Identification and functional expression of the mitochondrial pyruvate carrier.* Science, 2012. **337**(6090): p. 93-6.
330. Li, Y., et al., *Mitochondrial pyruvate carrier function is negatively linked to Warburg phenotype in vitro and malignant features in esophageal squamous cell carcinomas.* Oncotarget, 2017. **8**(1): p. 1058-1073.
331. Li, X., et al., *MPC1 and MPC2 expressions are associated with favorable clinical outcomes in prostate cancer.* BMC Cancer, 2016. **16**(1): p. 894.

332. Zou, H., et al., *MPC1 deficiency accelerates lung adenocarcinoma progression through the STAT3 pathway.* Cell Death Dis, 2019. **10**(3): p. 148.
333. Bensard, C.L., et al., *Regulation of Tumor Initiation by the Mitochondrial Pyruvate Carrier.* Cell Metab, 2020. **31**(2): p. 284-300.e7.
334. Chai, Y., et al., *MPC1 deletion is associated with poor prognosis and temozolomide resistance in glioblastoma.* J Neurooncol, 2019. **144**(2): p. 293-301.
335. Duan, L., et al., *Histone lysine demethylase KDM4B regulates the alternative splicing of the androgen receptor in response to androgen deprivation.* Nucleic Acids Res, 2019. **47**(22): p. 11623-11636.
336. Ma, X., et al., *Function of mitochondrial pyruvate carriers in hepatocellular carcinoma patients.* Oncol Lett, 2018. **15**(6): p. 9110-9116.
337. Dan, L., et al., *PGC1α promotes cholangiocarcinoma metastasis by upregulating PDHA1 and MPC1 expression to reverse the Warburg effect.* Cell Death Dis, 2018. **9**(5): p. 466.
338. Corbet, C., et al., *Interruption of lactate uptake by inhibiting mitochondrial pyruvate transport unravels direct antitumor and radiosensitizing effects.* Nat Commun, 2018. **9**(1): p. 1208.
339. Ruiz-Iglesias, A. and S. Manes, *The Importance of Mitochondrial Pyruvate Carrier in Cancer Cell Metabolism and Tumorigenesis.* Cancers (Basel), 2021. **13**(7).
340. Corcoran, L.M. and S.L. Nutt, *Long-lived plasma cells have a sweet tooth.* Immunity, 2016. **45**(1): p. 3-5.
341. Dalva-Aydemir, S., et al., *Targeting the metabolic plasticity of multiple myeloma with FDA-approved ritonavir and metformin.* Clinical Cancer Research, 2015. **21**(5): p. 1161-1171.
342. Tompkins, S.C., et al., *Disrupting Mitochondrial Pyruvate Uptake Directs Glutamine into the TCA Cycle away from Glutathione Synthesis and Impairs Hepatocellular Tumorigenesis.* Cell Reports, 2019. **28**(10): p. 2608-2619.e6.
343. Prelowska, M.K., et al., *Inhibition of the L-glutamine transporter ASCT2 sensitizes plasma cell myeloma cells to proteasome inhibitors.* Cancer Lett, 2021. **507**: p. 13-25.
344. Austin, S. and J. St-Pierre, *PGC1α and mitochondrial metabolism – emerging concepts and relevance in ageing and neurodegenerative disorders.* Journal of Cell Science, 2012. **125**(21): p. 4963-4971.

345. St-Pierre, J., et al., *Suppression of reactive oxygen species and neurodegeneration by the PGC-1 transcriptional coactivators.* Cell, 2006. **127**(2): p. 397-408.
346. Koh, E., et al., *MPC1 is essential for PGC-1α-induced mitochondrial respiration and biogenesis.* Biochem J, 2018. **475**(10): p. 1687-1699.
347. Park, S., et al., *Inhibition of ERRα prevents mitochondrial pyruvate uptake exposing NADPH-generating pathways as targetable vulnerabilities in breast cancer.* Cell reports, 2019. **27**(12): p. 3587-3601. e4.
348. Zellner, M., et al., *Glutamine starvation of monocytes inhibits the ubiquitin-proteasome proteolytic pathway.* Biochim Biophys Acta, 2003. **1638**(2): p. 138-48.
349. Widjaja, C.E., et al., *Proteasome activity regulates CD8+ T lymphocyte metabolism and fate specification.* J Clin Invest, 2017. **127**(10): p. 3609-3623.
350. Tibullo, D., et al., *Mitochondrial Functions, Energy Metabolism and Protein Glycosylation are Interconnected Processes Mediating Resistance to Bortezomib in Multiple Myeloma Cells.* Biomolecules, 2020. **10**(5): p. 696.
351. Zaal, E.A., et al., *Targeting coenzyme Q10 synthesis overcomes bortezomib resistance in multiple myeloma.* Molecular Omics, 2022. **18**(1): p. 19-30.
352. Chesi, M., et al., *Drug response in a genetically engineered mouse model of multiple myeloma is predictive of clinical efficacy.* Blood, 2012. **120**(2): p. 376-85.
353. Fowler, J.A., et al., *A murine model of myeloma that allows genetic manipulation of the host microenvironment.* Dis Model Mech, 2009. **2**(11-12): p. 604-11.
354. Calimeri, T., et al., *Aberrant Non-Homologous End Joining in Multiple Myeloma: A Role in Genomic Instability and As Potential Prognostic Marker.* Blood, 2012. **120**(21): p. 2932.
355. Shammas, M.A., et al., *Dysfunctional homologous recombination mediates genomic instability and progression in myeloma.* Blood, The Journal of the American Society of Hematology, 2009. **113**(10): p. 2290-2297.
356. Walters, D.K., et al., *Evidence for ongoing DNA damage in multiple myeloma cells as revealed by constitutive phosphorylation of H2AX.* Leukemia, 2011. **25**(8): p. 1344-1353.
357. Ushie, C., et al., *The polymorphisms of base excision repair genes influence the prognosis of multiple myeloma.* Blood, 2012. **120**(21): p. 3981.

358. Episkopou, H., et al., *Association between transcriptional activity, local chromatin structure, and the efficiencies of both subpathways of nucleotide excision repair of melphalan adducts.* Cancer research, 2009. **69**(10): p. 4424-4433.
359. Kotoula, V., et al., *Mismatch repair gene expression in malignant lymphoproliferative disorders of B-cell origin.* Leukemia & lymphoma, 2002. **43**(2): p. 393-399.
360. Talluri, S., et al., *Dysregulated APOBEC3G causes DNA damage and promotes genomic instability in multiple myeloma.* Blood Cancer Journal, 2021. **11**(10): p. 166.
361. Herrero, A.B., J. San Miguel, and N.C. Gutierrez, *Deregulation of DNA double-strand break repair in multiple myeloma: implications for genome stability.* PLoS One, 2015. **10**(3): p. e0121581.
362. Bothmer, A., et al., *53BP1 regulates DNA resection and the choice between classical and alternative end joining during class switch recombination.* Journal of Experimental Medicine, 2010. **207**(4): p. 855-865.
363. Bunting, S.F., et al., *53BP1 inhibits homologous recombination in Brca1-deficient cells by blocking resection of DNA breaks.* Cell, 2010. **141**(2): p. 243-254.
364. Escribano-Díaz, C., et al., *A cell cycle-dependent regulatory circuit composed of 53BP1-RIF1 and BRCA1-CtIP controls DNA repair pathway choice.* Molecular cell, 2013. **49**(5): p. 872-883.
365. Chapman, J.R., et al., *RIF1 is essential for 53BP1-dependent nonhomologous end joining and suppression of DNA double-strand break resection.* Molecular cell, 2013. **49**(5): p. 858-871.
366. Callen, E., et al., *53BP1 mediates productive and mutagenic DNA repair through distinct phosphoprotein interactions.* Cell, 2013. **153**(6): p. 1266-1280.
367. Bhat, A., et al., *Rev7/Mad2B plays a critical role in the assembly of a functional mitotic spindle.* Cell Cycle, 2015. **14**(24): p. 3929-38.
368. Rizzo, A.A., et al., *Rev7 dimerization is important for assembly and function of the Rev1/Polζ translesion synthesis complex.* Proc Natl Acad Sci U S A, 2018. **115**(35): p. E8191-e8200.
369. Boersma, V., et al., *MAD2L2 controls DNA repair at telomeres and DNA breaks by inhibiting 5′ end resection.* Nature, 2015. **521**(7553): p. 537-540.

370. Xu, G., et al., *REV7 counteracts DNA double-strand break resection and affects PARP inhibition.* Nature, 2015. **521**(7553): p. 541-544.
371. Gupta, R., et al., *DNA repair network analysis reveals shieldin as a key regulator of NHEJ and PARP inhibitor sensitivity.* Cell, 2018. **173**(4): p. 972-988. e23.
372. Dev, H., et al., *Shieldin complex promotes DNA end-joining and counters homologous recombination in BRCA1-null cells.* Nature Cell Biology, 2018. **20**(8): p. 954-965.
373. Noordermeer, S.M., et al., *The shieldin complex mediates 53BP1-dependent DNA repair.* Nature, 2018. **560**(7716): p. 117-121.
374. Gao, S., et al., *An OB-fold complex controls the repair pathways for DNA double-strand breaks.* Nature Communications, 2018. **9**(1): p. 3925.
375. Ghezraoui, H., et al., *53BP1 cooperation with the REV7–shieldin complex underpins DNA structure-specific NHEJ.* Nature, 2018. **560**(7716): p. 122-127.
376. Mirman, Z., et al., *53BP1–RIF1–shieldin counteracts DSB resection through CST-and Polα-dependent fill-in.* Nature, 2018. **560**(7716): p. 112-116.
377. Tomida, J., et al., *FAM 35A associates with REV 7 and modulates DNA damage responses of normal and BRCA 1-defective cells.* The EMBO journal, 2018. **37**(12): p. e99543.
378. Roddam, P.L., et al., *Genetic variants of NHEJ DNA ligase IV can affect the risk of developing multiple myeloma, a tumour characterised by aberrant class switch recombination.* J Med Genet, 2002. **39**(12): p. 900-5.
379. Caracciolo, D., et al., *miR-22 suppresses DNA ligase III addiction in multiple myeloma.* Leukemia, 2019. **33**(2): p. 487-498.
380. Chen, Q., et al., *The FA/BRCA pathway is involved in melphalan-induced DNA interstrand cross-link repair and accounts for melphalan resistance in multiple myeloma cells.* Blood, 2005. **106**(2): p. 698-705.
381. Sousa, M.M.L., et al., *An inverse switch in DNA base excision and strand break repair contributes to melphalan resistance in multiple myeloma cells.* PloS one, 2013. **8**(2): p. e55493-e55493.
382. Gkotzamanidou, M., et al., *DNA repair of myeloma plasma cells correlates with clinical outcome: the effect of the nonhomologous end-joining inhibitor SCR7.* Blood, The Journal of the American Society of Hematology, 2016. **128**(9): p. 1214-1225.

383. Mitsiades, N., et al., *The proteasome inhibitor PS-341 potentiates sensitivity of multiple myeloma cells to conventional chemotherapeutic agents: therapeutic applications.* Blood, The Journal of the American Society of Hematology, 2003. **101**(6): p. 2377-2380.
384. Kiziltepe, T., et al., *5-Azacytidine, a DNA methyltransferase inhibitor, induces ATR-mediated DNA double-strand break responses, apoptosis, and synergistic cytotoxicity with doxorubicin and bortezomib against multiple myeloma cells.* Molecular cancer therapeutics, 2007. **6**(6): p. 1718-1727.
385. Kiziltepe, T., et al., *5-Azacytidine, a DNA methyltransferase inhibitor, induces ATR-mediated DNA double-strand break responses, apoptosis, and synergistic cytotoxicity with doxorubicin and bortezomib against multiple myeloma cells.* Molecular Cancer Therapeutics, 2007. **6**(6): p. 1718-1727.
386. Kiziltepe, T., et al., *JS-K, a GST-activated nitric oxide generator, induces DNA double-strand breaks, activates DNA damage response pathways, and induces apoptosis in vitro and in vivo in human multiple myeloma cells.* Blood, 2007. **110**(2): p. 709-718.
387. Chen, G. and et al., *A novel phosphoramide compound, DCZ0847, displays in vitro and in vivo anti-myeloma activity, alone or in combination with bortezomib.* Cancer Letters, 2020. **478**: p. 45.
388. Moyal, L., et al., *Requirement of ATM-Dependent Monoubiquitylation of Histone H2B for Timely Repair of DNA Double-Strand Breaks.* Molecular Cell, 2011. **41**(5): p. 529-542.
389. Botuyan, M.V., et al., *Structural Basis for the Methylation State-Specific Recognition of Histone H4-K20 by 53BP1 and Crb2 in DNA Repair.* Cell, 2006. **127**(7): p. 1361-1373.